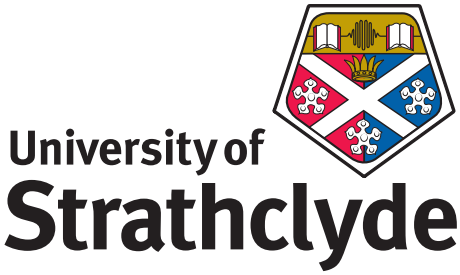

Thin-Film Flows on Cylinders

George Adam Leslie

Department of Mathematics and Statistics

University of Strathclyde

Glasgow, UK

March 2012

This thesis is submitted to the University of Strathclyde for the degree of Doctor of Philosophy in the Faculty of Science.

This thesis is the result of the authors original research. It has been composed by the author and has not been previously submitted for examination which has led to the award of a degree.

Signed: Date:

Abstract

Three different problems concerning thin-film flows on horizontal cylinders are studied. Firstly, steady two-dimensional gravity-driven flow with prescribed volume flux of a thin film of Newtonian fluid with temperature-dependent viscosity (i.e. thermoviscous flow) over a uniformly heated or cooled stationary horizontal cylinder is studied. Numerical results along with asymptotic solutions in appropriate limits are presented giving an insight into the effects of thermoviscosity and heat transfer at the free surface. Next, we consider steady two-dimensional flow of a prescribed load (mass) of Newtonian fluid with temperature-dependent viscosity on a uniformly heated or cooled rotating horizontal cylinder. The existence of a critical solution with a critical load above which no solutions exist is found, and both this critical solution and the case of prescribed subcritical load are studied in detail, with both numerical and asymptotic solutions presented. In particular, it is found that backflow (i.e. flow counter to the direction of rotation) occurs within a certain region of parameter space (backflow never occurs in the corresponding isothermal problem). Finally, the steady isothermal flow of a symmetric thin slowly-varying rivulet of a non-perfectly wetting Newtonian fluid on either the outside or the inside of a uniformly rotating horizontal cylinder is considered. Numerical and asymptotic solutions in appropriate limits are presented and it is found that rivulet flow on a rotating cylinder gives rise to a critical solution similar in nature to the critical solution found for the classical two-dimensional problem. We also show that backflow occurs within a particular region of parameter space.

Contents

Chapter 1

Introduction

1.1 Thin-Film Flow

Thin-film flows occur in a large number of situations, including many biological, industrial, geophysical and simple everyday contexts. For example, thin films in a biological context appear in several places in the human body, such as tear films, which lubricate the eyes, peritoneal fluid, which lubricates the outside of organs and tissue in the peritoneal cavity, synovial fluid, which lubricates joints, and mucus, which coats the airways. In industrial contexts thin-film flows occur in a wide variety of coating applications, such as painting, printing, dying, coating foodstuffs (for example, figure 1.1(a) shows doughnuts passing though an enrober which coats each doughnut with a thin film of glaze) and the coating of photographic film with photosensitive chemicals. Industrial coatings are applied through a variety of processes, such as blade coating, in which a blade is used to spread the coating fluid over an object to form a thin film, air-knife coating, which uses a jet of air instead of a physical blade, spin coating, in which the coating fluid is applied to an object which is spun until the fluid spreads to form the desired thickness, dip coating, in which the object to be coated is immersed in a vat of fluid and is then removed with a coating of the fluid, and curtain coating, in which the object to be coated passes through a falling film of the coating fluid (the coating of the doughnuts in

(a)

(b)

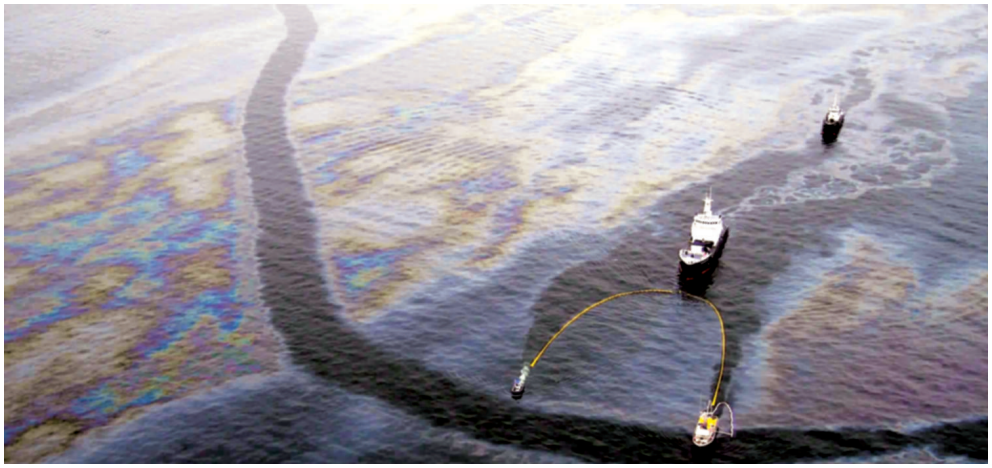

Figure 1.1: (a) Doughnuts passing though an enrober which coats each doughnut with a thin film of glaze; picture sourced from flickr.com/kathleenhaboc. (b) An oil spill in the sea; the oil floats on top of the water forming a thin film; picture sourced from NOAA Photo Library.

figure 1.1(a) being an example of this). Many industrial processes require various parts of machinery to be lubricated, which is often achieved using a thin film of a lubricant; for example, bearings, pumps, pistons and turbines all require lubrication. Heat exchangers often involve the evaporation of (or condensation to) a thin film of fluid, while distillation processes can form thin films when the distillate condenses. There are also a large number of everyday situations that give rise

to thin-film flows, such as oil spreading in a frying pan, the spreading of honey onto a piece of toast with a knife, and droplets and rivulets of rain flowing down a window. It is worth noting that the word thin does not necessarily mean "small" in the everyday sense of the word; thin simply means "depth significantly smaller than width". Examples of "large" but thin flows may be found in geophysical and environmental settings, such as in rivers, lava flows and mud flows, while oil spills in large bodies of water lead to thin films of oil floating on top of the water; figure 1.1(b) shows an example of an oil spill at sea.

1.2 Mathematical Modelling of Thin-Film Flows

The flow of an incompressible Newtonian fluid is modelled using the well-known Navier–Stokes equation

$$\rho\frac{\mathrm{D}\mathbf{u}}{\mathrm{D}t} = \rho\mathbf{f} - \nabla p + \mu\nabla^2\mathbf{u}, \tag{1.1}$$

together with the mass-conservation equation

$$\nabla\cdot\mathbf{u} = 0, \tag{1.2}$$

where ρ is the density of the fluid, p is the pressure in the fluid, μ is the viscosity of the fluid, $\mathbf{u}$ is the fluid velocity, t is time, $\mathbf{f}$ is any body forces acting on the fluid per unit volume, ∇ is the vector gradient operator, and $\dfrac{\mathrm{D}}{\mathrm{D}t} = \dfrac{\partial}{\partial t} + \mathbf{u}\cdot\nabla$ is the material derivative. At any fluid-fluid boundary one must also consider the stress balance equation

$$\mathbf{n}\cdot\boldsymbol{\sigma} - \mathbf{n}\cdot\hat{\boldsymbol{\sigma}} = \gamma\mathbf{n}(\nabla\cdot\mathbf{n}) - \nabla\gamma \tag{1.3}$$

where $\boldsymbol{\sigma} = -p\mathbf{I} + \mu[\nabla\mathbf{u} + (\nabla\mathbf{u})^{\mathrm{T}}]$ is the stress tensor in the "first" fluid (with $\hat{\boldsymbol{\sigma}}$ being the stress tensor in the "second" fluid), $\mathbf{n}$ is the unit outward normal to the surface pointing towards the first fluid, and γ is the surface tension between the fluids (which is often taken to be constant). In the case of a free surface the stress boundary equation reduces to $\mathbf{n}\cdot\boldsymbol{\sigma} = \gamma\mathbf{n}(\nabla\cdot\mathbf{n}) - \nabla\gamma$, while if it is also assumed

that the surface tension is constant (which it is often considered to be) then the stress boundary equation reduces to $\mathbf{n} \cdot \boldsymbol{\sigma} = \gamma \mathbf{n}(\nabla \cdot \mathbf{n})$. If there is zero mass flux across a fluid-fluid boundary then we must also use the kinematic boundary condition $\mathrm{D}F/\mathrm{D}t = 0$, where $F(\mathbf{x}, t) = 0$ is the equation for the boundary and $\mathbf{x}$ is the position vector. In the case of a fluid-solid boundary it is usual to impose the condition $\mathbf{u} = 0$, namely the no-slip and no-penetration conditions (thought it should be noted that slip conditions are possible). In general, these equations do not permit any meaningful analytical progress and can only be solved numerically; as a result of this, it is common practice to consider instead some practically relevant approximation to the equations. In particular, the relative smallness of one lengthscale of a thin film (for example, depth) compared to another (for example, length or width) can be used to simplify the problem greatly. The introduction of an appropriate small aspect ratio allows simplification of the governing equations by ignoring terms that are small compared to others, and often results in equations where analytical progress can be made; this form of approximation is often referred to as lubrication theory because of its applicability in the modelling of thin films of lubricant between two substrates (for example, in journal bearings).

We shall introduce the idea of lubrication theory by considering a basic example, namely the two-dimensional flow of a thin film of fluid down a plane inclined at an angle α ($0 \leq \alpha \leq \pi/2$) to the horizontal, and in doing so we reproduce the work of Huppert [1]. A diagram showing the setup of the problem is shown in figure 1.2, where L and H are typical lengthscales in the longitudinal and transverse directions, respectively, and the aspect ratio, denoted ϵ, is given by $\epsilon = H/L \ll 1$ and is taken to be small. We choose Cartesian coordinates Oxy with the x axis in the direction of flow and the y axis normal to the substrate, and take the substrate to be at $y = 0$ and the free surface to be at $y = h$, where $h = h(x, t)$ is the film thickness. We non-dimensionalise and scale the system appropriately by writing

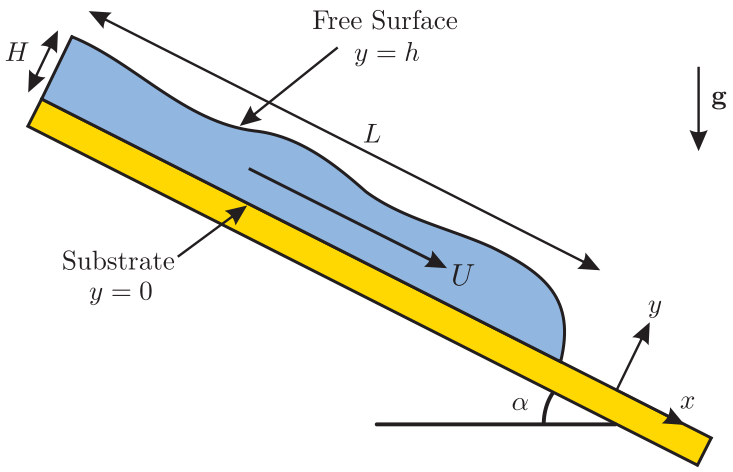

Figure 1.2: Geometry of two-dimensional thin-film flow down an incline.

$$\left.\begin{aligned} x = Lx^*, \quad y = Hy^*, \quad h = Hh^*, \quad t = \frac{L}{U}t^*, \\ u = Uu^*, \quad v = \frac{UH}{L}v^*, \quad p - p_\mathrm{a} = \frac{\mu U}{H}p^*, \quad U = \frac{\rho g H^2}{\mu}, \end{aligned}\right\} \tag{1.4}$$

where u and v are the components of velocity in the x and y directions, respectively, h is the film thickness, U is a characteristic velocity in the x direction, p_a is the constant pressure in the surrounding atmosphere, and g is the magnitude of gravitational acceleration. The star superscripts are immediately dropped for clarity. The mass-conservation and Navier–Stokes equations, (1.1) and (1.2), become

$$\frac{\partial u}{\partial y} + \frac{\partial v}{\partial y} = 0, \tag{1.5}$$

$$\epsilon^2 Re\left(\frac{\partial u}{\partial t} + u\frac{\partial u}{\partial x} + v\frac{\partial u}{\partial y}\right) = -\epsilon\frac{\partial p}{\partial x} + \epsilon^2\frac{\partial^2 u}{\partial x^2} + \frac{\partial^2 u}{\partial y^2} + \sin\alpha \tag{1.6}$$

and

$$\epsilon^3 Re\left(\frac{\partial v}{\partial t} + u\frac{\partial v}{\partial x} + v\frac{\partial v}{\partial y}\right) = -\frac{\partial p}{\partial y} + \epsilon^3\frac{\partial^2 v}{\partial x^2} + \epsilon\frac{\partial^2 v}{\partial y^2} - \cos\alpha, \tag{1.7}$$

where $Re^* = \epsilon^2 Re = \epsilon^2 \rho U L/\mu \ll 1$ is the reduced Reynolds number which is assumed to be small; in particular, this means that the Reynolds number itself need

not be small. At leading order in ϵ the governing equations simplify dramatically to

$$\frac{\partial u}{\partial x} + \frac{\partial v}{\partial y} = 0, \quad \frac{\partial^2 u}{\partial y^2} = -\sin\alpha \quad \text{and} \quad \frac{\partial p}{\partial y} = -\cos\alpha, \tag{1.8}$$

together with the boundary conditions of no-slip and no-penetration on the substrate:

$$u = v = 0 \quad \text{on} \quad y = 0, \tag{1.9}$$

and the balances of normal and tangential stress at the free surface:

$$\frac{\partial u}{\partial y} = 0 \quad \text{and} \quad p = 0 \quad \text{on} \quad y = h, \tag{1.10}$$

where it has been assumed that the effects of surface tension are negligible. The solution to (1.8)–(1.10) for the pressure p and velocities u and v is given by

$$p = \cos\alpha(h - y), \quad u = \frac{\sin\alpha}{2}(2h - y)y \quad \text{and} \quad v = -\frac{\sin\alpha}{2}\frac{\partial h}{\partial x}y^2, \tag{1.11}$$

while the kinematic condition, which may be written in the form

$$\frac{\partial h}{\partial t} + \frac{\partial Q}{\partial x} = 0, \tag{1.12}$$

where Q is the volume flux per unit width, given by

$$Q = \int_0^h u \, \mathrm{d}y = \frac{\sin\alpha}{3}h^3, \tag{1.13}$$

leads to an evolution equation for the film thickness h, namely

$$\frac{\partial h}{\partial t} + h^2 \sin\alpha \frac{\partial h}{\partial x} = 0, \tag{1.14}$$

which may be solved for h using the method of characteristics to yield the implicit solution

$$h = f(x - h^2 t \sin\alpha), \tag{1.15}$$

where $f = f(x)$ is the initial shape of the film when $t = 0$ (i.e. $h(x, 0) = f(x)$). A long time after the start of the flow the bulk of the fluid approaches the simple similarity solution

$$h = \left(\frac{x}{t\sin\alpha}\right)^{1/2}, \tag{1.16}$$

which is independent of the initial shape $f(x)$. It may also be shown the "nose" of the flow, denoted $x = x_{\mathrm{N}}(t)$, approaches

$$x_{\mathrm{N}} = \left(\frac{9}{4}A^2 t \sin\alpha\right)^{1/3}, \tag{1.17}$$

where A is the initial two-dimensional volume (i.e. area) of the film. The region near the nose is not described by the similarity solution (1.16) becasuse pressure gradients in the x direction will become important along with the effects of surface tension; to obtain a satisfactory solution one would have to construct an inner solution taking one or both of these effects into account.

As a result of the relative simplicity of the equations that result from lubrication theory there has been a vast amount of research using this approach, and there are several review articles devoted to it, including those by Oron et al. [2], Colineta et al. [3] and Craster and Matar [4].

1.3 Flow on a Horizontal Cylinder

The flow of a thin film of fluid on a cylindrical substrate is of great importance in a number of industrial contexts, for example, in the chemical process, food and paper industries. Heat exchangers, such as falling-film condensers and evaporators, are often made up of a series of cylinders where either a vapour condenses on the cooled cylinders forming a thin film of fluid or thin films of fluid on heated cylinders evaporate. Coating processes often involve the application of a thin film of fluid to one or more rotating cylindrical rollers, as is the case with the Fourdrinier machine in the paper industry, or in the coating of the inside of fluorescent tubes. As a result of the many applications there has been much interest in the problems considered in this section, namely the two-dimensional steady flow of a thin film of fluid of prescribed flux over a stationary horizontal cylinder (hereafter referred to as "curtain flow") and the two-dimensional steady flow of a thin film of fluid of prescribed load (that is, the prescribed mass of fluid per unit axial length on

the cylinder) on either the outside (hereafter referred to as "coating flow") or the inside (hereafter referred to as "rimming flow") of a uniformly rotating horizontal cylinder. The early work for curtain flow was done by Nusselt [5, 6], who studied the steady condensation of a quiescent surrounding vapour (steam) into a thin film of fluid (water) on a stationary horizontal cylinder, and in doing so obtained the solution for the fluid velocity of the leading-order lubrication theory. The pioneering study of the leading-order lubrication theory for coating and rimming flow was performed by Moffatt [7] who found that steady continuous, finite and non-zero solutions to his model (hereafter referred to as "full-film" solutions) are possible only below a critical load. In the following subsection we summarise the key ideas in these classical studies of two-dimensional thin-film flow on horizontal cylinders.

1.3.1 Leading-order lubrication theory

We will explore curtain, coating and rimming flow by modelling them using leading-order lubrication theory. Consider the steady two-dimensional flow of a thin film of a Newtonian fluid with constant density ρ and viscosity μ on a circular cylinder of radius a with its axis horizontal, the cylinder being either stationary or rotating in a counter-clockwise direction about its horizontal axis at uniform angular speed Ω (so that the circumferential speed is $a\Omega$). Referred to polar coordinates $r = a \pm y$ (with origin at the cylinder's axis) and θ (measured counter-clockwise from the horizontal), as shown in figure 1.3, we take the free surface of the fluid to be at $r = a + h$ for curtain flow or coating flow and $r = a - h$ for rimming flow, the film thickness being denoted by $h = h(\theta)$. For curtain flow the azimuthal volume flux of fluid per unit axial length crossing a station $\theta =$ constant, denoted Q, takes the prescribed constant values $Q = Q_{\mathrm{L}}$ (> 0) and $Q = Q_{\mathrm{R}}$ (< 0) on the left-hand side and right-hand side of the cylinder, respectively, and the supply flux Q_{S} satisfies $Q_{\mathrm{S}} = Q_{\mathrm{L}} - Q_{\mathrm{R}}$, whereas in coating and rimming flow the flux Q is constant (since the flow is steady) but is unknown a priori, and is determined

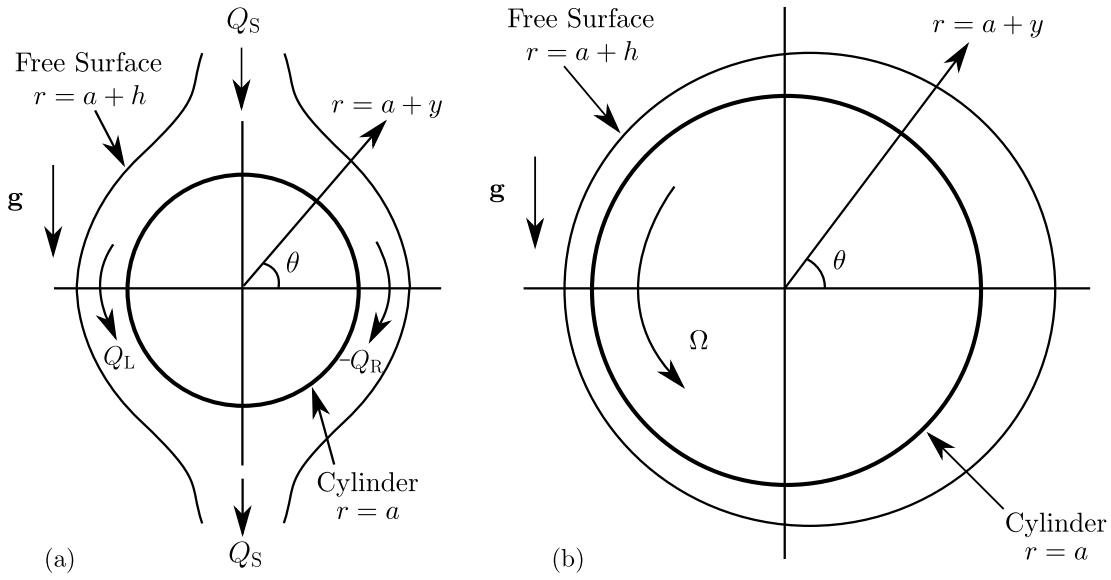

Figure 1.3: Geometry of steady two-dimensional flow of a thin film of Newtonian fluid on a horizontal cylinder, where (a) the volume flux of fluid is prescribed and the cylinder is stationary, and (b) the fluid load is prescribed and the cylinder is rotating.

through the condition of prescribed load. The fluid velocity $\mathbf{u} = u\mathbf{e}_\theta + v\mathbf{e}_r$ (where $\mathbf{e}_\theta$ and $\mathbf{e}_r$ denote unit vectors in the azimuthal and radial directions, respectively) and pressure p are governed by the mass-conservation and Navier–Stokes equations. Surface-tension and inertia effects are neglected. On the cylinder $r = a$ the velocity $\mathbf{u}$ satisfies no-slip and no-penetration conditions and on the free surface $r = a \pm h$ the normal and tangential stress balances and the kinematic condition apply. We consider only thin films with small aspect ratio $\epsilon = (\mu U_0/a^2\rho g)^{1/2} \ll 1$ where U_0 is the characteristic velocity defined by $U_0 = (\rho g Q_S^2/\mu)^{1/3}$ for curtain flow and $U_0 = a\Omega$ for coating and rimming flow. We non-dimensionalise and scale the system appropriately by writing

$$\left.\begin{aligned} r = a(1 \pm \epsilon y^*), \quad h = \epsilon a h^*, \quad u = U_0 u^*, \quad v = \pm\epsilon U_0 v^*, \\ p = p_a \pm \epsilon a\rho g p^*, \quad Q = \epsilon a U_0 Q^*, \quad M = \epsilon a^2 \rho M^*, \end{aligned}\right\} \tag{1.18}$$

in which the + in the ± corresponds to curtain or coating flow while the − corresponds to rimming flow, p_a is the constant pressure in the surrounding atmosphere, and $M\,(>0)$ is the constant fluid load on the cylinder. For clarity the star superscripts on non-dimensional variables will be omitted henceforth.

At leading order in ϵ the governing equations become

$$\frac{\partial u}{\partial \theta}+\frac{\partial v}{\partial y}=0, \quad \frac{\partial^2 u}{\partial y^2}=\cos\theta, \quad \frac{\partial p}{\partial y}=-\sin\theta, \tag{1.19}$$

together with the boundary conditions

$$u=U \quad \text{and} \quad v=0 \quad \text{on} \quad y=0 \tag{1.20}$$

and

$$\frac{\partial u}{\partial y}=0 \quad \text{and} \quad p=0 \quad \text{on} \quad y=h, \tag{1.21}$$

where $U=0$ for a stationary cylinder (which we use in curtain flow) and $U=1$ for a rotating cylinder (which we use in coating and rimming flow). Solving (1.19) subject to (1.20) and (1.21) for the azimuthal velocity $u=u(y,\theta)$ and pressure $p=p(y,\theta)$ yields

$$u=U-\frac{\cos\theta}{2}(2h-y)y \tag{1.22}$$

and

$$p=(h-y)\sin\theta. \tag{1.23}$$

Hence the volume flux Q is given by

$$Q=\int_0^h u\,\mathrm{d}y=Uh-\frac{h^3\cos\theta}{3}. \tag{1.24}$$

(a) Curtain flow

In the case of curtain flow on a stationary cylinder we have $U=0$ and the solution for h in terms of the constant prescribed flux Q is given from (1.24) by

$$h=\left(-\frac{3Q}{\cos\theta}\right)^{1/3}, \tag{1.25}$$

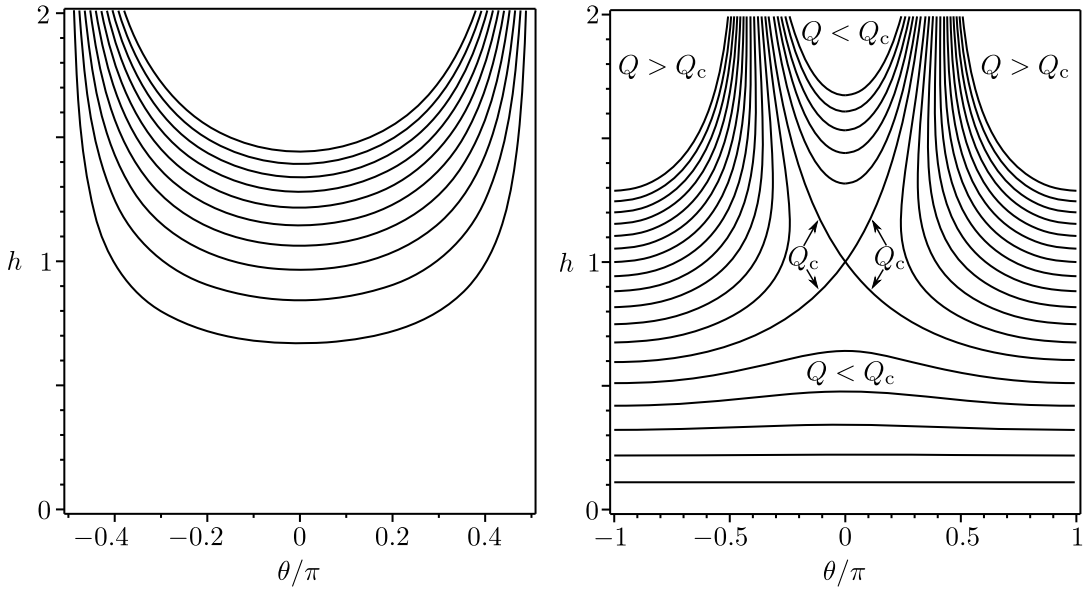

Figure 1.4: Contours of the expression for the flux Q given by (1.24) in the θ/π–h plane when (a) $U = 0$ (the cylinder is stationary) with the contours drawn for flow on the right-hand-side of the cylinder ($-\pi/2 < \theta < \pi/2$) with $Q = -1/10$, $-1/5$, $-3/10$, …, -1, and (b) $U = 1$ (the cylinder is rotating) with the contours drawn for $Q = 1/9, 2/9, 1/3, \ldots, 2$ where $Q_{\rm c} = 2/3$ is the critical flux above which full-film solutions do not exist.

while the velocity u and pressure p are given by equations (1.22) and (1.23), respectively, with $U = 0$, and the load M is given by

$$M = \int_{-\pi}^{-\pi/2} h\,\mathrm{d}\theta + \int_{\pi/2}^{\pi} h\,\mathrm{d}\theta = CQ^{1/3} \quad \text{or} \quad M = \int_{-\pi/2}^{\pi/2} h\,\mathrm{d}\theta = -CQ^{1/3}, \quad (1.26)$$

where

$$C = \frac{2^{5/3}\pi^2}{3^{2/3}\Gamma\left(\frac{2}{3}\right)^3} \simeq 6.06689, \quad (1.27)$$

depending on whether we are considering flow on the left-hand-side (where $Q = Q_{\rm L} > 0$) or the right-hand-side (where $Q = Q_{\rm R} < 0$) of the cylinder, respectively. Figure 1.4(a) shows the solution for h given by (1.25) plotted as a function of θ/π for different values of the flux Q (or, equivalently, contours of the expression for the flux Q given by (1.24)). In particular, figure 1.4(a) and equation (1.25) show

that h increases monotonically with $|\theta|$ away from its minimum value of $(3|Q|)^{1/3}$ at $\theta = 0$, becoming unbounded at the top and the bottom of the cylinder according to

$$h = \left(\frac{3Q}{|\theta| - \pi/2}\right)^{1/3} + O\left(|\theta| - \frac{\pi}{2}\right)^{5/3} \quad \text{as} \quad \theta \to \pm\frac{\pi}{2}, \tag{1.28}$$

where, of course, the lubrication theory fails, by which we mean that since both $h \to \infty$ and $|\mathrm{d}h/\mathrm{d}\theta| \to \infty$ as $|\theta| \to \pi/2$, higher order terms that were previously ignored may become relevant. In particular, the pressure and the velocity, together with their corresponding θ gradients, will also tend to infinity as $|\theta| \to \pi/2$ and the assumption that $\epsilon \ll 1$ may not be enough to "kill off" these terms. However, this may not be especially important since the flow near the top and bottom could be affected by other factors away from the cylinder (in particular, near the top where the manner in which the fluid is supplied would certainly be important) in which case the solution here acts as an outer solution describing the flow away from the top and the bottom.

(b) Coating and rimming flow

In the case of coating or rimming flow we have $U = 1$ without loss of generality, and so h is given from (1.24) in terms of the constant flux Q by the solution to a cubic polynomial equation. Figure 1.4(b) shows contours of the expression for the flux Q given by (1.24) in the θ/π–h plane for several values of Q, and highlights the existence of a critical flux, denoted $Q = Q_\mathrm{c} = 2/3$ above which full-film solutions (i.e. continuous, finite and non-zero solutions) do not exist. The root of the flux equation (1.24) that gives rise to full-film solutions is given by

$$h = \begin{cases} \dfrac{2}{(\cos\theta)^{1/2}} \cos\left[\dfrac{2\pi}{3} - \dfrac{1}{3}\cos^{-1}\left(-\dfrac{3}{2}Q[\cos\theta]^{1/2}\right)\right] & \text{if} \quad |\theta| < \pi/2, \\ Q & \text{if} \quad |\theta| = \pi/2, \\ \dfrac{2}{(-\cos\theta)^{1/2}} \sinh\left[\dfrac{1}{3}\sinh^{-1}\left(\dfrac{3}{2}Q[-\cos\theta]^{1/2}\right)\right] & \text{if} \quad \pi/2 < |\theta| \leq \pi, \end{cases} \tag{1.29}$$

where $0 < Q \leq 2/3$, while the load M is given by

$$M = \int_{-\pi}^{\pi} h \, \mathrm{d}\theta, \tag{1.30}$$

and the critical load, denoted M_c, is given by $M_\mathrm{c} \simeq 4.44272$[1]. With the load M prescribed, the flux Q is obtained from equations (1.24) and (1.30), and the film thickness h is given by (1.29), while the velocity u and pressure p are given by (1.22) and (1.23), respectively, with $U = 1$. The film thickness h is a monotonic increasing function of the load M and flux Q and is a monotonic decreasing function of $|\theta|$, achieving its maximum value at $\theta = 0$ where in the critical case (i.e. when $Q = Q_\mathrm{c} = 2/3$) there is, as can be seen in figure 1.4(b), a corner in the solution given by $h = 1 - |\theta|/\sqrt{6} + O(\theta^2)$ as $\theta \to 0$.[1]

1.3.2 Review of previous literature

(a) Flows on stationary horizontal cylinders

As we have already mentioned, the pioneering work on curtain flow was done by Nusselt [5, 6], who studied the steady condensation of a quiescent surrounding vapour (steam) into a thin film of fluid (water) on a stationary horizontal cylinder. Extensions of this basic problem have been considered by many subsequent authors, including, for example, Sparrow and Gregg [8], Nicol et al. [9] and Shu and Wilks [10], who included fluid inertia and thermal advection in the film, Shekriladze and Gomelauri [11], Fujii et al. [12], Rose [13] and Chen and Lin [14], who considered the influence of flow of the vapour, Sarma et al. [15] and Yang and Lin [16], who considered turbulent flow in the film, and Conlisk and Mao [17] who investigated the unsteady flow of a thin film of both one-component and two-component fluids. Condensation onto an elliptical (rather than a circular) cylinder has been studied by, for example, Yang and Hsu [18] who considered laminar flow and included the effects of flow in vapour, Lin and Yang [19] who extended the

[1] Note that Moffatt [7] gave slightly inaccurate values for M_c and the solution at the corner, corresponding to $M_\mathrm{c} = 4.428$ and $h \sim 1 - 0.577|\theta|$ in the present notation.

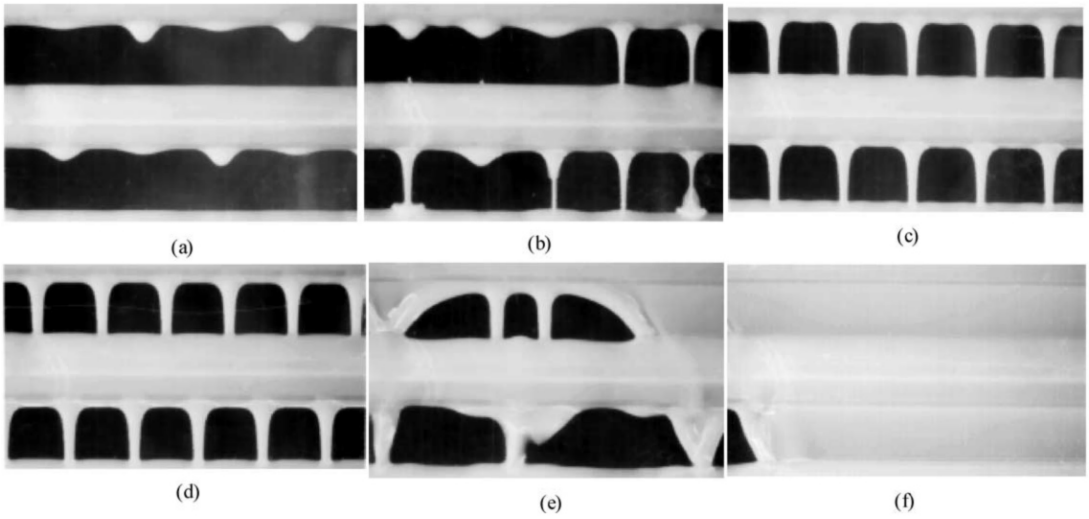

Figure 1.5: Images of the flow types of falling films between cylindrical tubes found by Hu and Jacobi [21]. These are (a) droplet, (b) droplet-jet, (c) in-line jet, (d) staggered jet, (e) jet-sheet, and (f) sheet. Reprinted from Hu and Jacobi [21] with permission, copyright 1996, ASME (American Society of Mechanical Engineers).

work of Sarma et al. [15] and Yang and Hsu [18] to consider turbulent flow in the film, and Li and Yang [20] who considered laminar flow and showed that as the ellipticity increases so does the entropy generation while the film thickness decreases.

The flow of a film over multiple horizontal cylindrical tubes that are vertically aligned, with applications in evaporators and absorbers used in refrigeration, has been well studied. Hu and Jacobi [21] conducted an experimental study of falling films between cylindrical tubes and suggested the following categorisations for the different flow types: droplet, droplet-jet, in-line jet, staggered jet, jet-sheet and sheet. Images of these flow types are shown in figure 1.5. Killion and Garimella [22] conducted an experimental study of falling films focusing on flows where drops fall between the cylindrical tubes, while Killion and Garimella [23] obtained numerical solutions to the Navier–Stokes equation that accurately modelled the observed drop formations. Figure 1.6 shows a comparison between the numerical solution

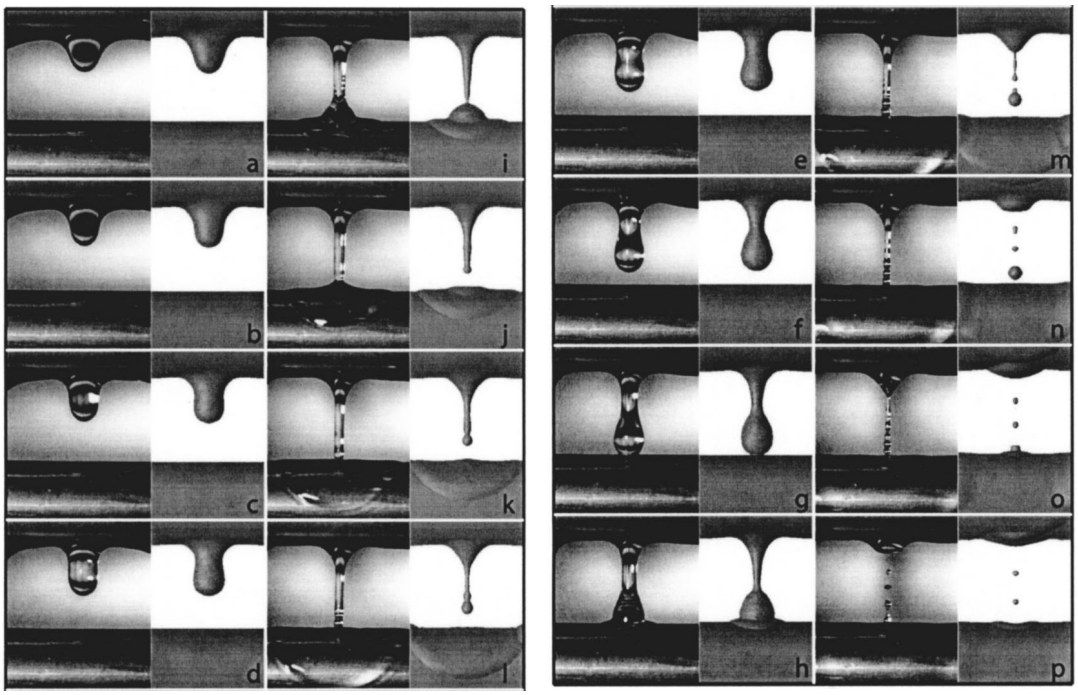

Figure 1.6: Comparison between the experimental (left-hand-side of each image a–p) and numerical (right-hand-side of each image a–p) results of Killion and Garimella [23] showing drops falling between stationary cylinders at different times. Reprinted from Killion and Garimella [23] with permission, copyright 2004, ASME (American Society of Mechanical Engineers).

and images of the experimental study. Sultana et al. [24] considered situations where a uniform film, drops or jets fall between the cylindrical tubes and included the effect of the flow of a coolant in the cylindrical tube, while Ruan et al. [25] considered the effect of flow in the surrounding vapour on the transitions between uniform films, drops and jets between the cylindrical tubes. Ribatskia and Jacobib [26] presented an extensive review of the literature on falling film evaporation on horizontal cylindrical tubes, while, Li et al. [27] and Yang and Wang [28] conducted experimental studies of falling film evaporation on horizontal cylindrical tubes with non-uniform surfaces, with Yang and Wang [28] also including numerical simulations; both Li et al. [27] and Yang and Wang [28] showed that the non-

uniform cylinder surfaces lead to increased heat transfer rates.

There have also been a number of studies on both two-dimensional and three-dimensional thin-film flow on both the inside and the outside of a horizontal cylinder that do not involve either evaporation or absorption. Reisfeld and Bankoff [29] undertook an investigation of unsteady flow on a heated or cooled cylinder incorporating the effects of gravity, surface tension, thermocapillarity (i.e. variation of surface tension with temperature) and van der Waals forces, while Lin et al. [30] investigated the three-dimensional evolution and rupture of a film due to van der Waals forces. King et al. [31] studied the three-dimensional evolution of a film on both a horizontal and an inclined cylinder. Band et al. [32] considered two-dimensional flow driven by prescribed azimuthal variations in surface tension. Haimovich and Oron [33] investigated the effect of axial oscillations of the cylinder on the evolution and rupture of an axisymmetric film, while Haimovich and Oron [34] extended the work of Haimovich and Oron [33] to the case of a non-isothermal fluid where thermocapillary effects are significant.

(b) Flows on rotating horizontal cylinders

Coating and rimming flows have been studied extensively, with most of the theoretical work building on the pioneering papers by Pukhnachev [35][2], Moffatt [7] and Johnson [36]. Pukhnachev [35] discussed the existence and uniqueness of solutions for coating flow of the steady two-dimensional Navier–Stokes equation and then used lubrication theory to derive an evolution equation that includes the effects of gravity, viscosity and surface tension, while, as we have already discussed, Moffatt [7] considered coating flow both theoretically using a model based on lubrication theory and experimentally and, in particular, found that steady solutions covering the entire cylinder are possible only below a critical load. Though their attention is focused on coating flow at leading order, the theoretical results of both

[2]This author's name has been transliterated into English as both "Pukhnachev" and "Pukhnachov".

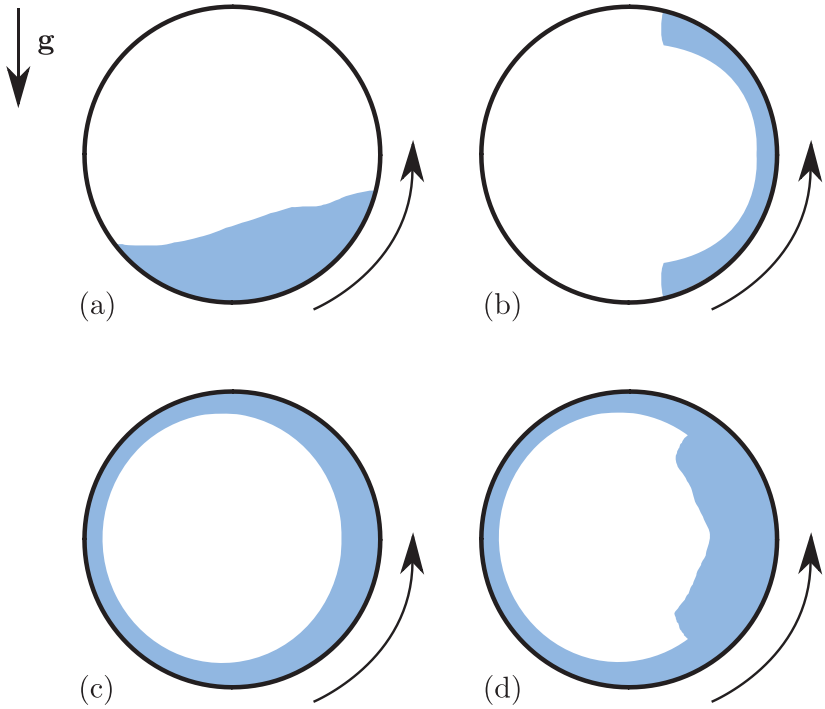

Figure 1.7: The four possible types of steady rimming flow found by Johnson [36].

Pukhnachev [35] and Moffatt [7] also apply to rimming flow. Steady rimming flow was considered by Johnson [36] who found four different types of free surface profile, two in which the fluid fully coats the cylinder, one in which the fluid pools at the bottom of the cylinder, and one in which the fluid coats part of only one side of the cylinder. A diagram depicting the four types of profile is shown in figure 1.7. The profile that coats only one side of the cylinder and one of the profiles that fully coats the cylinder ((b) and (d) in figure 1.7) involve shock-like jumps in the film thickness (often called "shock solutions") and have loads greater than the critical load found by Moffatt [7].

Subsequently, there have been a large number of studies of both coating and rimming flow, many (but not all) focusing on the two-dimensional problem. Solutions to the Stokes equations where there is no restriction on the thickness of the film have been considered by Hansen and Kelmanson [37] who obtained steady nu-

merical solutions for coating flow using integral-equation method, Peterson et al. [38] who obtained unsteady numerical solutions for coating flow using a finite-element method and found that steady-state solutions are more readily attained for near-critical loads than for significantly sub-critical loads, Wilson et al. [39] who obtained steady numerical solutions for both coating and rimming flow in the critical state and developed higher-order asymptotic solutions in the limit of a thin film, and concluded that the critical load always slightly exceeds Moffatt's value, and later by Hunt [40] who obtained unsteady numerical solutions for flow on an elliptical (rather than a circular) cylinder. The work of Moffatt [7] was extended by Duffy and Wilson [41] to include "curtain" solutions, that is, solutions that are unbounded at the top and bottom of the cylinder, representing fluid falling onto and off the cylinder at these locations. Tirumkudulu and Acrivos [42] extended leading-order lubrication theory in the case of rimming flow by adding a higher-order term arising from the hydrostatic pressure, and found good agreement with their own experimental measurements and numerical solutions of the Stokes equations; later Acrivos and Jin [43] investigated the stability of these solutions. Tougher et al. [44] analysed the approach to the leading order critical solution obtained by Moffatt [7] for both rimming and coating flow. The evolution equation derived by Pukhnachev [35] has formed the basis for many subsequent studies of coating flow, including that of Hinch and Kelmanson [45] who analysed and numerically solved the equation and found that perturbations to the solutions decay slowly to the steady state and exhibit a phase lag, Karabut [46] who obtained solutions to the equation representing a hanging drop, and Kelmanson [47] who extended the work of Pukhnachev [35] by including inertial effects. Rimming flows involving shocks of the type described by Johnson [36] have been studied further by Wilson and Williams [48] who derived and numerically solved an evolution equation (including the smoothing effect of surface tension) that determines the height and location of the shock, O'Brien and Gath [49] who used the approach of Johnson [36] to determine the height and location of the shock

without considering surface-tension effects, O'Brien [50] who extended the leading order lubrication theory to include higher-order terms arising from the hydrostatic pressure and surface tension and investigated the stability of both smooth and shock solutions, and Benilov et al. [51] who obtained numerical solutions to the Stokes equations that include a smoothed shock and showed that steady solutions do not exist if the shock is too close to the bottom of the cylinder. Ashmore et al. [52] considered steady rimming flow including the smoothing effect of surface tension and considered a situation in which gravitational forces are large compared to viscous forces, causing a pool of fluid to form at the bottom of the cylinder, while Benilov et al. [53] investigated this pooling behaviour and derived a matched asymptotic solution describing the pool, and Noakes et al. [54] included the effect of mass transfer and obtained shock solutions that exhibit the pooling behaviour. Various aspects of the stability of rimming flow were examined by Benilov et al. [55], Benilov et al. [56] and Benilov and O'Brien [57], the latter of whom considered the effect of inertia and found that, although it always causes instability, its effect may be counteracted by increasing the viscosity so as to make the time of growth so large that the solution is effectively stable, while Villegas-Díaz et al. [58] included a uniform surface shear stress together with the effects of surface tension and higher-order gravity. Rimming flow of non-Newtonian fluids has been considered by, amongst others, Rajagopalan et al. [59] who studied the flow of a viscoelastic fluid and obtained numerical solutions using a finite-element method, and found that steady solutions exist only below a certain rotation speed, Fomin et al. [60] who studied the flow of a shear-thinning generalised Newtonian fluid and found that the critical load is smaller than in the case of a Newtonian fluid, and Fomin et al. [61] who studied the flow of a power-law fluid and obtained analytical solutions in the particular case when the power-law index is equal to 1/2.

Studies of three-dimensional coating and rimming flow have also been undertaken. Moffatt [7] conducted experiments on coating flow and found that the steady two-dimensional solution can be realised at sufficiently low rotation speeds,

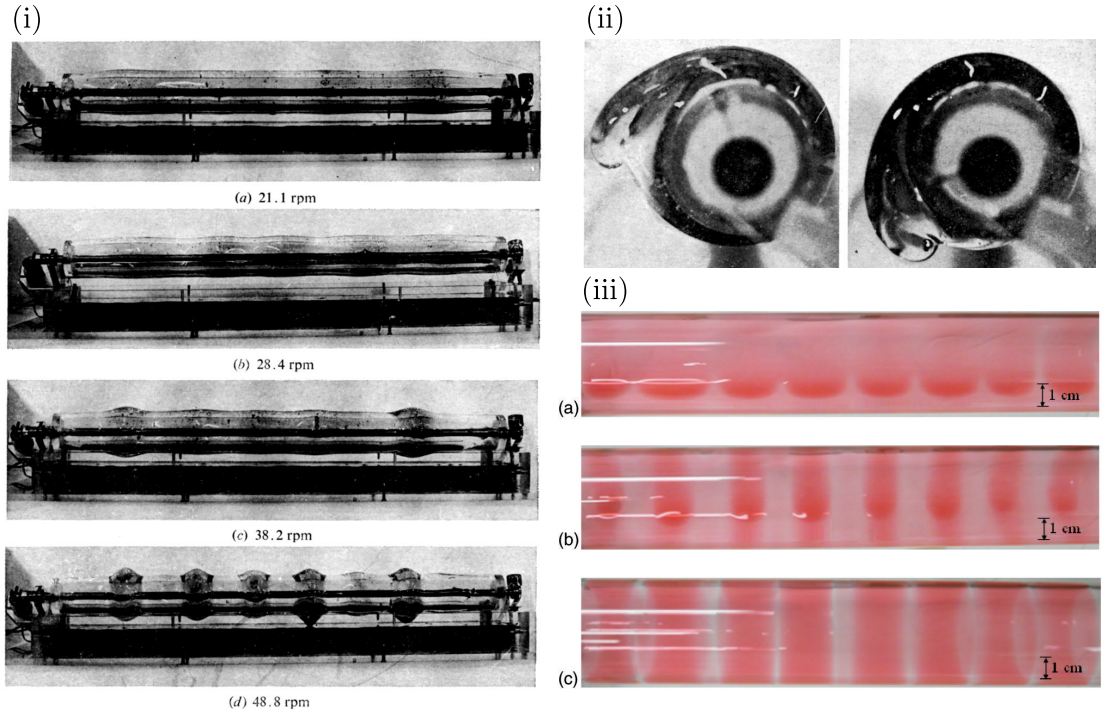

Figure 1.8: (i) Images of coating flow from the experimental work of Moffatt [7] showing the development from a uniform film at low rotation speeds to the ring formations at higher speeds. The higher rotation speed in (i)(d) causes lobes to develop; these can be seen side on in (ii). (iii) Images of rimming flow from the experimental work of Chen et al. [62] showing the ring formations. (i) and (ii) reprinted with the kind permission of Prof. Keith Moffatt. (iii) Reprinted from Chen et al. [62] with permission, copyright 2007, American Institute of Physics.

but that the flow becomes unstable and "rings" of fluid are formed at higher rotation speeds, and that at even higher rotations speeds depth discontinuities develop and "lobes" start to form. The rings and lobes can be seen in figures 1.8(i) and 1.8(ii) which shows images from the experimental work of Moffatt [7]. Thoroddsen and Mahadevan [63] carried out an experimental study of rimming flow and observed many different phenomena, including a shark's-teeth-like pattern in the axial direction, while Hosoi and Mahadevan [64] derived an evolution equation including the effect of weak surface tension and weak inertia and ob-

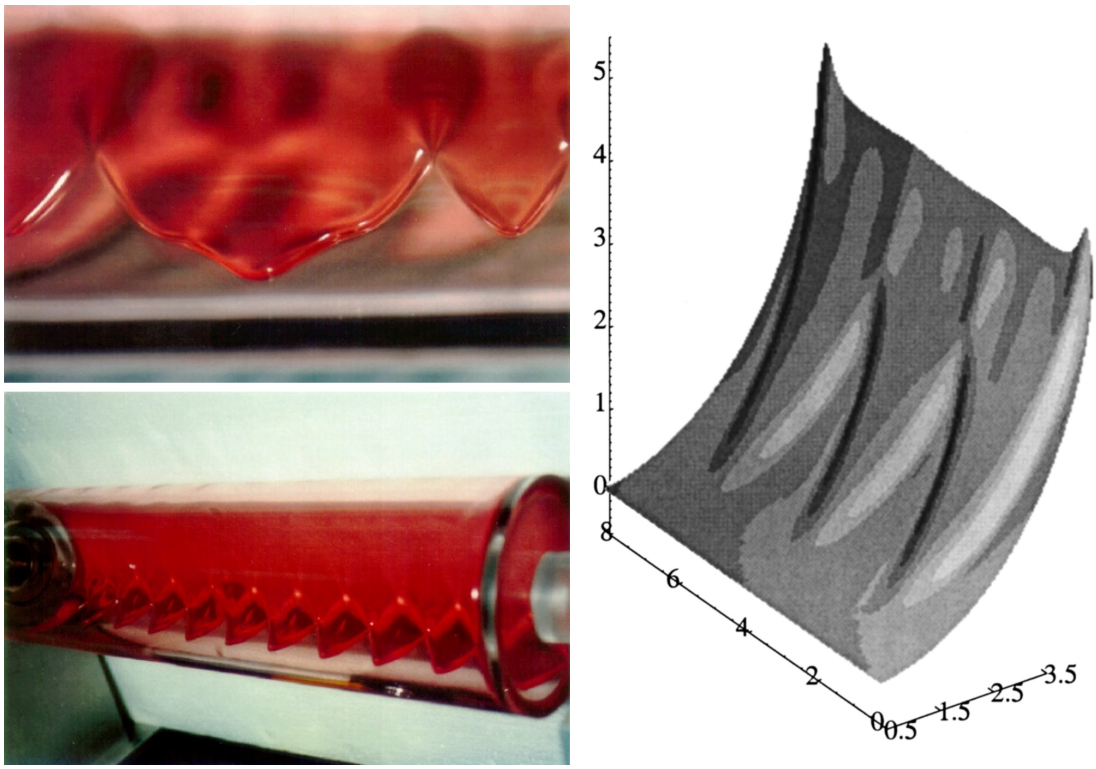

(a) (b)

Figure 1.9: The shark's-teeth-like pattern observed in rimming flow: (a) shows images from the experimental work of Thoroddsen and Mahadevan [63] while (b) shows the numerical solution of Hosoi and Mahadevan [64]. (a) Reprinted from Thoroddsen and Mahadevan [63] with permission, copyright 1997, Springer. (b) Reprinted from Hosoi and Mahadevan [64] with permission, copyright 1999, American Institute of Physics.

tained solutions showing the shark's-teeth pattern. The shark's-teeth-like pattern can be seen in figure 1.9(a) which shows images from the experimental work of Thoroddsen and Mahadevan [63] while figure 1.9(b) shows the numerical solution of Hosoi and Mahadevan [64]. Jin and Acrivos [65] extended the approach used by Tirumkudulu and Acrivos [42] to three dimensions for rimming flows with axially-varying viscosity. Evans et al. [66] derived a three-dimensional evolution equation for coating flow which includes the effects of rotation, gravity and surface

tension, and obtained two-dimensional numerical solutions for the case when axial flow is neglected; later Evans et al. [67] extended the work of Evans et al. [66] to obtain three-dimensional numerical solutions, and reported experimental results that confirm the general features of the numerical results. Noakes et al. [68] investigated the stability of three-dimensional coating flow in the absence of gravity, and Noakes et al. [69] used a multiple-time-scales approach to derive evolution equations describing rimming and coating flows in which inertial effects (including centrifugal effects) are significant, along with the effects of viscous, gravitational and surface-tension forces, while Pougatch and Frigaard [70] obtained numerical solutions to a three-dimensional evolution equation for rimming flow that retains first order terms and includes the effect of inertia. Chen et al. [62] carried out an experimental investigation into the conditions in which a uniform film occurs for rimming flow with a low volume fraction and found that the rotation speed must be sufficiently high for this to be possible. Figure 1.8(iii) shows the formation of rings in rimming flow in the experiment by Chen et al. [62]. Chicharro et al. [71] performed similar experiments to Chen et al. [62] and found six different possible patterns when the rotation speed is low, but that a uniform film occurs if the rotation speed is sufficiently high.

1.4 Rivulet Flow Down an Inclined Substrate

Flows involving rivulets of fluid on inclined substrates occur in a large number industrial situations including, for example, heat exchangers, distillation processes, desalination processes and trickle-bed reactors. They can also occur in everyday situations such as rainwater on a car windscreen and water flowing down the wall of a shower. Flows of thin films of fluid often breakup to form dry patches together with rivulets or drops, while the rivulets that may be formed can themselves give rise to many interesting features including spreading, meandering and break-up into droplets. Figure 1.10 shows examples of rivulet flows; specifically, the

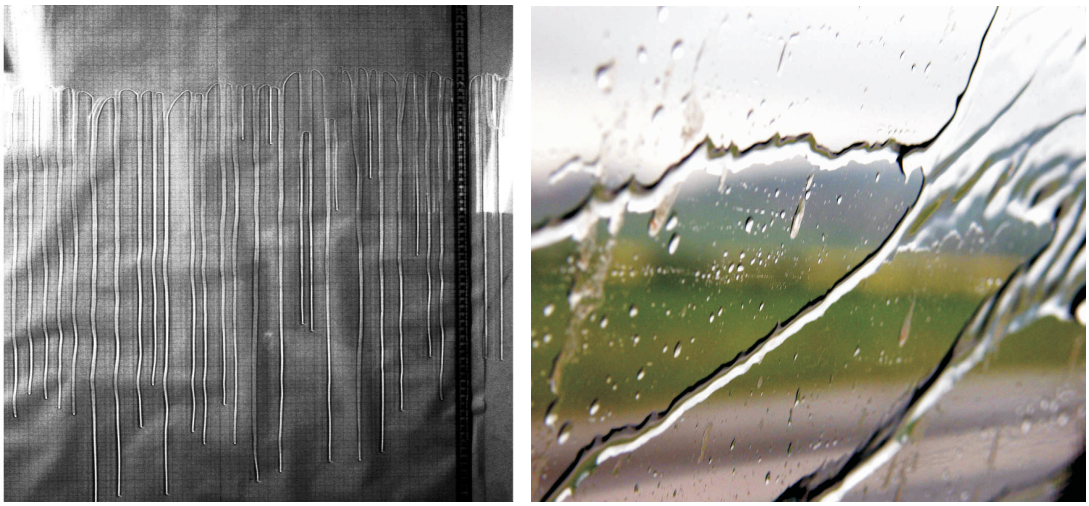

(a) (b)

Figure 1.10: (a) Image showing the break up of film of fluid into rivulets from the experiment by Hocking et al. [72]; reprinted with permission, copyright 1999, American Institute of Physics. (b) Image showing rivulets on a car windscreen; picture courtesy of Prof. S. K. Wilson.

break-up of a film into rivulets and rivulets on a car windscreen are shown. As a result of the many interesting features of rivulet flows there has been much interest in the problem of rivulet flow down an inclined substrate. The pioneering work on this problem was performed by Towell and Rothfeld [73] who studied the steady unidirectional flow of a uniform rivulet (i.e. a rivulet with constant width and cross-sectional profile) of Newtonian fluid down an inclined plane and obtained numerical solutions for the rivulet profile that are in good agreement with their own experimental results, while also obtaining asymptotic solutions in the limits of thin and wide rivulets and of thin and narrow rivulets. Allen and Biggin [74] used the lubrication approximation to investigate the limit of a thin rivulet and found good agreement between their first-order-accurate asymptotic solution and the numerical solution obtained using a finite element method, while Bentwich et al. [75] obtained an analytical solution for the flow of a rivulet down a

vertical plane, and also derived an approximate solution to describe the flow down an inclined plane. Duffy and Moffatt [76] followed the approach of Allen and Biggin [74] to obtain the leading order asymptotic solution in the limit of a thin rivulet on an inclined plane and interpreted their results as describing the locally unidirectional flow of a rivulet down a slowly varying substrate, and, in particular, as describing the flow in the azimuthal direction round a large horizontal cylinder. In the following subsection we reproduce the work of Duffy and Moffatt [76] to study the case of a locally unidirectional rivulet flowing down a slowly varying substrate.

1.4.1 Locally unidirectional rivulet flow down a slowly varying substrate

Consider the steady three-dimensional gravity-driven flow of a thin symmetric rivulet of Newtonian fluid with uniform density ρ and viscosity μ down a substrate inclined at an angle α ($0 \leq \alpha \leq \pi$) to the horizontal. We choose Cartesian axes $Oxyz$ as shown in figure 1.11, with the x axis in the direction of flow, the y axis horizontal and transverse to the direction of flow and the z axis normal to the substrate, and take the free surface to be at $z = h$, where $h = h(x, y)$ is the rivulet thickness, and take the contact lines of the rivulet (where $h = 0$) to be at $y = \pm a$, where $a = a(x)$ is the semi-width of the rivulet. The velocity $\mathbf{u} = u\mathbf{e}_x + v\mathbf{e}_y + w\mathbf{e}_z$ (where $\mathbf{e}_x$, $\mathbf{e}_y$ and $\mathbf{e}_z$ denote unit vectors in the x, y and z directions, respectively) and pressure p are governed by the usual mass-conservation and Navier–Stokes equations. On the substrate $z = 0$ the velocity $\mathbf{u}$ satisfies no-slip and no-penetration conditions, while on the free surface $z = h$ the normal and tangential stress balances apply. We consider only thin, slowly varying rivulets whose transverse aspect ratio is denoted $\delta \ll 1$, and whose longitudinal aspect ratio is denoted ϵ and is defined in terms of the capillary length $l_c = (\gamma/\rho g)^{1/2}$ to be $\epsilon = l_c/l$, where l is a typical length scale in the x direction, γ is the coefficient

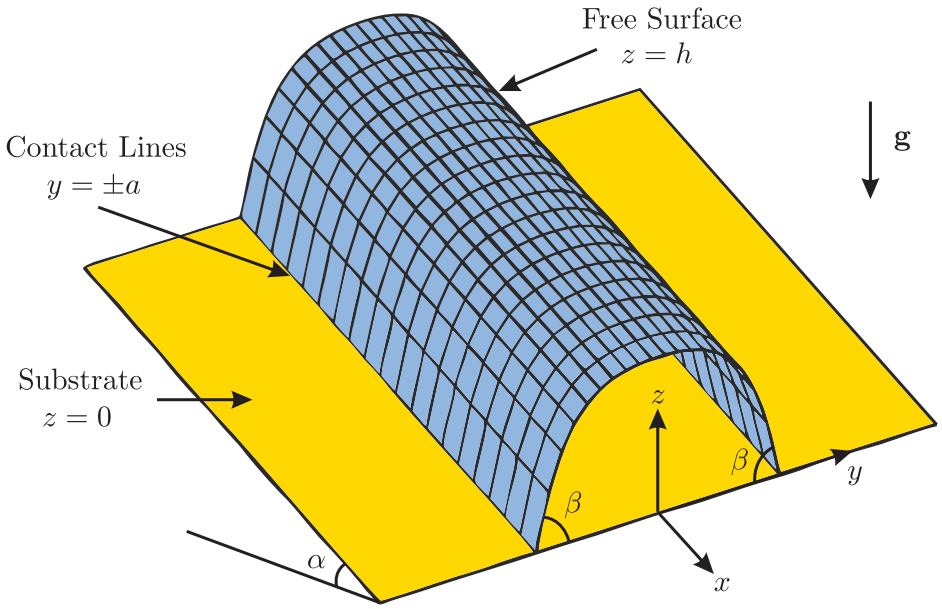

Figure 1.11: Geometry of steady three-dimensional flow of a thin uniform rivulet of Newtonian fluid on an inclined plane.

of surface tension (assumed constant), and g is the magnitude of gravitational acceleration. In particular, we consider the case where the rivulet is sufficiently slowly varying that $\epsilon \ll \delta \ll 1$; this is a sensible case to consider since it is easily realised by making the substrate (and therefore the length scale l) sufficiently long. One could also consider, for example, $\epsilon = O(\delta)$ or $\epsilon \ll \delta \ll 1$ instead. However $\epsilon = O(\delta)$ is somewhat restrictive (though entirely possilbe) while $\epsilon \ll \delta \ll 1$ would likey result in a rivulet so thin that surface tension would cause it to breakup with dry patches and drops forming. Hence we non-dimensionalise and scale the system appropriately by writing

$$\left.\begin{gathered} x = lx^*, \quad y = \epsilon l y^*, \quad z = \epsilon\delta l z^*, \quad a = \epsilon l a^*, \quad h = \epsilon\delta l h^*, \quad \beta = \delta\beta^*, \\ u = \frac{\epsilon^2\delta^2 l^2\rho g}{\mu}u^*, \quad v = \frac{\epsilon^3\delta^2 l^2\rho g}{\mu}v^*, \quad w = \frac{\epsilon^3\delta^3 l^2\rho g}{\mu}w^*, \\ p = p_\mathrm{a} + \epsilon\delta l\rho g p^*, \quad Q = \frac{\epsilon^4\delta^4 l^4\rho g}{\mu}Q^*, \end{gathered}\right\} \tag{1.31}$$

in which $\beta \ll 1$ is the prescribed contact angle, p_{a} is the constant pressure in the surrounding atmosphere, and Q is the prescribed constant volume flux of fluid down the substrate. For clarity the star superscripts on the non-dimensional quantities will be omitted henceforth.

At leading order in ϵ and δ the governing equations become

$$\frac{\partial u}{\partial x}+\frac{\partial v}{\partial y}+\frac{\partial w}{\partial z}=0, \quad \frac{\partial^2 u}{\partial z^2}=-\sin\alpha, \quad \frac{\partial p}{\partial y}=0 \quad \text{and} \quad \frac{\partial p}{\partial z}=-\cos\alpha, \tag{1.32}$$

together with the boundary conditions

$$u=v=w=0 \quad \text{on} \quad z=0, \tag{1.33}$$

$$p=-\frac{\partial^2 h}{\partial y^2} \quad \text{and} \quad \frac{\partial u}{\partial z}=\frac{\partial v}{\partial z}=0 \quad \text{on} \quad z=h, \tag{1.34}$$

and

$$h=0 \quad \text{and} \quad \frac{\partial h}{\partial y}=\mp\beta \quad \text{on} \quad y=\pm a. \tag{1.35}$$

Integrating $(1.32)_4$ subject to (1.34) yields the pressure distribution

$$p=(h-z)\cos\alpha-\frac{\partial^2 h}{\partial y^2}, \tag{1.36}$$

from which $(1.32)_3$ gives a third-order differential equation for the rivulet thickness h, namely

$$\frac{\partial}{\partial y}\left(h\cos\alpha-\frac{\partial^2 h}{\partial y^2}\right)=0, \tag{1.37}$$

which together with (1.35) shows that the rivulet thickness does not depend on the longitudinal coordinate x, and so $h=h(y)$. Integrating $(1.32)_2$ twice subject to (1.33) and (1.34) yields the velocity distribution

$$u=\frac{\sin\alpha}{2}(2h-z)z, \tag{1.38}$$

and hence the constant volume flux Q is given by

$$Q=\int_{-a}^{a}\int_{0}^{h} u \,\mathrm{d}z \,\mathrm{d}y=\frac{\sin\alpha}{3}\int_{-a}^{a} h^3 \,\mathrm{d}y, \tag{1.39}$$

which in general provides an implicit solution for the semi-width a in terms of the prescribed constant flux Q and the angle of inclination α; equation (1.39) also shows that a does not depend on x and is therefore simply a constant depending only on the flux Q.

(a) Perfectly wetting rivulet

In the case of a perfectly wetting rivulet we take the contact angle to be zero (i.e. let $\beta = 0$) and reproduce the solution obtained by Duffy and Wilson [77]. It is found that there are no solutions to (1.37) and (1.39) for $0 \leq \alpha \leq \pi/2$ (i.e. no solution corresponding to a sessile rivulet or a rivulet on a vertical substrate), but that there is a solution when $\pi/2 < \alpha \leq \pi$ (i.e. a solution corresponding to a pendent rivulet), namely

$$a = \frac{\pi}{m} \quad \text{and} \quad h = \frac{h_{\mathrm{m}}}{2}\big(1 + \cos(my)\big), \tag{1.40}$$

where the maximum thickness of the rivulet $h_{\mathrm{m}} = h(0)$ is given by

$$h_{\mathrm{m}} = 2\left(\frac{3Qm}{5\pi \sin\alpha}\right)^{1/3}, \tag{1.41}$$

where for convenience we have defined $m = |\cos\alpha|^{1/2}$. The solutions (1.40) and (1.41) show that the semi-width a (but not the rivulet thickness h) of the rivulet is, rather surprisingly, independent of the value of the prescribed flux Q. Figure 1.12(a) shows the semi-width a and the maximum thickness h_{m} plotted as functions of α/π when $Q = 1$, and figure 1.12(b) shows the rivulet thickness h plotted as a function of y for different values of α when $Q = 1$. Figure 1.12 together with the solutions (1.40) and (1.41) show that the rivulet becomes wide and thin according to

$$a = \pi\left(\alpha - \frac{\pi}{2}\right)^{-1/2} + O\left[\left(\alpha - \frac{\pi}{2}\right)^{3/2}\right] \tag{1.42}$$

and

$$h_{\mathrm{m}} = 2\left(\frac{3Q}{5\pi}\right)^{1/3}\left(\alpha - \frac{\pi}{2}\right)^{1/6} + O\left[\left(\alpha - \frac{\pi}{2}\right)^{13/6}\right] \tag{1.43}$$

as $\alpha \to \pi/2^{+}$ (i.e. as the substrate tends towards being vertical), and becomes deep with finite width according to

$$a = \pi + \frac{\pi}{4}(\pi - \alpha)^2 + O\left[(\pi - \alpha)^4\right] \tag{1.44}$$

and

$$h_{\mathrm{m}} = 2\left(\frac{3Q}{5\pi(\pi - \alpha)}\right)^{1/3} + O\left[(\pi - \alpha)^{5/3}\right] \tag{1.45}$$

as $\alpha \to \pi^{-}$ (i.e. as the substrate tends towards being horizontal).

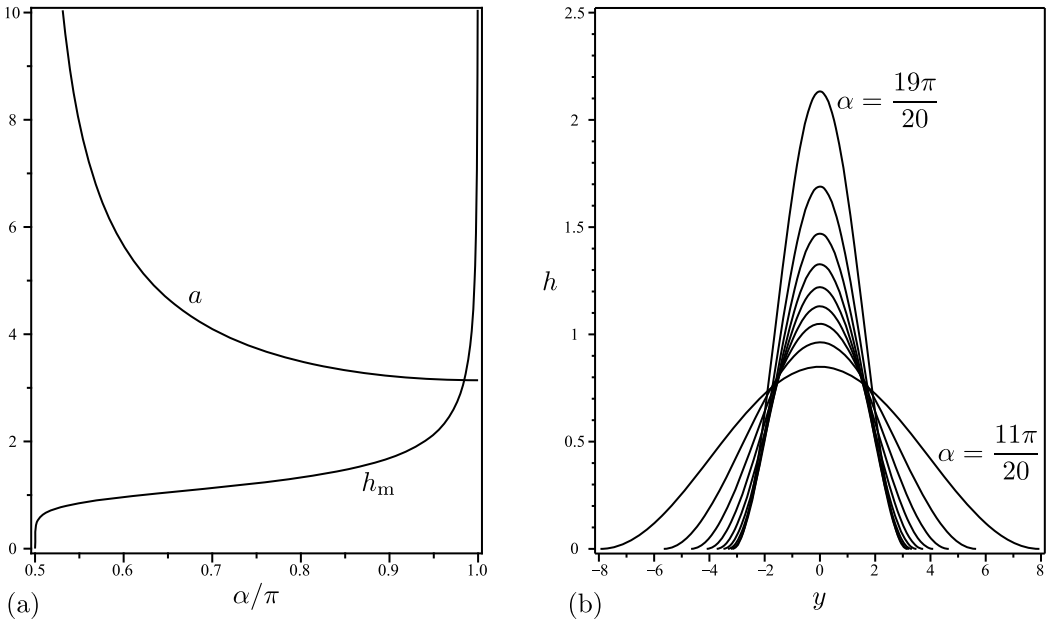

Figure 1.12: Perfectly wetting rivulet: (a) The semi-width a and the maximum thickness h_{m} plotted as functions of α/π when $Q = 1$. (b) The rivulet thickness h plotted as a function of y when $\alpha/\pi = 11/20$, $6/10$, $13/20$, $\ldots$, $19/20$ and $Q = 1$.

(b) Non-perfectly wetting rivulet

In the case of a non-perfectly wetting rivulet we take the contact angle to be $\beta = 1$, so that the transverse aspect ratio δ is equal to the original unscaled contact angle (which is, of course, small). As Duffy and Moffatt [76] showed, the solution to (1.37) for the rivulet thickness $h = h(y)$ is given by

$$h = \begin{cases} \dfrac{\cosh(ma) - \cosh(my)}{m\sinh(ma)} & \text{if } 0 \leq \alpha < \pi/2, \\ \dfrac{a^2 - y^2}{2a} & \text{if } \alpha = \pi/2, \\ \dfrac{\cos(my) - \cos(ma)}{m\sin(ma)} & \text{if } \pi/2 < \alpha \leq \pi, \end{cases} \tag{1.46}$$

and hence the flux Q is given from (1.39) as

$$Q = \frac{\sin\alpha}{9m^4} F(ma), \tag{1.47}$$

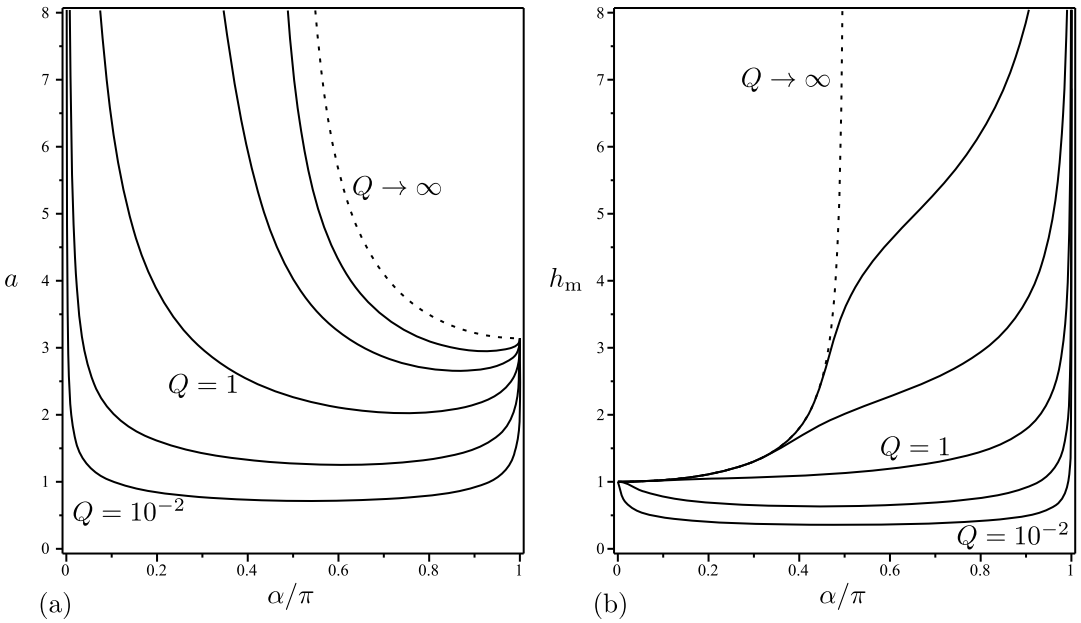

Figure 1.13: Non-perfectly wetting rivulet: (a) The semi-width a and (b) the maximum thickness $h_{\rm m}$ plotted as functions of α/π for $Q = 10^{-n}$ with $n = -2$, -1, 0, 1 and 2 together with the leading order result in the limit $Q \to \infty$ (dashed line).

where we have defined

$$F(ma) = \begin{cases} 15ma\coth^3(ma) - 15\coth^2(ma) \\ \qquad -9ma\coth(ma) + 4 \end{cases} \quad \text{if } 0 \le \alpha < \pi/2, \\ \begin{cases} -15ma\cot^3(ma) + 15\cot^2(ma) \\ \qquad -9ma\cot(ma) + 4 \end{cases} \quad \text{if } \pi/2 < \alpha \le \pi. \tag{1.48}$$

Appropriate interpretation of (1.47) as a limit is needed in the case $\alpha = \pi/2$, whereupon the flux equation becomes $Q = 4a^4/105$. For $0 \le \alpha < \pi/2$ there is a unique solution for a at each value of α, while for $\pi/2 < \alpha \le \pi$ there are infinitely many branches of solutions for a for each value of α; of these, however, only the lowest positive one, which connects smoothly with the solution in $0 \le \alpha < \pi/2$, is physically realisable. With a known from (1.47), the rivulet thickness is given by (1.46), which has a single maximum $h = h_{\rm m}$ at $y = 0$, where $h_{\rm m} = h(0)$. Figure 1.13 shows (a) the semi-width a and (b) the maximum thickness $h_{\rm m}$ plotted as

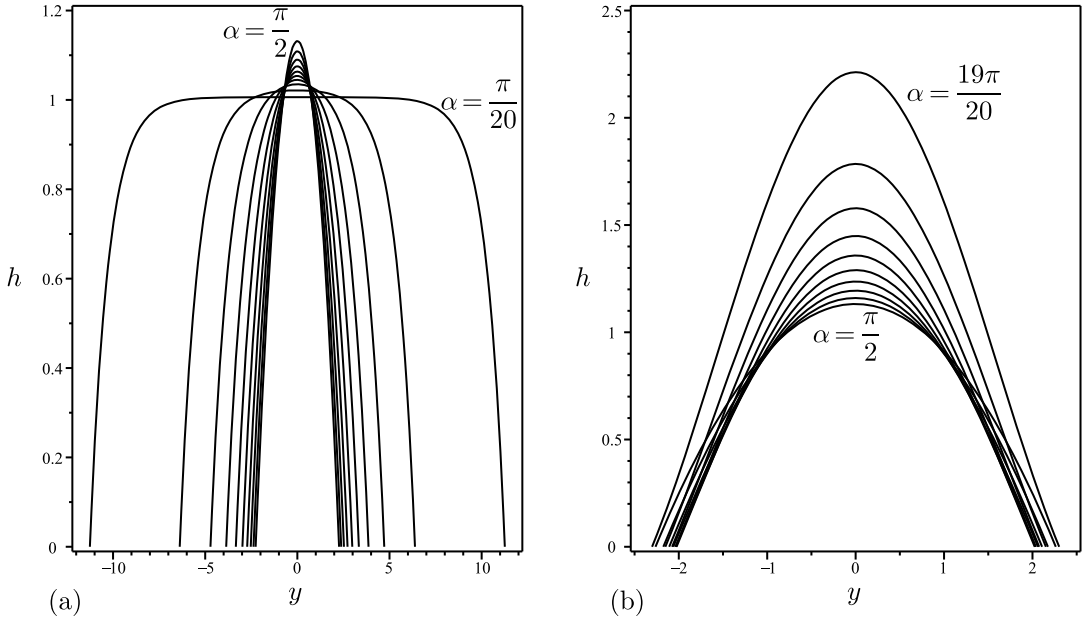

Figure 1.14: Non-perfectly wetting rivulet: The rivulet thickness h plotted as a function of y for (a) $\alpha/\pi = 1/20, 1/10, 3/20, \ldots, 1/2$, and (b) $\alpha/\pi = 1/2, 11/20, 6/10, \ldots, 19/20$, when $Q = 1$. Note the different h and y scales used in (a) and (b).

functions of α/π for a range of values of the flux Q, while figure 1.14 shows the rivulet thickness h plotted as a function of y for a range of values of α when $Q = 1$. In particular, figures 1.13 and 1.14 together with the solutions for a and h obtained from (1.47) and (1.46) show that the rivulet becomes wide with uniform depth unity according to

$$a = \frac{3Q}{2\alpha} + O(1) \quad \text{and} \quad h_{\mathrm{m}} = 1 + \frac{\alpha^2}{4} + O\big(\alpha^4\big) \tag{1.49}$$

as $\alpha \to 0^+$ (i.e. as the substrate tends towards being horizontal with a sessile rivulet), becomes of finite width and depth with

$$a = \left(\frac{105Q}{4}\right)^{1/4} \quad \text{and} \quad h_{\mathrm{m}} = \frac{1}{2}\left(\frac{105Q}{4}\right)^{1/4} \tag{1.50}$$

at $\alpha = \pi/2$ (i.e. when the substrate is vertical), and becomes deep with finite width according to

$$a = \pi - \left(\frac{5\pi(\pi-\alpha)}{3Q}\right)^{1/3} + O(\pi-\alpha), \quad h_{\mathrm{m}} = \left(\frac{24Q}{5\pi(\pi-\alpha)}\right)^{1/3} + O(\pi-\alpha)^{1/3} \tag{1.51}$$

as $\alpha \to \pi^-$ (i.e. as the substrate tends towards being horizontal with a pendent rivulet). In the limit of small flux $Q \to 0$ the rivulet becomes narrow and shallow according to

$$a = \left(\frac{105Q}{4\sin\alpha}\right)^{1/4} + O\left(Q^{3/4}\right) \quad \text{and} \quad h_{\mathrm{m}} = \frac{1}{2}\left(\frac{105Q}{4\sin\alpha}\right)^{1/4} + O\left(Q^{3/4}\right), \quad (1.52)$$

while in the limit of large flux $Q \to \infty$ the rivulet becomes wide with finite depth according to

$$a = \frac{3Qm^3}{2\sin\alpha} + O(1) \quad \text{and} \quad h_{\mathrm{m}} = \frac{1}{m} + O\left[\exp\left(-\frac{6Qm^4}{2\sin\alpha}\right)\right] \quad (1.53)$$

if $0 \leq \alpha < \pi/2$, becomes wide and deep with a and h_{m} given by (1.50) if $\alpha = \pi/2$, and becomes deep with finite width according to

$$a = \frac{\pi}{m} - \left(\frac{5\pi\sin\alpha}{3Qm^7}\right)^{1/3} + O\left(\frac{1}{Q}\right) \quad \text{and} \quad h_{\mathrm{m}} = \left(\frac{24Qm}{5\pi\sin\alpha}\right)^{1/3} + O\left(\frac{1}{Q^{1/3}}\right) \quad (1.54)$$

if $\pi/2 < \alpha \leq \pi$. Note that (1.52) fails near $\alpha = 0$ and $\alpha = \pi$ where there are boundary layers of width $O(Q)$, while (1.53) and (1.54) fail near $\alpha = \pi/2$ where there are boundary layers of width $O(Q^{-1/2})$.

1.4.2 Review of previous literature

Various aspects of the flow of rivulets have been studied extensively. At the beginning of the section we discussed some of the early work on the unidirectional flow of a rivulet down an inclined plane by Towell and Rothfeld [73], Allen and Biggin [74], Bentwich et al. [75] and Duffy and Moffatt [76]. Subsequently, Wilson and Duffy [78] extended the work of Duffy and Moffatt [76] to include the effect of substrate variation transverse to the direction of flow. In particular, Wilson and Duffy [78] found that a rivulet can run continuously from the top to the bottom of a large horizontal cylinder only if the transverse profile of the substrate is a sufficiently shallow trough; if the profile is a deeper trough then a rivulet is not possible near the bottom of the cylinder whereas if the profile is a ridge then a rivulet is not possible near the top of the cylinder. Later, Perazzo and Gratton

[79] revisited the basic flow considered by Towell and Rothfeld [73] and included discussion of the case when the contact angle is greater than $\pi/2$, while recently Tanasijczuk et al. [80] extended this work to include the effect of substrate variation transverse to the direction of flow. The flow of a rivulet down the underside of an inclined cylinder was considered by Kuibin [81], Alekseenko et al. [82] and Alekseenko et al. [83] both theoretically and experimentally. In particular, Kuibin [81] obtained the leading order asymptotic solution in the limit of small contact angle which corresponds to the flow of a perfectly wetting rivulet (i.e. a rivulet with zero contact angle). Further studies of the flow of a perfectly wetting rivulet down a slowly varying substrate have been performed by Duffy and Wilson [77] for the case when the viscosity is temperature-dependent (i.e. with thermoviscosity) and the substrate is uniformly heated or cooled, and Wilson and Duffy [84], who extended the work of Duffy and Moffatt [76] and Wilson and Duffy [78] to the case of a perfectly wetting rivulet. In particular, both Duffy and Wilson [77] and Wilson and Duffy [84] found that a perfectly wetting sessile rivulet (i.e. a rivulet on top of the substrate) is not possible but that a pendent rivulet (i.e. a rivulet hanging below the substrate) is.

Taking a somewhat different approach, Smith [85] and Duffy and Moffatt [86] obtained similarity solutions to the thin-film equations describing the steady gravity-driven flow of a slender non-uniform rivulet flowing either from a point source or to a point sink on an inclined plane in the cases of weak and strong surface-tension effects, respectively, while Wilson et al. [87] obtained the corresponding similarity solutions for the steady flow of a thin rivulet of a non-Newtonian power-law fluid down an inclined plane driven either by gravity or by a uniform surface shear stress. Snoeijer et al. [88] derived steady similarity solutions describing the flow of a drop down an inclined plane which show that there is a critical velocity above which a corner forms at the rear of the drop; as the velocity increases further this corner solution ultimately fails and thereafter a rivulet of fluid or droplets ("pearling") are left behind. Yatim et al. [89] derived

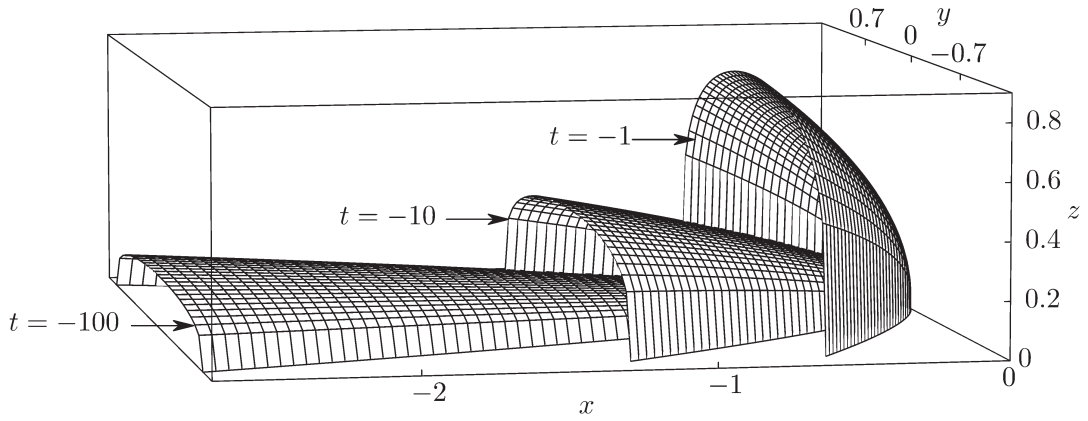

Figure 1.15: The solution obtained by Yatim et al. [89] for rivulet flow down an included plane in the case of a sessile rivulet with constant volume at different times. Reprinted from Yatim et al. [89] with permission of Oxford University Press.

an unsteady similarity solution corresponding to a rivulet with a fixed "nose" with either a "single-humped" or "double-humped" cross-sectional profile that widens (for a sessile rivulet) or narrows (for pendent a rivulet) with distance down the plane. Figure 1.15 shows the solution obtained Yatim et al. [89] in the case of a sessile rivulet with constant volume at different times.

In many situations involving the flow of rivulets non-isothermal effects are significant. Sultanović et al. [90] conducted an experimental study of the heat transfer in rivulets of water flowing down a heated inclined plane and found that if the rivulets develop waves or undergo meandering then the heat-transfer rate increases, while Kabov et al. [91] experimentally investigated the heat transfer to a film falling down a locally heated vertical plane and its breakup into rivulets. El-Genk and Saber [92] studied the steady flow of an evaporating film of fluid down a uniformly heated vertical plane and, via an argument based on minimisation of energy that they had previously used for the isothermal case [93], derived analytical expressions for the critical film thickness below which the film breaks up into rivulets. Holland et al. [94] used the lubrication approximation to study the steady locally unidirectional flow of a thin rivulet whose surface tension varies

linearly with temperature (i.e. with thermocapillarity) down a heated or cooled slowly varying substrate, and found that fluid particles spiral down the rivulet in helical vortices (something which does not occur in the corresponding isothermal problem), while Wilson and Duffy [95, 96] and Duffy and Wilson [77] considered the effects of thermoviscosity on a rivulet flowing down a heated or cooled slowly varying substrate for three different viscosity models (namely a linear, an exponential and an Eyring model) in the cases of both perfectly wetting [77] and non-perfectly wetting [95, 96] rivulets.

The important question of the stability of rivulet flows has been considered by many authors. Davis [97] considered the stability of a static rivulet on a horizontal plane in three different cases, namely fixed contact lines, fixed contact angles, and contact angles that are smooth functions of the speed of the moving contact line, while Young and Davis [98] studied the stability of a rivulet flowing down a vertical plane for the same three cases. Nakagawa and Scott [99] and Nakagawa [100] experimentally investigated the gravity-driven flow of a rivulet down an inclined plane and found four different regimes of flow depending on the flow rate, namely, drops, a stable meandering rivulet, an unstable meandering rivulet that breaks up into multiple rivulets, and a restabilised rivulet that no longer meanders but still has varying width; Schmuki and Laso [101] also investigated this flow both experimentally and theoretically and showed that uniform rivulets can also occur. In particular, by using an argument based on minimisation of energy, Schmuki and Laso [101] obtained predictions as to when the transitions from a single uniform rivulet to a meandering rivulet and from a meandering rivulet to multiple rivulets occur. Figure 1.16 shows images of five forms of rivulet flow obtained experimentally by Schmuki and Laso [101], namely a wetting film, droplets, a linear rivulet, a meandering rivulet and a oscillating or pendulum rivulet (essentially an unstable meandering rivulet). Roy and Schwartz [102] considered the stability of static rivulets on substrates of various shapes, including both wedges and cylinders, and found that stability is guaranteed if the pressure within the rivulet is an

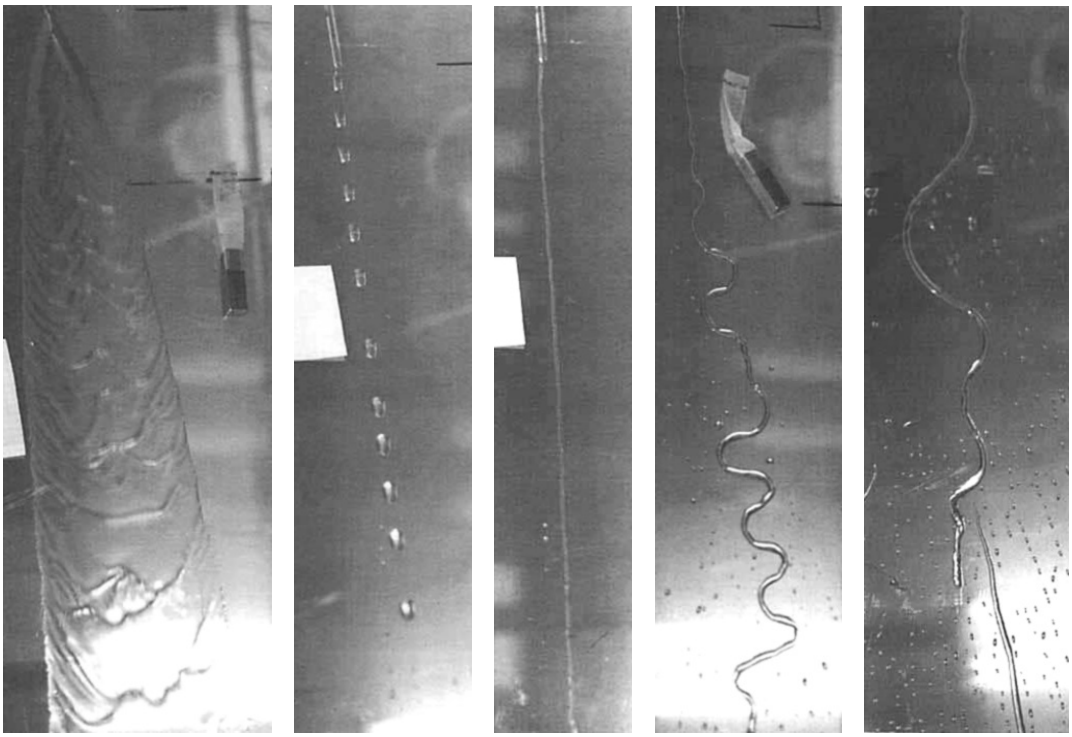

Figure 1.16: Images of five forms of rivulet flow obtained experimentally by Schmuki and Laso [101], namely (from left to right) a wetting film, droplets, a linear rivulet, a meandering rivulet and a oscillating or pendulum rivulet. Reprinted from Schmuki and Laso [101] with permission.

increasing function of its cross-sectional area. Saber and El-Genk [103] studied the flow of a uniform film down an inclined plane subject to a prescribed non-uniform longitudinal surface shear stress and, by using similar methods to El-Genk and Saber [93, 92], described the breakup of the film into rivulets. Myers et al. [104] considered the stability of a rivulet down an inclined plane subject to both the effects of gravity and a uniform longitudinal surface shear stress, and presented both numerical solutions and asymptotic solutions for a thin rivulet, finding good agreement between them for contact angles up to approximately $\pi/6$. Using an argument based on minimisation of energy they also calculated when it is ener-

getically favourable for the rivulet to split into two rivulets and hypothesised that a purely shear-driven rivulet will never split whereas a purely gravity-driven one may do so. Wilson and Duffy [105] and Wilson et al. [106] reconsidered the same problem for the particular case of a thin rivulet on a vertical plane, with Wilson and Duffy [105] finding that it can in fact be energetically favourable for a purely shear-driven rivulet to split, while Sullivan et al. [107] considered the stability of a thin perfectly wetting rivulet on an inclined plane. Le Grand-Piteira et al. [108] and Daerr et al. [109] experimentally investigated the meandering that can occur above a critical flow rate when a rivulet flows down an inclined plane. They considered the cases of both a non-perfectly wetting [108] and a perfectly wetting [109] rivulet. Benilov [110] considered the stability of the gravity-driven flow of a thin sessile or pendent rivulet on an inclined plane and found that whereas the sessile rivulet is always stable, the stability of the pendent rivulet depends on both the rivulet width and the angle of inclination of the plane. Diez et al. [111, 112] considered the stability of a static rivulet on a horizontal plane on both the macroscopic scale where gravitational effects are dominant and on the microscopic scale where van der Waals forces are dominant, and also discussed the case of a static rivulet of finite length.

1.5 Non-Isothermal Flow

In many thin-film flows, such as those found in heat exchangers, distillation processes and various coating problems, the effects of heating or cooling are important. In order to analyse the effects that temperature can have on a flow we must consider the energy in the system; the energy-balance equation for an incompressible Newtonian fluid is given by

$$\underbrace{\rho c_{\mathrm{p}}\left(\frac{\partial T}{\partial t}+\mathbf{u}\cdot\nabla T\right)}_{\substack{\text{thermal}\\ \text{advection}}}-\underbrace{\nabla\cdot(k_{\mathrm{th}}\nabla T)}_{\substack{\text{thermal}\\ \text{diffusion}}}-\underbrace{\frac{\mu}{2}\,\mathrm{tr}\Big(\big[\nabla\mathbf{u}+(\nabla\mathbf{u})^{T}\big]^{2}\Big)}_{\substack{\text{viscous}\\ \text{dissipation}}}+q=0, \tag{1.55}$$

where T is temperature, c_p is the specific heat, k_th is the thermal conductivity (which, in general, depends on temperature, but, is very often taken to be constant) and q is a heat source or sink. The different physical effects described by the terms in (1.55) are labelled. We note that in the case of the lubrication theory described in Section 1.1, equation (1.55) simplifies greatly to $\partial^2 T/\partial y^2 = 0$ at leading order in ϵ ($\ll 1$), provided that the suitably defined Péclet (a measure of the ratio of thermal advection to thermal diffusion) and Brinkman (a measure of the ratio of viscous dissipation to thermal diffusion) numbers are assumed to be small. Equation (1.55) requires boundary conditions; these may simply consist of fixed temperatures at the boundaries (be it at a substrate, a free surface or a fluid–fluid interface) or they may be more complicated and incorporate thermal effects such as heat transfer at the boundaries. In Chapters 2 and 3 we invoke a boundary condition involving heat transfer at a free surface; we model this with the commonly used Newton's law of cooling (see for example, Reisfeld and Bankoff [113], Selak and Lebon [114], Balmforth and Craster [115], Kabova and Kuznetsov [116], Wilson and Duffy [96] and Usha et al. [117]), which may be expressed as

$$-k_\mathrm{th}\nabla T \cdot \mathbf{n} = \alpha_\mathrm{th}(T - T_\infty) \tag{1.56}$$

where α_th is the heat transfer coefficient (a measure of the ratio of heat flux at the free surface to the temperature difference across the boundary; it is usually taken to be constant), $\mathbf{n}$ is the outward unit normal to the free surface, and T_∞ is the temperature in the surrounding atmosphere. This condition is applicable to cases where the heat transfer at the free surface is dominated by convective heat transfer, as is commonly the case at a liquid-gas boundary. Note that it is assumed there is a small airflow present in the atmosphere driving the convective heat transfer (though not enough to cause a significant shear on the surface of the fluid). Another thermal effect that is sometimes considered is that of thermocapillarity at a free surface, that is, the dependence of surface tension on temperature which is often called the Marangoni effect. In general, the density ρ and viscosity

μ vary with temperature, and a model describing their dependence on temperature is required; however, in many problems the variation of these quantities is sufficiently small that it is suitable to assume that one or both of them is constant. In Chapters 2 and 3 we consider flows that include thermoviscosity effects (with the density assumed constant). There are many models that can be used to describe the dependence of viscosity on temperature, including linear, exponential and Arrhenius/Eyring models; in Chapters 2 and 3 we use an exponential model. Thermoviscosity effects are significant in a wide range of problems, and because of this there have been a large number of studies of the effects of thermoviscosity on the non-isothermal flow of thin films of fluid on a variety of substrates. Thermoviscous flow of a thin film of fluid down an inclined substrate has been studied by, among others, Goussis and Kelly [118, 119] who used an exponential viscosity model to considered the stability of the film and found that heating destabilises the flow while cooling stabilises it, Hwang and Weng [120] who used an Arrhenius/Eyring viscosity model and gave the same conclusion as Goussis and Kelly [118, 119] regarding stability of the film. Kabova and Kuznetsov [116] used a linear viscosity model to consider the steady flow of a film flowing down a locally heated substrate with both thermoviscous and thermocapillarity (i.e. temperature-dependent surface tension) effects and found that the film thickens at the heated section of the substrate. Wilson and Duffy [95, 96] and Duffy and Wilson [77] studied the steady flow of a thin rivulet of fluid for three viscosity models (namely a linear, an exponential and an Arrhenius/Eyring model) and also included the effect of heat transfer at the free surface; they found that cooling the atmosphere widens and deepens the rivulet. There have also been many studies of thermoviscous flow of a thin film of fluid on a horizontal substrate; for example, Reisfeld and Bankoff [113] and Wu and Hwang [121] used a linear and an Arrhenius/Eyring viscosity model, respectively, to consider the evolution and eventual rupture of the film subject to surface tension and van der Waals; they found that heating reduces the rupture time while cooling increases it. Selak and Lebon [114] used both linear

and exponential viscosity models to investigate the onset of convection in a quiescent film subject to both buoyancy and thermocapillarity effects and found that the effect of thermoviscosity on stability depends on the sign of the of the viscosity's variation with temperature. Sansom et al. [122] considered the spreading of a film for three viscosity models (namely a linear, an exponential and a biviscosity model) and found that thicker regions of the droplet spread much faster that thinner ones. Motivated by lava flows, Bercovici [123] and Balmforth and Craster [115] studied the radial spreading of a film; Bercovici [123] used a viscosity model that is inversely proportional to temperature and included the effects of thermal advection, while Balmforth and Craster [115] used an exponential viscosity model and considered a viscoplastic fluid with a yield stress and found that finger-like instabilities can form. Also with applications to lava flows, Osiptsov [124] used an exponential viscosity model to consider the unsteady flow of a thin film of fluid over a conical surface with fluid being supplied at the apex. Unsteady flow of a thin film of fluid with thermoviscous and thermocapillary effects on a uniformly rotating disk was considered by Usha et al. [117], who used a linear viscosity model, and Wu [125], who used an Arrhenius/Eyring viscosity model.

1.6 Outline of Thesis

In this thesis we study three different problems concerning thin-film flows on horizontal cylinders.

In Chapter 2 we consider steady two-dimensional curtain flow with prescribed volume flux of a Newtonian fluid with temperature-dependent viscosity over a uniformly heated or cooled stationary horizontal cylinder. The problem is formulated for a general viscosity model and the effects of both thermoviscosity and heat transfer at the free surface are studied in detail in the particular case of an exponential viscosity model. We present and discuss numerical results along with asymptotic solutions in appropriate limits of the physical parameters of the problem.

In Chapter 3 we consider the steady two-dimensional coating and rimming flow of a Newtonian fluid with temperature-dependent viscosity on a uniformly heated or cooled rotating horizontal cylinder. As in Chapter 2, we formulate the problem for a general viscosity model and study the particular case of an exponential viscosity model in detail by giving numerical and asymptotic results. We show that there exists a critical solution with a critical load above which no solutions exist (analogous to that found in the corresponding isothermal problem); a detailed analysis of this critical solution and its dependence on the physical parameters of the problem is given. The case of prescribed subcritical load is also discussed in detail and we show the it is possible for backflow to occur within a particular region of parameter space.

In Chapter 4 we consider steady isothermal flow of a rivulet of Newtonian fluid on either the outside or the inside of a uniformly rotating horizontal cylinder. We present and discuss numerical and asymptotic solutions in appropriate limits, and find that the flow of a rivulet on a rotating cylinder also gives rise to a critical solution that is similar in nature to the critical solution found in the classical isothermal two-dimensional problem. We also show that backflow occurs within a particular region of parameter space.

Finally, in Chapter 5 we summarise Chapters 2–4 and discuss the key results and conclusions, and suggest ideas for possible further work.

1.7 Presentations and Publications

Aspects of the work given in Chapters 2 and 3 have been presented at the European Postgraduate Fluid Dynamics Conference at Keele University in 2008, the British Applied Mathematics Colloquium at the University of Nottingham in 2009, the 22$^{\text{nd}}$ Scottish Fluid Mechanics Meeting at The Scottish Association for Marine Science (SAMS), Oban in 2009, the EUROMECH Colloquium 497 on "Recent developments and New Directions in Thin-Film Flow" at the Royal Society of

Edinburgh in 2009, the 11$^{\text{th}}$ UK National Heat Transfer Conference at Queen Mary, University of London in 2009; including a short paper (Leslie et al. [126]) in the conference proceedings on the material in Chapter 2, and the 12$^{\text{th}}$ UK National Heat Transfer Conference at the University of Leeds in 2011; including a short paper (Leslie et al. [127]) in the conference proceedings on the material in Chapter 3. The work contained in Chapter 2 has been published in Physics of Fluids (Leslie et al. [128]), while the work in Chapter 3 has recently been submitted for publication in the Quarterly Journal of Mechanics and Applied Mathematics.

Parts of the work in Chapter 4 have been presented at the British Applied Mathematics Colloquium at the University of Edinburgh in 2010, and the 8$^{\text{th}}$ Euromech Fluid Mechanics Conference (EMFC8) in Bad Reichenhall, Germany in 2010. The work contained in Chapter 4 has recently been submitted for publication in the Journal of Fluid Mechanics.

Chapter 2

Thermoviscous Curtain Flow

In this chapter we use lubrication theory to study the steady two-dimensional thermoviscous gravity-driven flow of a Newtonian fluid on a stationary horizontal cylinder.

2.1 Problem Formulation

Consider steady two-dimensional gravity-driven flow of a thin film of Newtonian fluid with uniform (temperature-independent) density ρ and temperature-dependent viscosity $\mu = \mu(T)$, where T denotes the (in general) non-uniform temperature of the fluid, on a stationary circular cylinder of radius a with its axis horizontal, the cylinder being at a uniform temperature T_0, which may be either hotter or colder than the uniform temperature T_∞ ($\neq T_0$) of the surrounding atmosphere. Where possible we will consider a general viscosity model $\mu = \mu(T)$, where $\mu(T)$ is any monotonically decreasing function of T satisfying $\mu = \mu_0$ and $\mathrm{d}\mu/\mathrm{d}T = -\lambda\,(< 0)$ when $T = T_0$, where $\lambda\,(> 0)$ is a prescribed positive constant. When it is necessary to specify a particular viscosity model we will use the exponential viscosity model

$$\mu(T) = \mu_0 \exp\left(-\frac{\lambda(T - T_0)}{\mu_0}\right) \tag{2.1}$$

as used by, for example, Goussis and Kelly [118, 119], Hwang and Weng [120], Selak and Lebon [114], Balmforth and Craster [115] and Wilson and Duffy [95]. The choice of the cylinder temperature $T = T_0$ as the reference point for the viscosity model (as opposed to using the atmosphere temperature $T = T_\infty$) is made because the heat transfer from the cylinder to the fluid is usually much stronger than the heat transfer at the free surface and so the temperature of the fluid will be closer to that of the cylinder and hence the viscosity model will be more accurate (generally, the further the temperature goes from the reference temperature, the less accurate the viscosity model becomes). The appropriate non-dimensional measure of thermoviscosity (i.e. the variation of viscosity with temperature) is the *thermoviscosity number*, V, defined by

$$V = \frac{\lambda(T_0 - T_\infty)}{\mu_0}. \tag{2.2}$$

Since V has the same sign as $T_0 - T_\infty$, situations in which the cylinder is hotter (colder) than the atmosphere correspond to positive (negative) values of V. The physically realistic values of V vary over several orders of magnitude from arbitrarily small values (when the viscosity is effectively independent of temperature and/or when the magnitude of the heating or cooling is small) to reasonably large values (when the viscosity is strongly dependent on temperature and/or when the magnitude of the heating or cooling is large). For example, using the parameter values given by Selak and Lebon [114] in the case $|T_0 - T_\infty| = 25$ K yields $|V| = 0.3825$ for acetic acid, $|V| = 0.5225$ for silicone oil, $|V| = 0.625$ for water, and $|V| = 2.5125$ for glycerol, while Balmforth and Craster [115] give "typical" values of $|V| = 1$ for wax and slurry, $|V| = 5$ for basaltic lava, $|V| = 7$ for syrup, and $|V| = 10 - 18$ for silicic lava. Hence we will consider the full range of values from $V = 0$ to the limits $V \to \infty$ and $V \to -\infty$ in the present work.

Referred to polar coordinates $r = a + Y$ (with origin at the cylinder's axis) and θ (measured counter-clockwise from the horizontal) as shown in figure 2.1, we take the free surface of the fluid to be at $r = a + h$, the film thickness being denoted by

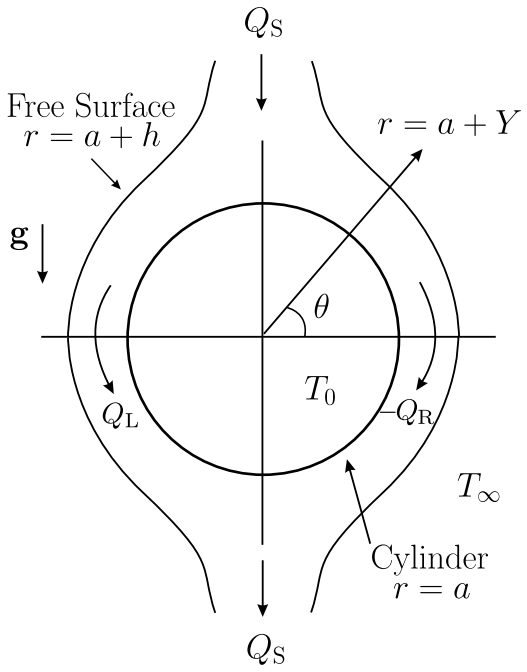

Figure 2.1: Geometry of the problem: steady two-dimensional flow of a thin film of Newtonian fluid with temperature-dependent viscosity on a stationary horizontal cylinder which may be either uniformly hotter or colder than the surrounding atmosphere.

h. The fluid velocity $\mathbf{u} = u\mathbf{e}_\theta + v\mathbf{e}_r$ (where $\mathbf{e}_\theta$ and $\mathbf{e}_r$ denote unit vectors in the azimuthal and radial directions, respectively), pressure p and temperature T are governed by the familiar mass-conservation, Navier–Stokes and energy equations. On the cylinder $r = a$ the velocity $\mathbf{u}$ satisfies the no-slip and no-penetration conditions, and the temperature is $T = T_0$ (a prescribed constant). On the free surface $r = a+h$ the usual normal and tangential stress balances and the kinematic condition apply, as does Newton's law of cooling

$$-k_{\rm th}\nabla T \cdot \mathbf{n} = \alpha_{\rm th}(T - T_\infty), \tag{2.3}$$

where $k_{\rm th}$ denotes the thermal conductivity of the fluid (assumed constant), $\alpha_{\rm th}$ (≥ 0) denotes an empirical surface heat-transfer coefficient, and $\mathbf{n}$ denotes the unit outward normal to the free surface. Surface tension, viscous dissipation, thermal

advection and inertia are all neglected (i.e. it is assumed that the appropriately defined Brinkman, Péclet and reduced Reynolds numbers are all small, while the Bond number is large).

Since the flow is steady, the volume flux per unit axial length Q (measured positive in the direction of increasing θ) is a piecewise constant, and since (as we shall show) the film thickness h always becomes unbounded at the top ($\theta = \pi/2$) and the bottom ($\theta = -\pi/2$) of the cylinder (where the tangential component of gravity is zero), it is natural to follow previous studies of the isothermal problem (see, for example, Duffy and Wilson [41]) and to interpret this as a curtain of fluid with prescribed constant volume flux $Q_{\mathrm{S}}\,(>0)$ falling onto the top of the cylinder and splitting into two films with constant azimuthal fluxes $Q = Q_{\mathrm{R}}$ and $Q = Q_{\mathrm{L}}$ round the right-hand and left-hand sides of the cylinder, respectively, with a corresponding curtain (also with flux Q_{S}) falling off at the bottom of the cylinder. By global conservation of mass these fluxes are related by $Q_{\mathrm{S}} = Q_{\mathrm{L}} - Q_{\mathrm{R}}$, but the relative split of the flux between the two sides of the cylinder is not determined by the present theory. In particular, the flow need not necessarily have left-to-right symmetry (i.e. Q_{R} and Q_{L} need not necessarily be equal to $-Q_{\mathrm{S}}/2$ and $Q_{\mathrm{S}}/2$, respectively). If $Q_{\mathrm{R}} \neq Q_{\mathrm{L}}$ then there will be a resultant torque τ on the cylinder given by

$$\tau = a^2 \mu_0 \int_{-\pi}^{\pi} \left.\frac{\partial u}{\partial Y}\right|_{Y=0} \mathrm{d}\theta, \tag{2.4}$$

however, we shall assume that the cylinder can resist this torque and will remain stationary.

The total fluid load (i.e. the mass of fluid) per unit axial length on either side of the cylinder M is denoted by $M = M_{\mathrm{R}}$ and $M = M_{\mathrm{L}}$ on the right-hand and left-hand sides of the cylinder, respectively, and hence the total fluid load on the cylinder is given by $M_{\mathrm{R}} + M_{\mathrm{L}}$.

We will consider only thin films, whose aspect ratio ϵ, defined by

$$\epsilon = \left(\frac{\mu_0 Q_{\mathrm{S}}}{\rho g a^3}\right)^{1/3} \ll 1, \tag{2.5}$$

is small. We non-dimensionalise and scale the system by writing

$$\left.\begin{gathered} r = a(1+\epsilon Y^*), \quad h = \epsilon a h^*, \quad u = U u^*, \quad v = \epsilon U v^*, \\ p = p_\mathrm{a} + \epsilon a \rho g p^*, \quad T = T_\infty + (T_0 - T_\infty) T^*, \quad \psi = Q_\mathrm{S}\psi^*, \quad \mu = \mu_0 \mu^*, \\ Q = Q_\mathrm{S} Q^* = \epsilon a U Q^*, \quad Q_\mathrm{R} = Q_\mathrm{S} Q_\mathrm{R}^* = \epsilon a U Q_\mathrm{R}^*, \quad Q_\mathrm{L} = Q_\mathrm{S} Q_\mathrm{L}^* = \epsilon a U Q_\mathrm{L}^*, \\ M = \epsilon \rho a^2 M^*, \quad M_\mathrm{R} = \epsilon \rho a^2 M_\mathrm{R}^*, \quad M_\mathrm{L} = \epsilon \rho a^2 M_\mathrm{L}^*, \end{gathered}\right\} \tag{2.6}$$

where the characteristic azimuthal fluid velocity U, defined to be equal to $Q_\mathrm{S}/\epsilon a$, is given by

$$U = \left(\frac{\rho g Q_\mathrm{S}^2}{\mu_0}\right)^{1/3}, \tag{2.7}$$

p_a is the constant pressure in the surrounding atmosphere and ψ is the stream-function satisfying $u = \partial\psi/\partial Y$ and $v = -\partial\psi/\partial\theta$ with $\psi = 0$ on $Y = 0$. Note that the non-dimensionalisation of temperature given in (2.6) incorporates the factor $T_0 - T_\infty$, which can be either positive or negative, and so a little care is required in interpreting results for the non-dimensional temperature T^* in terms of the dimensional temperature T. For clarity the star superscripts on non-dimensional variables will be omitted henceforth.

Expressed in non-dimensional variables the fluid occupies $0 \le Y \le h$ for $-\pi < \theta \le \pi$, the flux Q takes the values $Q = Q_\mathrm{R}$ on the right-hand side of the cylinder $|\theta| < \pi/2$ and $Q = Q_\mathrm{L}$ on the left-hand side of the cylinder $\pi/2 < |\theta| \le \pi$, with $Q_\mathrm{L} - Q_\mathrm{R} = 1$; also the general viscosity model $\mu = \mu(T)$ satisfies $\mu = 1$ and $\mathrm{d}\mu/\mathrm{d}T = -V$ when $T = 1$, and, in particular, the exponential viscosity model (2.1) is given by

$$\mu = \exp(-V(T-1)). \tag{2.8}$$

At leading order in ϵ the governing equations become

$$\frac{\partial u}{\partial \theta} + \frac{\partial v}{\partial Y} = 0, \quad \frac{\partial}{\partial Y}\left(\mu \frac{\partial u}{\partial Y}\right) = \cos\theta, \quad \frac{\partial p}{\partial Y} = -\sin\theta, \quad \frac{\partial^2 T}{\partial Y^2} = 0, \tag{2.9}$$

together with the boundary conditions

$$u = 0, \quad v = 0 \quad \text{and} \quad T = 1 \quad \text{on} \quad Y = 0, \tag{2.10}$$

$$\frac{\partial u}{\partial Y} = 0, \quad p = 0 \quad \text{and} \quad \frac{\partial T}{\partial Y} + BT = 0 \quad \text{on} \quad Y = h, \tag{2.11}$$

where $B = \epsilon a \alpha_{\text{th}}/k_{\text{th}}$ (≥ 0) is the non-dimensional Biot number (a non-dimensional measure of heat transfer to or from the atmosphere at the free surface). The special case $B = 0$ corresponds to that of a perfectly insulated free surface with no heat transfer (i.e. $\partial T/\partial Y = 0$ at $Y = h$), while at leading order in the limit $B \to \infty$ the free surface is at the same uniform temperature as the atmosphere (i.e. $T = 0$ at $Y = h$), and so we will consider the full range of values from $B = 0$ to the limit $B \to \infty$ in the present work.

Introducing the rescaled variable $y = Y/h$ (so that the fluid occupies $0 \leq y \leq 1$) and solving (2.9) subject to (2.10) and (2.11) for the temperature $T = T(y, \theta)$, the azimuthal velocity $u = u(y, \theta)$ and the pressure $p = p(y, \theta)$ yields

$$T(y, \theta) = 1 - \frac{Bhy}{1 + Bh}, \tag{2.12}$$

$$u(y, \theta) = -h^2 \cos\theta \int_0^y \frac{1 - \tilde{y}}{\mu(T(\tilde{y}, \theta))} \, \mathrm{d}\tilde{y} \tag{2.13}$$

and

$$p(y, \theta) = h(1 - y) \sin\theta. \tag{2.14}$$

The stream function $\psi = \psi(y, \theta)$[1] is given by

$$\psi = -h^3 \cos\theta \int_0^y \int_0^{\bar{y}} \frac{1 - \tilde{y}}{\mu(T(\tilde{y}, \theta))} \, \mathrm{d}\tilde{y} \, \mathrm{d}\bar{y} = -h^3 \cos\theta \int_0^y \frac{(1 - \tilde{y})(y - \tilde{y})}{\mu(T(\tilde{y}, \theta))} \, \mathrm{d}\tilde{y}. \tag{2.15}$$

The volume flux Q ($= \psi(1, \theta)$) is given by

$$Q = h \int_0^1 u \, \mathrm{d}y = -h^3 \cos\theta \int_0^1 \int_0^y \frac{1 - \tilde{y}}{\mu(T(\tilde{y}, \theta))} \, \mathrm{d}\tilde{y} \, \mathrm{d}y, \tag{2.16}$$

leading to

$$Q = -\frac{h^3 \cos\theta}{3} f, \tag{2.17}$$

where $f = f(\theta)$ (> 0) is a measure of the fluidity of the fluid film (herein referred to simply as the fluidity), defined by

$$f = 3 \int_0^1 \int_0^y \frac{1 - \tilde{y}}{\mu(T(\tilde{y}, \theta))} \, \mathrm{d}\tilde{y} \, \mathrm{d}y = 3 \int_0^1 \frac{(1 - y)^2}{\mu(T(y, \theta))} \, \mathrm{d}y. \tag{2.18}$$

[1]Note that the rescaled stream function $\psi = \psi(y, \theta)$ satisfies $u = \frac{1}{h}\frac{\partial \psi}{\partial y}$ and $v = -\frac{\partial \psi}{\partial \theta} + \frac{y}{h}\frac{\mathrm{d}h}{\mathrm{d}\theta}\frac{\partial \psi}{\partial y}$.

In the special case of constant viscosity $\mu \equiv 1$ the fluidity is simply equal to unity, i.e. $f \equiv 1$. Note that, since the flux Q is prescribed, (2.17) is the key equation which determines the film thickness h. Furthermore, since by definition $f > 0$ and $h > 0$, (2.17) shows that $-Q/\cos\theta > 0$, i.e. that Q must always have the same sign as $-\cos\theta$. Thus we deduce that $-1 < Q_{\mathrm{R}} < 0$ and $0 < Q_{\mathrm{L}} < 1$, where the sign difference between Q_{R} and Q_{L} arises because the flux is everywhere downwards, and so it is in the direction of increasing θ on the left-hand side of the cylinder but is in the direction of decreasing θ on the right-hand side of the cylinder. In fact, the present analysis also applies to the flow on the left-hand side of the cylinder in the case $Q_{\mathrm{R}} = 0$, $Q_{\mathrm{L}} = 1$ (in which there is no fluid on the right-hand side of the cylinder), and to the flow on the right-hand side of the cylinder in the case $Q_{\mathrm{R}} = -1$, $Q_{\mathrm{L}} = 0$ (in which there is no fluid on the left-hand side of the cylinder).

The fluid loads on the right-hand and the left-hand sides of the cylinder are given by

$$M_{\mathrm{R}} = \int_{-\pi/2}^{\pi/2} h \,\mathrm{d}\theta \tag{2.19}$$

and

$$M_{\mathrm{L}} = \int_{\pi/2}^{\pi} h \,\mathrm{d}\theta + \int_{-\pi}^{-\pi/2} h \,\mathrm{d}\theta, \tag{2.20}$$

respectively.

Thus, for a specific choice of viscosity model $\mu = \mu(T)$, the film thickness h is determined in terms of $Q = Q_{\mathrm{R}}$ $(-1 \leq Q_{\mathrm{R}} < 0)$ on the right-hand side of the cylinder and in terms of $Q = Q_{\mathrm{L}}$ $(0 < Q_{\mathrm{L}} \leq 1)$ on the left-hand side of the cylinder by the algebraic equation (2.17) in which f is given by (2.18), and the solutions for T, u, p, M_{R} and M_{L} are given explicitly by (2.12)–(2.14), (2.19) and (2.20), respectively.

Note that while the present problem has been obtained as the leading-order approximation to the steady flow of a thin film of fluid on a large horizontal circular cylinder, exactly the same problem also describes the leading-order approximation to the steady flow of a thin film of fluid down any sufficiently slowly varying substrate with local angle of inclination to the horizontal $\alpha = \pi/2 - \theta$, where

$0 \leq \alpha \leq \pi$. In particular, the present analysis applies to the widely studied problem of rectilinear flow down a planar substrate inclined at an angle α to the horizontal.

From (2.12), (2.13), (2.15), (2.17) and (2.18) it is clear that the Biot number B appears only in the combinations Bh, B^2u, $B^3\psi$ and B^3Q, and that Bh is a function of $-B^3Q/\cos\theta\,(>0)$. Thus, in particular, we could remove B explicitly from the mathematical problem by rescaling h, u, ψ and Q appropriately; however, since this obscures the physical interpretation of the results obtained we retain B explicitly in what follows.

Combining (2.12), (2.13), (2.15), (2.17) and (2.18) shows that h, T, u, ψ and f depend on θ only through $\cos\theta$, and so the flow has top-to-bottom symmetry, but (as we have already mentioned) not necessarily left-to-right symmetry.

Using (2.12) and (2.18) one may show that

$$\frac{\mathrm{d}\,(fh^3)}{\mathrm{d}h} = \frac{3h^2}{1+Bh}\int_0^1 \frac{(1-y)\,[2+3Bh(1-y)]}{\mu(T(y,\theta))}\,\mathrm{d}y > 0, \tag{2.21}$$

and hence from (2.17) we find that $\partial h/\partial Q$ has the same sign as Q, which means that the film thickness at each station θ increases monotonically with $|Q|$.

Similarly, from (2.17) we find that $\mathrm{d}h/\mathrm{d}\theta$ has the same sign as $\tan\theta$, which means that the film thickness on the right-hand (left-hand) side of the cylinder increases monotonically away from its minimum value at $\theta = 0$ ($\theta = \pi$).

Near the top and the bottom of the cylinder we have $h \to \infty$, $T \sim 1-y$, and $f \to \hat{f}$ as $\theta \to \pm\pi/2$, where from (2.18) the constant $\hat{f}\,(>0)$, which depends only on the specific viscosity model considered, is defined by

$$\hat{f} = 3\int_0^1 \frac{T^2}{\mu(T)}\,\mathrm{d}T. \tag{2.22}$$

Specifically, from (2.17) the thin-film approximation ultimately fails as the film thickness becomes unbounded according to

$$h = \left(\frac{3Q}{(|\theta|-\pi/2)\,\hat{f}}\right)^{1/3} - \frac{\hat{f}-\hat{g}}{\hat{f}B} + O\left(|\theta|-\frac{\pi}{2}\right)^{1/3} \quad \text{as} \quad \theta \to \pm\frac{\pi}{2}, \tag{2.23}$$

where the constant $\hat{g}\,(>0)$, which (like $\hat{f}$) also depends only on the specific viscosity model considered, is defined by

$$\hat{g} = 2\int_0^1 \frac{T}{\mu(T)}\,\mathrm{d}T. \tag{2.24}$$

Hereafter we will, for simplicity, restrict our attention to the flow on the right-hand side of the cylinder ($|\theta| < \pi/2$) with flux $Q = Q_{\mathrm{R}}$ ($-1 \le Q_{\mathrm{R}} < 0$) and load $M = M_{\mathrm{R}}$, from which the corresponding results for the flow on the left-hand side of the cylinder ($\pi/2 < |\theta| < \pi$) with flux $Q = Q_{\mathrm{L}}$ ($0 < Q_{\mathrm{L}} \le 1$) and load $M = M_{\mathrm{L}}$ can be readily obtained.

2.2 Special Case of Constant Viscosity

If either there is no heat transfer to or from the atmosphere at the free surface (i.e. in dimensional terms if $\alpha_{\mathrm{th}} = 0$) so that $B = 0$ (in which case the fluid film is isothermal with constant temperature $T \equiv 1$) or the viscosity is independent of temperature (i.e. in dimensional terms if $\lambda = 0$) so that $V = 0$ (in which case the fluid film is non-isothermal with non-constant temperature $T \not\equiv 1$), then the fluid has constant viscosity $\mu \equiv 1$ and fluidity $f \equiv 1$. In either case we recover the classical isothermal solution in which $h = h_0$, $u = u_0$ and $\psi = \psi_0$, where

$$h_0 = \left(-\frac{3Q}{\cos\theta}\right)^{1/3}, \tag{2.25}$$

$$u_0 = -\frac{h_0^2\cos\theta}{2}(2-y)y \tag{2.26}$$

and

$$\psi_0 = -\frac{h_0^3\cos\theta}{6}(3-y)y^2. \tag{2.27}$$

In particular, (2.25) shows that the film thickness h_0 increases monotonically with $|\theta|$ away from its minimum value of $(3|Q|)^{1/3}$ at $\theta = 0$, becoming unbounded at the top and the bottom of the cylinder according to

$$h_0 = \left(\frac{3Q}{|\theta| - \pi/2}\right)^{1/3} + O\left(|\theta| - \frac{\pi}{2}\right)^{5/3} \quad \text{as} \quad \theta \to \pm\frac{\pi}{2}, \tag{2.28}$$

in agreement with the corresponding general results obtained in Section 2.1. The load $M = M_0$ is given by

$$M_0 = 2\int_0^{\pi/2} h_0 \,\mathrm{d}\theta = C_0|Q|^{1/3}, \tag{2.29}$$

in which the numerical coefficient C_0 is given by

$$C_0 = 2\int_0^{\pi/2} \left(\frac{3}{\cos\theta}\right)^{1/3} \mathrm{d}\theta = \frac{2^{5/3}\pi^2}{3^{2/3}\Gamma\left(\frac{2}{3}\right)^3} \simeq 6.0669. \tag{2.30}$$

2.3 General Case of Non-Constant Viscosity

In general, if there is heat transfer to or from the atmosphere at the free surface (i.e. in dimensional terms if $\alpha_{\mathrm{th}} > 0$) so that $B > 0$ and the viscosity depends on temperature (i.e. in dimensional terms if $\lambda > 0$) so that $V \neq 0$, then the fluid film is non-isothermal with, in general, non-constant temperature, viscosity and fluidity. In the particular case of the exponential viscosity model (2.8) we have

$$\mu = \exp(-V(T-1)) = \exp\left(\frac{BVhy}{1+Bh}\right) = \exp(\mathcal{V}y), \tag{2.31}$$

where, for brevity, we have introduced the notation $\mathcal{V} = \mathcal{V}(\theta)$ defined by

$$\mathcal{V} = \frac{BVh}{1+Bh}, \tag{2.32}$$

so that (2.13) yields the azimuthal velocity

$$u = -\frac{h^2\cos\theta}{\mathcal{V}^2}\left[\mathcal{V} - 1 + (1 - \mathcal{V}(1-y))\exp(-\mathcal{V}y)\right], \tag{2.33}$$

(2.15) yields the stream function

$$\psi = -\frac{h^3\cos\theta}{\mathcal{V}^3}\left[(\mathcal{V}-1)(\mathcal{V}y-1) + 1 - (2 - \mathcal{V}(1-y))\exp(-\mathcal{V}y)\right] \tag{2.34}$$

and (2.18) yields the fluidity

$$f = \frac{3}{\mathcal{V}^3}\left[(\mathcal{V}-1)^2 + 1 - 2\exp(-\mathcal{V})\right]. \tag{2.35}$$

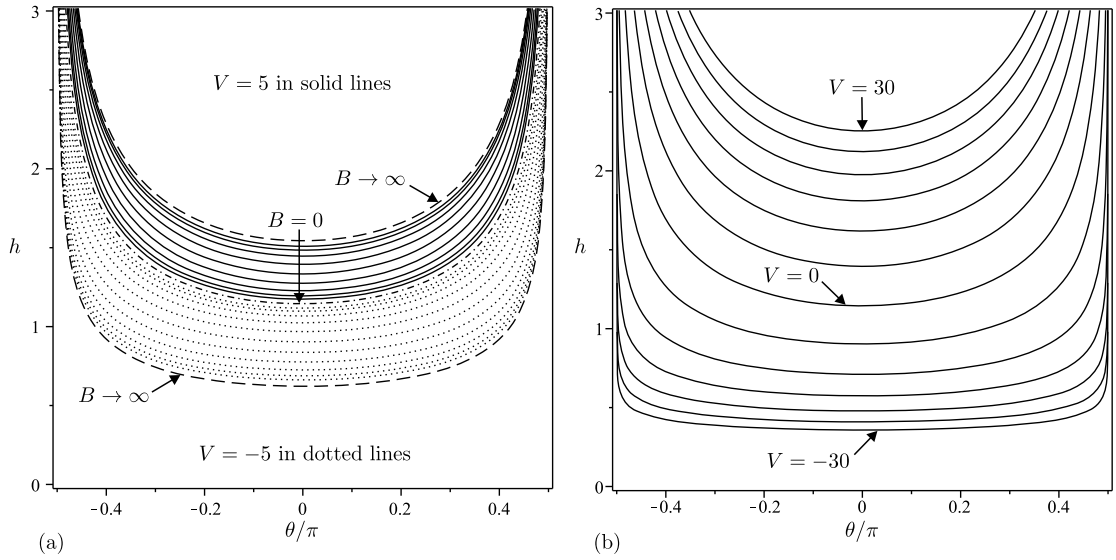

Figure 2.2: Film thickness h plotted as a function of θ/π for (a) $B = 0$ (dash-dotted line), $B = 10^n$ ($n = -1.25, -1, -0.75, \ldots, 1.25$) in the case $V = -5$ (dotted lines) and $B = 10^n$ ($n = -1.25, -1, -0.75, \ldots, 0.75$) in the case $V = 5$ (solid lines) together with the leading order asymptotic solutions in the limit $B \to \infty$ in the cases $V = -5$ and $V = 5$ (dashed lines), and for (b) $V = -30, -25, -20, \ldots, 30$ in the case $B = 1$, when $Q = -1/2$.

Note that f is a monotonically decreasing function of $\mathcal{V}$ satisfying

$$f \sim \frac{6\exp(-\mathcal{V})}{(-\mathcal{V})^3} \to \infty \quad \text{as} \quad \mathcal{V} \to -\infty, \tag{2.36}$$

$$f = 1 - \frac{\mathcal{V}}{4} + O(\mathcal{V}^2) \quad \text{as} \quad \mathcal{V} \to 0 \tag{2.37}$$

and

$$f \sim \frac{3}{\mathcal{V}} \to 0 \quad \text{as} \quad \mathcal{V} \to \infty. \tag{2.38}$$

Figures 2.2 and 2.3 show the film thickness h plotted as a function of θ/π for a range of values of B and V, and the film thickness at $\theta = 0$, $h(0)$, plotted as a function of B for a range of values of V and of V for a range of values of B, respectively. In particular, figures 2.2 and 2.3 illustrate that h is a monotonically increasing (decreasing) function of B for positive (negative) V, and a monotonically

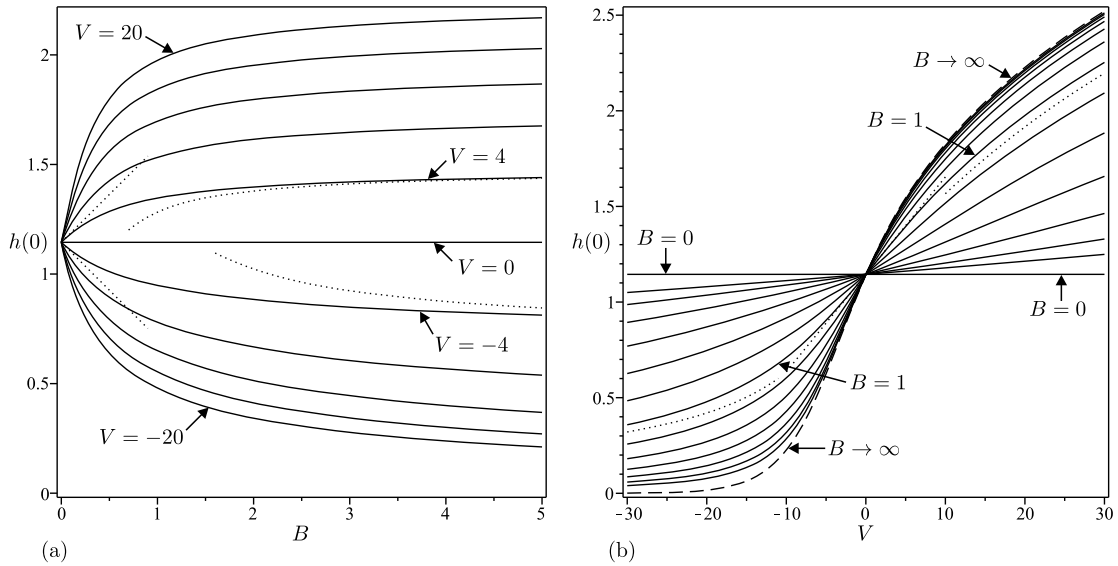

Figure 2.3: Film thickness at $\theta = 0$, $h(0)$, plotted as a function (a) of B for $V = -20$, -16, -12, ..., 20 (solid lines) together with the asymptotic solutions in the limits $B \to 0^+$ and $B \to \infty$ in the cases $V = -4$ and 4 (dotted lines), and (b) of V for $B = 0$ and $B = 10^n$ ($n = -1.5$, -1.25, -1, ..., 1.5) (solid lines) together with the asymptotic solutions in the limits $V \to 0$, $V \to \infty$ and $V \to -\infty$ in the case $B = 1$ (dotted lines) and the leading order asymptotic solution in the limit $B \to \infty$ (dashed line), when $Q = -1/2$.

increasing function of V. In addition, figure 2.3 shows good agreement with the asymptotic results for h obtained subsequently.

Figure 2.4 shows the free-surface temperature at $\theta = 0$, $T(1, 0)$, plotted as a function of B for a range of values of V and of V for a range of values of B. Taken together with the results for h shown in figures 2.2 and 2.3, figure 2.4 illustrates that the free-surface temperature, $T(1, \theta)$, is a monotonically decreasing function of both B and V.

Figure 2.5 shows the velocity u plotted as a function of $Y = hy$ for a range of values of θ for both a negative and a positive value of V, and Figure 2.6 shows the free-surface velocity at $\theta = 0$, $u(1, 0)$, plotted as a function of B for a range of values of V and of V for a range of values of B. In particular, figure 2.5 shows that

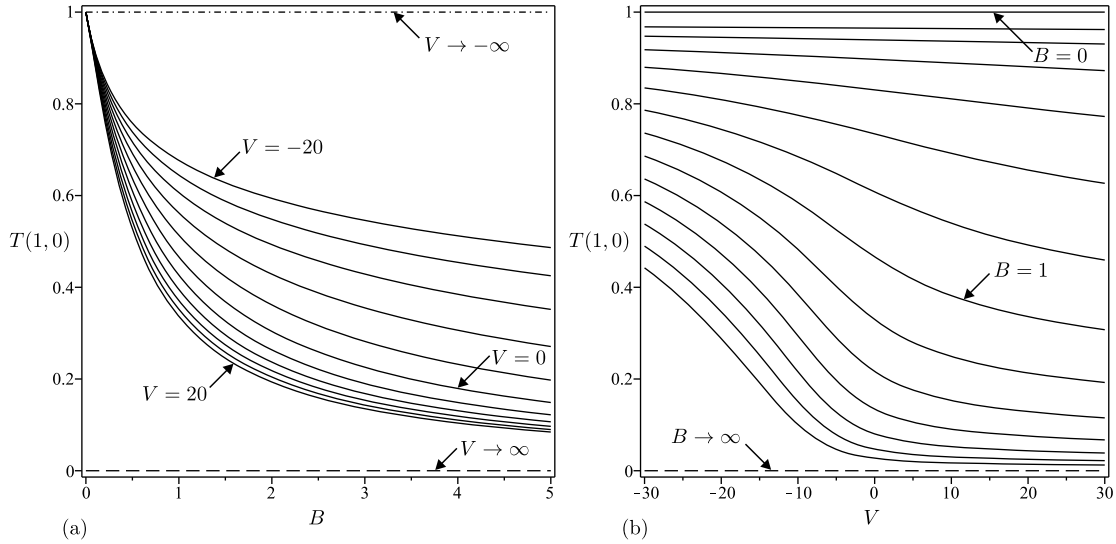

Figure 2.4: Free-surface temperature at $\theta = 0$, $T(1,0)$, plotted as a function (a) of B for $V = -20, -16, -12, \ldots, 20$ (solid lines) together with the leading order asymptotic solution in the limit $V \to \infty$ (i.e. $T(1,0) = 0$) (dashed line) and the leading order asymptotic solution in the limit $V \to -\infty$ (i.e. $T(1,0) = 1$) (dash-dotted line), and (b) of V for $B = 0$ and $B = 10^n$ ($n = -1.5, -1.25, -1, \ldots, 1.5$) (solid lines) together with the leading order asymptotic solution in the limit $B \to \infty$ (i.e. $T(1,0) = 0$) (dashed line), when $Q = -1/2$.

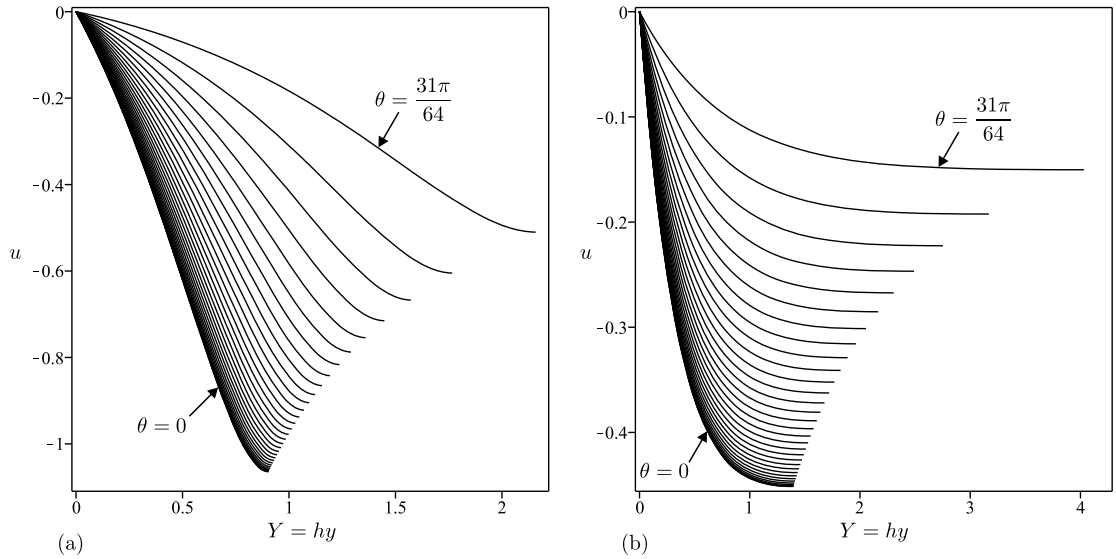

Figure 2.5: Velocity u plotted as a function of $Y = hy$ for $\theta = 0$, $\pi/64$, $\pi/32$, $\ldots$, $31\pi/64$ in the cases (a) $V = -5$ and (b) $V = 5$, when $Q = -1/2$ and $B = 1$.

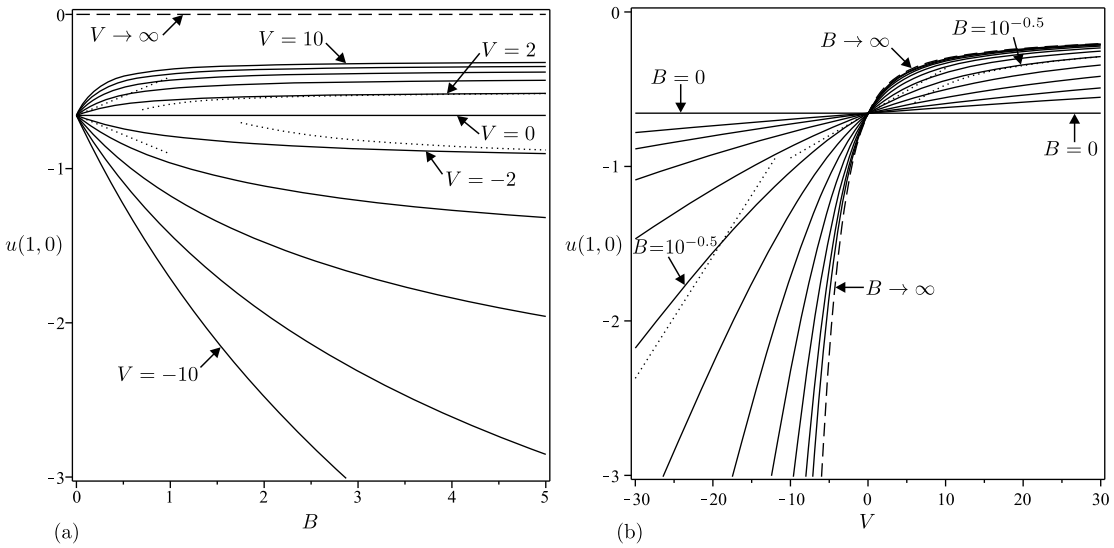

Figure 2.6: Free-surface velocity at $\theta = 0$, $u(1,0)$, plotted as a function (a) of B for $V = -10, -8, -6, \ldots, 10$ (solid lines) together with the asymptotic solutions in the limits $B \to 0^+$ and $B \to \infty$ in the cases $V = -2$ and 2 (dotted lines) and the leading order asymptotic solution in the limit $V \to \infty$ (i.e. $u(1,0) = 0$) (dashed line), and (b) of V for $B = 0$ and $B = 10^n$ ($n = -1.5, -1.25, -1, \ldots, 1$) (solid lines) together with the asymptotic solutions in the limits $V \to 0$, $V \to \infty$ and $V \to -\infty$ in the case $B = 10^{-0.5} \simeq 0.3162$ (dotted lines) and the leading order asymptotic solution in the limit $B \to \infty$ (dashed line), when $Q = -1/2$.

the velocity profiles for non-zero values of V are, in general, quite different from the familiar semi-parabolic profile (2.26) in the constant viscosity case $V = 0$. Figure 2.7 shows typical streamlines of the flow on the right-hand side of the cylinder.

Figure 2.8 shows the load M plotted as a function of B for a range of values of V and of V for a range of values of B. In particular, figure 2.8 shows that M is a monotonically increasing (decreasing) function of B for positive (negative) V, and a monotonically increasing function of V. In addition, figure 2.8 shows good agreement with the asymptotic results for M obtained subsequently.

In order to obtain a complete understanding of the influence of varying B and V, in the following Subsections 2.3.1–2.3.5 we analyse the behaviour in the asymp-

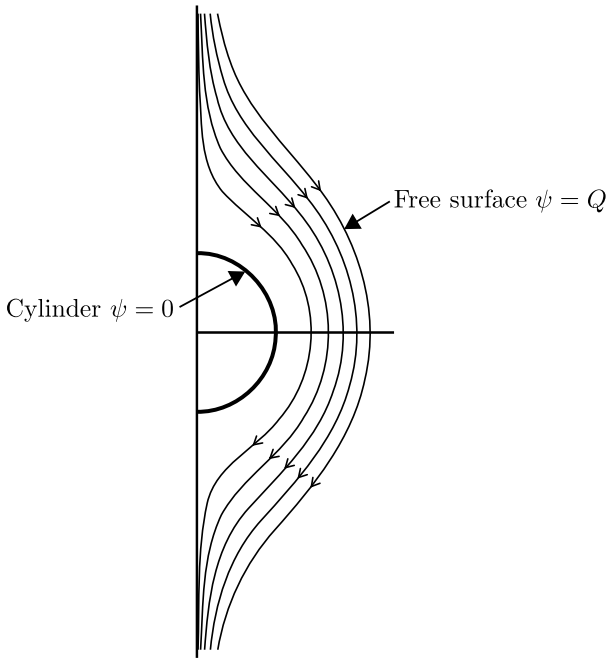

Figure 2.7: Typical streamlines of the flow on the right-hand side of the cylinder plotted for $\psi = 0$ (the cylinder), $Q/5$, $2Q/5$, $3Q/5$, $4Q/5$ and Q (the free surface) when $Q = -1/2$, $B = 1$ and $V = 1$.

totic limits of weak heat transfer at the free surface, $B \to 0^+$, strong heat transfer at the free surface, $B \to \infty$, weak thermoviscosity, $V \to 0$, strong positive thermoviscosity, $V \to \infty$, and strong negative thermoviscosity, $V \to -\infty$, respectively. In addition, in Section 2.4 we analyse the distinguished limit of strong thermoviscosity and weak heat transfer, $|V| \to \infty$ and $B \to 0^+$ with $BV = O(1)$, in which, although the variation in temperature across the fluid film small, thermoviscosity effects still enter the problem at leading order.

2.3.1 The limit of weak heat transfer $B \to 0^+$

At leading order in the limit of weak heat transfer at the free surface, $B \to 0^+$, the free surface is insulated (i.e. $\partial T/\partial y = 0$ at $y = 1$) and, as already discussed in Section 2.2, the fluid film is isothermal with constant temperature $T \equiv 1$, viscosity

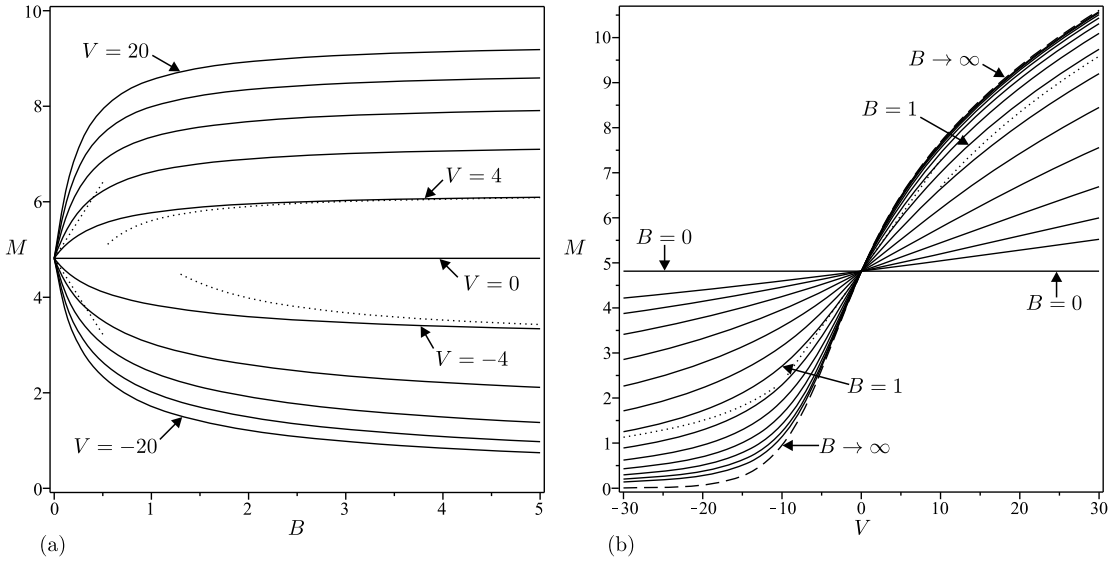

Figure 2.8: Load M plotted as a function (a) of B for $V = -20, -16, -12, \ldots, 20$ (solid lines) together with the asymptotic solutions in the limits $B \to 0^+$ and $B \to \infty$ in the cases $V = -4$ and 4 (dotted lines), and (b) of V for $B = 0$ and $B = 10^n$ ($n = -1.5, -1.25, -1, \ldots, 1.5$) (solid lines) together with the asymptotic solutions in the limits $V \to 0$, $V \to \infty$ and $V \to -\infty$ in the case $B = 1$ (dotted lines) and the leading order asymptotic solution in the limit $B \to \infty$ (dashed line), when $Q = -1/2$.

$\mu \equiv 1$ and fluidity $f \equiv 1$. Hence the leading-order solutions for h, u and M are simply the isothermal solutions h_0, u_0 and M_0 given by (2.25), (2.26) and (2.29), respectively.

The effect of variations in B first appear at $O(B)$, to which order the solutions for h, T, u and M are given by

$$h = h_0 + \frac{BVh_0^2}{12} + O(B^2), \tag{2.39}$$

$$T = 1 - Bh_0 y + \frac{B^2(12 - V)h_0^2 y}{12} + O(B^3), \tag{2.40}$$

$$u = u_0 - \frac{BVh_0^3 \cos\theta}{12}(4y^2 - 7y + 2)y + O(B^2) \tag{2.41}$$

and

$$M = M_0 + C_1 Q^{2/3} BV + O(B^2), \tag{2.42}$$

where the numerical coefficient C_1 is given by

$$C_1 = \frac{1}{6}\int_0^{\pi/2} \left(\frac{3}{\cos\theta}\right)^{2/3} \mathrm{d}\theta = \frac{\pi^2}{2^{1/3}3^{5/6}\Gamma\left(\frac{2}{3}\right)^3} = \frac{C_0}{4\times 3^{1/6}} \simeq 1.2629. \tag{2.43}$$

Note that the solutions (2.39)–(2.42) are valid for a general viscosity model satisfying $\mu = 1$ and $\mathrm{d}\mu/\mathrm{d}T = -V$ when $T = 1$ to the order shown (but not to higher orders). The solution (2.40) shows that the effect of weak heat transfer at the free surface is to decrease T from its constant isothermal value $T \equiv 1$ throughout the fluid film. Thus for positive (negative) thermoviscosity $V > 0$ ($V < 0$) the viscosity is increased (decreased) from its constant isothermal value $\mu \equiv 1$, and determining the sign of u_1 shows that the magnitude of the velocity is increased (decreased) from its value in the isothermal case when $0 < y < (7-\sqrt{17})/8 \simeq 0.3596$ and decreased (increased) when $(7-\sqrt{17})/8 < y \leq 1$, with the net effect that the magnitude of the average fluid velocity is decreased (increased) and hence that the film thickness (and hence the load) is increased (decreased) everywhere in order to accommodate the fixed volume flux of fluid.

2.3.2 The limit of strong heat transfer $B \to \infty$

At leading order in the limit of strong heat transfer at the free surface, $B \to \infty$, the free surface is at the same uniform temperature as the atmosphere (i.e. $T = 0$ at $y = 1$) and the fluid film has non-constant temperature $T = \hat{T} = 1 - y$ and viscosity $\mu = \hat{\mu} = \mu(\hat{T})$. As Duffy and Wilson [129] showed, the leading-order solutions for u and f, denoted by $\hat{u}$ and $\hat{f}$, are given by

$$\hat{u} = -\hat{h}^2 \cos\theta \int_{\hat{T}}^{1} \frac{T}{\mu(T)}\,\mathrm{d}T \tag{2.44}$$

and (2.22), respectively, where $\hat{h}$ denotes the leading-order solution for h. Closed-form expressions for $\hat{f}$ for linear, exponential and Eyring viscosity models are

described in detail by Wilson and Duffy [95]. Since $\hat{f}$ is a constant (and not a function of θ as, in general, f is) the leading-order solutions for h and M, the latter denoted by $\hat{M}$, are simply given by

$$\hat{h} = \frac{h_0}{\hat{f}^{1/3}} = \left(-\frac{3Q}{\hat{f}\cos\theta} \right)^{1/3}, \quad \hat{M} = \frac{M_0}{\hat{f}^{1/3}} = C_0 \left(\frac{|Q|}{\hat{f}} \right)^{1/3}, \tag{2.45}$$

where h_0 and M_0 are the solutions for h and M of the corresponding isothermal problem with the same flux given by (2.25) and (2.29) in which the constant C_0 is again given by (2.30). Thus, rather remarkably, for a general viscosity model the film thickness and the load (but *not* the temperature or the velocity) at leading order in the limit of strong heat transfer are simply re-scaled versions of their values for the corresponding isothermal problem with the same flux. In particular, this means that for positive (negative) thermoviscosity the leading-order film thickness and load are increased (decreased) from their values for the corresponding isothermal problem with the same flux. Furthermore, in this limit $\mathcal{V} \sim V$, and so the leading order expressions for μ, u, ψ and f are simply given by (2.31), (2.33), (2.34) and (2.35) with $\mathcal{V}$ replaced by V, respectively.

Note that the re-scaling (2.45) differs from that proposed by Duffy and Wilson [129]. In general, the leading-order solutions for h, Q and M in the limit of strong heat transfer, denoted by $\hat{h}$, $\hat{Q}$ and $\hat{M}$, are given simply by $\hat{h} = \hat{f}^{-m} h_0$, $\hat{Q} = \hat{f}^{1-3m} Q_0$, and $\hat{M} = \hat{f}^{-m} M_0$ for *any* non-zero value of m, where h_0 and M_0 are the solutions for h and M of the corresponding isothermal problem with flux Q_0. Thus at leading order in the limit of strong heat transfer, the film thickness and the load are simply re-scaled versions of their values for the corresponding isothermal problem with the appropriate flux. The present scaling (2.45) corresponds to the choice $m = 1/3$ and is simply the special case in which the flux remains unscaled. The scaling proposed by Duffy and Wilson [129] corresponds to the choice $m = 1/2$, who showed that this the only possible choice for the corresponding problem of non-isothermal flow on a *uniformly rotating* cylinder at leading order in the limit of strong heat transfer, but failed to notice that there is no restriction on the value

of m for the present problem of non-isothermal flow on a *stationary* cylinder.

As might have been anticipated, this simple re-scaling property does not extend to higher orders. Specifically, extending the analysis to $O(1/B^2)$ the solutions for h, T, u and M are given by

$$h = \hat{h} - \frac{(V+3)\hat{f} - 3}{3\hat{f}B} + O\left(\frac{1}{B^2}\right), \tag{2.46}$$

$$T = \hat{T} + \frac{y}{B\hat{h}} + \frac{(V\hat{f} - 3)y}{3\hat{f}B^3\hat{h}^2} + O\left(\frac{1}{B^3}\right), \tag{2.47}$$

$$\begin{aligned} u = \hat{u} - \frac{\hat{h}\cos\theta}{3\hat{f}BV}\Bigg[&\frac{6(V-1)}{V} - (2V+1)\hat{f} \\ &+ \left(\frac{6[1-V(1-y)]}{V} + [1+V(1-y)(2-3y)]\hat{f}\right)\exp(-Vy)\Bigg] + O\left(\frac{1}{B^2}\right) \end{aligned} \tag{2.48}$$

and

$$M = \hat{M} - \frac{\pi\left[(V+3)\hat{f} - 3\right]}{3\hat{f}B} + O\left(\frac{1}{B^2}\right). \tag{2.49}$$

The solution (2.47) shows that the effect of large-but-finite heat transfer at the free surface is to increase T from its leading-order value $T = \hat{T} = 1 - y$ throughout the fluid film. Thus for positive (negative) thermoviscosity $V > 0$ ($V < 0$) the viscosity is decreased (increased) from its leading-order value $\mu = \hat{\mu}$ with the net effect that the film thickness is decreased (increased) uniformly in order to accommodate the fixed volume flux of fluid, and hence that the load is decreased (increased).

2.3.3 The limit of weak thermoviscosity $V \to 0$

As already discussed in Section 2.2, at leading order in the limit of weak thermoviscosity, $V \to 0$, the fluid film has non-constant temperature $T \not\equiv 1$ but constant viscosity $\mu \equiv 1$ and fluidity $f \equiv 1$. From (2.17) and (2.18) the solution for h is given by

$$h = h_0 + \frac{BVh_0^2}{12(1+Bh_0)} + O(V^2), \tag{2.50}$$

and hence from (2.12), (2.13) and (2.19) the solutions for T, u and M are given by

$$T = 1 - \frac{Bh_0 y}{1 + Bh_0} - \frac{B^2 V h_0^2 y}{12(1 + Bh_0)^3} + O(V^2), \tag{2.51}$$

$$u = u_0 - \frac{BVh_0^3 \cos\theta}{12(1 + Bh_0)}(4y^2 - 7y + 2)y + O(V^2) \tag{2.52}$$

and

$$M = M_0 + \frac{Q^{2/3} BV}{2 \times 3^{1/3}} \int_0^{\pi/2} \frac{\mathrm{d}\theta}{(\cos\theta)^{2/3} + B(3|Q|\cos\theta)^{1/3}} + O(V^2), \tag{2.53}$$

where h_0, u_0 and M_0 are the isothermal solutions given by (2.25), (2.26) and (2.29), respectively. Note that the solutions (2.50)–(2.53) are valid for a general viscosity model satisfying $\mu = 1$ and $\mathrm{d}\mu/\mathrm{d}T = -V$ when $T = 1$ to the order shown (but not to higher orders). The solutions in this limit are similar to those in the limit $B \to 0^+$ described in Subsection 2.3.1 and have a similar physical interpretation. This behaviour is illustrated in figure 2.9 which shows the film thickness h plotted as a function of θ/π and the velocity u at $\theta = 0$ plotted as a function of $Y = hy$ for a range of values of V near $V = 0$.

2.3.4 The limit of strong positive thermoviscosity $V \to \infty$

In the limit of strong positive thermoviscosity, $V \to \infty$, from (2.17) and (2.18) the solution for h is given by

$$h = h_0 \left(\frac{V}{3}\right)^{1/3} - \frac{1}{3B} + O\left(\frac{1}{V^{1/3}}\right), \tag{2.54}$$

and hence from (2.12), (2.13) and (2.19) the solutions for T, u and M are given by

$$T = 1 - y + \frac{y}{Bh_0}\left(\frac{3}{V}\right)^{1/3} - \frac{2y}{3B^2 h_0^2}\left(\frac{3}{V}\right)^{2/3} + O\left(\frac{1}{V}\right), \tag{2.55}$$

$$u = -\frac{h_0^2 \cos\theta}{3}\left(\frac{3}{V}\right)^{1/3}[1 - \exp(-Vy)]$$
$$- \frac{h_0 \cos\theta}{9B}\left(\frac{3}{V}\right)^{2/3}[1 - (1 + 3Vy)\exp(-Vy)] + O\left(\frac{1}{V}\right) \tag{2.56}$$

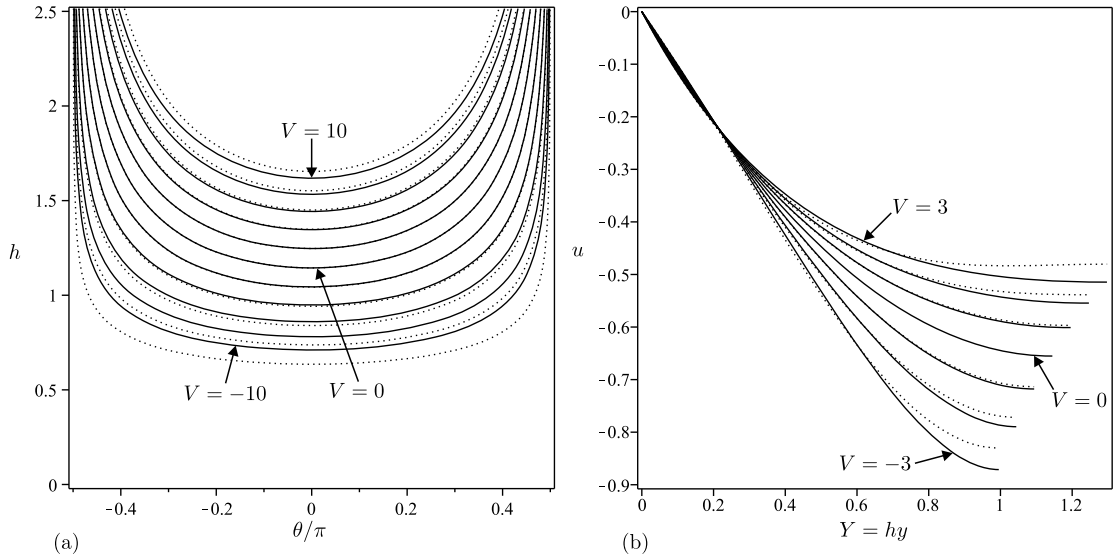

Figure 2.9: (a) Film thickness h plotted as a function of θ/π for $V = -10$, -8, -6, $\ldots$, 10 (solid lines), and (b) velocity u at $\theta = 0$ plotted as a function of $Y = hy$ for $V = -3$, -2, -1, $\ldots$, 3 (solid lines), together with the corresponding asymptotic solutions in the limit $V \to 0$ (dotted lines), when $Q = -1/2$ and $B = 1$.

and

$$M = M_0 \left(\frac{V}{3}\right)^{1/3} - \frac{\pi}{3B} + O\left(\frac{1}{V^{1/3}}\right), \tag{2.57}$$

where h_0 and M_0 are the isothermal solutions for h and M given by (2.25) and (2.29), respectively. In particular, these solutions show that at leading order in the limit of strong positive thermoviscosity the temperature is given by $T = 1 - y$ and the viscosity $\mu = O(\exp(Vy))$ is exponentially large outside a narrow boundary layer of width $O(1/V) \ll 1$ near the cylinder $y = 0$, resulting in a slow "plug flow" with a uniform (i.e. independent of y) velocity of $O(V^{-1/3}) \ll 1$ outside the boundary layer and a large film thickness of $O(V^{1/3}) \gg 1$. This behaviour is illustrated in figure 2.10 which shows the film thickness h plotted as a function of θ/π and the velocity u at $\theta = 0$ plotted as a function of $Y = hy$ for a range of positive values of V.

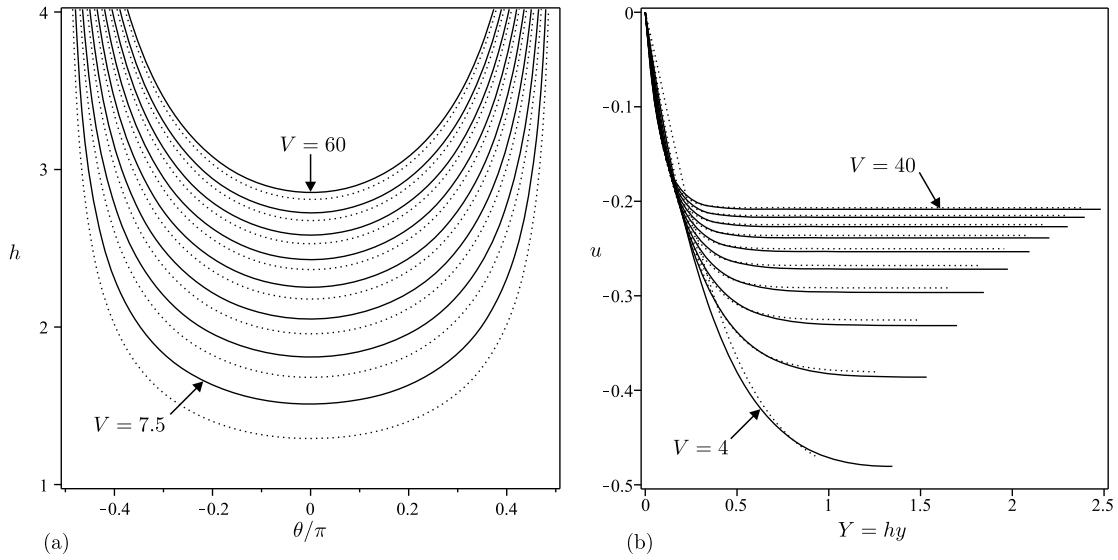

Figure 2.10: (a) Film thickness h plotted as a function of θ/π for $V = 7.5$, 15, 22.5, ..., 60 (solid lines), and (b) velocity u at $\theta = 0$ plotted as a function of $Y = hy$ for $V = 4$, 8, 12, ..., 40 (solid lines), together with the corresponding asymptotic solutions in the limit $V \to \infty$ (dotted lines), when $Q = -1/2$ and $B = 1$.

2.3.5 The limit of strong negative thermoviscosity $V \to -\infty$

In the limit of strong negative thermoviscosity, $V \to -\infty$, from (2.17) and (2.18) the solution for h is given by

$$h = \frac{1}{B(-V)} \log\left(\frac{QB^3V^3}{2\cos\theta}\right) + O\left(\frac{\log(-V)^2}{V^2}\right), \tag{2.58}$$

and hence from (2.12), (2.13) and (2.19) the solutions for T, u and M are given by

$$T = 1 - \frac{y}{(-V)} \log\left(\frac{QB^3V^3}{2\cos\theta}\right) + O\left(\frac{\log(-V)}{V^2}\right), \tag{2.59}$$

$$u = -\frac{\cos\theta}{B^2V^2}\left[\left(\frac{QB^3V^3}{2\cos\theta}\right)^y \left\{\log\left(\frac{QB^3V^3}{2\cos\theta}\right)(1-y)+1\right\} - \log\left(\frac{QB^3V^3}{2\cos\theta}\right) - 1\right] + O\left(\log(-V)\right) \tag{2.60}$$

and

$$M = \frac{\pi \log(|Q|B^3(-V)^3)}{B(-V)} + O\left(\frac{\log(-V)^2}{V^2}\right). \tag{2.61}$$

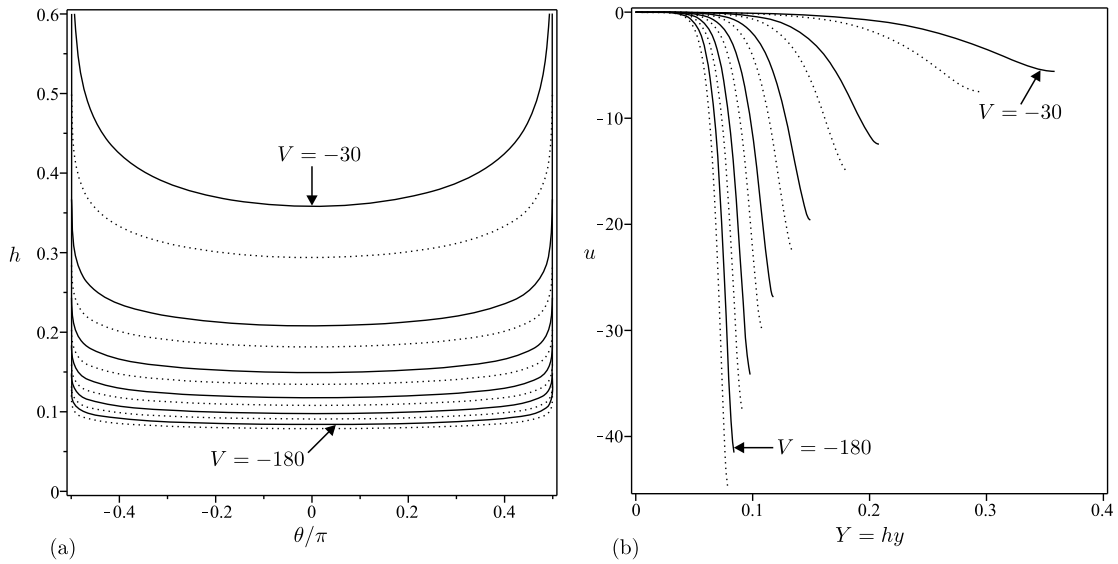

Figure 2.11: (a) Film thickness h plotted as a function of θ/π for $V = -30$, -60, -90, ..., -180 (solid lines), and (b) velocity u at $\theta = 0$ plotted as a function of $Y = hy$ also for $V = -30$, -60, -90, ..., -180 (solid lines), together with the corresponding asymptotic solutions in the limit $V \to -\infty$ (dotted lines), when $Q = -1/2$ and $B = 1$.

In particular, these solutions show that at leading order in the limit of strong negative thermoviscosity the temperature is given by $T = 1$ and the viscosity

$$\mu = \left(\frac{2\cos\theta}{QB^3V^3} \right)^y \tag{2.62}$$

decreases from $O(1)$ at the cylinder $y = 0$ to $O((-V)^{-3}) \ll 1$ at the free surface $y = 1$ and that the velocity increases from zero at the cylinder (where there is a narrow boundary layer of width $O(1/\log(-V)) \ll 1$) to $O(-V) \gg 1$ at the free surface (where there is another narrow boundary layer also of width $O(1/\log(-V)) \ll 1$), resulting in a small film thickness of $O(\log(-V)/(-V)) \ll 1$. This behaviour is illustrated in figure 2.11 which shows the film thickness h plotted as a function of θ/π and the velocity u at $\theta = 0$ plotted as a function of $Y = hy$ for a range of negative values of V.

2.4 Distinguished Limit of Strong Thermoviscosity and Weak Heat Transfer $|V| \to \infty$ and $B \to 0^+$ With $\hat{V} = BV = O(1)$

Another interesting case also worth considering is the distinguished limit discussed by Wilson and Duffy [96] of strong thermoviscosity, $|V| \to \infty$, *and* weak heat transfer at the free surface, $B \to 0^+$, such that $\hat{V} = BV = O(1)$, in which, although the variation in temperature across the fluid film is small, specifically $T = 1 - Bhy + O(B^2)$, thermoviscosity effects still enter the problem at leading order, i.e. the variation in viscosity across the fluid film is still $O(1)$. This case is physically relevant since the Biot number is often found to be small. By making the substitution $V = \hat{V}/B$ and taking the limit $B \to 0$ we are able to consider this interesting case with one less parameter than we had previously thereby simplifying the analysis of the problem. Note that in this limit the *effective thermoviscosity number*, $\hat{V} = BV$, defined in terms of dimensional quantities by

$$\hat{V} = \frac{\lambda(T_0 - T_\infty)\epsilon a \alpha_{\text{th}}}{\mu_0 k_{\text{th}}}, \tag{2.63}$$

and not the previously defined thermoviscosity number, V, is the appropriate non-dimensional measure of thermoviscosity effects. In the particular case of the exponential viscosity model (2.31) in this limit $\mathcal{V} \sim \hat{V}h$ and so the leading order expressions for μ, u, ψ and f are simply given by (2.31), (2.33)–(2.35) with $\mathcal{V}$ replaced by $\hat{V}h$, respectively.

Note that, in an analogous way to being able to remove B explicitly from the general mathematical problem by rescaling appropriately (discussed in Section 2.1), in this case we could remove $\hat{V}$ explicitly from the mathematical problem by rescaling h, u, ψ and Q appropriately; however, since this again obscures the physical interpretation of the results obtained we retain $\hat{V}$ explicitly in what follows.

In the limit of "weak" thermoviscosity, $\hat{V} \to 0$, the solutions for h, u and M are given by the corresponding results in the limit $B \to 0$ given in Subsection

2.3.1, namely (2.39), (2.41) and (2.42), with BV replaced by $\hat{V}$, and hence have the same physical interpretation.

In the limit of strong positive thermoviscosity, $\hat{V} \to \infty$, the solutions for h, u and M are given by

$$h = \left(-\frac{Q\hat{V}}{\cos\theta}\right)^{1/2} + \frac{1}{\hat{V}} + O\left(\frac{1}{\hat{V}^{5/2}}\right), \tag{2.64}$$

$$u = -\frac{\cos\theta}{\hat{V}}\left(-\frac{Q\hat{V}}{\cos\theta}\right)^{1/2}\left\{1 - \exp\left[-\left(-\frac{Q\hat{V}^3}{\cos\theta}\right)^{1/2} y\right]\right\} + O\left(\frac{1}{\hat{V}^2}\right) \tag{2.65}$$

and

$$M = \hat{C}\left(|Q|\hat{V}\right)^{1/2} + \frac{\pi}{\hat{V}} + O\left(\frac{1}{\hat{V}^{5/2}}\right), \tag{2.66}$$

in which the numerical coefficient $\hat{C}$ is given by

$$\hat{C} = 2\int_0^{\pi/2}\left(\frac{1}{\cos\theta}\right)^{1/2} \mathrm{d}\theta = 2\sqrt{2}\,\mathrm{K}\left(\frac{1}{\sqrt{2}}\right) \simeq 5.2441, \tag{2.67}$$

where $\mathrm{K}(k)$ is the complete elliptic integral of the first kind with modulus k defined by

$$\mathrm{K}(k) = \int_0^1 \frac{\mathrm{d}x}{\sqrt{1-x^2}\sqrt{1-k^2x^2}} \tag{2.68}$$

(see, for example, Gradshteyn and Ryzhik [130]). These solutions differ from the corresponding results in the limit $V \to \infty$ given in Subsection 2.3.4, namely (2.54), (2.56) and (2.57), but have a qualitatively similar physical interpretation. In particular, these solutions show that at leading order in the limit of strong positive thermoviscosity the viscosity

$$\mu = \exp\left[\left(-\frac{Q\hat{V}^3}{\cos\theta}\right)^{1/2} y + y\right] \tag{2.69}$$

is exponentially large outside a narrow boundary layer of width $O(\hat{V}^{-3/2}) \ll 1$ near the cylinder $y = 0$, resulting in a slow "plug flow" with a uniform (i.e. independent of y) velocity of $O(\hat{V}^{-1/2}) \ll 1$ outside the boundary layer and a large film thickness of $O(\hat{V}^{1/2}) \gg 1$.

In the limit of strong negative thermoviscosity, $\hat{V} \to -\infty$, the solutions for h, u and M are given by

$$h = \frac{1}{(-\hat{V})} \log\left(\frac{Q\hat{V}^3}{2\cos\theta}\right) + O\left(\frac{\log((-\hat{V})^6)}{\hat{V}^4}\right), \tag{2.70}$$

$$u = -\frac{\cos\theta}{\hat{V}^2}\left[\left(\frac{Q\hat{V}^3}{2\cos\theta}\right)^y \left\{\log\left(\frac{Q\hat{V}^3}{2\cos\theta}\right)(1-y)+1\right\} - \log\left(\frac{Q\hat{V}^3}{2\cos\theta}\right) - 1\right] + O\left(\frac{\log((-\hat{V})^6)}{\hat{V}^2}\right) \tag{2.71}$$

and

$$M = \frac{\pi \log(|Q|(-\hat{V})^3)}{(-\hat{V})} + O\left(\frac{\log((-\hat{V})^6)}{\hat{V}^4}\right). \tag{2.72}$$

At leading (but not higher) order these solutions coincide with the corresponding results in the limit $V \to -\infty$ given in Subsection 2.3.5, namely (2.58), (2.60) and (2.61), and hence have the same physical interpretation.

2.5 Conclusions

In the present work we obtained a comprehensive description of the two-dimensional steady gravity-driven flow with prescribed volume flux of a thin film of Newtonian fluid with temperature-dependent viscosity on a heated or cooled stationary horizontal cylinder. In particular, we showed that for the exponential viscosity model (2.8) the effect of increasing B depends on the sign of V. When the cylinder is hotter than the surrounding atmosphere (i.e. when $V > 0$) the effect of increasing B is to decrease the average temperature and so to increase the average viscosity and hence reduce the average velocity within the film, with the net effect that the film thickness (and hence the total fluid load on the cylinder) is increased to maintain the fixed volume flux of fluid. When the cylinder is colder than the surrounding atmosphere (i.e. when $V < 0$) the opposite occurs. Similarly, we showed that the effect of increasing V is always to increase the film thickness and hence the load.

In order to obtain a complete understanding of the influence of varying B and V, we also analysed the behaviour in the asymptotic limits of weak heat transfer, $B \to 0^+$, strong heat transfer, $B \to \infty$, weak thermoviscosity, $V \to 0$, strong positive thermoviscosity, $V \to \infty$, and strong negative thermoviscosity, $V \to -\infty$, as well as in the distinguished limit of strong thermoviscosity and weak heat transfer, $|V| \to \infty$ and $B \to 0^+$ with $BV = O(1)$. The asymptotic analysis in the limits $B \to 0^+$ and $B \to \infty$ revealed that increasing B from zero to infinity changes the film thickness everywhere (and hence the load, but not the temperature or the velocity) by a constant factor of $\hat{f}^{-1/3}$, where $\hat{f}$ is given by (2.22), which depends only on the specific viscosity model considered. The asymptotic analysis in the limits $V \to 0$, $V \to \infty$ and $V \to -\infty$ revealed that for the exponential viscosity model (2.8) the behaviour of the solution for large positive thermoviscosity is very different from that for large negative thermoviscosity, and that both are very different from that in the constant viscosity case $V = 0$. Specifically, in the limit $V \to \infty$ the viscosity is exponentially large of $O(\exp(V)) \gg 1$ and the velocity is small and uniform (i.e. independent of y) of $O(V^{-1/3}) \ll 1$ outside a narrow boundary layer of width $O(1/V) \ll 1$ near the cylinder, leading to a large film thickness of $O(V^{1/3}) \gg 1$, while in the limit $V \to -\infty$ the viscosity decreases from $O(1)$ at the cylinder to $O((-V)^{-3}) \ll 1$ at the free surface and the velocity increases from zero at the cylinder to a large value of $O(-V) \gg 1$ at the free surface, leading to a small film thickness of $O(\log(-V)/(-V)) \ll 1$.

Chapter 3

Thermoviscous Coating and Rimming Flows

In this chapter we use lubrication theory to study the steady two-dimensional thermoviscous flow of a Newtonian fluid on either the outside or the inside of a rotating horizontal cylinder.

3.1 Problem Formulation

Consider the steady two-dimensional thermoviscous flow of a thin film of a Newtonian fluid with uniform (temperature-independent) density ρ and temperature-dependent viscosity $\mu = \mu(T)$, where T denotes the (in general) non-uniform temperature of the fluid, on either the outside ("coating flow") or the inside ("rimming flow") of a circular cylinder of radius a rotating in a counter-clockwise direction about its horizontal axis at uniform angular speed Ω (so that the circumferential speed is $a\Omega$), the cylinder being at the uniform temperature T_0, which may be either hotter or colder than the uniform temperature of the surrounding atmosphere, denoted by T_∞ ($\neq T_0$). Where possible we will consider a general viscosity model $\mu = \mu(T)$, where $\mu(T)$ is any monotonically decreasing function of T satisfying $\mu = \mu_0$ and $\mathrm{d}\mu/\mathrm{d}T = -\lambda\,(< 0)$ when $T = T_0$, where $\lambda\,(> 0)$ is a prescribed

positive constant. When it is necessary to specify a particular viscosity model we will use the exponential viscosity model

$$\mu(T) = \mu_0 \exp\left(-\frac{\lambda(T - T_0)}{\mu_0}\right) \tag{3.1}$$

as used by, for example, Goussis and Kelly [118, 119], Hwang and Weng [120], Selak and Lebon [114], Balmforth and Craster [115] and Wilson and Duffy [95]. The choice of the cylinder temperature $T = T_0$ as the reference point for the viscosity model (as opposed to using the atmosphere temperature $T = T_\infty$) is made because the heat transfer from the cylinder to the fluid is usually much stronger that the heat transfer at the free surface and so the temperature of the fluid will be closer to that of the cylinder and hence the viscosity model will be more accurate (the further the temperature goes from the reference temperature, the less accurate the viscosity model becomes). The appropriate non-dimensional measure of thermoviscosity (i.e. the variation of viscosity with temperature) is the *thermoviscosity number*, V, defined by

$$V = \frac{\lambda(T_0 - T_\infty)}{\mu_0}. \tag{3.2}$$

Since V has the same sign as $T_0 - T_\infty$, situations in which the cylinder is hotter (colder) than the atmosphere correspond to positive (negative) values of V. The physically realistic values of V vary over several orders of magnitude from arbitrarily small values (when the viscosity is effectively independent of temperature and/or when the magnitude of the heating or cooling is small) to reasonably large values (when the viscosity is strongly dependent on temperature and/or when the magnitude of the heating or cooling is large). For example, using the parameter values given by Selak and Lebon [114] in the case $|T_0 - T_\infty| = 25$ K yields $|V| = 0.3825$ for acetic acid, $|V| = 0.5225$ for silicone oil, $|V| = 0.625$ for water, and $|V| = 2.5125$ for glycerol, while Balmforth and Craster [115] give "typical" values of $|V| = 1$ for wax and slurry, $|V| = 5$ for basaltic lava, $|V| = 7$ for syrup, and $|V| = 10 - 18$ for silicic lava. Hence we will consider the full range of values from $V = 0$ to the limits $V \to \infty$ and $V \to -\infty$ in the present work.

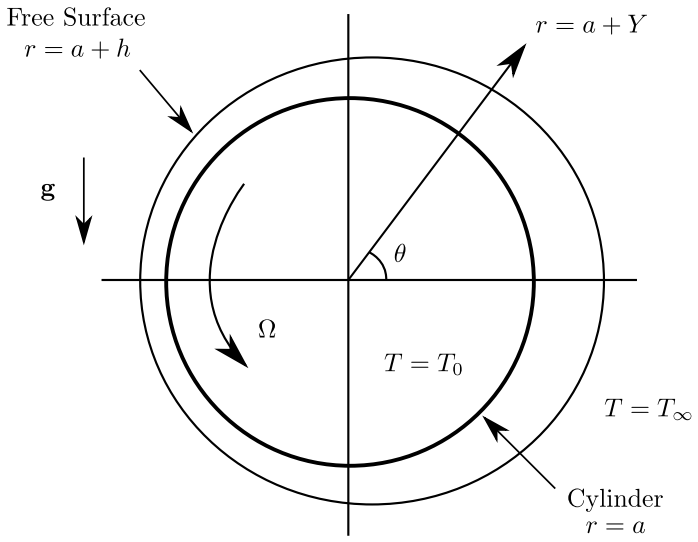

Figure 3.1: Geometry of the problem (drawn for coating flow): steady two-dimensional thermoviscous flow of a thin film of Newtonian fluid on a uniformly rotating horizontal cylinder which is uniformly hotter or colder than the surrounding atmosphere.

Referred to polar coordinates $r = a \pm Y$ (with origin at the cylinder's axis) and θ (measured counter-clockwise from the horizontal), as shown in figure 3.1 (drawn for coating flow), we take the free surface of the fluid to be at $r = a+h$ for coating flow and $r = a-h$ for rimming flow, the film thickness being denoted by $h = h(\theta)$. The fluid velocity $\mathbf{u} = u\mathbf{e}_\theta + v\mathbf{e}_r$ (where $\mathbf{e}_\theta$ and $\mathbf{e}_r$ denote unit vectors in the azimuthal and radial directions, respectively), the pressure p, and the temperature T are governed by the usual mass-conservation, Navier–Stokes and energy equations. On the cylinder $r = a$ the velocity $\mathbf{u}$ satisfies no-slip and no-penetration conditions, and the temperature is $T = T_0$ (a prescribed constant). On the free surface $r = a \pm h$ the usual normal and tangential stress balances and the kinematic condition apply, as does Newton's law of cooling $-k_{\text{th}} \nabla T \cdot \mathbf{n} = \alpha_{\text{th}}(T - T_\infty)$, where k_{th} denotes the thermal conductivity of the fluid (assumed constant), $\alpha_{\text{th}}\,(\geq 0)$ denotes an (empirical) surface heat-transfer coefficient, and $\mathbf{n}$ denotes the unit outward normal to the free surface. Surface tension, viscous dissipation, inertia

and thermal advection are all neglected.

We consider only thin films with small aspect ratio ϵ defined by

$$\epsilon = \left(\frac{\mu_0 \Omega}{\rho g a}\right)^{1/2} \ll 1, \tag{3.3}$$

where g denotes the magnitude of gravitational acceleration, and we scale and non-dimensionalise the system appropriately by writing

$$\left.\begin{gathered} r = a(1 \pm \epsilon Y^*), \quad h = \epsilon a h^*, \quad u = a\Omega u^*, \quad v = \pm \epsilon a \Omega v^*, \\ \psi = \pm \epsilon a^2 \Omega \psi^*, \quad p = p_\mathrm{a} \pm \epsilon a \rho g p^*, \quad T = T_\infty + (T_0 - T_\infty) T^*, \\ \mu = \mu_0 \mu^*, \quad Q = \epsilon a^2 \Omega Q^*, \quad M = \epsilon a^2 \rho M^*, \end{gathered}\right\} \tag{3.4}$$

in which the $+$ in the $\pm$ corresponds to coating flow while the $-$ corresponds to rimming flow, ψ is the streamfunction satisfying $u = \partial\psi/\partial Y$ and $v = -\partial\psi/\partial\theta$ with $\psi = 0$ on $Y = 0$, p_a is the constant pressure in the surrounding atmosphere, Q is the constant azimuthal volume flux of fluid per unit axial length crossing a station $\theta =$ constant, and $M\,(>0)$ is the constant fluid load on/in the cylinder (that is, the mass of fluid per unit length on/in the cylinder). Note that since the non-dimensionalisation of temperature given in (3.4) incorporates the factor $T_0 - T_\infty$, which can be either positive or negative, care is required when interpreting results for the non-dimensional temperature T^* in terms of the dimensional temperature T. For clarity the star superscripts on non-dimensional variables will be omitted henceforth. In terms of non-dimensional variables the fluid occupies $0 \le Y \le h$ for $-\pi < \theta \le \pi$, the general viscosity model $\mu = \mu(T)$ satisfies $\mu = 1$ and $\mathrm{d}\mu/\mathrm{d}T = -V$ when $T = 1$, and the exponential viscosity model (3.1) is given by

$$\mu = \exp(-V(T-1)). \tag{3.5}$$

For both coating and rimming flow at leading order in ϵ the governing equations become

$$\frac{\partial u}{\partial \theta} + \frac{\partial v}{\partial Y} = 0, \quad \frac{\partial}{\partial Y}\left(\mu \frac{\partial u}{\partial Y}\right) = \cos\theta, \quad \frac{\partial p}{\partial Y} = -\sin\theta, \quad \frac{\partial^2 T}{\partial Y^2} = 0, \tag{3.6}$$

together with the boundary conditions

$$u = 1, \quad v = 0 \quad \text{and} \quad T = 1 \quad \text{on} \quad Y = 0 \tag{3.7}$$

and

$$\frac{\partial u}{\partial Y} = 0, \quad p = 0 \quad \text{and} \quad \frac{\partial T}{\partial Y} + BT = 0 \quad \text{on} \quad Y = h, \tag{3.8}$$

where the Biot number, $B\,(\geq 0)$, defined by

$$B = \frac{\epsilon a \alpha_{\text{th}}}{k_{\text{th}}}, \tag{3.9}$$

is the appropriate non-dimensional measure of heat transfer to or from the atmosphere at the free surface. The special case $B = 0$ corresponds to a perfectly insulated free surface with no heat transfer to or from the atmosphere (i.e. $\partial T/\partial Y = 0$ on $Y = h$), while at leading order in the limit $B \to \infty$ the free surface is at the same uniform temperature as the atmosphere (i.e. $T = 0$ on $Y = h$).

Introducing the rescaled radial coordinate $y = Y/h$ (so that the fluid lies within the fixed range $0 \leq y \leq 1$) and solving (3.6) subject to (3.7) and (3.8) for the azimuthal velocity $u = u(y, \theta)$, the streamfunction $\psi = \psi(y, \theta)$[1] the pressure $p = p(y, \theta)$ and the temperature $T = T(y, \theta)$ yields

$$u = 1 - h^2 \cos\theta \int_0^y \frac{1 - \tilde{y}}{\mu(T(\tilde{y}, \theta))}\, \mathrm{d}\tilde{y}, \tag{3.10}$$

$$\begin{aligned} \psi &= hy - h^3 \cos\theta \int_0^y \int_0^{\bar{y}} \frac{1 - \tilde{y}}{\mu(T(\tilde{y}, \theta))}\, \mathrm{d}\tilde{y}\, \mathrm{d}\bar{y} \\ &= hy - h^3 \cos\theta \int_0^y \frac{(1 - \tilde{y})(y - \tilde{y})}{\mu(T(\tilde{y}, \theta))}\, \mathrm{d}\tilde{y}, \end{aligned} \tag{3.11}$$

$$p = h(1 - y)\sin\theta \tag{3.12}$$

and

$$T = 1 - \frac{Bhy}{1 + Bh}. \tag{3.13}$$

Hence the volume flux Q $(= \psi(1, \theta))$ is given by

$$Q = h \int_0^1 u\, \mathrm{d}y = h - h^3 \cos\theta \int_0^1 \int_0^y \frac{1 - \tilde{y}}{\mu(T(\tilde{y}, \theta))}\, \mathrm{d}\tilde{y}\, \mathrm{d}y, \tag{3.14}$$

[1]Note that the rescaled stream function $\psi = \psi(y, \theta)$ satisfies $u = \frac{1}{h}\frac{\partial \psi}{\partial y}$ and $v = -\frac{\partial \psi}{\partial \theta} + \frac{y}{h}\frac{\mathrm{d}h}{\mathrm{d}\theta}\frac{\partial \psi}{\partial y}$.

which may be re-written as

$$Q = h - \frac{h^3 \cos\theta}{3} f, \tag{3.15}$$

where $f = f(\theta)$ (> 0) is a measure of the fluidity of the fluid film (herein referred to simply as the fluidity), defined by

$$f = 3\int_0^1 \int_0^y \frac{1-\tilde{y}}{\mu(T(\tilde{y},\theta))}\,\mathrm{d}\tilde{y}\,\mathrm{d}y = 3\int_0^1 \frac{(1-y)^2}{\mu(T(y,\theta))}\,\mathrm{d}y. \tag{3.16}$$

In the special case of constant viscosity $\mu \equiv 1$ the fluidity is simply equal to unity, i.e. $f \equiv 1$.

In the present work we shall be concerned only with "full-film" solutions, i.e. solutions for which h is continuous, finite and non-zero for all $-\pi < \theta \leq \pi$, corresponding to a continuous film of fluid covering the entire outside or inside of the cylinder. In particular, for such solutions equations (3.13) and (3.16) show that f depends on θ only through its dependence on h, and hence, using (3.15), only through its dependence on $\cos\theta$. Hence h, u and T depend on θ only through $\cos\theta$, and so the flow has top-to-bottom symmetry (but not left-to-right symmetry). This symmetry is due to the balance between the viscous and gravitational forces at leading order and would not be found if the higher order term corresponding to pressure gradients in the θ direction was included. Moreover, at the top and the bottom of the cylinder ($\theta = \pm\pi/2$) the film thickness is simply $h = Q$ (from which we trivially deduce that $Q > 0$) and the velocity is a uniform (i.e. independent of y) "plug flow" $u \equiv 1$ across the film.

The fluid load in/on the cylinder, M (> 0), is given by

$$M = \int_{-\pi}^{\pi} h\,\mathrm{d}\theta = 2\int_0^{\pi} h\,\mathrm{d}\theta. \tag{3.17}$$

With the viscosity model $\mu = \mu(T)$ prescribed, the film thickness h is determined in terms of Q by the algebraic equation (3.15) in which f is given by (3.16). The value of Q is determined from either an appropriate criticality condition (given in Section 3.4) or from the condition of prescribed load using (3.17). The properties and behaviour of the solutions in these two cases are discussed in detail in

Sections 3.4 and 3.5, respectively, but in both cases, the solutions for u, ψ, p and T are given explicitly by (3.10)–(3.13), respectively.

3.2 The Special Case of Constant Viscosity

If either there is no heat transfer to or from the atmosphere at the free surface (i.e. in dimensional terms if $\alpha_{\text{th}} = 0$) so that $B = 0$ (in which case the fluid film is isothermal with constant temperature $T \equiv 1$) or the viscosity is independent of temperature (i.e. in dimensional terms if $\lambda = 0$) so that $V = 0$ (in which case the fluid film is non-isothermal with non-constant temperature $T \not\equiv 1$), then the fluid has constant viscosity $\mu \equiv 1$ and fluidity $f \equiv 1$. In either case we recover the classical constant-viscosity solution derived by Moffatt [7], denoted by $h = h_0$, $u = u_0$, $\psi = \psi_0$, $Q = Q_0$ and $M = M_0$, where

$$u_0 = 1 - \frac{h_0^2 \cos\theta}{2}(2 - y)y, \tag{3.18}$$

$$\psi_0 = h_0 y - \frac{h_0^3 \cos\theta}{6}(3 - y)y^2, \tag{3.19}$$

$$Q_0 = h_0 - \frac{h_0^3 \cos\theta}{3} \tag{3.20}$$

and

$$M_0 = 2\int_0^\pi h_0 \,\mathrm{d}\theta. \tag{3.21}$$

Figure 3.2 shows contours of the flux Q_0 given by (3.20) in the θ/π–h_0 plane, which, since they are by definition curves on which $Q_0 =$ constant, represent candidate solutions for the free surface $h_0 = h_0(\theta)$. In particular, figure 3.2 shows that full-film solutions are possible only for values of Q_0 satisfying $0 < Q_0 \leq Q_{\text{c}0}$, where $Q_{\text{c}0} = 2/3$ denotes the flux of the critical solution above which full-film solutions are not possible, and that these solutions have loads M_0 satisfying $0 < M_0 \leq M_{\text{c}0}$, where $M_{\text{c}0}$ denotes the load of the critical solution. A detailed description of the other (i.e. non-full-film) solutions of (3.20) is given by Duffy and Wilson [41].

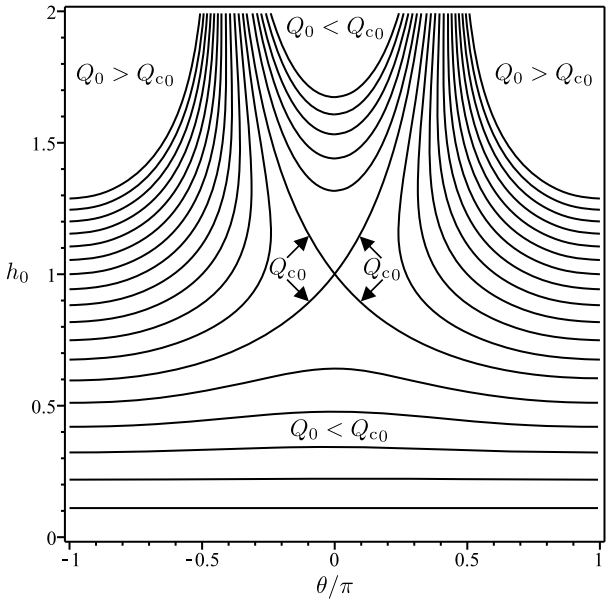

Figure 3.2: Contours of the flux in the constant-viscosity case, Q_0, given by (3.20) in the θ/π–h_0 plane. The contours are drawn for $Q_0/Q_{c0} = 1/6,\ 1/3,\ 1/2,\ \ldots,\ 3$, where $Q_{c0} = 2/3$.

When $0 < Q_0 \leq Q_{c0}$ the full-film solution of (3.20) for h_0 may be written explicitly in terms of Q_0 and θ as

$$h_0 = \begin{cases} \dfrac{2}{(\cos\theta)^{1/2}} \cos\left[\dfrac{2\pi}{3} - \dfrac{1}{3}\cos^{-1}\left(-\dfrac{3}{2}Q_0[\cos\theta]^{1/2}\right)\right] & \text{if } |\theta| < \pi/2, \\ Q_0 & \text{if } |\theta| = \pi/2, \\ \dfrac{2}{(-\cos\theta)^{1/2}} \sinh\left[\dfrac{1}{3}\sinh^{-1}\left(\dfrac{3}{2}Q_0[-\cos\theta]^{1/2}\right)\right] & \text{if } \pi/2 < |\theta| \leq \pi, \end{cases} \tag{3.22}$$

and has load M_0 satisfying $0 < M_0 \leq M_{c0}$ given by (3.21). The critical solution, denoted by $h_0 = h_{c0}$, $u_0 = u_{c0}$ and $\psi_0 = \psi_{c0}$, is obtained by substituting $Q_0 = Q_{c0} = 2/3$ into (3.18), (3.19) and (3.22), and from (3.21) has load $M_0 = M_{c0}$, where

$$M_{c0} = 2\int_0^\pi h_{c0}\,\mathrm{d}\theta \simeq 4.44272. \tag{3.23}$$

As figure 3.2 shows, the critical film thickness h_{c0} has a corner at $\theta = 0$ (with corresponding corners in all of the other streamlines $\psi_{c0} =$ constant also at $\theta = 0$)

given by $h_{c0} = 1 - H_{c0}|\theta| + O(\theta^2)$, where the magnitude of the slope of the corner, denoted by H_{c0}, is given by $H_{c0} = 1/\sqrt{6} \simeq 0.40825$.[2] It is worth mentioning that at the corner the fluid undergoes infinite acceleration and so the lubrication theory breaks down; the corner could be "smoothed out" by the inclusion of higher order effects. Wilson et al. [39] obtained an inner expansion for the solution near $\theta = 0$ for the case of constant viscosity and showed that even in the absence of surface tension (which one would certainly assume smooths out the corner) the inclusion of higher order terms eliminated the corner. In what follows we will not obtain the inner solution near $\theta = 0$ since doing so would complicate the full solution enormously and obscure the interpretation of the effects of interest, namely the non-isothermal effects.

3.3 The General Case of Non-Constant Viscosity

In general, if there is heat transfer to or from the atmosphere at the free surface (i.e. in dimensional terms if $\alpha_{th} > 0$) so that $B > 0$ and the viscosity depends on temperature (i.e. in dimensional terms if $\lambda > 0$) so that $V \neq 0$, then the fluid film is non-isothermal with, in general, non-constant temperature, viscosity and fluidity. In the particular case of the exponential viscosity model (3.5) we have

$$\mu = \exp(-V(T-1)) = \exp\left(\frac{BVhy}{1+Bh}\right) = \exp(\mathcal{V}y), \tag{3.24}$$

where, for brevity, we have introduced the notation $\mathcal{V} = \mathcal{V}(\theta)$ defined by

$$\mathcal{V} = \frac{BVh}{1+Bh}, \tag{3.25}$$

so that (3.10) yields the azimuthal velocity

$$u = 1 - \frac{h^2\cos\theta}{\mathcal{V}^2}\left[\mathcal{V} - 1 + (1 - \mathcal{V}(1-y))\exp(-\mathcal{V}y)\right], \tag{3.26}$$

[2]Note that Moffatt [7] gave slightly inaccurate values of M_{c0} and H_{c0}, corresponding to $M_{c0} = 4.428$ and $H_{c0} = 0.577$ in the present notation.

(3.11) yields the stream function

$$\psi = hy - \frac{h^3 \cos\theta}{\mathcal{V}^3}\left[(\mathcal{V}-1)(\mathcal{V}y-1) + 1 - (2-\mathcal{V}(1-y))\exp(-\mathcal{V}y)\right] \qquad (3.27)$$

and (3.16) yields the fluidity

$$f = \frac{3}{\mathcal{V}^3}\left[(\mathcal{V}-1)^2 + 1 - 2\exp(-\mathcal{V})\right]. \qquad (3.28)$$

Note that the azimuthal velocity profile (3.26) is, in general, very different from the simple parabolic velocity profile in the constant-viscosity case (3.18), and that the fluidity (3.28) is a monotonically decreasing function of $\mathcal{V}$ satisfying $f = O(\exp(-\mathcal{V})/(-\mathcal{V})^3) \to \infty$ as $\mathcal{V} \to -\infty$, $f = 1 + O(\mathcal{V})$ as $\mathcal{V} \to 0$, and $f = O(1/\mathcal{V}) \to 0^+$ as $\mathcal{V} \to \infty$.

Figure 3.3 shows contours of the flux Q given by (3.15) and (3.28) when $B = 1$ for (a) $V = -5$ and (b) $V = 5$. These plots are typical of those for all values of B and V, and show that, as in the constant-viscosity case, there is a critical flux $Q_c = Q_c(B, V)$ with a corresponding critical load $M_c = M_c(B, V)$ (both of which, of course, now depend on both B and V) such that full-film solutions exist only for $0 < Q \leq Q_c$ (i.e. for $0 < M \leq M_c$). For future reference, the corresponding critical solution (with $Q = Q_c$ and $M = M_c$) is denoted by $\mu = \mu_c$, $h = h_c$, $u = u_c$, $\psi = \psi_c$, $T = T_c$ and $f = f_c$.

Figure 3.4 shows streamlines of the flow (drawn for coating flow) when $B = 1$ and $V = 1$ for (a) a prescribed load $M = 4\,(< M_c \simeq 4.73590)$ and (b) the critical case $M = M_c$. In particular, in the case shown in Figure 3.4 the azimuthal velocity u is always in the same direction as the rotation of the cylinder (i.e. $u \geq 0$ for all $0 \leq y \leq 1$), and so backflow (i.e. $u < 0$ somewhere in $0 < y \leq 1$) does not occur. While this is by far the most common behaviour (i.e. for most values of B and V backflow does not occur), unlike in the special case of constant viscosity in which backflow never occurs, in Section 3.6 we will show that in the general case of non-constant viscosity there is a region of the B–V parameter plane in which backflow occurs in a region on the right-hand side of the cylinder containing the point on the free surface at $\theta = 0$ (i.e. the point $y = 1$ and $\theta = 0$).

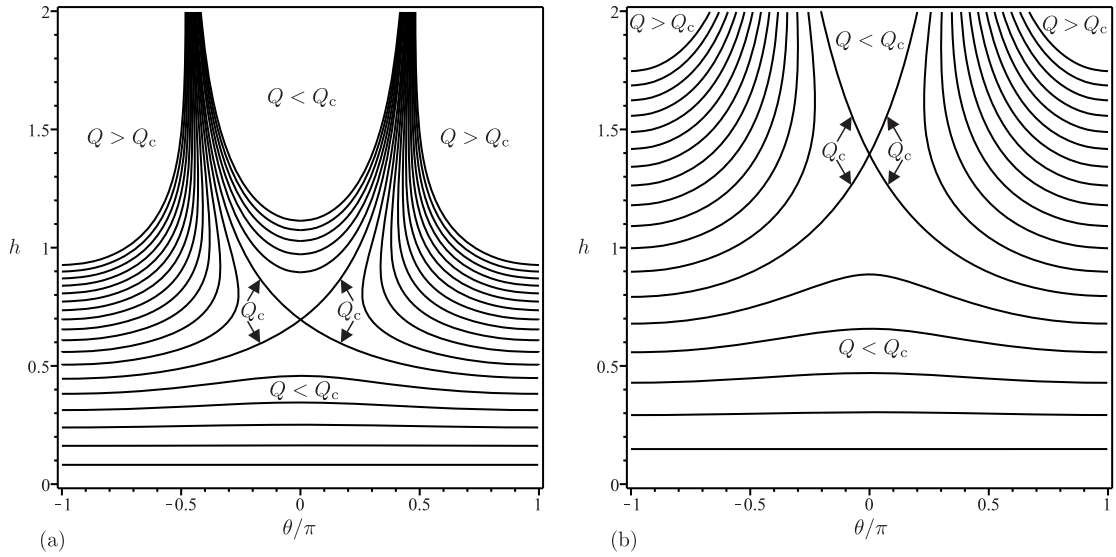

Figure 3.3: Contours of the flux in the non-constant-viscosity case, Q, given by (3.15) and (3.28) in the θ/π–h plane when $B = 1$ for (a) $V = -5$ and (b) $V = 5$. The contours are drawn for $Q/Q_c = 1/6,\ 1/3,\ 1/2,\ \ldots,\ 3$, where (a) $Q_c \simeq 0.49107$ and (b) $Q_c \simeq 0.89514$.

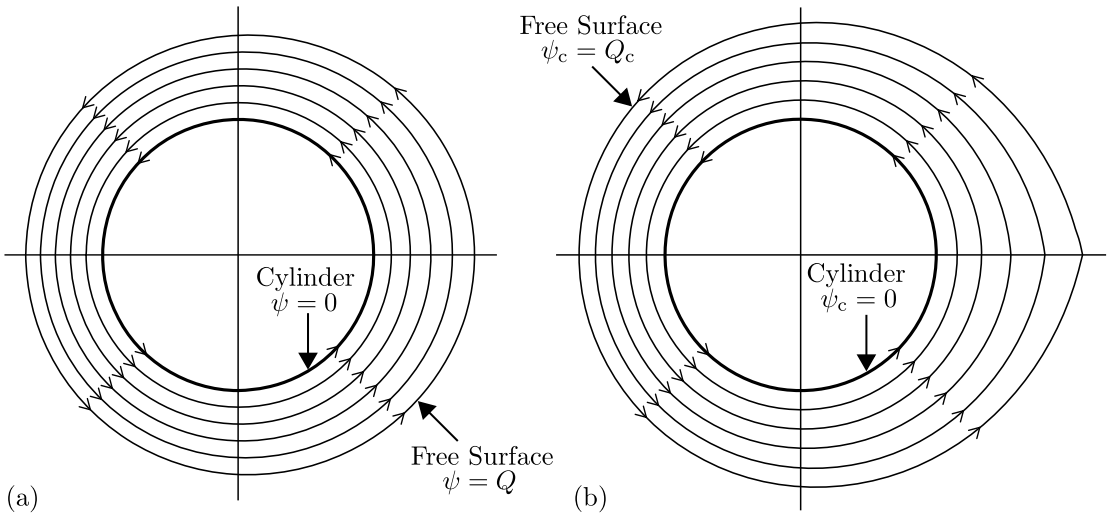

Figure 3.4: Streamlines of the flow (drawn for coating flow) plotted for $\psi/Q = 0$ (the cylinder), 1/5, 2/5, 3/5, 4/5 and 1 (the free surface) when $B = 1$ and $V = 1$ for (a) a prescribed load $M = 4\,(< M_c \simeq 4.73590)$ with $Q \simeq 0.62083\,(< Q_c \simeq 0.70942)$ and (b) the critical case $M = M_c$ with $Q = Q_c$.

3.4 The Critical Solution

In this Section we consider the properties and behaviour of the non-constant-viscosity critical solution with load $M = M_c$ introduced in Section 3.3 such that full-film solutions exist only for $0 < M \leq M_c$. Not only is this generalisation of the classical constant-viscosity critical solution of some interest in its own right, but, as we shall see subsequently in Section 3.5, it is crucial to understanding the properties and behaviour of solutions with a prescribed load.

As figures 3.2 and 3.3 clearly show, the unique feature of the critical solution is that Q has a saddle point at $\theta = 0$ and $h = h_c(0)$, at which point $\partial Q/\partial\theta = 0$ and $\partial Q/\partial h = 0$, which leads to the criticality condition

$$\frac{\mathrm{d}}{\mathrm{d}h}\left(\frac{fh^3}{3}\right) = 1 \tag{3.29}$$

evaluated at $\theta = 0$. For the exponential viscosity model (3.24) the criticality condition (3.29) yields

$$\mathcal{V}^2 + 2\mathcal{V}(V-2) - 2V + 6 - B^2V(V-\mathcal{V})^2 - 2(\mathcal{V} - V + 3)\exp(-\mathcal{V}) = 0 \tag{3.30}$$

evaluated at $\theta = 0$, where $\mathcal{V}$ is given by (3.25). Solving (3.30) yields the value of $\mathcal{V}(0)$ and hence the value of $h_c(0)$, and then (3.15) with f_c given by (3.28) yields the value of Q_c and the solution for h_c. The solutions for u_c, ψ_c, T_c and M_c are then given by (3.26), (3.27), (3.13) and (3.17), respectively. As in the constant-viscosity case, the critical film thickness h_c has a corner at $\theta = 0$ (with corresponding corners in all of the other streamlines $\psi_c =$ constant also at $\theta = 0$) given by $h_c = h_c(0) - H_c|\theta| + O(\theta^2)$, where the magnitude of the slope of the corner, denoted by $H_c = H_c(B, V)$ (which, of course, now depends on both B and V) is given by

$$H_c = \left(\frac{V^2\left[(\mathcal{V}-1)^2 + 1 - 2\exp(-\mathcal{V})\right]}{2B^2(V-\mathcal{V})^2\left[V^2 + 2V(\mathcal{V}-2) - 2\mathcal{V} + 6 - \left[(V-\mathcal{V}-2)^2+2\right]\exp(-\mathcal{V})\right]}\right)^{1/2} \tag{3.31}$$

evaluated at $\theta = 0$. In fact, rather unexpectedly, a general version of (3.31) valid for any viscosity model can be also obtained and is given by

$$H_{\mathrm{c}} = \left[\frac{\displaystyle\int_{\bar{T}}^{1} \frac{(T-\bar{T})^2}{\mu(T)} \mathrm{d}T}{\displaystyle 2\int_{\bar{T}}^{1} \frac{T(3T-2\bar{T})}{\mu(T)} \mathrm{d}T \int_{\bar{T}}^{1} \frac{(T-\bar{T})(3T-\bar{T})}{\mu(T)} \mathrm{d}T} \right]^{1/2}, \tag{3.32}$$

where $\bar{T} = T_{\mathrm{c}}(1,0) = 1/(1 + Bh_{\mathrm{c}}(0))$ is the critical free-surface temperature evaluated at $\theta = 0$.

Figure 3.5 shows the critical film thickness h_{c} plotted as a function of θ/π for a range of values of (a) B and (b) V, and figure 3.6 shows the critical film thickness at $\theta = 0$, $h_{\mathrm{c}}(0)$, plotted as a function of (a) B for a range of values of V and (b) V for a range of values of B. In particular, figures 3.5 and 3.6 show that h_{c} is a decreasing function of $|\theta|$, an increasing (decreasing) function of B for positive (negative) V, and an increasing function of V.

Figures 3.7 and 3.8 show the magnitude of the slope of the corner in the critical film thickness at $\theta = 0$, H_{c}, and the critical load M_{c}, respectively, plotted as functions of (a) B for a range of values of V and (b) V for a range of values of B. In particular, figures 3.7 and 3.8 show that both H_{c} and M_{c} are increasing (decreasing) functions of B for positive (negative) V, and increasing functions of V.

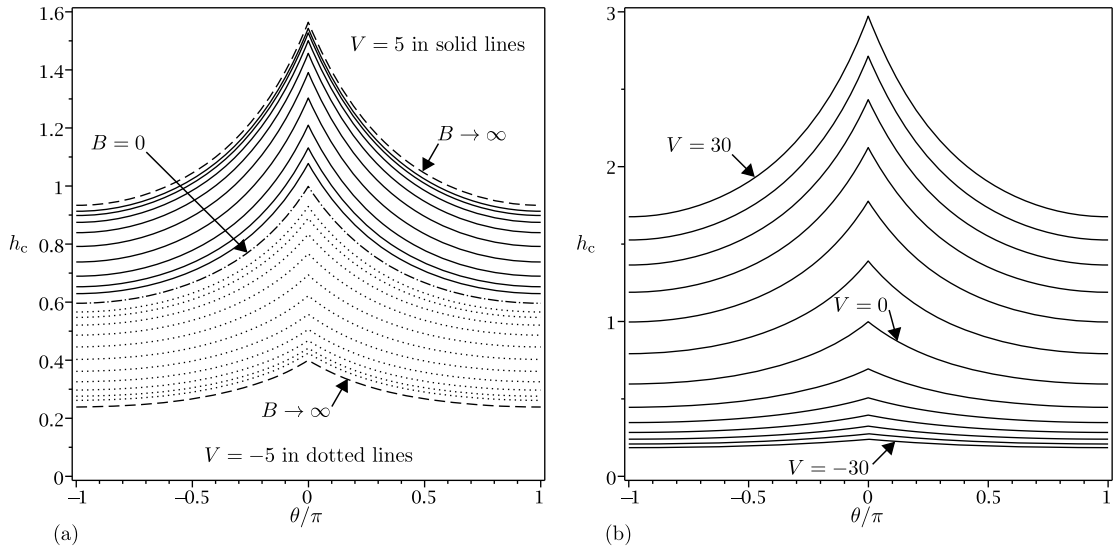

Figure 3.5: Critical film thickness h_c plotted as a function of θ/π for (a) $B = 0$ (dash-dot line) and $B = 10^n$ ($n = -1, -0.75, -0.5, \ldots, 1.5$) for $V = -5$ (dotted lines) and $B = 10^n$ ($n = -1, -0.75, -0.5, \ldots, 1$) for $V = 5$ (solid lines) and the leading-order asymptotic solution in the limit $B \to \infty$ for $V = -5$ and $V = 5$ (dashed lines), and (b) $V = -30, -25, -20, \ldots, 30$ for $B = 1$.

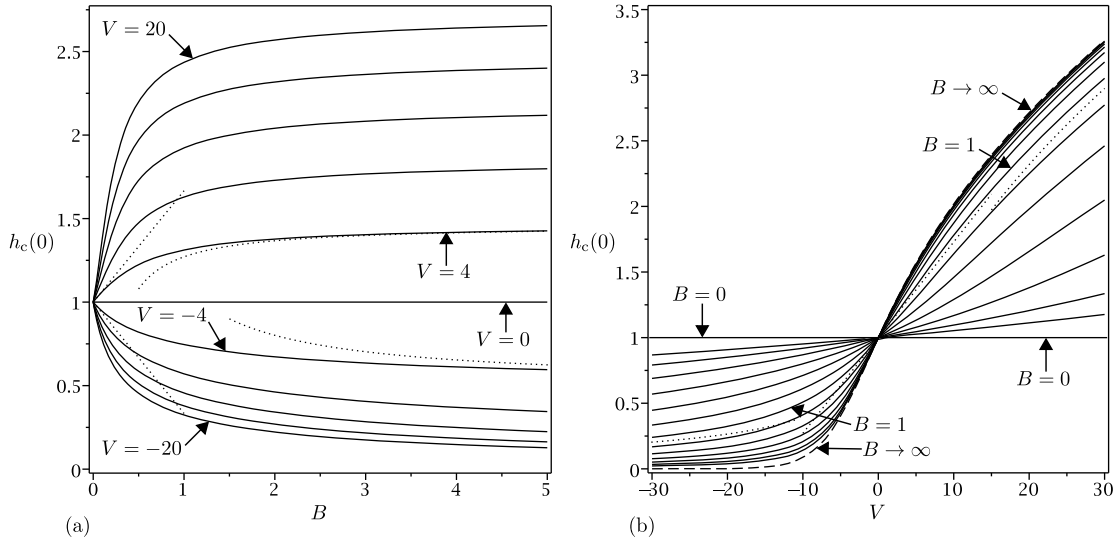

Figure 3.6: Critical film thickness at $\theta = 0$, $h_c(0)$, plotted as a function of (a) B for $V = -20, -16, -12, \ldots, 20$ with the asymptotic solutions in the limits $B \to 0^+$ and $B \to \infty$ for $V = -4$ and 4 (dotted lines), and (b) V for $B = 0$ and $B = 10^n$ ($n = -1.5, -1.25, -1, \ldots, 1.5$) with the asymptotic solutions in the limits $V \to 0$, $V \to \infty$ and $V \to -\infty$ for $B = 1$ (dotted lines) and the leading-order asymptotic solution in the limit $B \to \infty$ (dashed line).

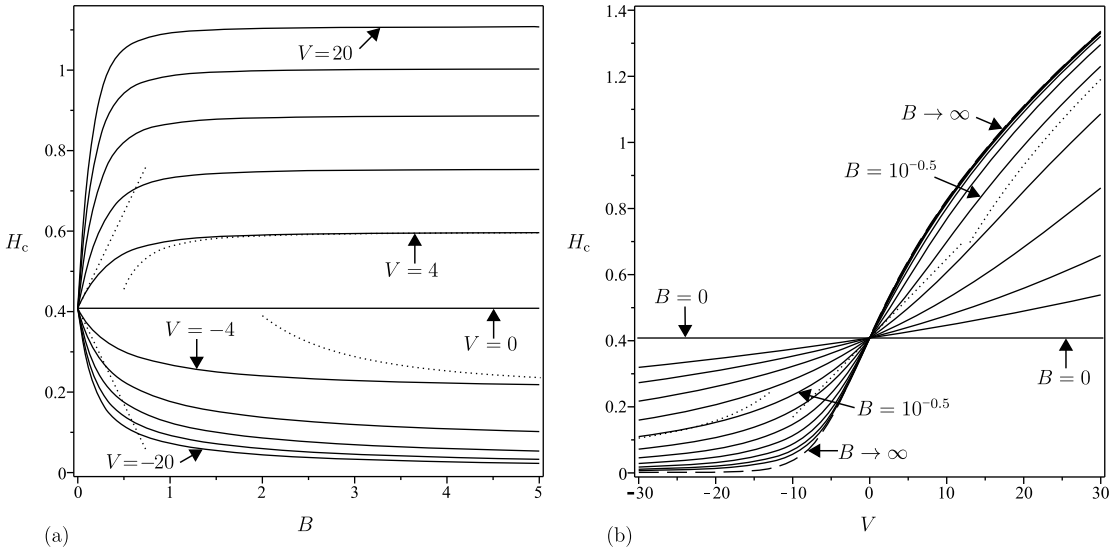

Figure 3.7: Magnitude of the slope of the corner in the critical film thickness at $\theta = 0$, H_c, plotted as a function of (a) B for $V = -20, -16, -12, \ldots, 20$ with the asymptotic solutions in the limits $B \to 0^+$ and $B \to \infty$ for $V = -4$ and 4 (dotted lines), and (b) V for $B = 0$ and $B = 10^n$ ($n = -1.5, -1.25, -1, \ldots, 1$) with the asymptotic solutions in the limits $V \to 0$, $V \to \infty$ and $V \to -\infty$ for $B = 10^{-0.5}$ (dotted lines) and the leading-order asymptotic solution in the limit $B \to \infty$ (dashed line).

Figure 3.9 shows critical velocity profiles u_c at various values of θ in the range $0 \le \theta \le \pi$ when $B = 1$ for (a) $V = -5$ and (b) $V = 5$. The corresponding profiles in the range $-\pi < \theta < 0$ follow immediately from the top-to-bottom symmetry of the flow. In particular, figure 3.9 shows that u_c is an increasing function of $|\theta|$, a decreasing (increasing) function of y on the right-hand side $0 \le |\theta| < \pi/2$ (the left-hand side $\pi/2 < |\theta| \le \pi$) of the cylinder, and a uniform plug flow $u_c \equiv 1$ at the top and bottom of the cylinder $|\theta| = \pi/2$. Figure 3.10 shows the critical free-surface velocity at $\theta = 0$, $u_c(1, 0)$, plotted as a function of (a) B for a range of values of V and (b) V for a range of values of B. In particular, figure 3.10 shows that $u_c(1, 0)$ is an increasing (decreasing) function of B for positive (negative) V, an increasing function of V for positive V, but a non-monotonic function of V for negative V.

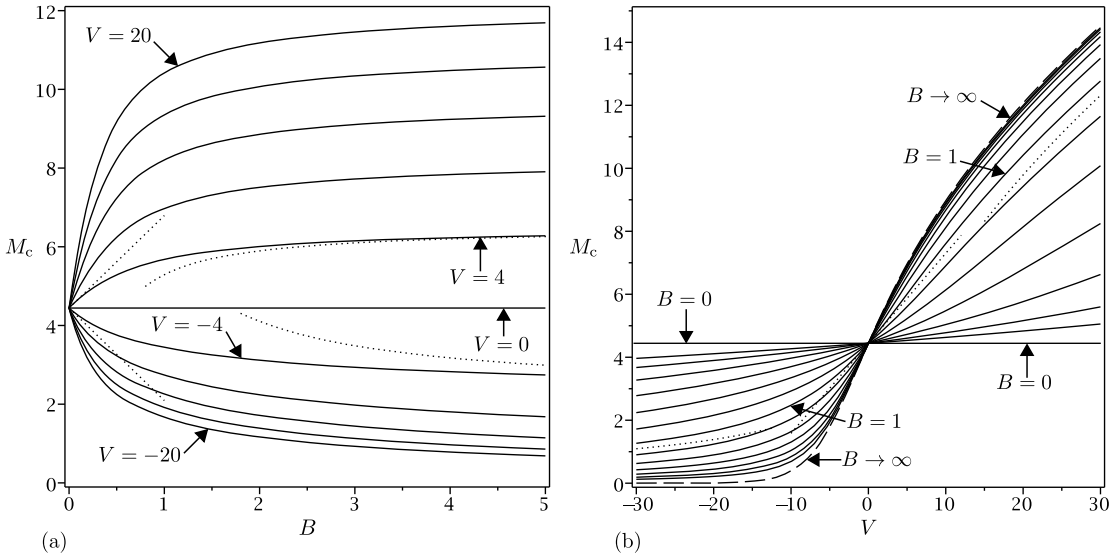

Figure 3.8: Critical load M_c plotted as a function of (a) B for $V = -20, -16, -12, \ldots, 20$ with the asymptotic solutions in the limits $B \to 0^+$ and $B \to \infty$ for $V = -4$ and 4 (dotted lines), and (b) V for $B = 0$ and $B = 10^n$ ($n = -1.5, -1.25, -1, \ldots, 1.5$) with the asymptotic solutions in the limits $V \to 0$, $V \to \infty$ and $V \to -\infty$ for $B = 1$ (dotted lines) and the leading-order asymptotic solution in the limit $B \to \infty$ (dashed line).

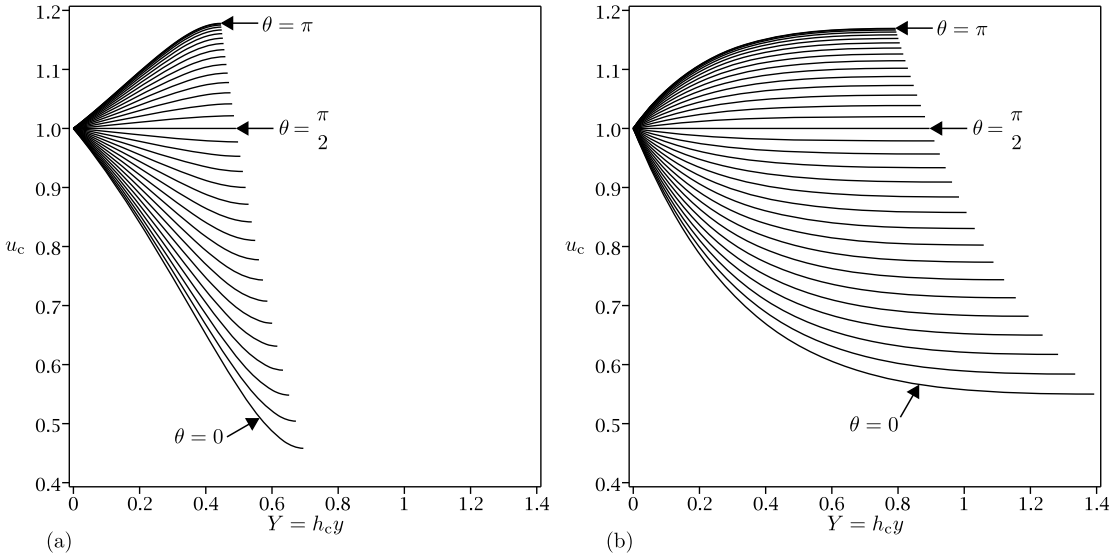

Figure 3.9: Critical velocity profiles u_c plotted as a function of $Y = h_c y$ at $\theta = 0$, $\pi/32$, $\pi/16$, $\ldots$, π when $B = 1$ for (a) $V = -5$ and (b) $V = 5$.

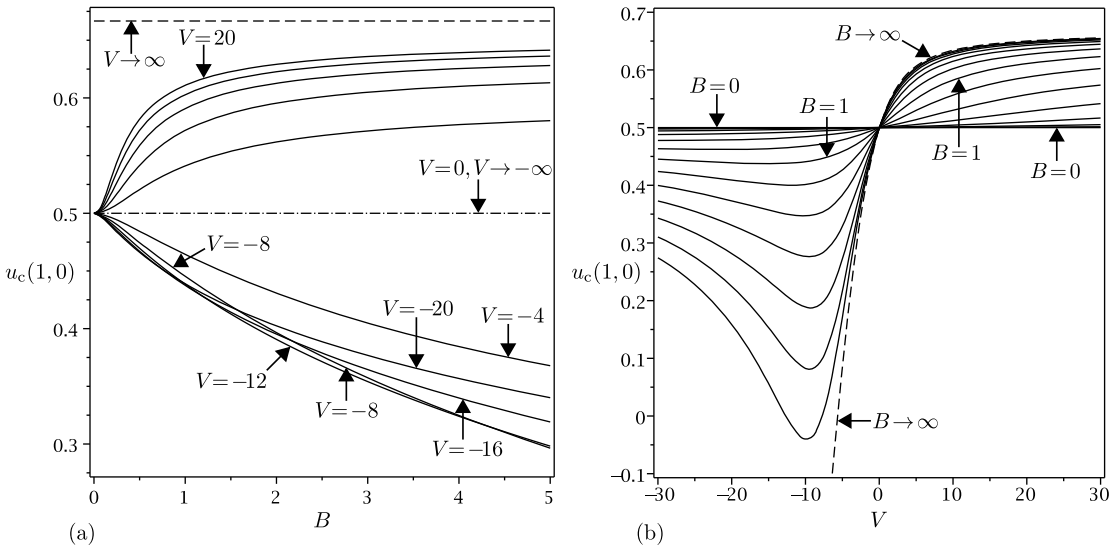

Figure 3.10: Critical free-surface velocity at $\theta = 0$, $u_c(1,0)$, plotted as a function of (a) B for $V = -20, -16, -12, \ldots, 20$ with the leading-order asymptotic solution in the limit $V \to \infty$ (i.e. $u_c(1,0) = 2/3$) (dashed line) and the solution for $V = 0$ and the leading-order asymptotic solution in the limit $V \to -\infty$ (i.e. $u_c(1,0) = 1/2$) (dash-dot line), and (b) V for $B = 0$ (i.e. $u_c(1,0) = 1/2$) and $B = 10^n$ ($n = -1.5, -1.25, -1, \ldots, 1.5$) with the leading-order asymptotic solution in the limit $B \to \infty$ (dashed line).

Figure 3.11 shows the critical free-surface temperature at $\theta = 0$, $T_c(1,0)$, plotted as a function of (a) B for a range of values of V and (b) V for a range of values of B. In particular, figure 3.11 shows that $T_c(1,0)$ is a decreasing function of both B and V.

In order to complete our understanding of the effects of varying B and V on the critical solution, in the following Subsections we analyse the behaviour of the critical solution in the asymptotic limits $B \to 0^+$, $B \to \infty$, $V \to 0$, $V \to \infty$ and $V \to -\infty$.

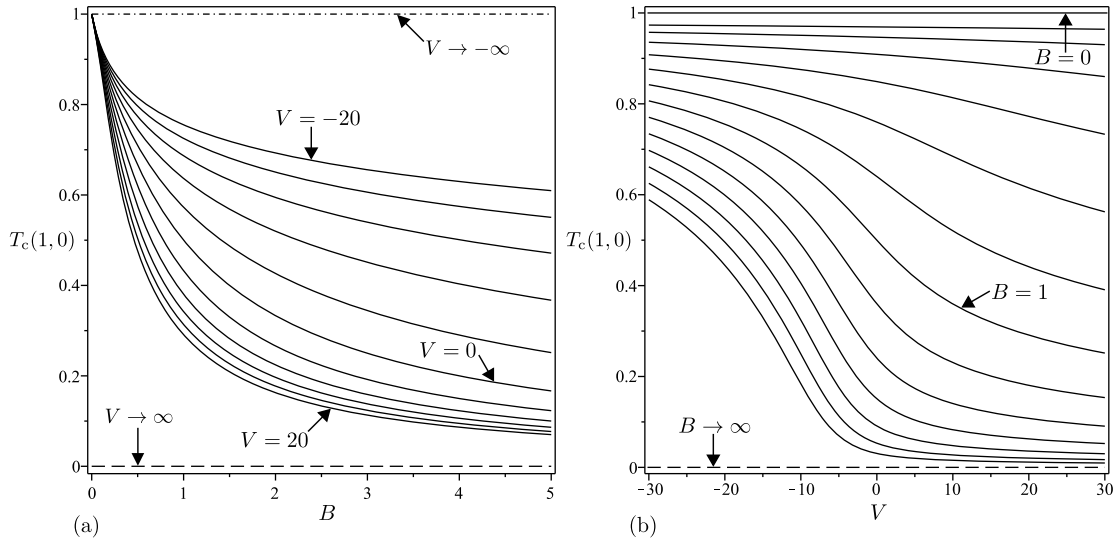

Figure 3.11: The critical free-surface temperature at $\theta = 0$, $T_c(1,0)$, plotted as a function of (a) B for $V = -20, -16, -12, \ldots, 20$ with the leading-order asymptotic solution in the limit $V \to \infty$ (i.e. $T_c(1,0) = 0$) (dashed line) and the leading-order asymptotic solution in the limit $V \to -\infty$ (i.e. $T_c(1,0) = 1$) (dash-dot line), and (b) V for $B = 0$ (i.e. $T_c(1,0) = 1$) and $B = 10^n$ ($n = -1.5, -1.25, -1, \ldots, 1.5$) with the leading-order asymptotic solution in the limit $B \to \infty$ (i.e. $T_c(1,0) = 0$) (dashed line).

3.4.1 The limit of weak heat transfer $B \to 0^+$

At leading order in the limit of weak heat transfer at the free surface, $B \to 0^+$, the free surface is perfectly insulated (i.e. $\partial T_c/\partial y = 0$ on $y = 1$) and the fluid film is isothermal with constant temperature $T_c \equiv 1$, viscosity $\mu_c \equiv 1$ and fluidity $f_c \equiv 1$. Hence the leading-order solutions for h_c, H_c, M_c and u_c are simply the constant-viscosity solutions h_{c0}, H_{c0}, M_{c0} and u_{c0} given in Section 3.2. The effect of variations in B first appear at $O(B)$, to which order the solutions for h_c, H_c, M_c, u_c and T_c are given by

$$h_c = h_{c0} + \frac{BVh_{c0}}{24}(3h_{c0} + 1) + O(B^2), \tag{3.33}$$

$$H_c = H_{c0} + \frac{7BV}{24\sqrt{6}} + O(B^2), \tag{3.34}$$

$$M_{\rm c} = M_{\rm c0} + \frac{BV}{24}(3C_{B0} + M_{\rm c0}) + O(B^2), \tag{3.35}$$

$$u_{\rm c} = u_{\rm c0} - \frac{BVh_{\rm c0}^2 y\cos\theta}{24}\left[h_{\rm c0}(8y^2 - 15y + 6) + 2 - y\right] + O(B^2) \tag{3.36}$$

and

$$T_{\rm c} = 1 - Bh_{\rm c0}y - \frac{B^2 h_{\rm c0}y}{24}\left[V(3h_{\rm c0} + 1) - 24h_{\rm c0}\right] + O(B^3), \tag{3.37}$$

where the constant C_{B0} is given by

$$C_{B0} = 2\int_0^\pi h_{\rm c0}^2\,{\rm d}\theta \simeq 3.21962. \tag{3.38}$$

Note that the solutions (3.33)–(3.37) are valid for a general viscosity model satisfying $\mu = 1$ and ${\rm d}\mu/{\rm d}T = -V$ when $T_{\rm c} = 1$ to the order shown (but not to higher orders). The same is true for the asymptotic solution in the limit of weak thermoviscosity $V \to 0$ presented subsequently in Subsection 3.4.3. The solution (3.37) shows that the effect of weak heat transfer at the free surface is to decrease the temperature from its constant isothermal value $T_{\rm c} \equiv 1$ throughout the fluid film, and thus to increase (decrease) the viscosity from its constant isothermal value $\mu_{\rm c} \equiv 1$, causing $h_{\rm c}$, $H_{\rm c}$ and $M_{\rm c}$ to increase (decrease) from their isothermal values when $V > 0$ ($V < 0$). Furthermore, since the sign of the first-order term in (3.36) is simply the sign of $-V\cos\theta$, the effect of weak heat transfer at the free surface is to decrease (increase) $u_{\rm c}$ from its isothermal value $u_{\rm c0}$ when $V\cos\theta > 0$ ($V\cos\theta < 0$). The asymptotic results (3.33)–(3.35) are included in figures 3.6(a), 3.7(a) and 3.8(a), respectively.

3.4.2 The limit of strong heat transfer $B \to \infty$

At leading order in the limit of strong heat transfer at the free surface, $B \to \infty$, the free surface is at the same uniform temperature as the atmosphere (i.e. $T_{\rm c} = 0$ on $y = 1$) and the fluid film has non-constant temperature $T_{\rm c} = \hat{T} = 1 - y$ and viscosity $\mu_{\rm c} = \hat{\mu} = \mu(\hat{T})$. As Duffy and Wilson [129] showed, from (3.10) and (3.16) the leading-order solutions for $u_{\rm c}$ and $f_{\rm c}$, denoted by $\hat{u}$ and $\hat{f}$, are given by

$$\hat{u} = 1 - \hat{h}^2\cos\theta\int_{\hat{T}}^1 \frac{T}{\mu(T)}\,{\rm d}T \tag{3.39}$$

and

$$\hat{f} = 3\int_0^1 \frac{T^2}{\mu(T)}\,\mathrm{d}T, \tag{3.40}$$

where $\hat{h}$ denotes the leading-order solution for h_c. Moreover, since, for any viscosity model, $\hat{f} = \hat{f}(V)$ is a constant (and not a function of θ as, in general, f is) the leading-order solutions for h_c, H_c and M_c, denoted by $\hat{h}$, $\hat{H}$ and $\hat{M}$, are given simply by rescaling the corresponding constant-viscosity solutions $h_{\mathrm{c}0}$, $H_{\mathrm{c}0}$, $Q_{\mathrm{c}0}$ and $M_{\mathrm{c}0}$ according to $\hat{h} = \hat{f}^{-1/2}h_{\mathrm{c}0}$, $\hat{H} = \hat{f}^{-1/2}H_{\mathrm{c}0} = (6\hat{f})^{-1/2}$, $\hat{Q} = \hat{f}^{-1/2}Q_{\mathrm{c}0}$ and $\hat{M} = \hat{f}^{-1/2}M_{\mathrm{c}0}$. For the exponential viscosity model $\mathcal{V} \sim V$ in the limit $B \to \infty$, and so the leading-order solutions for μ_c, u_c, ψ_c and f_c are given simply by (3.24), (3.26)–(3.28) with $\mathcal{V}$ replaced by V, respectively.

As might have been anticipated, this simple re-scaling property does not extend to higher orders. Specifically, to higher order the solutions for h_c, H_c, M_c, u_c and T_c are given by

$$h_\mathrm{c} = \hat{h} + \frac{3-(V+3)\hat{f}}{3B\hat{f}} + O\left(\frac{1}{B^2}\right), \tag{3.41}$$

$$H_\mathrm{c} = \hat{H} + \frac{V^2\hat{f}^2 + 3(V+6)\hat{f} - 18}{3B^2(6\hat{f})^{3/2}} + O\left(\frac{1}{B^3}\right), \tag{3.42}$$

$$M_\mathrm{c} = \hat{M} + \frac{2\pi[3-(V+3)\hat{f}]}{3B\hat{f}} + O\left(\frac{1}{B^2}\right), \tag{3.43}$$

$$\begin{aligned} u_\mathrm{c} = \hat{u} - \frac{h_{\mathrm{c}0}\cos\theta}{3V^2B\hat{f}^{3/2}}\Big[&\Big\{V(3y-5)\hat{f}+6\Big\}Vy\exp(-Vy) \\ &-\Big\{V(1+2V)\hat{f}+6(1-V)\Big\}(1-\exp(-Vy))\Big] + O\left(\frac{1}{B^2}\right) \end{aligned} \tag{3.44}$$

and

$$T_\mathrm{c} = \hat{T} + \frac{\hat{f}^{1/2}y}{Bh_{\mathrm{c}0}} - \frac{(3-V\hat{f})y}{3B^2h_{\mathrm{c}0}^2} + O\left(\frac{1}{B^3}\right). \tag{3.45}$$

The solution (3.45) shows that the effect of large-but-finite heat transfer at the free surface is to increase the temperature from its leading-order value $T_\mathrm{c} = \hat{T} = 1-y$ throughout the fluid film, and thus to decrease (increase) the viscosity from its leading-order value $\mu_\mathrm{c} = \hat{\mu} = \exp(Vy)$, causing h_c, H_c and M_c to decrease

(increase) from their leading-order values when $V > 0$ ($V < 0$). The asymptotic results (3.41)–(3.43) are included in figures 3.6(a), 3.7(a), and 3.8(a), respectively.

3.4.3 The limit of weak thermoviscosity $V \to 0$

At leading order in the limit of weak thermoviscosity, $V \to 0$, the fluid film has non-constant temperature $T_\mathrm{c} \not\equiv 1$ but constant viscosity $\mu_\mathrm{c} \equiv 1$ and fluidity $f_\mathrm{c} \equiv 1$. Hence, like in the limit $B \to 0^+$, the leading-order solutions for h_c, H_c, M_c and u_c are simply the constant-viscosity solutions $h_{\mathrm{c}0}$, $H_{\mathrm{c}0}$, $M_{\mathrm{c}0}$ and $u_{\mathrm{c}0}$ given in Section 3.2. The effect of variations in V first appear at $O(V)$, to which order the solutions for h_c, H_c, M_c, u_c and T_c are given by

$$h_\mathrm{c} = h_{\mathrm{c}0} + \frac{BVh_{\mathrm{c}0}[3(1+B)h_{\mathrm{c}0}+1]}{24(1+B)(1+Bh_{\mathrm{c}0})} + O(V^2), \tag{3.46}$$

$$H_\mathrm{c} = H_{\mathrm{c}0} + \frac{BV(3B^2+9B+7)}{24\sqrt{6}(1+B)^3} + O(V^2), \tag{3.47}$$

$$M_\mathrm{c} = M_{\mathrm{c}0} + \frac{BV}{12(1+B)} \int_0^\pi \frac{h_{\mathrm{c}0}[3(1+B)h_{\mathrm{c}0}+1]}{1+Bh_{\mathrm{c}0}} \,\mathrm{d}\theta + O(V^2), \tag{3.48}$$

$$u_\mathrm{c} = u_{\mathrm{c}0} - \frac{BVh_{\mathrm{c}0}^2 y\cos\theta[(1+B)h_{\mathrm{c}0}(8y^2-15y+6)+2-y]}{24(1+B)(1+Bh_{\mathrm{c}0})} + O(V^2) \tag{3.49}$$

and

$$T_\mathrm{c} = 1 - \frac{Bh_{\mathrm{c}0}y}{1+Bh_{\mathrm{c}0}} - \frac{B^2Vh_{\mathrm{c}0}y[3(1+B)h_{\mathrm{c}0}+1]}{24(1+B)(1+Bh_{\mathrm{c}0})^3} + O(V^2). \tag{3.50}$$

The solutions in this limit are somewhat similar to those in the limit $B \to 0^+$ described previously in Subsection 3.4.1 and have the corresponding physical interpretation. There is, however, one noteworthy difference. Whereas in the limit $B \to 0^+$ the sign of the first-order term in (3.36) is simply the sign of $-V\cos\theta$, in the present limit it is the sign of the somewhat more complicated expression $-V\cos\theta[(1+B)h_{\mathrm{c}0}(8y^2-15y+6)+2-y]$. Thus for $0 < h_{\mathrm{c}0} \leq 1/(1+B)$ and for $0 < y < y_{\mathrm{c}0}$ when $1/(1+B) < h_{\mathrm{c}0} \leq 1$ the effect of weak thermoviscosity is to decrease (increase) u_c from its isothermal value $u_{\mathrm{c}0}$ when $V\cos\theta > 0$ ($V\cos\theta < 0$), whereas for $y_{\mathrm{c}0} < y \leq 1$ when $1/(1+B) < h_{\mathrm{c}0} \leq 1$ the effect is the opposite, where

$y = y_{c0}$ $(0 < y_{c0} \leq 1)$ satisfies $(1+B)h_{c0}(8y^2-15y+6)+2-y = 0$. This behaviour is the first hint of the occurrence of the backflow described subsequently in Section 3.6. The asymptotic results (3.46)–(3.48) are included in figures 3.6(b), 3.7(b) and 3.8(b), respectively.

3.4.4 The limit of strong positive thermoviscosity $V \to \infty$

In the limit of strong positive thermoviscosity, $V \to \infty$, the solutions for h_c, H_c, M_c, u_c and T_c are given by

$$h_c = \frac{V^{1/2}h_{c0}}{\sqrt{3}} - \frac{1}{3B} + O\left(\frac{1}{V^{1/2}}\right), \tag{3.51}$$

$$H_c = \frac{V^{1/2}}{3\sqrt{2}} + \frac{\sqrt{2}(3B^2-1)}{18B^2V^{1/2}} + O\left(\frac{1}{V}\right), \tag{3.52}$$

$$M_c = \frac{V^{1/2}M_{c0}}{\sqrt{3}} - \frac{2\pi}{3B} + O\left(\frac{1}{V^{1/2}}\right), \tag{3.53}$$

$$u_c = 1 - \frac{h_{c0}^2\cos\theta}{3}[1-\exp(-Vy)] - \frac{\sqrt{3}h_{c0}\cos\theta}{9BV^{1/2}}[1-(3Vy+1)\exp(-Vy)] + O\left(\frac{1}{V}\right) \tag{3.54}$$

and

$$T_c = 1 - y + \frac{\sqrt{3}y}{BV^{1/2}h_{c0}} - \frac{2y}{B^2Vh_{c0}^2} + O\left(\frac{1}{V^{3/2}}\right). \tag{3.55}$$

These solutions show that at leading order in the limit of strong positive thermoviscosity the temperature is given by $T_c = 1-y$ and the viscosity $\mu_c = O(\exp(Vy))$ is exponentially large outside a narrow boundary layer of width $O(1/V) \ll 1$ near the cylinder $y = 0$, resulting in a uniform plug flow $u_c \equiv 1 - h_{c0}^2\cos\theta/3$ outside the boundary layer and a large film thickness and load of $O(V^{1/2}) \gg 1$. The asymptotic results (3.51)–(3.53) are included in figures 3.6(b), 3.7(b) and 3.8(b), respectively.

3.4.5 The limit of strong negative thermoviscosity $V \to -\infty$

In the limit of strong negative thermoviscosity, $V \to -\infty$, the solutions for h_c, H_c, M_c, u_c and T_c are given by

$$h_\mathrm{c} = \frac{1}{B(-V)}\left[\log\left(\frac{B^2V^2}{2}\right) - W_{V\infty} - 1\right] + O\left(\frac{\log(-V)^2}{V^2}\right), \tag{3.56}$$

$$H_\mathrm{c} = \frac{1}{B(-V)} + O\left(\frac{\log(-V)}{V^2}\right), \tag{3.57}$$

$$M_\mathrm{c} = \frac{1}{B(-V)}\left[2\pi\log\left(\frac{B^2V^2}{2}\right) - C_{V\infty} - 2\pi\right] + O\left(\frac{\log(-V)^2}{V^2}\right), \tag{3.58}$$

$$u_\mathrm{c} = 1 - \frac{\cos\theta}{B^2V^2}\left[\left(-\frac{B^2V^2W_{V\infty}}{2\cos\theta}\right)^y\left\{\left[\log\left(\frac{B^2V^2}{2}\right) - W_{V\infty}\right](1-y) + y\right\} - \log\left(\frac{B^2V^2}{2}\right) + W_{V\infty}\right] + O\left(\frac{\log(-V)^2}{-V}\right) \tag{3.59}$$

and

$$T_\mathrm{c} = 1 - \frac{y}{(-V)}\left[\log\left(\frac{B^2V^2}{2}\right) - W_{V\infty} - 1\right] + O\left(\frac{\log(-V)}{V^2}\right), \tag{3.60}$$

where the function $W_{V\infty} = W_{V\infty}(\theta)$ is given by

$$W_{V\infty} = W_0\left(-\frac{\cos\theta}{\mathrm{e}}\right) \tag{3.61}$$

and the constant $C_{V\infty}$ is given by

$$C_{V\infty} = 2\int_0^\pi W_{V\infty}\,\mathrm{d}\theta \simeq -0.73144, \tag{3.62}$$

in which $W_0 = W_0(x)$ denotes the principal real branch of the Lambert W function. Figure 3.12(a) shows the two real branches of the Lambert W function, which is defined to be the solution for $W = W(x)$ of $W\exp(W) = x$, namely the principal real branch $W_0(x)$ with domain $[-1/\mathrm{e}, \infty)$ and range $[-1, \infty)$ and the lower real branch $W_{-1}(x)$ with domain $[-1/\mathrm{e}, 0)$ and range $(-\infty, -1]$. Figure 3.12(b) shows the function $W_{V\infty}$ given by (3.61) plotted as a function of θ/π and, in particular, shows that the sign of $W_{V\infty}$ is simply the sign of $-\cos\theta$. The solutions (3.56)–(3.60) show that at leading order in the limit of strong negative thermoviscosity

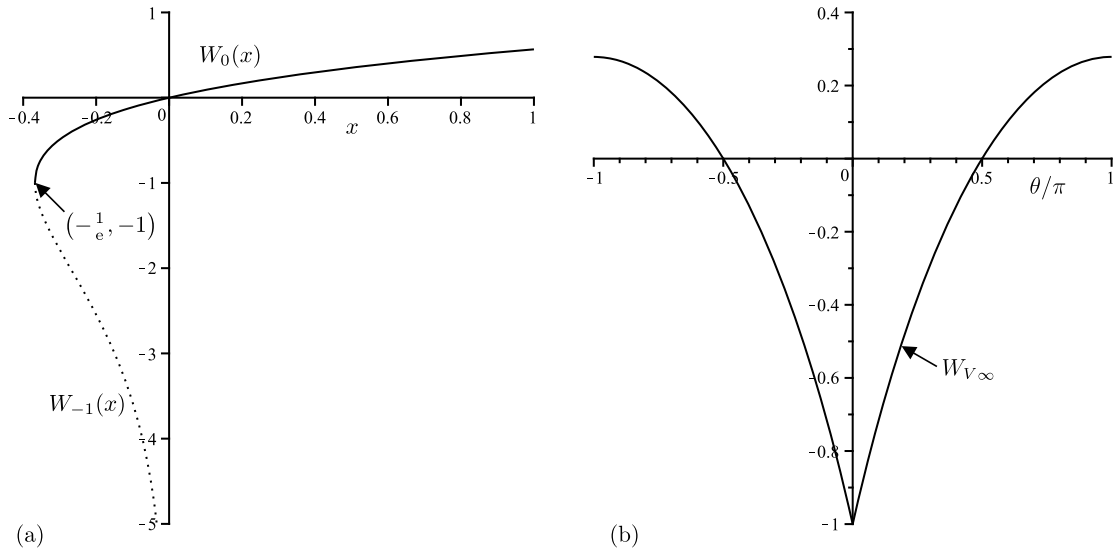

Figure 3.12: (a) The two real branches of the Lambert W function, $W_0(x)$ and $W_{-1}(x)$, plotted as functions of x. (b) The function $W_{V\infty} = W_0(-\cos\theta/\mathrm{e})$ plotted as a function of θ/π.

the temperature is given by $T_\mathrm{c} \equiv 1$ and the viscosity $\mu = O(V^{-2y})$ decreases from $O(1)$ at the cylinder $y = 0$ to $O((-V)^{-2}) \ll 1$ at the free surface $y = 1$, resulting in a velocity that increases (decreases) from $u_\mathrm{c} = 1$ at the cylinder [where there is a narrow boundary layer of width $O(1/\log(-V)) \ll 1$] to $u_\mathrm{c} = 1 + W_{V\infty}/2$ at the free surface [where there is another narrow boundary layer also of width $O(1/\log(-V)) \ll 1$] when $\cos\theta < 0$ ($\cos\theta > 0$), and a small film thickness and load of $O(\log(-V)/(-V)) \ll 1$. The asymptotic results (3.56)–(3.58) are included in figures 3.6(b), 3.7(b) and 3.8(b), respectively.

3.5 Full-Film Solution with a Prescribed Load

In this Section we consider the properties and behaviour of the non-constant-viscosity full-film solution with a prescribed load M. As described in Section 3.3, such solutions exist only when $0 < M \leq M_\mathrm{c}$, where M_c is the load of the critical solution described in Section 3.4 and shown in Figure 3.8. Thus for a prescribed

value of M such solutions exist, in general, only for restricted ranges of values of B and V, and the critical values of B and V for such solutions to exist, denoted by $B_{\rm c}$ and $V_{\rm c}$, are precisely the values of B and V for which the critical solution has load $M_{\rm c} = M$. The ranges of values of B and V depend on the relative size of the prescribed load M compared to the load of the critical solution in the limit $B \to 0^+$ (i.e. in the constant-viscosity case), namely $M_{\rm c0} \simeq 4.44272$, and the load of the critical solution in the limit $B \to \infty$, namely $\hat{M} = \hat{f}^{-1/2} M_{\rm c0}$, where $\hat{f} = \hat{f}(V)$ is given by (3.40), described previously. Specifically, as Figure 3.8(a) shows, for positive V there are no full-film solutions for any value of B when $M \geq \hat{M}$, full-film solutions for $B \geq B_{\rm c}$ when $M_{\rm c0} < M < \hat{M}$, and full-film solutions for all values of B when $M \leq M_{\rm c0}$, while for negative V there are no full-film solutions for any value of B when $M > M_{\rm c0}$, full-film solutions for $B \leq B_{\rm c}$ when $\hat{M} < M \leq M_{\rm c0}$, and full-film solutions for all values of B when $M \leq \hat{M}$. In particular, if we denote the value of V satisfying $M = \hat{M}$ by $V = V_\infty$, then there are full-film solutions in the limit $B \to \infty$ for $V \geq V_\infty$, but not for $V < V_\infty$. Similarly, as Figure 3.8(b) shows, for all values of B there are full-film solutions for $V \geq V_{\rm c}$, but not for $V < V_{\rm c}$. This behaviour is summarised in Figure 3.13, which shows the critical curves $(B_{\rm c}, V_{\rm c})$ for a range of values of M. For each value of M the corresponding critical curve $(B_{\rm c}, V_{\rm c})$ divides the B–V parameter plane into the region above the curve in which full-film solutions exist and the region below the curve in which they do not exist.

Figure 3.14 shows the film thickness h when $M = 2\,(< M_{\rm c0})$ plotted as a function of θ/π for a range of values of B for (a) $V = \pm 4$ and (b) $V = \pm 5$. Figure 3.14 shows that when $M = 2$ for $V = 5$, $V = 4$ and $V = -4$ (all of which satisfy $V > V_\infty \simeq -4.51567$) there are full-film solutions for all values of B, but for $V = -5 < V_\infty$ there are full-film solutions only for $B \leq B_{\rm c} \simeq 19.84427$. Figure 3.15(a) shows the film thickness h plotted as a function of θ/π for a range of values of B when $M = 6\,(> M_{\rm c0})$ and $V = 5$, in which case there are full-film solutions for $B \geq B_{\rm c} \simeq 0.99344$. Note that there is no corresponding plot for $M = 6\,(> M_{\rm c0})$

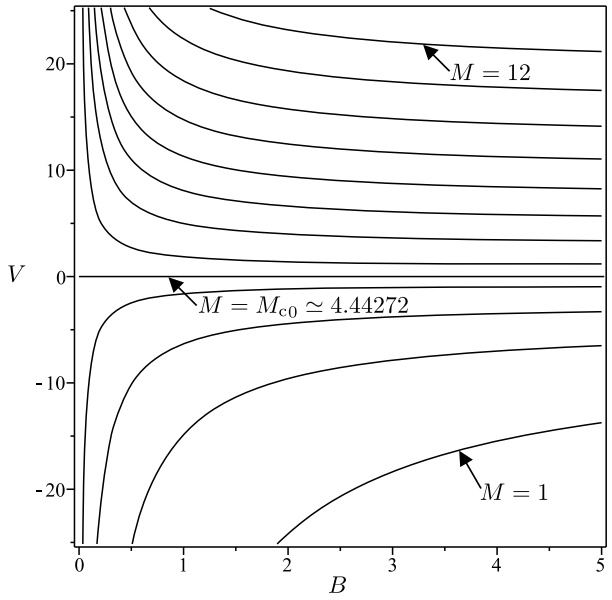

Figure 3.13: The critical curves (B_c, V_c) for $M = 1, 2, 3, \ldots, 12$ and $M = M_{c0} \simeq 4.44272$. For each value of M the corresponding curve (B_c, V_c) divides the B–V parameter plane into the region above the curve in which full-film solutions exist and the region below the curve in which they do not exist.

and $V = -5$ because there are no full-film solutions when $M > M_{c0}$ and $V < 0$. Figure 3.15(b) shows the film thickness h plotted as a function of θ/π for a range of values of V when $M = 2\,(< M_{c0})$ and $B = 1$, in which case there are full-film solutions for $V \geq V_c \simeq -14.83331\,(< 0)$. Note that the corresponding plot for $M = 6\,(> M_{c0})$ (which is omitted for brevity) is qualitatively similar to figure 3.15(b) except that $V_c > 0$. Figures 3.14 and 3.15 also show that h is a decreasing function of $|\theta|$, but, in contrast to the corresponding results for h_c shown in Figure 3.5, show that near $\theta = 0$ the film thickness h is a decreasing (increasing) function of B for positive (negative) V and a decreasing function of V, but that near $\theta = \pi$ it behaves in the opposite way in order to satisfy the condition of prescribed load.

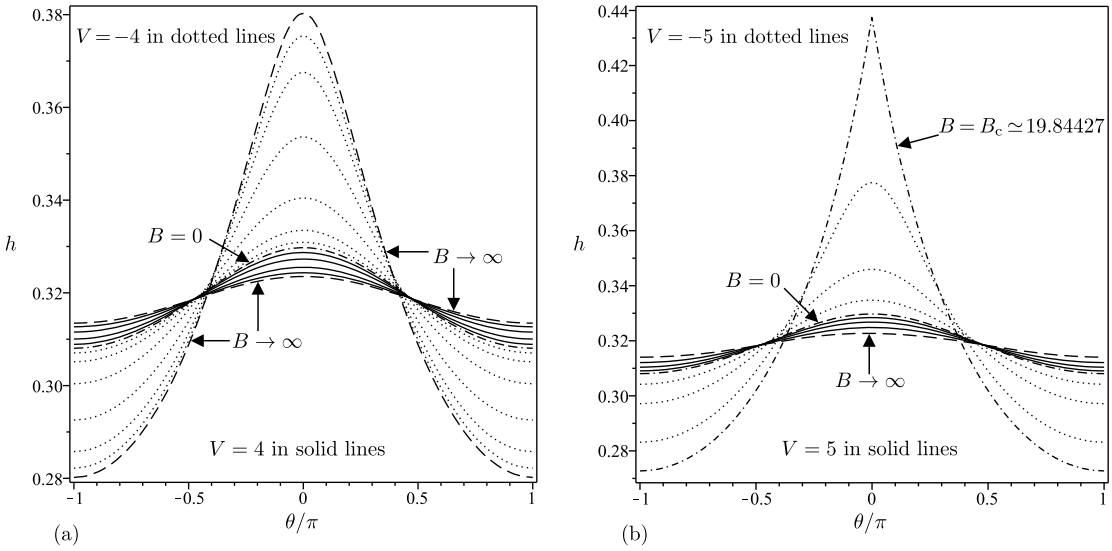

Figure 3.14: Film thickness h when $M = 2\,(< M_{\rm c0})$ plotted as a function of θ/π for (a) $B = 0$ (dash-dash-dotted line), $B = 10^n$ ($n = -0.5$, 0, 0.5, 1, 1.5, 2) for $V = -4$ (dotted lines) and $B = 10^n$ ($n = -0.5$, 0, 0.5, 1) for $V = 4$ (solid lines) together with the leading-order asymptotic solution in the limit $B \to \infty$ for $V = -4$ and $V = 4$ (dashed lines), and (b) $B = 0$ (dash-dash-dotted line), $B = 10^n$ ($n = 0$, 0.5, 1) for $V = -5$ (dotted lines) and $B = 10^n$ ($n = -0.5$, 0, 0.5) for $V = 5$ (solid lines) together with the leading-order asymptotic solution in the limit $B \to \infty$ for $V = 5$ (dashed line) and the critical solution for $V = -5$ with $B = B_{\rm c} \simeq 19.84427$ (dash-dotted line).

Figures 3.16 and 3.17 show the film thickness at $\theta = 0$, $h(0)$, and at $\theta = \pi$, $h(\pi)$, plotted as a function of (a,c) B for a range of values of V and (b,d) V for a range of values of B when $M = 2\,(< M_{\rm c0})$ and $M = 6\,(> M_{\rm c0})$, respectively. Note that in figure 3.16(a,c) the curve $V = V_\infty \simeq -4.51567$ divides curves that attain the limit $B \to \infty$ from those that terminate at the finite value $B = B_{\rm c}$ on the curve corresponding to $V = V_{\rm c}$. In particular, figures 3.16 and 3.17 show that $h(0)$ is a decreasing (increasing) function of B for positive (negative) V and a decreasing function of V, and that $h(\pi)$ behaves in the opposite way.

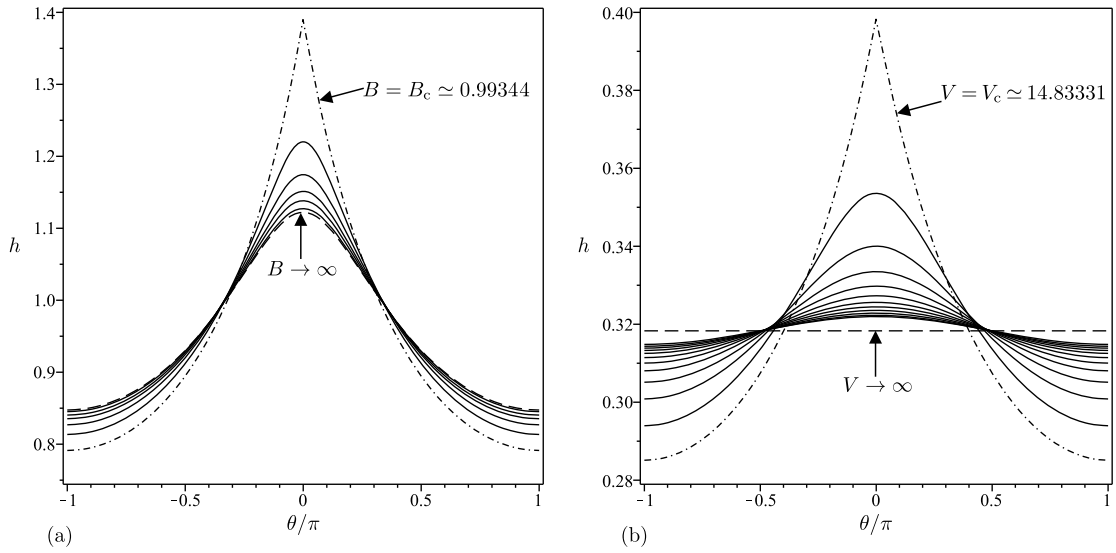

Figure 3.15: Film thickness h plotted as a function of θ/π for (a) $B = 10^n$ ($n = 0.25$, 0.5, 0.75, 1, 1.25) (solid lines) together with the leading-order asymptotic solution in the limit $B \to \infty$ (dashed line) and the critical solution with $B = B_c \simeq 0.99344$ (dash-dotted line) when $M = 6\,(> M_{c0})$ and $V = 5$, and (b) $V = -12$, -8, -4, $\ldots$, 20 (solid lines) together with the leading-order asymptotic solution in the limit $V \to \infty$ (i.e. $h \simeq 0.31831$) (dashed line) and the critical solution with $V = V_c \simeq -14.83331$ (dash-dotted line) when $M = 2\,(< M_{c0})$ and $B = 1$.

Figure 3.18 shows velocity profiles u at various values of θ in the range $0 \leq \theta \leq \pi$ when $M = 2$ and $B = 1$ for (a) $V = -5$ and (b) $V = 5$. Again the corresponding profiles in the range $-\pi < \theta < 0$ follow immediately from the top-to-bottom symmetry of the flow. In particular, figure 3.18 shows that the velocity profiles u are qualitatively similar to the critical velocity profiles u_c shown in figure 3.9. Figures 3.19 and 3.20 show the free-surface velocity at $\theta = 0$, $u(1,0)$, and at $\theta = \pi$, $u(1,\pi)$, plotted as a function of (a,c) B for a range of values of V and (b,d) V for a range of values of B when $M = 2\,(< M_{c0})$ and $M = 6\,(> M_{c0})$, respectively. In particular, figures 3.19 and 3.20 show that $u(1,0)$ is an increasing (decreasing) function of B for positive (negative) V and an increasing function of V, and that $u(1,\pi)$ behaves in the opposite way.

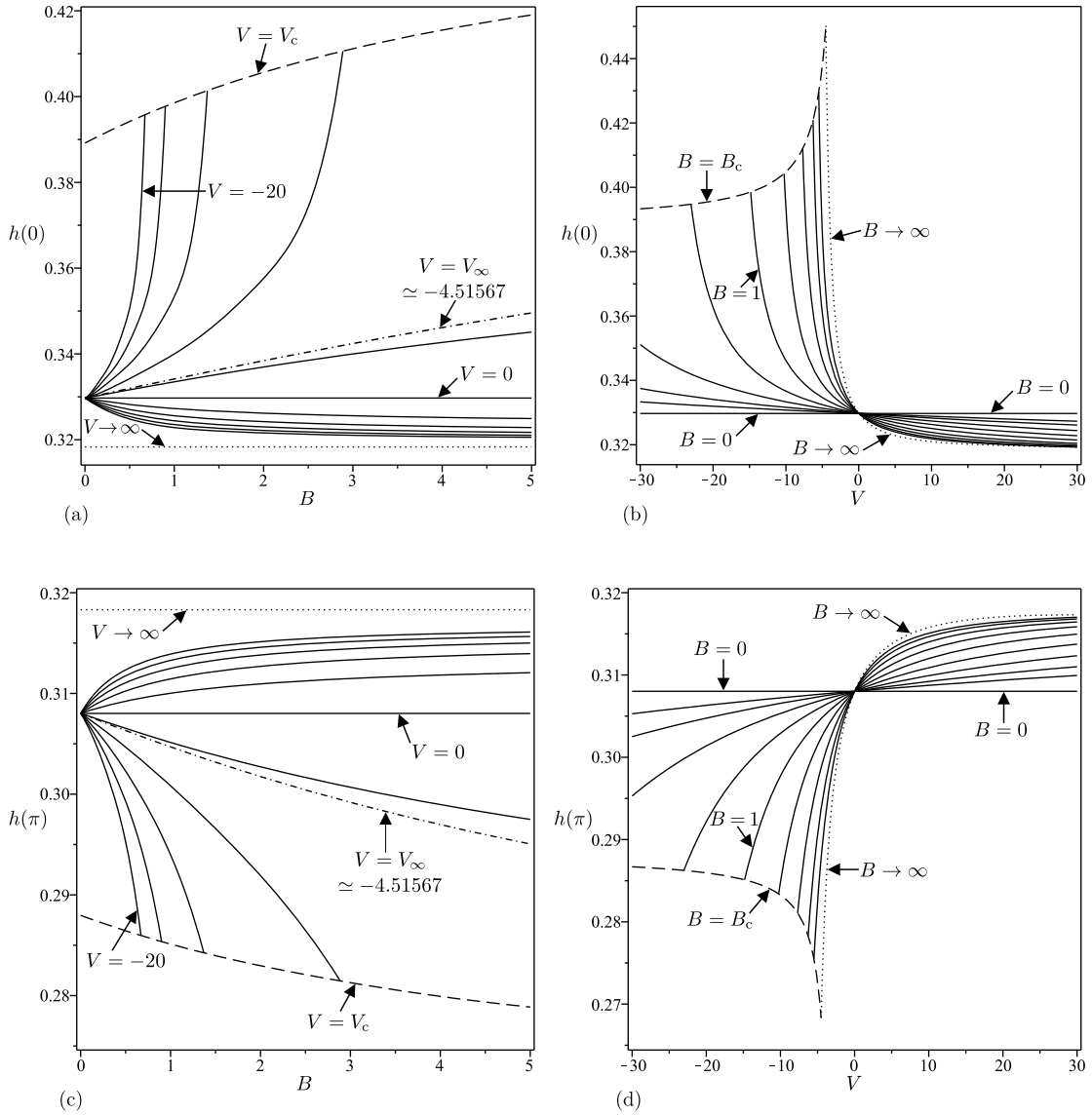

Figure 3.16: Film thickness at $\theta = 0$, $h(0)$, and at $\theta = \pi$, $h(\pi)$, when $M = 2\,(< M_{c0})$ plotted as a function of (a,c) B for $V = -20, -16, -12, \ldots, 20$ (solid lines) and $V = V_\infty \simeq -4.51567$ (dash-dotted line) together with the leading-order asymptotic solution in the limit $V \to \infty$ (i.e. $h(0) = h(\pi) \simeq 0.31831$) (dotted lines) and the critical solution with $V = V_c$ (dashed line), and (b,d) V for $B = 0$ (i.e. $h(0) \simeq 0.32971$ and $h(\pi) \simeq 0.30802$) and $B = 10^n$ ($n = -1, -0.75, -0.5, \ldots, 1$) (solid lines) together with the leading-order asymptotic solution in the limit $B \to \infty$ (dotted line) and the critical solution with $B = B_c$ (dashed line).

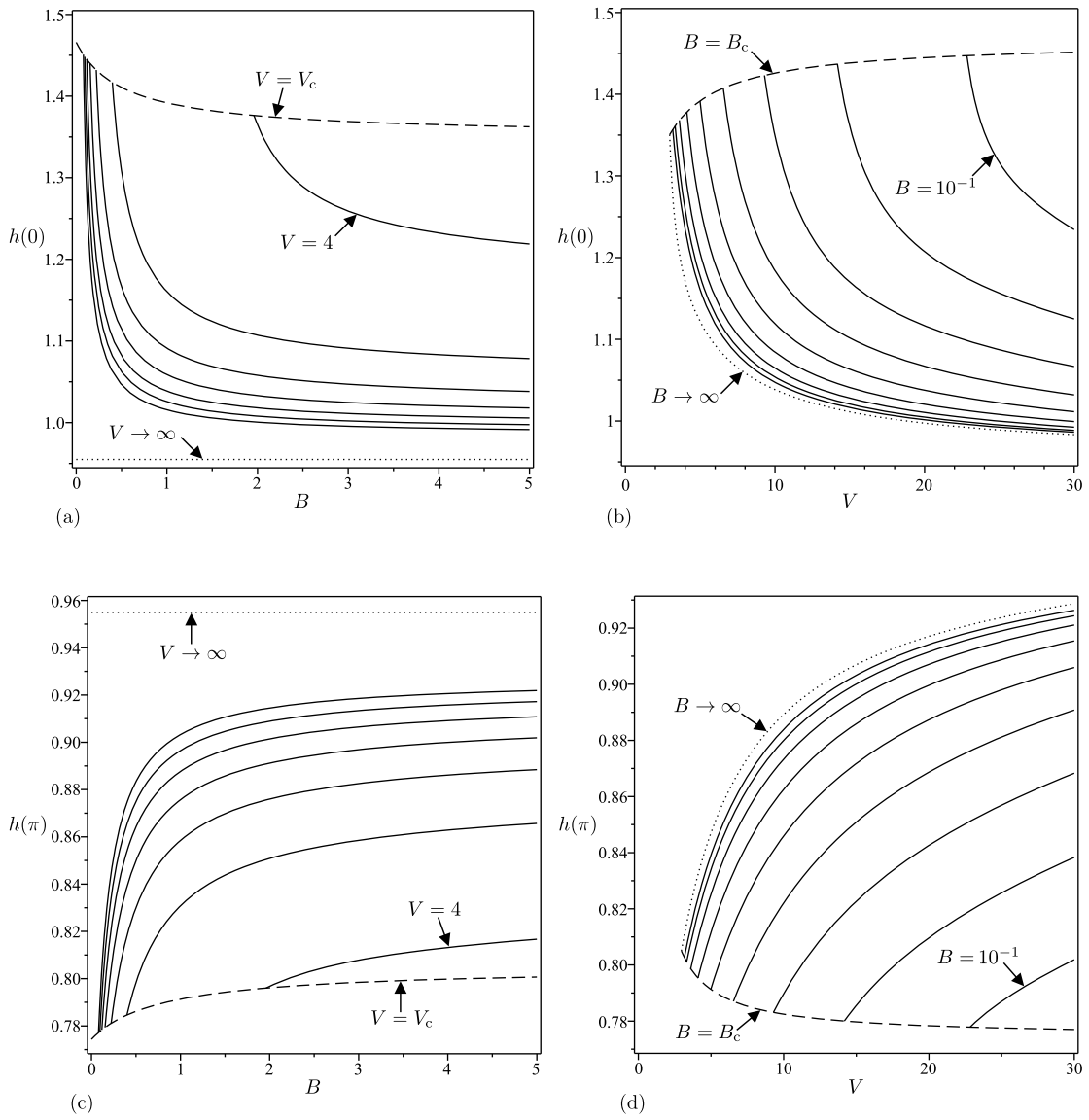

Figure 3.17: Film thickness at $\theta = 0$, $h(0)$, and at $\theta = \pi$, $h(\pi)$, when $M = 6\,(> M_{c0})$ plotted as a function of (a,c) B for $V = 4, 8, 12, \ldots, 28$ (solid lines) together with the leading-order asymptotic solution in the limit $V \to \infty$ (i.e. $h(0) = h(\pi) \simeq 0.95493$) (dotted lines) and the critical solution with $V = V_c$ (dashed line), and (b,d) V for $B = 10^n$ ($n = -1, -0.75, -0.5, \ldots, 1$) (solid lines) together with the leading-order asymptotic solution in the limit $B \to \infty$ (dotted line) and the critical solution with $B = B_c$ (dashed line).

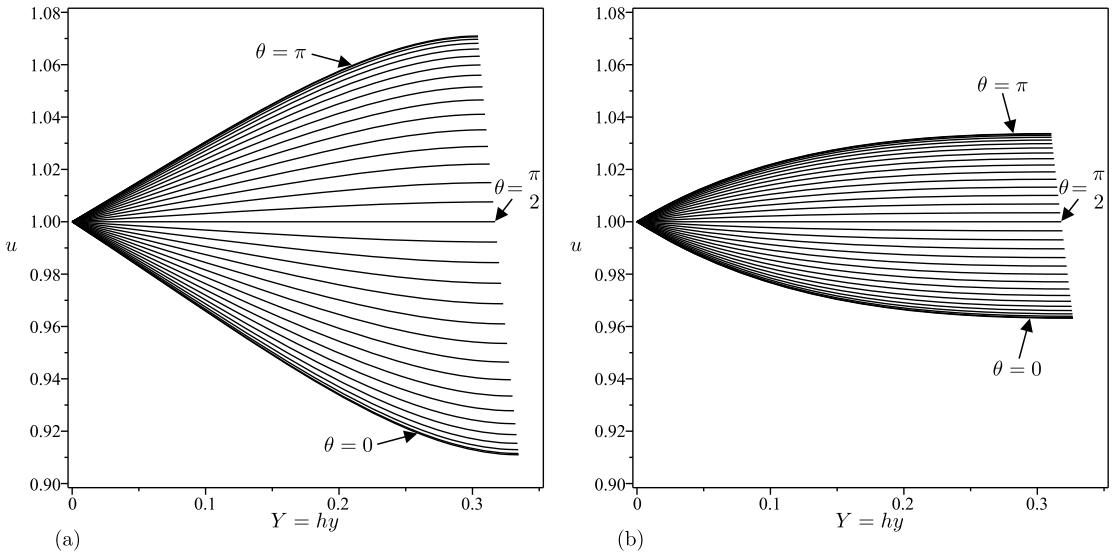

Figure 3.18: Velocity profiles u plotted as a function of $Y = hy$ at $\theta = 0$, $\pi/32$, $\pi/16$, ..., π when $M = 2$ and $B = 1$ for (a) $V = -5$ and (b) $V = 5$.

Figures 3.21 and 3.22 show the free-surface temperature at $\theta = 0$, $T(1, 0)$, and at $\theta = \pi$, $T(1, \pi)$, plotted as a function of (a,c) B for a range of values of V and (b,d) V for a range of values of B, when $M = 2\,(< M_{c0})$ and $M = 6\,(> M_{c0})$, respectively. In particular, figures 3.21 and 3.22 show that $T(1, 0)$ is a decreasing function of B and an increasing function of V, and that $T(1, \pi)$ is also a decreasing function of B but a decreasing function of V.

In the following Subsections we analyse the behaviour of the full-film solution with a prescribed load in the asymptotic limits $B \to 0^+$, $B \to \infty$, $V \to 0$, $V \to \infty$ and $M \to 0$. Note that (unlike in the corresponding analysis of the critical solution described in Subsection 3.4.5) there is no solution with prescribed load in the limit $V \to -\infty$, and, of course, there is no solution with prescribed load in the limit $M \to \infty$. Moreover, there are solutions with a prescribed load in the limits $B \to 0^+$ and $V \to 0$ only when $M \leq M_{c0}$.

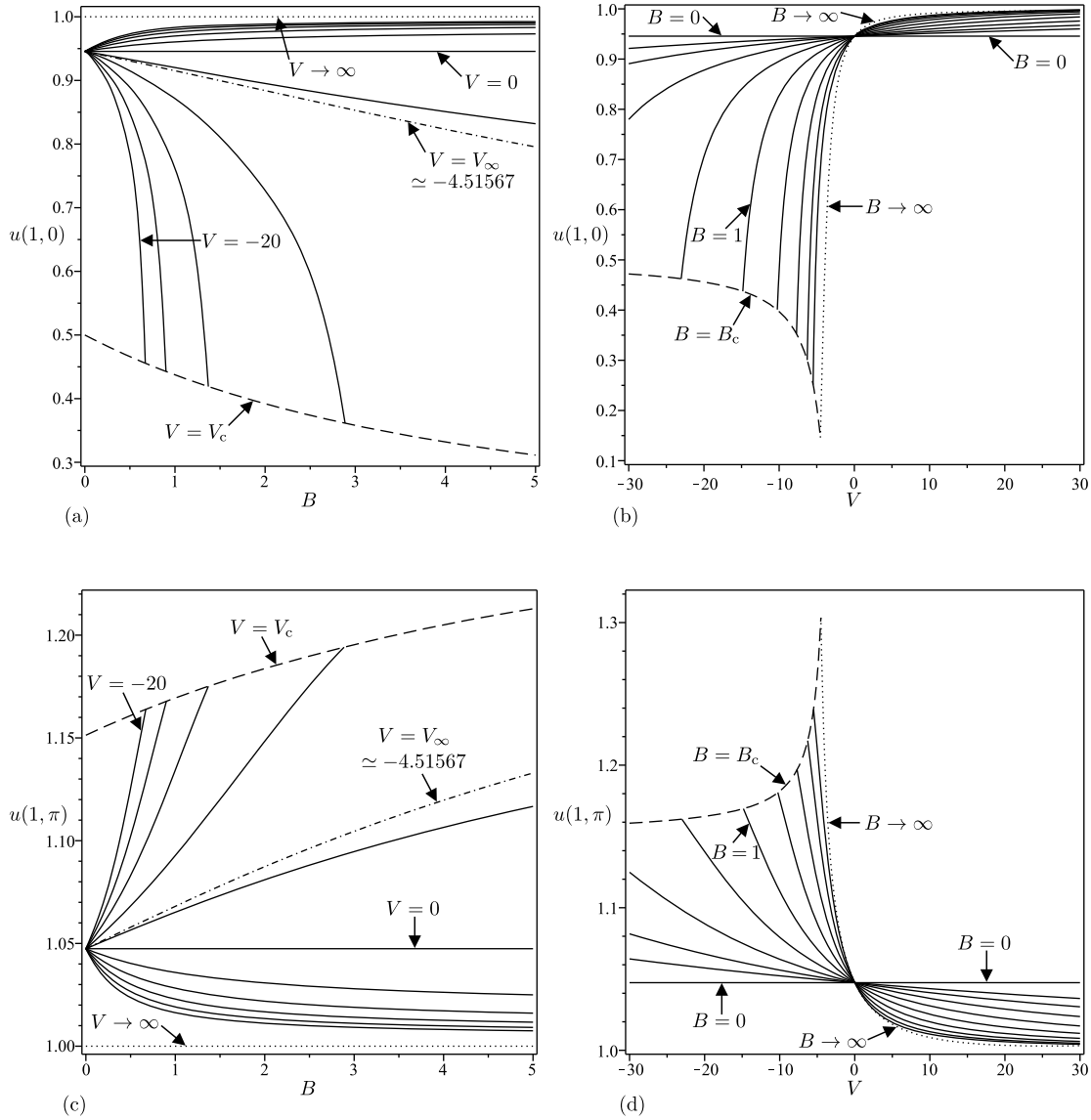

Figure 3.19: Free-surface velocity at $\theta = 0$, $u(1,0)$, and at $\theta = \pi$, $u(1,\pi)$, when $M = 2\,(< M_{c0})$ plotted as a function of (a,c) B for $V = -20$, -16, -12, $\ldots$, 20 (solid lines) and $V = V_\infty \simeq -4.51567$ (dash-dotted line) together with the leading-order asymptotic solution in the limit $V \to \infty$ (i.e. $u(1,0) = u(1,\pi) = 1$) (dotted lines) and the critical solution with $V = V_c$ (dashed line), and (b,d) V for $B = 0$ (i.e. $u(1,0) \simeq 0.94565$ and $u(1,\pi) \simeq 1.04744$) and $B = 10^n$ ($n = -1$, -0.75, -0.5, $\ldots$, 1) (solid lines) together with the leading-order asymptotic solution in the limit $B \to \infty$ (dotted line) and the critical solution with $B = B_c$ (dashed line).

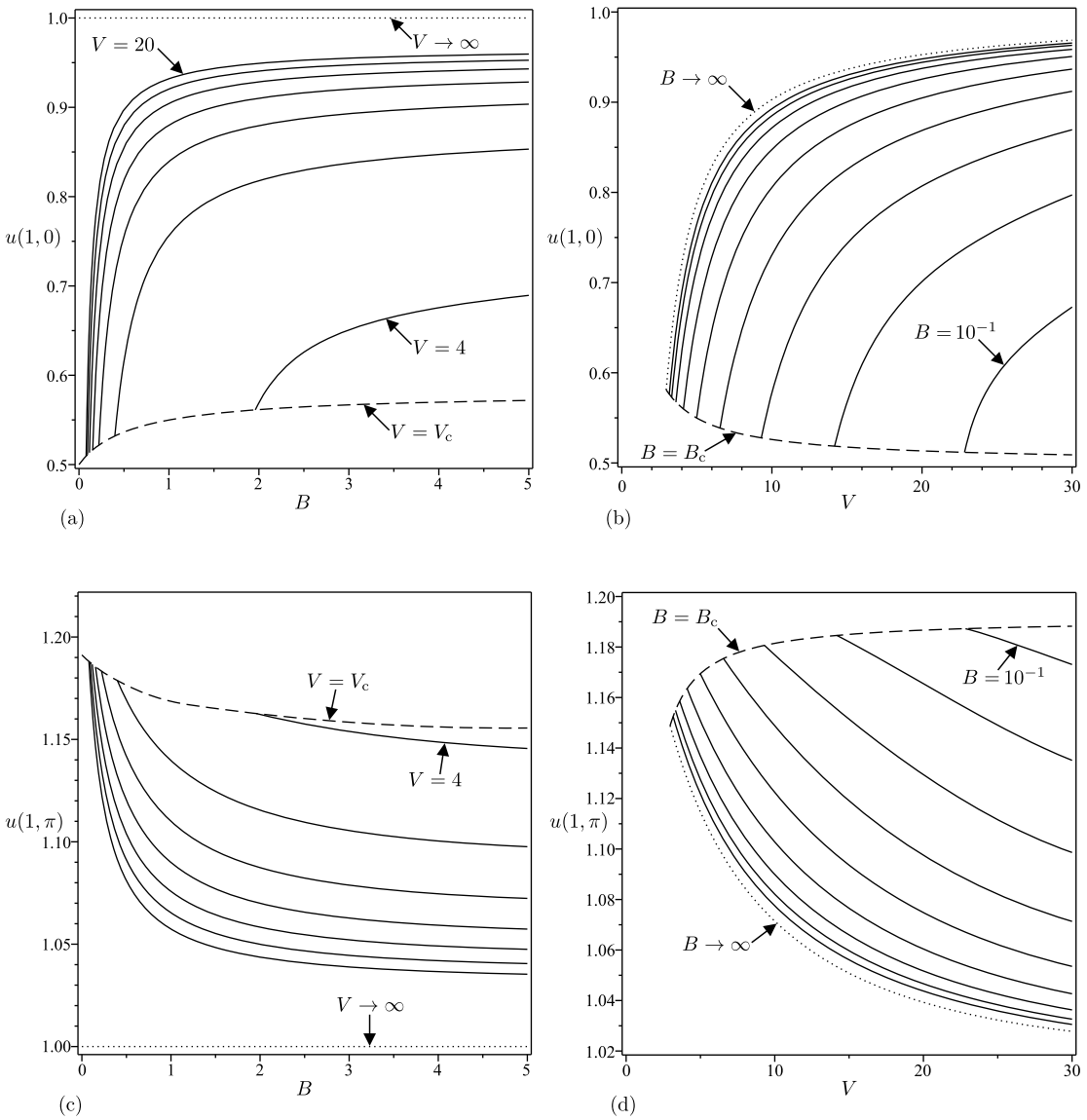

Figure 3.20: Free-surface velocity at $\theta = 0$, $u(1,0)$, and at $\theta = \pi$, $u(1,\pi)$, when $M = 6\,(> M_{c0})$ plotted as a function of (a,c) B for $V = 4$, 8, 12, ..., 28 (solid lines) together with the leading-order asymptotic solution in the limit $V \to \infty$ (i.e. $u(1,0) = u(1,\pi) = 1$) (dotted lines) and the critical solution with $V = V_c$ (dashed line), and (b,d) V for $B = 10^n$ ($n = -1$, -0.75, -0.5, ..., 1) (solid lines) together with the leading-order asymptotic solution in the limit $B \to \infty$ (dotted line) and the critical solution with $B = B_c$ (dashed line).

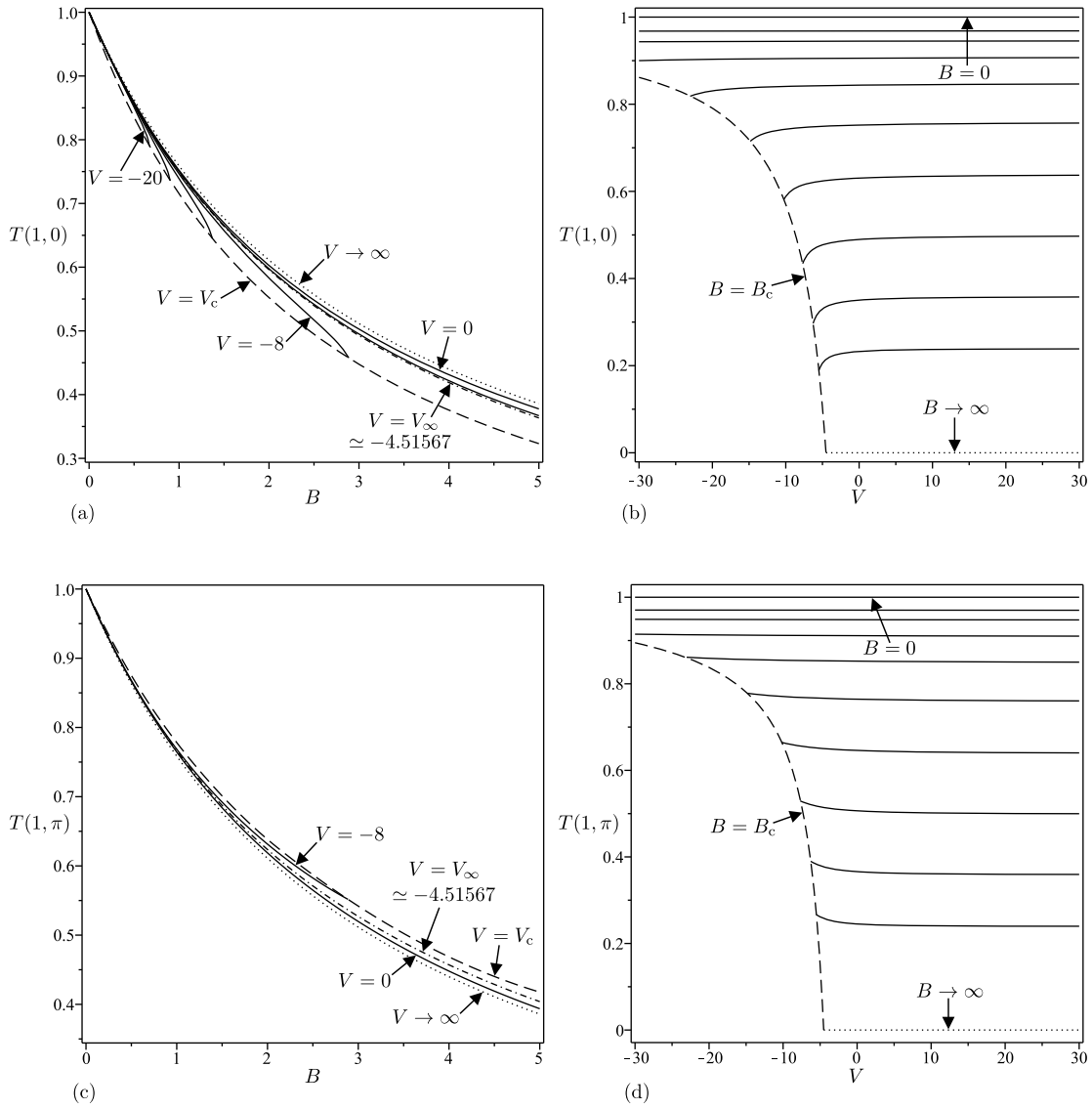

Figure 3.21: Free-surface temperature at $\theta = 0$, $T(1,0)$, and at $\theta = \pi$, $T(1,\pi)$, when $M = 2\,(< M_{c0})$ plotted as a function of (a,c) B for $V = -20$, -16, -12, -8, -4, 0 [for clarity, only the curves corresponding to $V = -8$ and $V = 0$ are shown in (c)] (solid lines) and $V = V_\infty \simeq -4.51567$ (dash-dotted line) together with the leading-order asymptotic solution in the limit $V \to \infty$ (dotted line) and the critical solution with $V = V_c$ (dashed line), and (b,d) V for $B = 0$ (i.e. $T(1,0) = T(1,\pi) = 1$) and $B = 10^n$ ($n = -1$, -0.75, -0.5, $\ldots$, 1) (solid lines) together with the leading-order asymptotic solution in the limit $B \to \infty$ (i.e. $T(1,0) = T(1,\pi) = 0$) (dotted lines) and the critical solution with $B = B_c$ (dashed line).

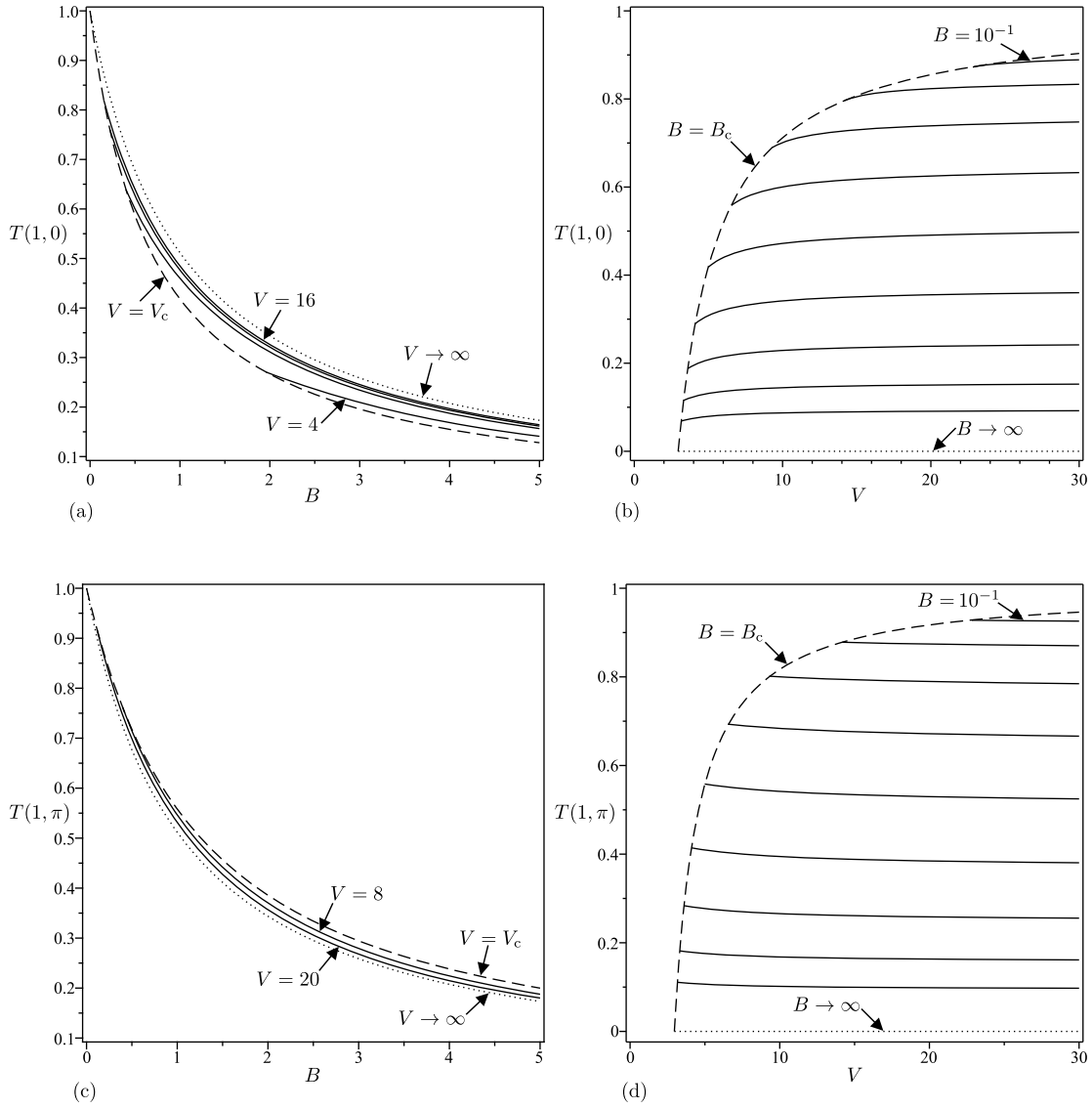

Figure 3.22: Free-surface temperature at $\theta = 0$, $T(1,0)$, and at $\theta = \pi$, $T(1,\pi)$, when $M = 6\,(> M_{c0})$ plotted as a function of (a,c) B for $V = 4$, 8, 12, 16 [for clarity, only the curves corresponding to $V = 8$ and $V = 20$ are shown in (c)] (solid lines) together with the leading-order asymptotic solution in the limit $V \to \infty$ (dotted line) and the critical solution with $V = V_c$ (dashed line), and (b,d) V for $B = 10^n$ ($n = -1, -0.75, -0.5, \ldots, 1$) (solid lines) together with the leading-order asymptotic solution in the limit $B \to \infty$ (i.e. $T(1,0) = T(1,\pi) = 0$) (dotted lines) and the critical solution with $B = B_c$ (dashed line).

3.5.1 The limit of weak heat transfer $B \to 0^+$

In the limit of weak heat transfer at the free surface, $B \to 0^+$, the solutions for h, u and T are given by

$$h = h_0 + \frac{BV(I_{B0} - h_0^4 \cos\theta)}{12(1 - h_0^2 \cos\theta)} + O(B^2), \tag{3.63}$$

$$u = u_0 - \frac{BVh_0 y \cos\theta}{12(1 - h_0^2 \cos\theta)} \left[h_0^2(1 - h_0^2 \cos\theta)(4y^2 - 7y + 2) + (I_{B0} - h_0^2)(2 - y)\right] + O(B^2) \tag{3.64}$$

and

$$T = 1 - Bh_0 y - \frac{B^2 y \left[V(I_{B0} - h_0^4 \cos\theta) - 12h_0^2(1 - h_0^2 \cos\theta)\right]}{12(1 - h_0^2 \cos\theta)} + O(B^3), \tag{3.65}$$

where the constant $I_{B0} = I_{B0}(M_0)$ $(0 < I_{B0} < 1)$ is given by

$$I_{B0} = \frac{\displaystyle\int_0^\pi \frac{h_0^4 \cos\theta}{1 - h_0^2 \cos\theta}\,\mathrm{d}\theta}{\displaystyle\int_0^\pi \frac{1}{1 - h_0^2 \cos\theta}\,\mathrm{d}\theta}, \tag{3.66}$$

and h_0 and u_0 are the constant-viscosity solutions with load $M_0 = M\,(\leq M_{\mathrm{c}0})$ given in Section 3.2. Note that the solutions (3.63)–(3.65) are valid for a general viscosity model satisfying $\mu = 1$ and $\mathrm{d}\mu/\mathrm{d}T = -V$ when $T = 1$ to the order shown (but not to higher orders). The same is true for the asymptotic solution in the limit of weak thermoviscosity $V \to 0$ presented subsequently in Subsection 3.5.3. Like the corresponding behaviour of the critical solution described in Subsection 3.4.1, the solution (3.65) shows that the effect of weak heat transfer at the free surface is to decrease the temperature from its constant isothermal value $T \equiv 1$ throughout the fluid film, and thus to increase (decrease) the viscosity from its constant isothermal value $\mu \equiv 1$ when $V > 0$ $(V < 0)$. However, unlike the corresponding behaviour of the critical solution, the effect on h depends on the sign of $V(I_{B0} - h_0^4 \cos\theta)$ (rather than just V). Thus when $V > 0$ $(V < 0)$ the effect of weak heat transfer at the free surface is to decrease (increase) h from its

isothermal value when $|\theta| < \bar{\theta}$ with the opposite behaviour when $|\theta| > \bar{\theta}$, where $\theta = \bar{\theta}$ $(0 < \bar{\theta} \leq \pi/2)$ satisfies $I_{B0} - h_0^4 \cos\theta = 0$.

3.5.2 The limit of strong heat transfer $B \to \infty$

In the limit of strong heat transfer at the free surface, $B \to \infty$, the solutions for h, u and T are given by

$$h = \hat{h} + \frac{h_1}{B} + O\left(\frac{1}{B^2}\right), \tag{3.67}$$

$$u = \hat{u} + \frac{h_0 \cos\theta}{V^2 B \hat{f}^{1/2}} \left[\{V(1-y) - 2(1+h_1)\} V y \exp(-Vy) \right. \\ \left. - \{V(1+2h_1) - 2(1+h_1)\} (1 - \exp(-Vy))\right] + O\left(\frac{1}{B^2}\right) \tag{3.68}$$

and

$$T = \hat{T} + \frac{\hat{f}^{1/2} y}{B h_0} - \frac{\hat{f}(1+h_1) y}{B^2 h_0^2} + O\left(\frac{1}{B^3}\right), \tag{3.69}$$

where $h_1 = h_1(\theta)$ is given by

$$h_1 = \frac{(I_{B\infty} - h_0^2 \cos\theta)[3 - (V+3)\hat{f}]}{3\hat{f}(1 - h_0^2 \cos\theta)} \tag{3.70}$$

and the constant $I_{B\infty} = I_{B\infty}(M_0)$ $(0 < I_{B\infty} < 1)$ is given by

$$I_{B\infty} = 1 - \pi \left(\int_0^\pi \frac{1}{1 - h_0^2 \cos\theta} \, d\theta \right)^{-1}. \tag{3.71}$$

As in the corresponding analysis of the critical solution described in Subsection 3.4.2, the leading-order solutions for h and Q, denoted by $\hat{h}$ and $\hat{Q}$, are given simply by rescaling the corresponding constant-viscosity solutions h_0 and Q_0 according to $\hat{h} = \hat{f}^{-1/2} h_0$ and $\hat{Q} = \hat{f}^{-1/2} Q_0$, where $M = \hat{f}^{-1/2} M_0$, and the leading-order solutions for u and f, denoted by $\hat{u}$ and $\hat{f}$, are again given by (3.39) and (3.40), respectively. Like the corresponding behaviour of the critical solution described in Subsection 3.4.2, the solution (3.69) shows that the effect of large-but-finite heat transfer at the free surface is to increase the temperature from its leading-order value $T = \hat{T} = 1 - y$ throughout the fluid film, and thus to decrease (increase)

the viscosity from its leading-order value $\mu = \hat{\mu} = \exp(Vy)$ when $V > 0$ ($V < 0$). However, unlike the corresponding behaviour of the critical solution, the effect on h depends on the sign of $(I_{B\infty} - h_0^2 \cos\theta)[3-(V+3)\hat{f}]$ (rather than just $3-(V+3)\hat{f}$). Thus when $V > 0$ ($V < 0$), the effect of large-but-finite heat transfer at the free surface is to increase (decrease) h from its isothermal value when $|\theta| < \bar{\theta}$ with the opposite behaviour when $|\theta| > \bar{\theta}$, where $\theta = \bar{\theta}$ ($0 < \bar{\theta} \leq \pi/2$) satisfies $I_{B\infty} - h_0^2 \cos\theta = 0$.

3.5.3 The limit of weak thermoviscosity $V \to 0$

In the limit of weak thermoviscosity, $V \to 0$, the solutions for h, u and T are given by

$$h = h_0 + \frac{BV[I_{V0}(1+Bh_0) - h_0^4 \cos\theta]}{12(1-h_0^2\cos\theta)(1+Bh_0)} + O(V^2), \tag{3.72}$$

$$u = u_0 - \frac{BVh_0 y \cos\theta}{12(1-h_0^2\cos\theta)(1+Bh_0)} \left\{h_0^2(1-h_0^2\cos\theta)(4y^2-7y+2) + \left[I_{V0}(1+Bh_0) - h_0^2\right](2-y)\right\} + O(V^2) \tag{3.73}$$

and

$$T = 1 - \frac{Bh_0 y}{1+Bh_0} - \frac{B^2 Vy\,[I_{V0}(1+Bh_0) - h_0^4\cos\theta]}{12(1-h_0^2\cos\theta)(1+Bh_0)^3} + O(V^2), \tag{3.74}$$

where the constant $I_{V0} = I_{V0}(M_0, B)$ ($0 < I_{V0} < 1$) is given by

$$I_{V0} = \frac{\displaystyle\int_0^\pi \frac{h_0^4\cos\theta}{(1-h_0^2\cos\theta)(1+Bh_0)}\,\mathrm{d}\theta}{\displaystyle\int_0^\pi \frac{1}{1-h_0^2\cos\theta}\,\mathrm{d}\theta}, \tag{3.75}$$

and h_0 and u_0 are the constant-viscosity solutions with load $M_0 = M\,(\leq M_{\mathrm{c}0})$ given in Section 3.2. Like the corresponding behaviour of the critical solution described in Subsection 3.4.3, the solutions in this limit are somewhat similar to those in the limit $B \to 0^+$ described previously in Subsection 3.5.1 and have the corresponding physical interpretation.

3.5.4 The limit of strong positive thermoviscosity $V \to \infty$

In the limit of strong positive thermoviscosity, $V \to \infty$, the solutions for h, u and T are given by

$$h = \frac{M}{2\pi} + \frac{M^2 \cos\theta(2\pi + BM)}{8\pi^3 BV} + O\left(\frac{1}{V^2}\right), \tag{3.76}$$

$$u = 1 - \frac{M\cos\theta(2\pi + BM)}{4\pi^2 BV}\left[1 - \exp\left(-\frac{BVMy}{2\pi + BM}\right)\right] + O\left(\frac{1}{V^2}\right) \tag{3.77}$$

and

$$T = 1 - \frac{BMy}{2\pi + BM} - \frac{M^2 y\cos\theta}{2\pi(2\pi + BM)V} + O\left(\frac{1}{V^2}\right). \tag{3.78}$$

These solutions show that, like the corresponding behaviour of the critical solution described in Subsection 3.4.4, at leading order in the limit of strong positive thermoviscosity the temperature is given by $T = 1 - BMy/(2\pi + BM)$ and the viscosity

$$\mu = O\left[\exp\left(\frac{BVMy}{2\pi + BM}\right)\right] \tag{3.79}$$

is exponentially large outside a narrow boundary layer of width $O(1/V) \ll 1$ near the cylinder $y = 0$, resulting in a uniform plug flow $u \equiv 1$ outside the boundary layer. However, unlike the corresponding behaviour of the critical solution, the leading-order film thickness is an $O(1)$ constant, and the effect of large-but-finite positive thermoviscosity is to decrease T from its leading-order value throughout the fluid film, and thus to decrease (increase) u outside the boundary layer and increase (decrease) h, respectively, from their leading-order values when $\cos\theta > 0$ ($\cos\theta < 0$).

3.5.5 The limit of small load $M \to 0$

In the limit of small load, $M \to 0$, the solutions for h, u and T are given by

$$h = \frac{M}{2\pi} + \frac{M^3\cos\theta}{24\pi^3} + O(M^4), \tag{3.80}$$

$$u = 1 - \frac{M^2\cos\theta(2-y)y}{8\pi^2} + \frac{M^3 BV\cos\theta(3-2y)y^2}{48\pi^3} + O(M^4) \tag{3.81}$$

and

$$T = 1 - \frac{MBy}{2\pi} + \frac{M^2B^2y}{4\pi^2} + O(M^3). \tag{3.82}$$

These solutions show that, as might have been anticipated, at leading order in the limit of small load the film is isothermal, $T \equiv 1$, the viscosity is constant, $\mu \equiv 1$, the film thickness is a small $O(M) \ll 1$ constant, and there is a uniform plug flow $u \equiv 1$.

3.6 Backflow

As we noted near the end of Section 3.3, in the special case of constant viscosity the azimuthal velocity u is always in the same direction as the rotation of the cylinder (i.e. $u \geq 0$ for all $0 \leq y \leq 1$) and so backflow (i.e. $u < 0$ somewhere in $0 < y \leq 1$) never occurs. It is therefore interesting to discover that in the general case of non-constant viscosity there is a region of the B–V parameter plane in which backflow occurs in a region on the right-hand side of the cylinder containing the point on the free surface at $\theta = 0$ (i.e. the point furthest from the cylinder at the azimuthal location where the strongest local effect of gravity occurs). Figure 3.23 shows the regions of the B–V parameter plane in which backflow occurs for a range of values of M and shows that backflow only occurs when the atmosphere is sufficiently heated and there is sufficient heat transfer at the free surface. The backflow that occurs is due to the reduction in viscosity of the fluid allowing gravity to "win" oven the rotation of the cylinder. The "bounding" curve corresponding to $u_c(1, 0) = 0$ divides the B–V parameter plane into the region to the left of the curve in which $u_c(1, 0) > 0$ in which backflow is impossible from the region to the right of the curve in which $u_c(1, 0) < 0$ in which backflow is possible (but may or may not actually occur). As we have already seen, for each prescribed value of M full-film solutions exist only above the corresponding critical curve (B_c, V_c) (described in Section 3.5 and shown in figure 3.8). Hence, for sufficiently small prescribed values of M backflow occurs in the narrow region bounded below by

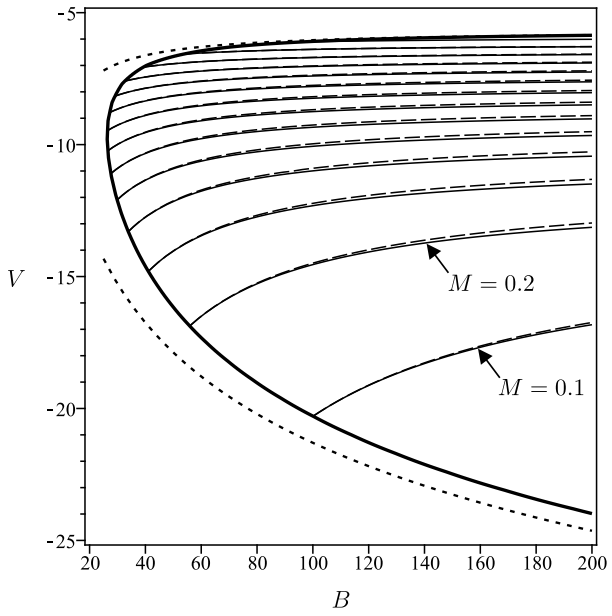

Figure 3.23: The regions of the B–V parameter plane in which backflow occurs for $M = 0.1, 0.2, 0.3, \ldots, 1.4$. For each value of M the region in which backflow occurs is bounded below by the critical curve (B_c, V_c) (solid lines) and above by the curve on which $u(1,0) = 0$ (dashed lines), which meet on the bounding curve on which $u_c(1,0) = 0$ (thick solid line). Also shown are the asymptotic solutions for the upper and lower branches of the bounding curve given by (3.83) and (3.84), respectively, (dashed lines).

the critical curve (B_c, V_c) and above by the curve on which $u(1,0) = 0$, and these curves meet on the bounding curve on which $u_c(1,0) = 0$. In the limit $B \to \infty$ the upper and lower branches of the bounding curve satisfy

$$V = V_{\max} + \frac{2\sqrt{3}V_{\max}(V_{\max}+3)}{B\sqrt{V_{\max}+6}(2V_{\max}+9)} + O\left(\frac{1}{B^2}\right) \tag{3.83}$$

where $V_{\max} \simeq -5.65658$ satisfies $2V_{\max}^2 - 5V_{\max} + 6 - (V_{\max}+6)\exp(-V_{\max}) = 0$, and

$$V = -4\log B - 4\log(\log B) + 6 - 4\log 2 + O\left(\frac{\log(\log B)}{\log B}\right), \tag{3.84}$$

respectively. In particular, equations (3.83) and (3.84) show that backflow never occurs for any value of B when $V \geq V_{\max}$, or, equivalently, when $M \geq M_{\max} =$

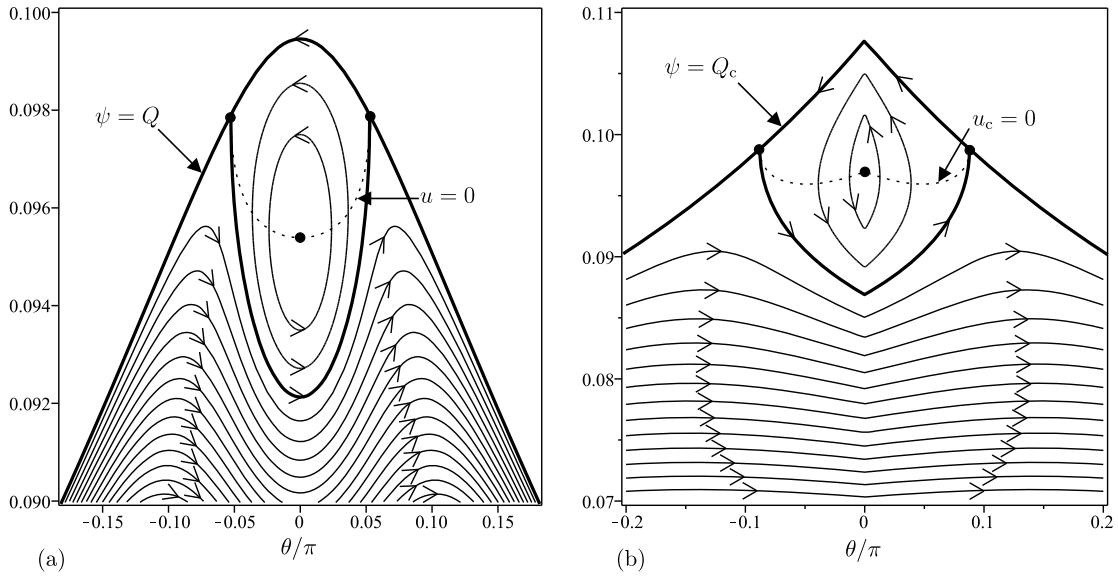

Figure 3.24: Details of the streamlines of the flow near $y = 1$ and $\theta = 0$ when $B = 100$ and $V = -10$ for (a) the solution with prescribed load $M = 1/2$ ($Q \simeq 0.07642$) in which the streamlines are drawn for $\psi/Q = 1487/1500$ (the lowest visible streamline), 1488/1500, 1489/1500, ..., 1 (the stagnation streamline), 1501/1500 and 1502/1500 (inside the recirculation region), and (b) the critical solution with load $M = M_c \simeq 0.50800$ ($Q = Q_c \simeq 0.07716$) in which the streamlines are drawn for $\psi/Q = 87/100$ (the lowest visible streamline), 88/100, 89/100, ..., 1 (the stagnation streamline), 101/100 and 102/100 (inside the recirculation region). In both cases the curve on which $u = 0$ is shown with a dashed line and the stagnation points are shown with large dots.

$\hat{f}(V_{\max})^{-1/2} M_{c0} \simeq 1.50315$. Furthermore, since the bounding curve lies to the right of the point $(26.29946, -9.69044)$, backflow never occurs for any value of V when $B < B_{\min} \simeq 26.29946$.

In order to illustrate backflow, Figure 3.24 shows details of the streamlines of the flow near $y = 1$ and $\theta = 0$ when $B = 100$ and $V = -10$ in two situations in which backflow occurs. Specifically, figure 3.24(a) shows streamlines of the solution with prescribed load $M = 1/2$, while figure 3.24(b) shows streamlines of the critical solution with load $M = M_c \simeq 0.50800$.

3.7 The Distinguished Limit of Strong Thermoviscosity and Weak Heat Transfer $|V| \to \infty$ and $B \to 0^+$ with $\hat{V} = BV = O(1)$

Another interesting case also worth considering is the distinguished limit discussed by Wilson and Duffy [96] of strong thermoviscosity, $|V| \to \infty$, *and* weak heat transfer at the free surface, $B \to 0^+$, such that $\hat{V} = BV = O(1)$, in which, although the variation in temperature across the fluid film is small, specifically $T = 1 - Bhy + O(B^2)$, thermoviscosity effects still enter the problem at leading order, i.e. the variation in viscosity across the fluid film is still $O(1)$. This case is physically relevant since the Biot number is often found to be small. By making the substitution $V = \hat{V}/B$ and taking the limit $B \to 0$ we are able to consider this interesting case with one less parameter than we had previously thereby simplifying the analysis of the problem. Note that in this limit the *effective thermoviscosity number*, $\hat{V} = BV$, defined in terms of dimensional quantities by

$$\hat{V} = \frac{\lambda(T_0 - T_\infty)\epsilon a \alpha_{\text{th}}}{\mu_0 k_{\text{th}}}, \tag{3.85}$$

and not the previously defined thermoviscosity number, V, is the appropriate non-dimensional measure of thermoviscosity effects. In the particular case of the exponential viscosity model (3.24) in this limit $\mathcal{V} \sim \hat{V}h$ and so the leading-order expressions for μ, u, ψ and f are given simply by (3.24), (3.26)–(3.28) with $\mathcal{V}$ replaced by $\hat{V}h$, respectively.

3.7.1 The critical solution

Unlike in the general case considered in Section 3.4, in the present distinguished limit explicit expressions can be obtained for the critical film thickness at $\theta = 0$, $h_{\text{c}}(0)$, the magnitude of the slope of the corner in h_{c} at $\theta = 0$, H_{c}, and the critical

flux, $Q_{\rm c}$, namely

$$h_{\rm c}(0) = \frac{\hat{V}^2 + 2(W_{\hat{V}} + 1)}{2\hat{V}}, \tag{3.86}$$

$$H_{\rm c} = \left(\frac{\hat{V}^4 + 4\hat{V}^2 W_{\hat{V}} + 4(W_{\hat{V}} + 1)^2}{8\hat{V}(W_{\hat{V}} + 1)} \right)^{1/2} \tag{3.87}$$

and

$$Q_{\rm c} = \frac{\hat{V}^2(\hat{V}^2 + 4) - 4(W_{\hat{V}} + 1)^2}{4\hat{V}^3}, \tag{3.88}$$

where $W_{\hat{V}} = W_{\hat{V}}(\hat{V})$ is given by

$$W_{\hat{V}} = \begin{cases} W_0\left(-\exp\left[-\dfrac{\hat{V}^2}{2} - 1 \right] \right) & \text{if} \quad \hat{V} \geq 0, \\ W_{-1}\left(-\exp\left[-\dfrac{\hat{V}^2}{2} - 1 \right] \right) & \text{if} \quad \hat{V} < 0, \end{cases} \tag{3.89}$$

where $W_0(x)$ and $W_{-1}(x)$ are again the principal and lower real branches of the Lambert W function, respectively. Figure 3.25 shows the quantities $h_{\rm c}(0)$, $H_{\rm c}$, $Q_{\rm c}$ and $M_{\rm c}$ plotted as functions of $\hat{V}$.

In the limit of weak thermoviscosity, $\hat{V} \to 0$, the solutions for $h_{\rm c}$, $H_{\rm c}$, $M_{\rm c}$ and $u_{\rm c}$ are given by the corresponding results in the limit $B \to 0$ given in Subsection 3.4.1, namely (3.33)–(3.36), with BV and $O(B^2)$ replaced by $\hat{V}$ and $O(\hat{V}^2)$, respectively, and hence have the same physical interpretation.

In the limit of strong positive thermoviscosity, $\hat{V} \to \infty$, the solutions for $h_{\rm c}$, $H_{\rm c}$, $M_{\rm c}$ and $u_{\rm c}$ are given by

$$h_{\rm c} = \frac{\hat{V}\left[1 - (1 - \cos\theta)^{1/2}\right]}{2\cos\theta} + \frac{1}{\hat{V}} + O\left(\frac{1}{\hat{V}^3}\right), \tag{3.90}$$

$$H_{\rm c} = \frac{\hat{V}}{2\sqrt{2}} + O\left(\frac{1}{\hat{V}^3}\right), \tag{3.91}$$

$$M_{\rm c} = 2\hat{V}\log(1 + \sqrt{2}) + \frac{2\pi}{\hat{V}} + O\left(\frac{1}{\hat{V}^3}\right) \tag{3.92}$$

and

$$u_{\rm c} = 1 - \frac{1}{2}\Big[1 - (1 - \cos\theta)^{1/2}\Big]\left[1 - \exp\left(-\frac{\hat{V}^2\left[1 - (1 - \cos\theta)^{1/2}\right]y}{2\cos\theta}\right)\right] + O\left(\frac{1}{\hat{V}^2}\right). \tag{3.93}$$

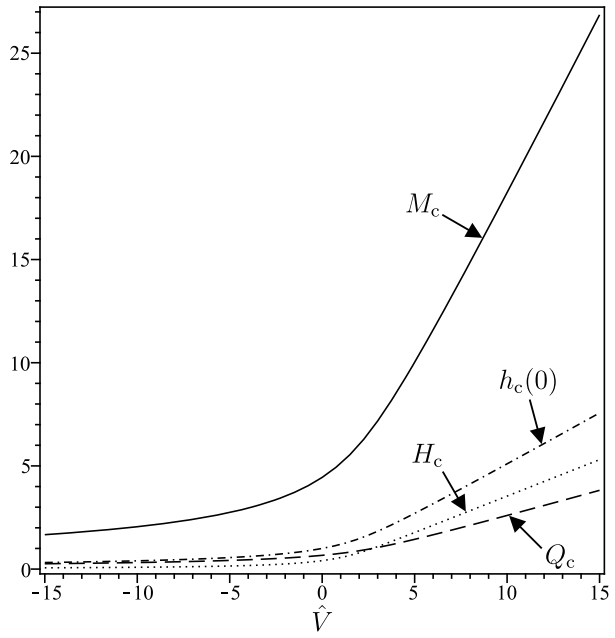

Figure 3.25: The quantities $h_c(0)$ given by (3.86) (dash-dotted line), H_c given by (3.87) (dotted line), Q_c given by (3.88) (dashed line), and M_c (solid line) plotted as functions of $\hat{V}$.

These solutions differ from the corresponding results in the limit $V \to \infty$ given in Subsection 3.4.4, namely (3.51)–(3.54), but have a qualitatively similar physical interpretation. In particular, these solutions show that at leading order in the limit of strong positive thermoviscosity the viscosity

$$\mu = \exp\left(\frac{\hat{V}^2\left[1-(1-\cos\theta)^{1/2}\right]y}{2\cos\theta} + y\right) \tag{3.94}$$

is exponentially large outside a narrow boundary layer of width $O(1/\hat{V}^2) \ll 1$ near the cylinder $y = 0$, resulting in a uniform plug flow $u_c \equiv [1+(1-\cos\theta)^{1/2}]/2$ outside the boundary layer and a large film thickness and load of $O(\hat{V}) \gg 1$.

In the limit of strong negative thermoviscosity, $\hat{V} \to -\infty$, the solutions for h_c, H_c, M_c, and u_c are given by

$$h_c = \frac{1}{(-\hat{V})}\left[\log\left(\frac{\hat{V}^2}{2}\right) - W_{V\infty} - 1\right] + O\left(\frac{\log(-\hat{V})^2}{\hat{V}^3}\right), \tag{3.95}$$

$$H_{\mathrm{c}} = \frac{1}{(-\hat{V})} + O\left(\frac{\log(-\hat{V})^2}{\hat{V}^3}\right), \tag{3.96}$$

$$M_{\mathrm{c}} = \frac{1}{(-\hat{V})}\left[2\pi \log\left(\frac{\hat{V}^2}{2}\right) - C_{V\infty} - 2\pi\right] + O\left(\frac{\log(-\hat{V})^2}{(-\hat{V})^3}\right) \tag{3.97}$$

and

$$u_{\mathrm{c}} = 1 - \frac{\cos\theta}{\hat{V}^2}\left[\left(-\frac{\hat{V}^2 W_{V\infty}}{2\cos\theta}\right)^y \left\{\left[\log\left(\frac{\hat{V}^2}{2}\right) - W_{V\infty}\right](1-y) + y\right\} - \log\left(\frac{\hat{V}^2}{2}\right) + W_{V\infty}\right] + O\left(\frac{\log(-\hat{V})^2}{\hat{V}^2}\right), \tag{3.98}$$

where the function $W_{V\infty} = W_{V\infty}(\theta)$ and the constant $C_{V\infty}$ are again given by (3.61) and (3.62), respectively. At leading (but not higher) order these solutions coincide with the corresponding results in the limit $V \to -\infty$ given in Subsection 3.4.5, namely (3.56)–(3.59), and hence have the same physical interpretation.

3.7.2 Full-film solution with a prescribed load

In the limit of weak thermoviscosity, $\hat{V} \to 0$, the solutions for h and u are given by the corresponding results in the limit $B \to 0$ given in Subsection 3.5.1, namely (3.63) and (3.64), with BV and $O(B^2)$ replaced by $\hat{V}$ and $O(\hat{V}^2)$, respectively, and hence have the same physical interpretation.

In the limit of strong positive thermoviscosity, $\hat{V} \to \infty$, the solutions for h and u are given by

$$h = \frac{M}{2\pi} + \frac{M^2\cos\theta}{4\pi^2\hat{V}} + O\left(\frac{1}{\hat{V}^2}\right) \tag{3.99}$$

and

$$u = 1 - \frac{M\cos\theta}{2\pi\hat{V}}\left[1 - \exp\left(-\frac{M\hat{V}y}{2\pi}\right)\right] + O\left(\frac{1}{\hat{V}^2}\right). \tag{3.100}$$

These solutions are similar to the corresponding results in the limit $V \to \infty$ given in Subsection 3.5.4, namely (3.76) and (3.77), from which they can be obtained by writing $V = \hat{V}/B$ and taking the limit $B \to 0$, and hence have the same physical interpretation.

In the limit of small load, $M \to 0$, the solutions for h and u are given by the corresponding results in the limit $M \to 0$ given in Subsection 3.5.5, namely (3.80) and (3.81), with BV replaced by $\hat{V}$, and hence have the same physical interpretation.

3.8 Conclusions

In the present work we obtained a comprehensive description of steady thermoviscous coating and rimming flow on a uniformly rotating horizontal cylinder. We found that, as in the corresponding isothermal problem studied by Moffatt [7], there is a critical solution with a corresponding critical load (which depends, in general, on both the Biot number B and the thermoviscosity number V) above which no full-film solutions exist.

In Section 3.4 we showed that the critical film thickness, h_c, the magnitude of the slope of the corner in the critical film thickness at $\theta = 0$, H_c, and the critical load, M_c, are increasing (decreasing) functions of B for positive (negative) V, and increasing functions of V. For a positive (negative) fixed value of V the maximum (minimum) possible critical load is attained in the limit of strong heat transfer at the free surface $B \to \infty$ and is given by $\hat{M} = \hat{f}^{-1/2} M_{c0}$, where $\hat{f} = \hat{f}(V)$ is given by (3.40) and $M_{c0} \simeq 4.44272$ is the critical load in the constant-viscosity case. For a fixed value of B the critical film thickness, and hence the critical load, become small like $O(\log(-V)/(-V)) \ll 1$ in the limit of strong negative thermoviscosity $V \to -\infty$ and become large like $O(V^{1/2}) \gg 1$ in the limit of strong positive thermoviscosity $V \to \infty$.

Full-film solutions with a prescribed load M exist only when $0 < M \leq M_c$, and figure 3.13 shows how for each prescribed value of M the corresponding critical curve (B_c, V_c) divides the B–V parameter plane into the region above the curve in which full-film solutions exist from the region below the curve in which they do not exist. In particular, there are no full-film solutions with a prescribed load

for any value of B when $M \geq \hat{M}$ for positive V and when $M > M_{c0}$ for negative V. In Section 3.5 we showed that near $\theta = 0$ the film thickness h is a decreasing (increasing) function of B for positive (negative) V, and a decreasing function of B, but that near $\theta = \pi$ it behaves in the opposite way. For a fixed value of V there are full-film solutions in the limit $B \to \infty$ for $V \geq V_\infty$, but not for $V < V_\infty$, where $V = V_\infty$ satisfies $M = \hat{M}$. For a fixed value of B there is no full-film solution in the limit $V \to -\infty$, while the leading-order film thickness is the $O(1)$ constant $h = M/2\pi$ in the limit $V \to \infty$.

In Section 3.6 we showed that, while by far the most common behaviour of the azimuthal velocity is that it is always in the same direction as the rotation of the cylinder, for sufficiently small prescribed values of M satisfying $M < M_{\max} \simeq 1.50315$ there is a narrow region of the B–V parameter plane shown in figure 3.23 in which backflow occurs in a region on the right-hand side of the cylinder containing the point of the free surface at $\theta = 0$. In particular, backflow never occurs for any value of B when $V \geq V_{\max} \simeq -5.65658$ or for any value of V when $B < B_{\min} \simeq 26.29946$.

Lastly, in Section 3.7 we considered the distinguished limit of strong thermoviscosity $|V| \to \infty$ and weak heat transfer $B \to 0^+$ with $\hat{V} = BV = O(1)$ in which the variation of temperature across the film is small but the variation of viscosity across the film is still $O(1)$, and found qualitative agreement with but some quantitative differences from the previous results. In particular, unlike in the limit $V \to \infty$ described above, in the limit $\hat{V} \to \infty$ the critical film thickness, and hence the critical load, become large like $O(\hat{V}) \gg 1$.

Chapter 4

Rivulet Flow on a Rotating Horizontal Cylinder

In this chapter we use lubrication theory to study the steady three-dimensional flow of a rivulet of Newtonian fluid on either the outside or the inside of a rotating horizontal cylinder.

4.1 Problem Formulation

Consider the three-dimensional steady flow of a thin, slowly varying, symmetric rivulet of Newtonian fluid with uniform density ρ and viscosity μ on either the outside or the inside of a large circular cylinder of radius R rotating in a counter-clockwise direction about its horizontal axis at uniform angular speed Ω (> 0) (so that the circumferential speed, denoted by U, is $U = R\Omega$). Referred to polar coordinates θ (the azimuthal coordinate measured counter-clockwise from the horizontal), Y (the axial coordinate with origin at the axis of symmetry of the rivulet) and $r = R \pm Z$ (the radial coordinate with origin at the cylinder's axis), as shown in figure 4.1 (drawn for the case of flow on the outside of the cylinder), we take the free surface of the rivulet to be at $r = R + h$ for flow on the outside of the cylinder and $r = R - h$ for flow on the inside of the cylinder, the rivulet profile

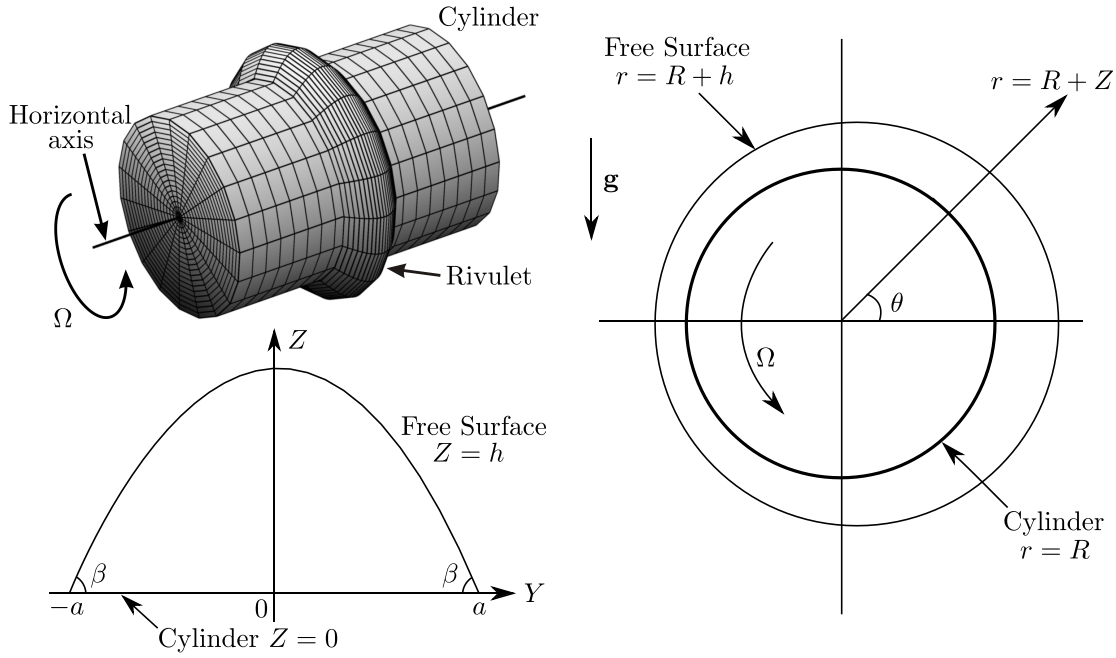

Figure 4.1: Geometry of the problem: steady flow of a thin, slowly varying, symmetric rivulet of Newtonian fluid on a uniformly rotating horizontal cylinder

being denoted by $h = h(\theta, Y)$, and take the contact lines of the rivulet (where $h = 0$) to be at $Y = \pm a$, the semi-width being denoted by $a = a(\theta)$ (> 0). Hence the fluid lies in the intervals $-a \leq Y \leq a$ and $0 \leq Z \leq h$ for $-\pi < \theta \leq \pi$. The fluid velocity $\mathbf{u} = u\mathbf{e}_\theta + v\mathbf{e}_Y + w\mathbf{e}_r$ (where $\mathbf{e}_\theta$, $\mathbf{e}_Y$ and $\mathbf{e}_r$ denote unit vectors in the azimuthal, axial and radial directions, respectively) and pressure p are governed by the usual mass-conservation and Navier–Stokes equations. On the cylinder $r = R$ the velocity $\mathbf{u}$ satisfies no-slip and no-penetration conditions, while on the free surface $r = R \pm h$ the usual normal and tangential stress balances and the kinematic condition apply.

We consider only thin, slowly varying rivulets whose transverse aspect ratio is defined to be the prescribed contact angle, denoted by $\beta \ll 1$, and whose longitudinal aspect ratio, denoted ϵ, is defined in terms of the capillary length $l = (\gamma/\rho g)^{1/2}$ to be $\epsilon = l/R \ll 1$, where γ is the coefficient of surface tension (assumed

constant) and g is the magnitude of gravitational acceleration. In particular, we consider the case where the rivulet is sufficiently slowly varying such that $\epsilon \ll \beta \ll 1$; this is a sensible case to consider since it is easily realised by making the cylinder (and therefore the radius of the cylinder R) sufficiently large. Hence we non-dimensionalise and scale the system appropriately by writing

$$\left.\begin{gathered} r = R(1 \pm \epsilon\beta Z^*), \quad Y = \epsilon R Y^*, \quad \theta = \pm\theta^*, \quad h = \epsilon\beta R h^*, \quad a = \epsilon R a^*, \\ u = \frac{\epsilon^2\beta^2 R^2 \rho g}{\mu} u^*, \quad v = \pm\frac{\epsilon^3\beta^2 R^2 \rho g}{\mu} v^*, \quad w = \frac{\epsilon^3\beta^3 R^2 \rho g}{\mu} w^*, \\ p = p_{\mathrm{a}} + \epsilon\beta R\rho g p^*, \quad U = R\Omega = \frac{\epsilon^2\beta^2 R^2 \rho g}{\mu} U^*, \\ Q = \frac{\epsilon^4\beta^3 R^4 \rho g}{\mu} Q^*, \quad M = \epsilon^2\beta R^3 \rho M^*, \end{gathered}\right\} \tag{4.1}$$

in which the + sign (− sign) corresponds to flow on the outside (inside) of the cylinder, p_{a} is the constant pressure in the surrounding atmosphere, Q is the constant azimuthal volume flux of fluid crossing a station θ = constant, and M (> 0) is the constant fluid load (i.e. the mass of fluid) on the cylinder. For clarity the star superscripts on the non-dimensional quantities will be omitted henceforth. We shall describe what follows in terms of flow on the outside of the cylinder only (i.e. we choose the + in the ± above) so that, in particular, positive values of θ correspond to the top of the cylinder and negative values to the bottom; to interpret the results that follow for flow on the inside of the cylinder it is simply necessary to let positive values of θ correspond to the bottom of the cylinder and negative values to the top. Note that physically this "swapping" of top and bottom when switching between coating and rimming flow also occurs in the corresponding two-dimensional "full-film" problem considered by Moffatt [7], however, since this flow exhibits top-to-bottom symmetry (unlike in the present problem), the sign change is unnecessary.

At leading order in ϵ and β the governing equations for the flow on the cylinder become

$$\frac{\partial u}{\partial \theta} + \frac{\partial v}{\partial Y} + \frac{\partial w}{\partial Z} = 0, \quad \frac{\partial p}{\partial Z} = -\sin\theta, \quad \frac{\partial^2 u}{\partial Z^2} = \cos\theta \quad \text{and} \quad \frac{\partial p}{\partial Y} = 0, \tag{4.2}$$

together with the boundary conditions

$$u = U \quad \text{and} \quad v = w = 0 \quad \text{on} \quad Z = 0, \tag{4.3}$$

$$p = -\frac{\partial^2 h}{\partial Y^2} \quad \text{and} \quad \frac{\partial u}{\partial Z} = \frac{\partial v}{\partial Z} = 0 \quad \text{on} \quad Z = h, \tag{4.4}$$

the kinematic condition on $Z = h$, which may be written in the form

$$\frac{\partial \bar{u}}{\partial \theta} + \frac{\partial \bar{v}}{\partial Y} = 0, \tag{4.5}$$

where the local fluxes $\bar{u} = \bar{u}(\theta, Y)$ and $\bar{v} = \bar{v}(\theta, Y)$ are defined by

$$\bar{u} = \int_0^h u \, \mathrm{d}Z, \quad \bar{v} = \int_0^h v \, \mathrm{d}Z, \tag{4.6}$$

and

$$h = 0 \quad \text{and} \quad \frac{\partial h}{\partial Y} = \mp 1 \quad \text{on} \quad Y = \pm a. \tag{4.7}$$

Introducing the rescaled axial coordinate $y = Y/a$ and rescaled radial coordinate $z = Z/h$ (so that the fluid lies within the fixed intervals $-1 \leq y \leq 1$ and $0 \leq z \leq 1$ for $-\pi < \theta \leq \pi$) and integrating $(4.2)_2$ subject to $(4.4)_1$ at the free surface $z = 1$ gives the pressure distribution

$$p = h \sin\theta (1 - z) - \frac{1}{a^2} \frac{\partial^2 h}{\partial y^2}, \tag{4.8}$$

from which $(4.2)_4$ gives a third-order differential equation for the rivulet profile $h = h(\theta, y)$, namely

$$\frac{\partial}{\partial y} \left(a^2 h \sin\theta - \frac{\partial^2 h}{\partial y^2} \right) = 0, \tag{4.9}$$

whose solution satisfying (4.7) at the contact lines $y = \pm 1$ is

$$h = \begin{cases} \dfrac{\cosh(ma) - \cosh(may)}{m \sinh(ma)} & \text{if } 0 < \theta < \pi, \\ \dfrac{a}{2}(1 - y^2) & \text{if } \theta = 0 \text{ or } \theta = \pi, \\ \dfrac{\cos(may) - \cos(ma)}{m \sin(ma)} & \text{if } -\pi < \theta < 0, \end{cases} \tag{4.10}$$

where for convenience we have introduced the notation $m = |\sin\theta|^{1/2}$. Note that this solution for the rivulet profile h is exactly the same as that given by Duffy

and Moffatt [76] for the unidirectional flow of a rivulet down a plane inclined at an angle $\pi/2 - \theta$ to the horizontal.

We shall be concerned only with "full-rivulet" solutions, i.e. solutions for which h and a are continuous, finite and non-zero for all $-\pi < \theta \leq \pi$ and $-1 < y < 1$, corresponding to a continuous rivulet of finite, non-zero thickness and width that runs all the way round the cylinder. This may be thought of as a three-dimensional generalisation of the two-dimensional "full-film" coating and rimming solutions first considered by Moffatt [7]. At any station $\theta =$ constant the rivulet profile h, given by (4.10), is symmetric about $y = 0$, with a single maximum at $y = 0$, and the maximum thickness of the rivulet, denoted $h_{\mathrm{m}} = h_{\mathrm{m}}(\theta) = h(\theta, 0)$, is given by

$$h_{\mathrm{m}} = \begin{cases} \dfrac{1}{m}\tanh\left(\dfrac{ma}{2}\right) & \text{if } 0 < \theta < \pi, \\ \dfrac{a}{2} & \text{if } \theta = 0 \text{ or } \theta = \pi, \\ \dfrac{1}{m}\tan\left(\dfrac{ma}{2}\right) & \text{if } -\pi < \theta < 0. \end{cases} \tag{4.11}$$

For future reference it is useful to note that in both of the limits $a \to 0^+$ or $m \to 0^+$ the rivulet profile h is given by

$$h = \frac{a}{2}\left(1 - y^2\right) - \mathrm{sgn}(\theta)\frac{m^2 a^3}{24}\left(1 - y^2\right)^2 + O\left(m^4 a^5\right), \tag{4.12}$$

while in the limit $a \to \infty$ if $0 < \theta < \pi$ the rivulet profile h is given by

$$h = \frac{1}{m}\left(1 - 2\mathrm{e}^{-ma}\cosh(may)\right) + O\left(\mathrm{e}^{-2ma}\right), \tag{4.13}$$

and in the limit $ma \to \pi$ if $-\pi < \theta < 0$ the rivulet profile h is given by

$$h = \frac{1 + \cos(\pi y)}{m(\pi - ma)} + \frac{y\sin(\pi y)}{m} + O(\pi - ma). \tag{4.14}$$

Integrating $(4.2)_3$ twice subject to $(4.3)_1$ on the cylinder at $z = 0$ and $(4.4)_2$ on the free-surface $z = 1$ gives the azimuthal velocity

$$u = U + \frac{h^2 z}{2}(z - 2)\cos\theta, \tag{4.15}$$

and so the local azimuthal flux $\bar{u}$ is given by

$$\bar{u} = Uh - \frac{1}{3}h^3 \cos\theta, \tag{4.16}$$

and hence the constant volume flux Q is given by

$$Q = a\int_{-1}^{1} \overline{u}\,\mathrm{d}y = Ua\int_{-1}^{1} h\,\mathrm{d}y - \frac{a}{3}\cos\theta\int_{-1}^{1} h^3\,\mathrm{d}y, \tag{4.17}$$

which leads to

$$Q = -\frac{\cos\theta}{9m^4}F(ma) + \frac{U}{m^2}G(ma), \tag{4.18}$$

where appropriate interpretation of the cases $\theta = 0$ and $\theta = \pi$ as limits is required. Equation (4.18) provides an implicit solution for the semi-width $a = a(\theta)$ in terms of the constant (but as yet unknown) flux Q, where the functions $F(ma)$ and $G(ma)$ are defined by

$$F(ma) = \begin{cases} 15ma\coth^3(ma) - 15\coth^2(ma) - 9ma\coth(ma) + 4 & \text{if } 0 < \theta < \pi, \\ -15ma\cot^3(ma) + 15\cot^2(ma) - 9ma\cot(ma) + 4 & \text{if } -\pi < \theta < 0, \end{cases} \tag{4.19}$$

and

$$G(ma) = \begin{cases} 2(ma\coth(ma) - 1) & \text{if } 0 < \theta < \pi, \\ 2(1 - ma\cot(ma)) & \text{if } -\pi < \theta < 0, \end{cases} \tag{4.20}$$

and are plotted together with their derivatives $F'(ma)$ and $G'(ma)$ in figure 4.2. For $0 < \theta < \pi$ the functions $F(ma)$, $G(ma)$, $F'(ma)$ and $G'(ma)$ are positive functions of ma, increasing monotonically from zero at $ma = 0$ to infinity, infinity, 6 and 2, respectively, as $ma \to \infty$, whereas for $-\pi < \theta < 0$ the functions $F(ma)$, $G(ma)$, $F'(ma)$ and $G'(ma)$ have multiple branches; however, one may show that in the latter case the branch that gives rise to full-rivulet solutions lies in the interval $0 < ma < \pi$ within which $F(ma)$, $G(ma)$, $F'(ma)$ and $G'(ma)$ are positive functions of ma, increasing monotonically from zero at $ma = 0$ to infinity as $ma \to \pi$. For future reference it is useful to note that in the limit $ma \to 0$, $F(ma)$

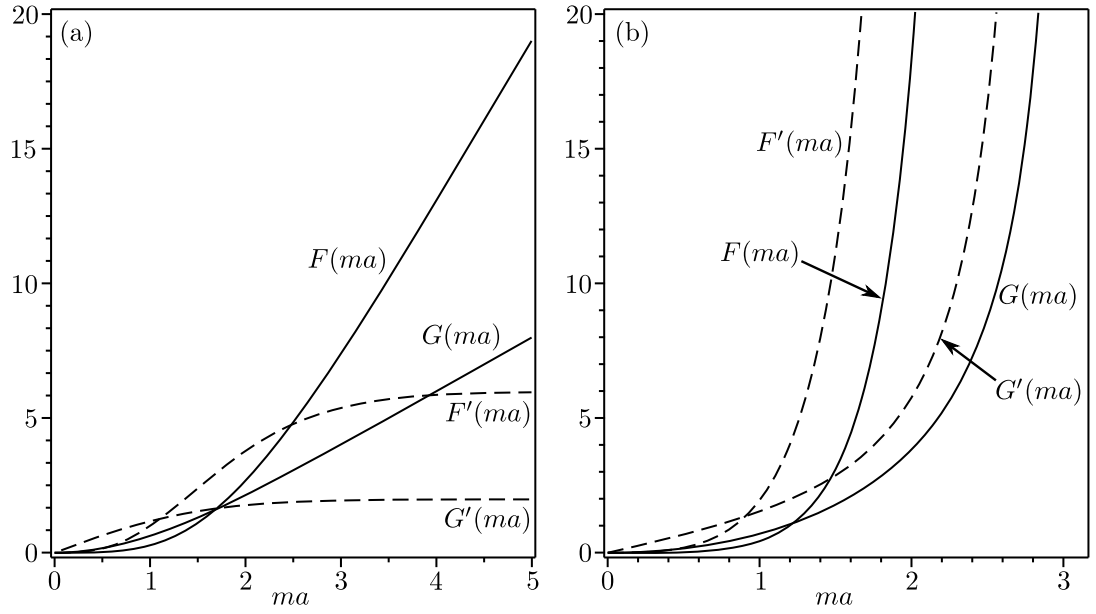

Figure 4.2: The functions $F(ma)$ and $G(ma)$ (solid lines), defined by (4.19) and (4.20), respectively, together with their derivatives $F'(ma)$ and $G'(ma)$ (dashed lines) when (a) $0 < \theta < \pi$ and (b) $-\pi < \theta < 0$ in the interval $0 < ma < \pi$.

and $G(ma)$ are given by

$$F(ma) = \begin{cases} \dfrac{12}{35}(ma)^4 - \dfrac{8}{105}(ma)^6 + O\left((ma)^8\right) & \text{if } 0 < \theta < \pi, \\ \dfrac{12}{35}(ma)^4 + \dfrac{8}{105}(ma)^6 + O\left((ma)^8\right) & \text{if } -\pi < \theta < 0, \end{cases} \tag{4.21}$$

and

$$G(ma) = \begin{cases} \dfrac{2}{3}(ma)^2 - \dfrac{2}{45}(ma)^4 + O\left((ma)^6\right) & \text{if } 0 < \theta < \pi, \\ \dfrac{2}{3}(ma)^2 + \dfrac{2}{45}(ma)^4 + O\left((ma)^6\right) & \text{if } -\pi < \theta < 0, \end{cases} \tag{4.22}$$

while in the limit $ma \to \infty$ when $0 < \theta < \pi$, $F(ma)$ and $G(ma)$ are given by

$$F(ma) = 6ma - 11 + 12(6ma - 5)\exp(-2ma) + O\big(ma\exp(-4ma)\big) \tag{4.23}$$

and

$$G(ma) = 2ma - 2 + 4ma\exp(-2ma) + O\big(ma\exp(-4ma)\big), \tag{4.24}$$

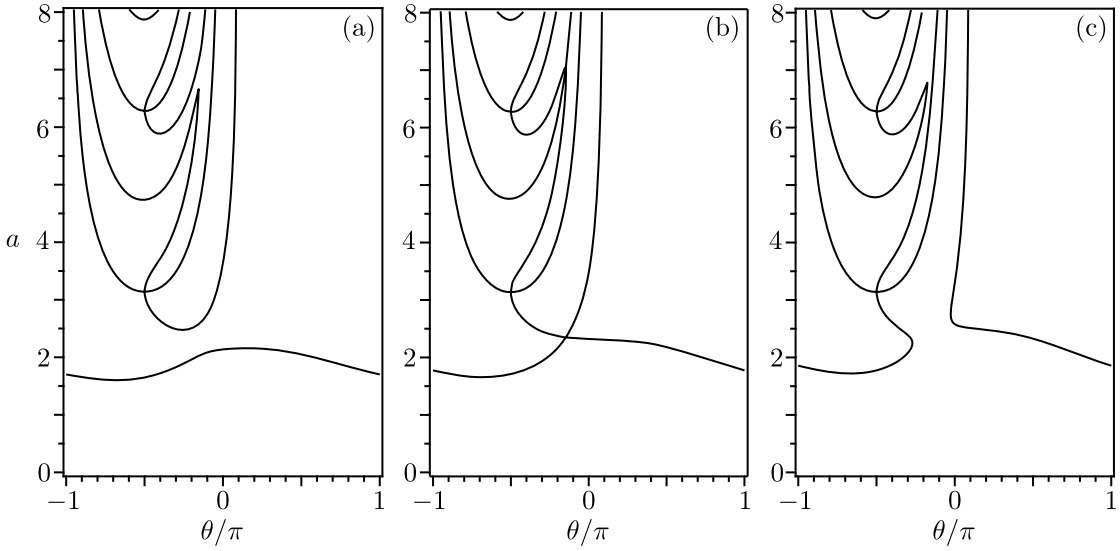

Figure 4.3: Three contours of the expression for the flux Q given by (4.18) in the θ/π–a plane when $U = 1$. The contours are drawn for (a) $Q = 2.25$, (b) $Q = Q_{\rm c} = 10\sqrt{5}/9 \simeq 2.48452$ and (c) $Q = 2.75$, which together illustrate that full-rivulet solutions exist when $Q \leq Q_{\rm c}$ but not when $Q > Q_{\rm c}$.

and in the limit $ma \to \pi$ when $-\pi < \theta < 0$, $F(ma)$ and $G(ma)$ are given by

$$F(ma) = \frac{15\pi}{(\pi - ma)^3} - \frac{6\pi}{\pi - ma} + O(\pi - ma) \tag{4.25}$$

and

$$G(ma) = \frac{2\pi}{\pi - ma} - \frac{2\pi}{3}(\pi - ma) + O(\pi - ma)^2. \tag{4.26}$$

At the top and bottom of the cylinder ($\theta = \pm\pi/2$) the flux Q given by equation (4.18) takes the form $Q = UG(a)$, which shows that $Q > 0$, while at $\theta = 0$ and $\theta = \pi$ careful interpretation of (4.18) as a limit is required whereupon (4.18) becomes $Q = -4a^4/105 + 2Ua^2/3$ and $Q = 4a^4/105 + 2Ua^2/3$ for $\theta = 0$ and $\theta = \pi$, respectively. By considering the roots the equation for the flux when $\theta = 0$ it can be shown that Q satisfies $0 < Q < 35U^2/12$. Figure 4.3 shows three contours of the expression for the flux Q given by (4.18) in the θ/π–a plane when $U = 1$ (these plots are typical for any value of U), which, since they are by definition curves on which $Q =$ constant, represent candidate solutions for the

semi-width $a = a(\theta)$. It can also been seen from Figure 4.3 that only the lowest positive solution for a can possibly correspond to a full-rivulet solution (that is, a solution corresponding to a rivulet with continuous, finite and non-zero width and thickness). This figure also clearly demonstrates one of the key features of the present problem, namely the existence of a critical solution with critical flux $Q = Q_c$ above which no full-rivulet solution exists (the critical solution is discussed in detail in Section 4.2). This result is similar in nature to the critical full-film solution found by Moffatt [7] for two-dimensional flow; however, as we shall see in Section 4.2, unlike the two-dimensional problem, the critical flux in the present problem depends on a condition of criticality and either the rotation speed U or the load M. In particular, figure 4.3(a) shows that when $Q < Q_c$ only the lowest branch is a full-rivulet solution while the higher branches form a rather complicated "network" which does not extend over all $-\pi < \theta \leq \pi$ and so cannot be full-rivulet solutions. Figure 4.3(b) shows that when $Q = Q_c$ a critical full-rivulet solution again exists; however, it is made up of two branches of solutions which meet to form a corner at some point $\theta = \hat{\theta}_c$, $a = \hat{a}_c$ (similar to the corner found by Moffatt [7] in the critical two-dimensional full-film flow), while again the higher branches cannot be full-rivulet solutions. Figure 4.3(c) shows that when $Q > Q_c$ there is no branch that is continuous for all $-\pi < \theta \leq \pi$ and so no full-rivulet solution exists.

The total fluid load on the cylinder, $M(> 0)$, is given by

$$M = \int_{-\pi}^{\pi} \int_{-1}^{1} \int_{0}^{1} a(\theta) h(\theta, y) \, \mathrm{d}z \, \mathrm{d}y \, \mathrm{d}\theta, \tag{4.27}$$

leading to

$$M = \int_{-\pi}^{\pi} \frac{G(ma)}{m^2} \, \mathrm{d}\theta, \tag{4.28}$$

where the function $G(ma)$ is again given by (4.20).

With the rotation speed U prescribed, the semi-width a, and hence the rivulet profile h, is determined in terms of Q by the algebraic equation (4.18) in which F and G are given by (4.19) and (4.20), respectively. The value of Q is determined either from an appropriate criticality condition or from the condition of prescribed

load using (4.28). The properties and behaviour of the solutions in these two cases are discussed in detail in Sections 4.2 and 4.3, respectively, but in both cases, the solutions for p, h and u are given explicitly by (4.8), (4.10) and (4.15), respectively.

4.2 The Critical Solution

In this Section we consider in detail the behaviour of the critical full-rivulet solution with critical flux $Q = Q_c$. Not only is this of interest in its own right but, as we shall see, investigating this critical case is necessary to understand when a full-rivulet solution exists when both the rotation speed U and load M are prescribed (this non-critical solution is discussed in detain in Section 4.3). In the critical case either U or M may be prescribed with the other being determined by the condition of criticality; specifically, as we shall see, if the rotation speed U is prescribed then there is a critical load, denoted M_c, above which no full-rivulet solutions are possible, whereas if the load M is prescribed then there is a critical rotation speed, denoted U_c, below which no full-rivulet solutions are possible. For future reference we note here that variables in the critical case will be denoted with a subscript c, e.g. a_c, h_c, M_c, etc. For simplicity and to avoid repetition we present the following analysis for the case of prescribed rotation speed U and leave the reader to interpret the results appropriately for the case of prescribed load M.

As may be seen from figure 4.3(b), a key feature of the critical solution is that the expression for Q in (4.18) has a saddle point at some $\theta = \hat{\theta}_c$ and $a = \hat{a}_c$ which gives rise to a corner in the critical full-rivulet profile h_c (similar in nature to that found by Moffatt [7] for the case of two-dimensional full-film flow). Variables in the critical case relating to the corner will be denoted with both a subscript c and a hat e.g. $\hat{\theta}_c$, $\hat{a}_c$, $\hat{h}_c$, etc. At the saddle point we have $\partial Q/\partial\theta = 0$ and $\partial Q/\partial a = 0$, which, from (4.18), leads to the criticality conditions

$$\begin{aligned}(1+\cos^2\hat{\theta}_c)F(\hat{m}_c\hat{a}_c) &= 9U\cos\hat{\theta}_c|\sin\hat{\theta}_c|G(\hat{m}_c\hat{a}_c),\\ \cos\hat{\theta}_c F'(\hat{m}_c\hat{a}_c) &= 9U|\sin\hat{\theta}_c|G'(\hat{m}_c\hat{a}_c),\end{aligned} \tag{4.29}$$

where we have defined $\hat{m}_{\rm c} = |\sin\hat{\theta}_{\rm c}|^{1/2}$. We may eliminate $\hat{a}_{\rm c}$ and $\hat{\theta}_{\rm c}$ from (4.29) in favour of $B_{\rm c} = \hat{m}_{\rm c}\hat{a}_{\rm c}$ (> 0) in order to obtain a single algebraic equation for $B_{\rm c}$ involving the parameter U only, namely

$$\frac{F(B_{\rm c})F'(B_{\rm c})^2}{G'(B_{\rm c})\left[F'(B_{\rm c})G(B_{\rm c}) - 2F(B_{\rm c})G'(B_{\rm c})\right]} = 81U^2. \tag{4.30}$$

From the criticality conditions (4.29) it is clear that $\cos\hat{\theta}_{\rm c} > 0$ and so we deduce that the corner lies on the right-hand-side of the cylinder (i.e. in the interval $-\pi/2 < \hat{\theta}_{\rm c} < \pi/2$). When $0 < \hat{\theta}_{\rm c} < \pi/2$ the function on the left-hand side of (4.30) is negative for all $B_{\rm c} > 0$, and so (4.30) has no full-rivulet solution for $B_{\rm c}$ for any U; on the other hand, when $-\pi/2 < \hat{\theta}_{\rm c} < 0$ this function is positive for $0 < B_{\rm c} < \pi$, increasing monotonically from zero at $B_{\rm c} = 0$ to infinity as $B_{\rm c} \to \pi$, so that for any prescribed U equation (4.30) has a unique solution for $B_{\rm c}$. Then, with $B_{\rm c}$ determined numerically from (4.30), the position of the corner $\hat{\theta}_{\rm c} = \hat{\theta}_{\rm c}(U)$ is given by (4.29) as

$$\hat{\theta}_{\rm c} = -\tan^{-1}\left(\frac{F'(B_{\rm c})}{9UG'(B_{\rm c})}\right), \tag{4.31}$$

which together with (4.19), (4.20) and (4.30) can be used to show that $\hat{\theta}_{\rm c}$ satisfies $-\pi/4 < \hat{\theta}_{\rm c} < 0$. In particular, if $B_{\rm c} \to 0$ then $\hat{\theta}_{\rm c} \to 0$, while if $B_{\rm c} \to \pi$ then $\hat{\theta}_{\rm c} \to -\pi/4$. The semi-width at the corner $\hat{a}_{\rm c} = \hat{a}_{\rm c}(U)$ is then given by

$$\hat{a}_{\rm c} = \frac{B_{\rm c}}{\hat{m}_{\rm c}} = \frac{B_{\rm c}}{\left(-\sin\hat{\theta}_{\rm c}\right)^{1/2}}, \tag{4.32}$$

and from (4.18) and (4.29) the critical flux $Q_{\rm c} = Q_{\rm c}(U)$ is given by

$$Q_{\rm c} = \frac{F(B_{\rm c})}{9\sin^2\hat{\theta}_{\rm c}\cos\hat{\theta}_{\rm c}}. \tag{4.33}$$

With the rotation speed U prescribed and the value of $Q_{\rm c}$ obtained from (4.33), the solution for the critical semi-width $a_{\rm c}$, critical rivulet profile $h_{\rm c}$, critical maximum thickness $h_{\rm mc}$, critical pressure $p_{\rm c}$, critical velocity $u_{\rm c}$ and critical load $M_{\rm c}$ may be obtained from (4.18), (4.10), (4.11), (4.8), (4.15) and (4.28), respectively. Figure 4.4 shows (a) the scaled position of the corner $\hat{\theta}_{\rm c}/\pi$, (b) the critical flux $Q_{\rm c}$ and (c) the critical load $M_{\rm c}$, plotted as functions of U. In particular, figure 4.4 shows

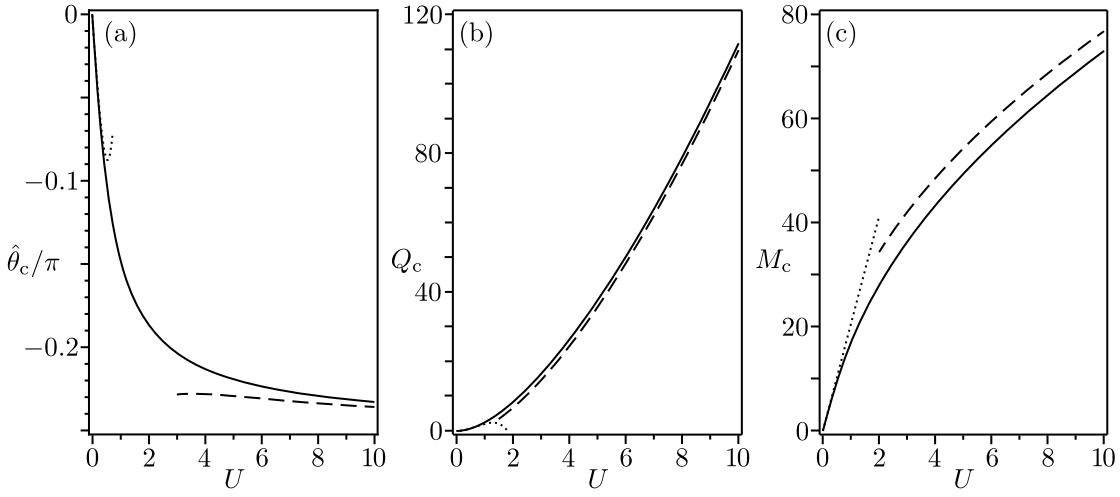

Figure 4.4: (a) The scaled position of the corner in the critical solution $\hat{\theta}_c/\pi$, (b) the critical flux Q_c and (c) the critical load M_c plotted as functions of U (solid lines) together with the asymptotic solutions (4.35), (4.36) and (4.41), and (4.42), (4.43) and (4.60) in the limits $U \to 0$ (dotted lines) and $U \to \infty$ (dashed lines), respectively. Full-rivulet solutions exist only for values of U and M that lie below the solid line in (c).

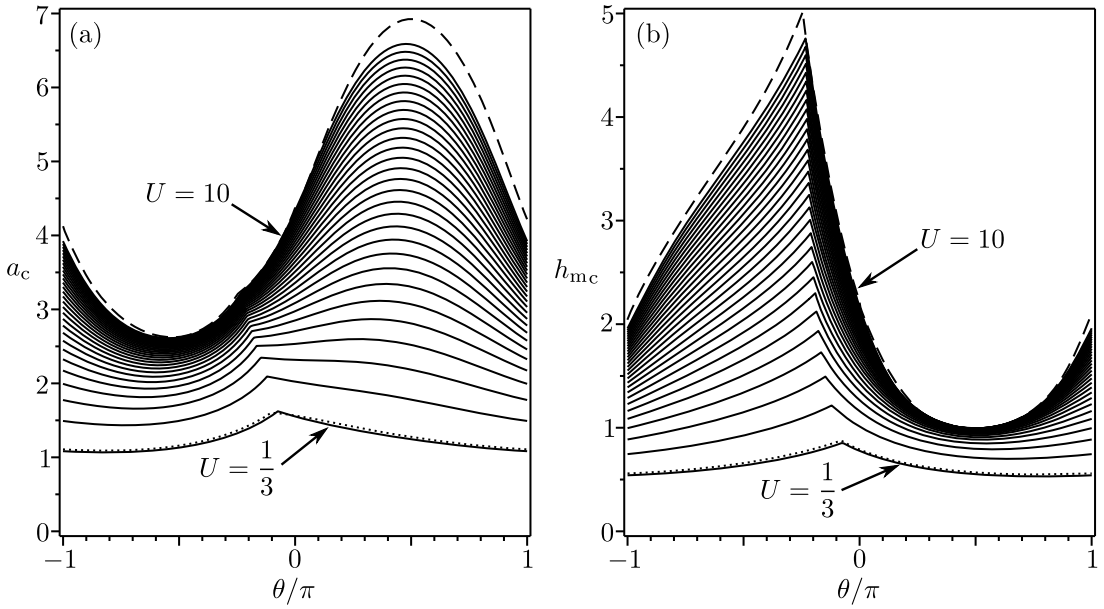

Figure 4.5: (a) The critical semi-width a_c and (b) the critical maximum thickness h_{mc} plotted as functions of θ/π for $U = 1/3$, $2/3$, 1, …, 10 (solid lines) together with the asymptotic solutions (4.37) and (4.38), and (4.50), (4.51), (4.56) and (4.57) in the limits $U \to 0$ (dotted lines) and $U \to \infty$ (dashed lines) for $U = 1/3$ and $U = 10$, respectively.

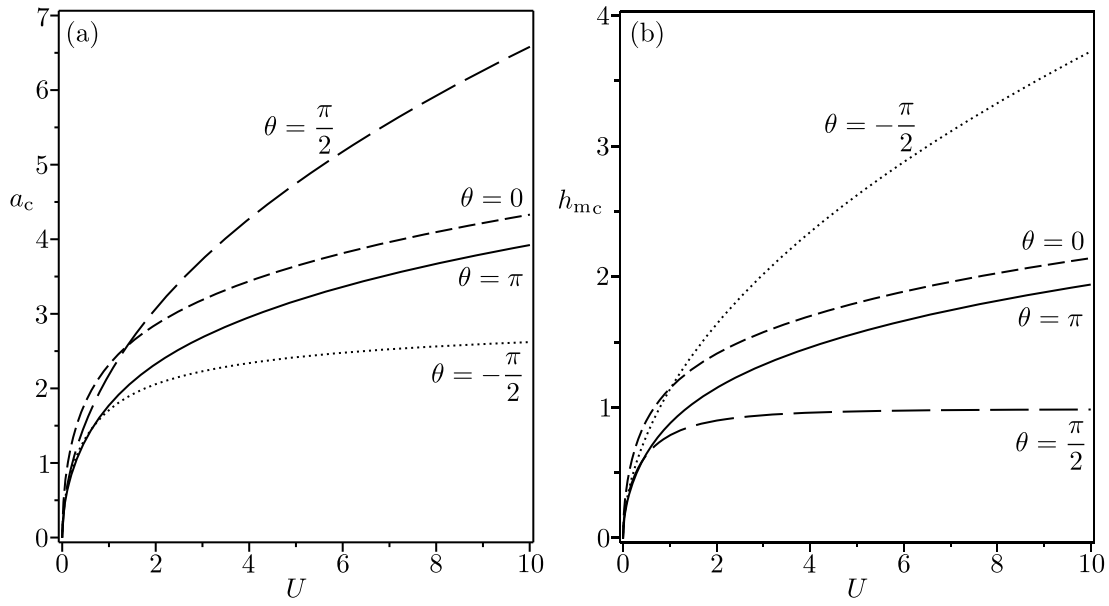

Figure 4.6: (a) The critical semi-width a_c and (b) the critical maximum thickness h_{mc} plotted as functions of U for $\theta = \pi$ (solid lines), $\theta = \pi/2$ (long-dashed lines), $\theta = 0$ (short-dashed lines) and $\theta = -\pi/2$ (dotted lines).

that $\hat{\theta}_c$ is a decreasing function of U, decreasing from zero at $U = 0$ to $-\pi/4$ as $U \to \infty$, and so, unlike in the two-dimensional full-film flow considered by Moffatt [7], in which the corner is always at $\theta = 0$, the position of the corner in the present problem varies with the rotation speed U. Figure 4.4 also shows that both the critical flux Q_c and critical load M_c are increasing functions of U, increasing from zero at $U = 0$ to infinity as $U \to \infty$, and so full-rivulet solutions, which exist only for values of U and M that lie below the solid line in figure 4.4(c), are possible for larger loads when the rotation speed is increased. The fact that the corner in the solution moves towards the bottom of the cylinder as U is increased may seem counterintuitive, however, one must keep in mind that as U is increased the critical load M_c is also increased and it is the effect of gravity on the resultant increased film thickness that causes the corner to move down. Figure 4.5 shows (a) the critical semi-width a_c and (b) the critical maximum thickness h_{mc} plotted as functions of θ/π for a range of values of U, and figure 4.6 shows the same

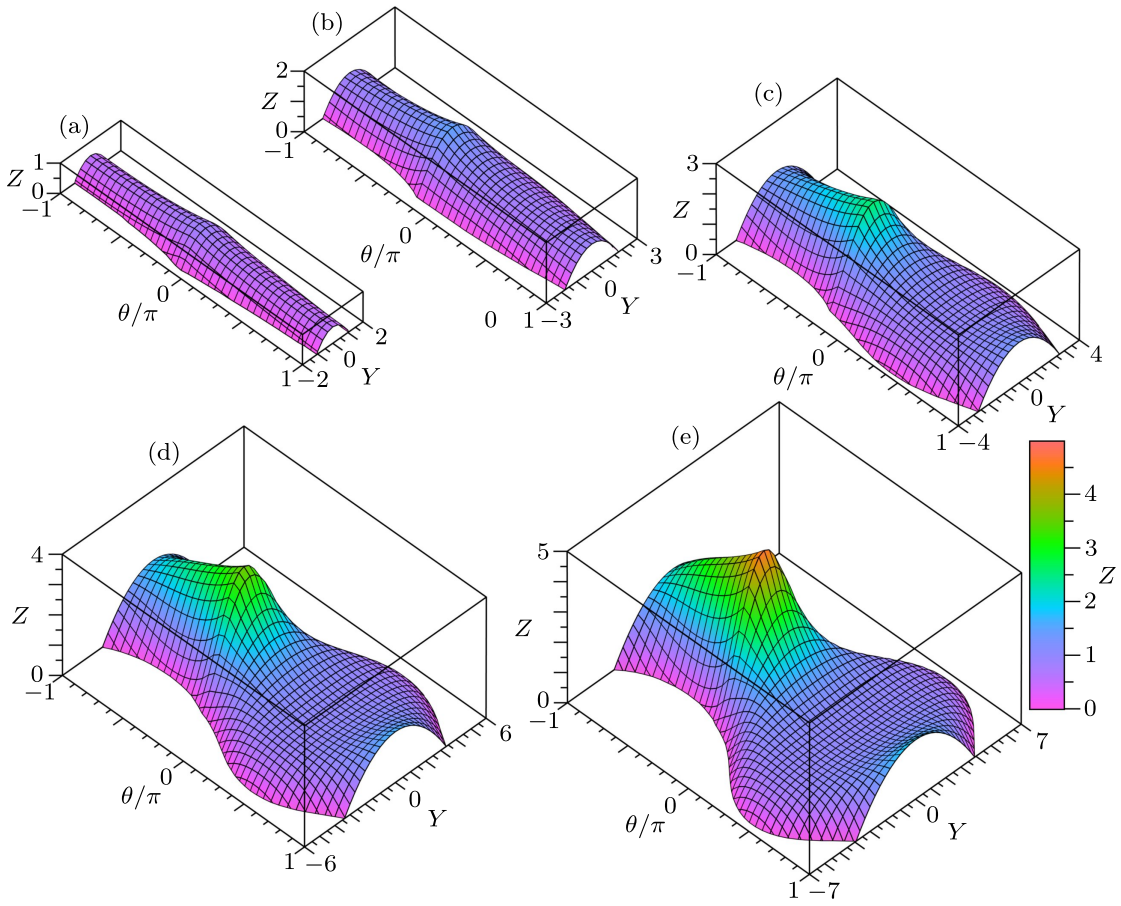

Figure 4.7: Three-dimensional plots of the critical rivulet profile h_c as a function of $Y = a_c y$ and θ/π for (a) $U = 1/3$, (b) $U = 1$, (c) $U = 3$, (d) $U = 6$ and (e) $U = 10$.

quantities plotted as functions of U for a range of values of θ. In particular, figures 4.5 and 4.6 show that both a_c and h_{mc} are increasing functions of U (a property that also holds for the critical rivulet profile h_c) and that the critical semi-width a_c (critical maximum thickness h_{mc}) is a decreasing (increasing) function of θ on the left-hand side of the cylinder near $\theta = \pi$ but is a non-monotonic function of θ elsewhere. Figure 4.7 shows three-dimensional plots of the critical rivulet profile h_c for different values of the rotation speed U, clearly illustrating the shape of the rivulet and how it changes as U varies. In particular, figures 4.5–4.7 show that when U is small the rivulet is almost uniform, whereas when U is large the rivulet

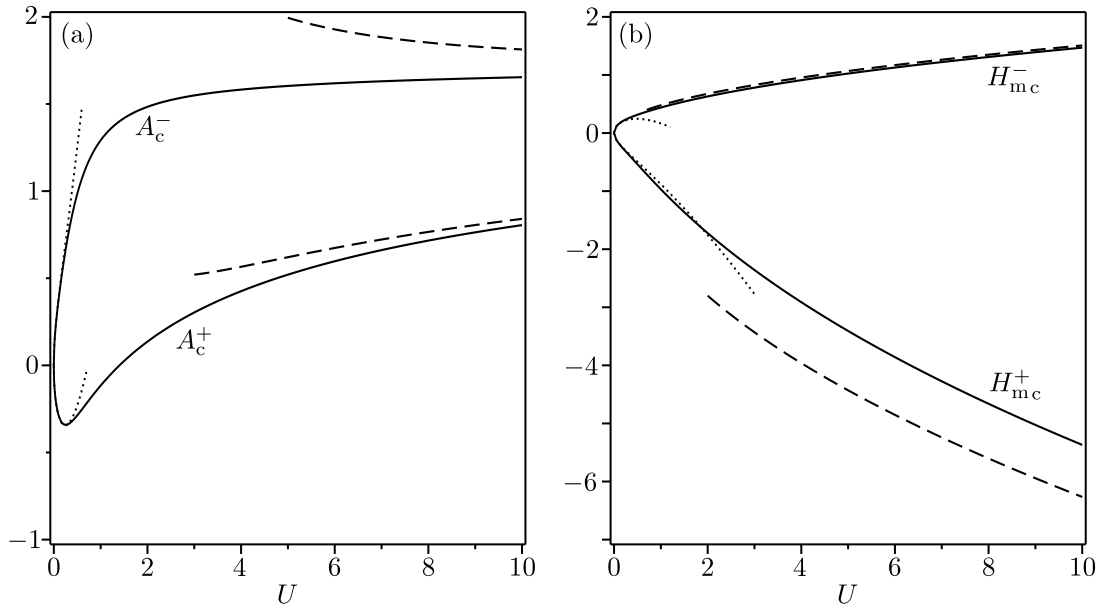

Figure 4.8: (a) The slopes of the critical semi-width a_c as $\theta \to \hat{\theta}_c^{\pm}$, $A_c^{\pm}$, and (b) the slopes of the critical maximum thickness h_{mc} as $\theta \to \hat{\theta}_c^{\pm}$, $H_{mc}^{\pm}$, plotted as functions of U (solid lines) together with the asymptotic solutions (4.39) and (4.40), and (4.58) and (4.59) in the limits $U \to 0$ (dotted lines) and $U \to \infty$ (dashed lines), respectively.

is wide and thin at the top of the cylinder near $\theta = \pi/2$ and is narrow and thick at the bottom of the cylinder near $\theta = -\pi/2$. The asymptotic limits of small and large U will be considered in detail in subsections 4.2.1 and 4.2.2, respectively.

Figures 4.3(b), 4.5 and 4.7 clearly illustrate the corner in the critical rivulet profile, the position and shape of which depends on the rotation speed U. The slopes of a_c and h_c on either side of this corner (i.e. as $\theta \to \hat{\theta}_c^{\pm}$) are denoted by

$$A_c^{\pm} = \left.\frac{\mathrm{d}a_c}{\mathrm{d}\theta}\right|_{\theta=\hat{\theta}_c^{\pm}} \quad \text{and} \quad H_c^{\pm} = \left.\frac{\partial h_c}{\partial \theta}\right|_{\theta=\hat{\theta}_c^{\pm}}. \tag{4.34}$$

Figure 4.8 shows (a) the slopes of a_c, $A_c^{\pm}$, and (b) the slopes of h_{mc}, $H_{mc}^{\pm}$, plotted as functions of U. In particular, figure 4.8 shows that A_c^- and H_{mc}^- are positive increasing functions of U (a property that also holds for H_c^-), whereas H_{mc}^+ is a negative decreasing function of U (a property that also holds for H_c^+) and A_c^+

is a negative decreasing function of U when $U < 0.25452$, a negative increasing function of U when $0.25452 < U < 1.40264$, and a positive increasing function of U when $U > 1.40264$. This behaviour of the slopes of h_c differs significantly from the two-dimensional full-film situation considered by Moffatt [7], not only because the slopes vary with the rotation speed U but also because the corner is not symmetric, i.e. the slope of h_c as $\theta \to \hat{\theta}_c^-$ is not simply the negative of the slope as $\theta \to \hat{\theta}_c^+$ as it is in the two-dimensional case.

In order to obtain a thorough understanding of the effect of varying the rotation speed U on the critical solution, in the following two subsections we analyse the behaviour of the critical solution in the asymptotic limits $U \to 0$ and $U \to \infty$, respectively.

4.2.1 The limit of small rotation speed $U \to 0$

In the limit of small rotation speed $U \to 0$ the position of the corner in the critical solution $\hat{\theta}_c$ is given from (4.30) and (4.31) by

$$\hat{\theta}_c = -\frac{7U}{9} + \frac{22148U^3}{24057} + O(U^5), \tag{4.35}$$

while from (4.33) the critical flux Q_c is given by

$$Q_c = \frac{35U^2}{12} - \frac{1715U^4}{1944} + O(U^6). \tag{4.36}$$

These solutions for $\hat{\theta}_c$ and Q_c are shown as dotted lines in figures 4.4(a) and 4.4(b), respectively, and show that the effect of small rotation speed is to decrease $\hat{\theta}_c$ from zero at $U = 0$ (specifically $O(U)$ as $U \to 0$) and to increase Q_c from zero at $U = 0$ (specifically $O(U^2)$ as $U \to 0$). With the solution for Q_c known we may show from (4.18), (4.21) and (4.22) that the critical semi-width a_c is given by

$$a_c = \frac{1}{2}\left(\frac{35U}{1+\sqrt{2}\,S\sin(\theta/2)}\right)^{1/2} + \frac{7\sqrt{35}\,U^{3/2}S\cos(\theta/2)\left(5S\sin(\theta/2)-\sqrt{2}\right)}{72\left(1+\sqrt{2}\,S\sin(\theta/2)\right)^{3/2}} + O(U^{5/2}), \tag{4.37}$$

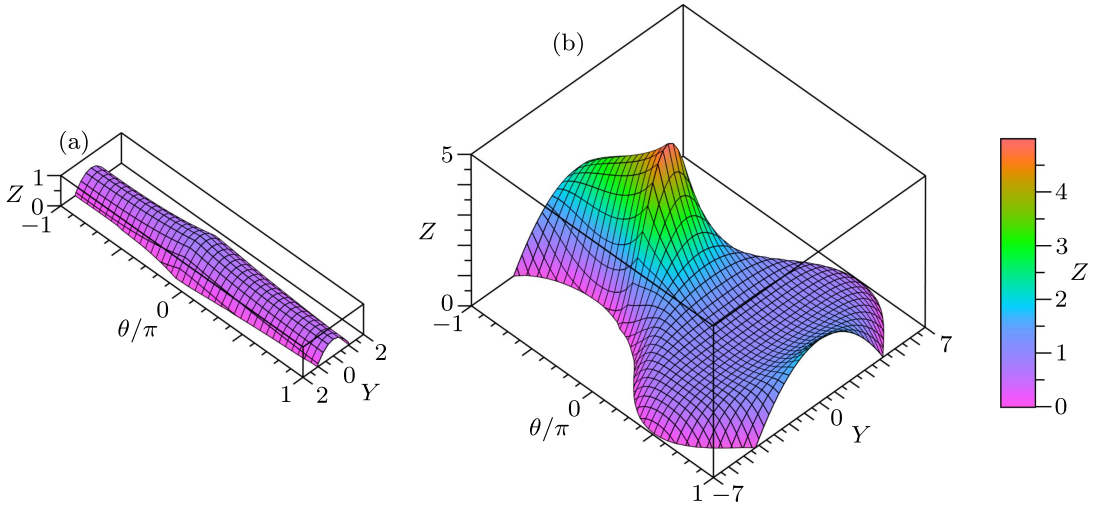

Figure 4.9: Three-dimensional plots of the asymptotic solutions for the critical rivulet profile h_c in the limit (a) $U \to 0$, given by (4.38), shown for $U = 1/3$ and (b) $U \to \infty$, given by (4.56) and (4.57), shown for $U = 10$, and plotted as functions of $Y = a_c y$ and θ/π. These figures may be compared with the corresponding numerical solutions shown in figures 4.7(a) and 4.7(e), respectively.

and hence from (4.10) and (4.12) that the critical rivulet profile h_c is given by

$$h_c = \frac{1-y^2}{4}\left(\frac{35U}{1+\sqrt{2}\,S\sin(\theta/2)}\right)^{1/2} + \frac{7\sqrt{35}\,U^{3/2}S(1-y^2)\cos(\theta/2)\left(5S\sin(\theta/2)(3y^2-1)-2\sqrt{2}\right)}{288\left(1+\sqrt{2}\,S\sin(\theta/2)\right)^{3/2}} + O(U^{5/2}), \quad (4.38)$$

where we have defined $S = \mathrm{sgn}(\theta - \hat{\theta}_c)$. These solutions for the critical semi-width a_c and critical maximum thickness $h_{mc} = h_c(\theta, 0)$ are shown as dotted lines in figure 4.5 and also in figure 4.9(a), which shows a three-dimensional plot of the asymptotic solution (4.38) for the critical rivulet profile h_c for $U = 1/3$, which may be compared with the corresponding three-dimensional plot of the numerical solution shown in figure 4.7(a). In particular, the solutions show that the effect of small rotation speed is to increase both the critical semi-width a_c and the critical rivulet profile h_c from zero when $U = 0$ (specifically both are $O(U^{1/2})$ as $U \to 0$).

The slopes on either side of the corners in a_c and h_c, $A_c^{\pm}$ and $H_c^{\pm}$, are given by

$$A_c^{\pm} = \mp\frac{(70U)^{1/2}}{8} + \frac{(35U)^{3/2}}{144} + O\left(U^{5/2}\right) \tag{4.39}$$

and

$$H_c^{\pm} = \mp\frac{(70U)^{1/2}(1-y^2)}{16} + \frac{(35U)^{3/2}(1-y^2)(3y^2-1)}{576} + O\left(U^{5/2}\right). \tag{4.40}$$

These solutions are shown as dotted lines in figure 4.8, and show that the effect of small rotation speed is to increase A_c^- and H_c^-, and decrease A_c^+ and H_c^+ from zero at $U = 0$, with all of the slopes being $O(U^{1/2})$ in the limit $U \to 0$.

From the solution for a_c given by (4.37) and the expression for the load (4.28) we find that the critical load M_c is given by

$$M_c = \frac{70U}{3}\log\left(1+\sqrt{2}\right) + O(U^3); \tag{4.41}$$

this is shown as a dotted line in figure 4.4(c) and shows that the effect of small rotation speed U is to increase the critical load from zero at $U = 0$ (specifically $O(U)$ as $U \to 0$).

4.2.2 The limit of large rotation speed $U \to \infty$

In the limit of large rotation speed $U \to \infty$ the position of the corner in the critical solution $\hat{\theta}_c$ is given from (4.30) and (4.31) by

$$\hat{\theta}_c = -\frac{\pi}{4} + \frac{3}{4U} - \frac{15}{8\pi}\left(\frac{5}{2U^3}\right)^{1/2} + O\left(\frac{1}{U^2}\right), \tag{4.42}$$

and from (4.33) the critical flux Q_c is given by

$$Q_c = \frac{8\pi U^{3/2}}{3\sqrt{5}} - \frac{2\pi U^{1/2}}{\sqrt{5}} + O\left(1\right). \tag{4.43}$$

These solutions for $\hat{\theta}_c$ and Q_c are shown as dashed lines in figures 4.4(a) and 4.4(b), respectively, and show that the effect of large but finite rotation speed is to increase $\hat{\theta}_c$ from its leading order value $\hat{\theta}_c = -\pi/4$ (specifically $\hat{\theta}_c = -\pi/4 + O(1/U)$ as

$U \to \infty$), while at leading order in the limit of large rotation speed the critical flux Q_c is large (specifically $O(U^{3/2})$ as $U \to \infty$).

Unlike the behaviour of the solution in the limit $U \to 0$, the behaviour of the solution for a_c in the limit $U \to \infty$ is qualitatively different for positive and negative θ with boundary layers near $\theta = 0$ and $\theta = \pi$ of width $O(1/U^{1/2})$. With the solution for Q_c given by (4.43) we may show from (4.18) and (4.23)–(4.26) that the solution for the critical semi-width a_c is given by

$$a_c = \frac{4\pi m U^{1/2}}{3\sqrt{5}} + \frac{1}{m} + O\left(\frac{1}{U^{1/2}}\right) \tag{4.44}$$

if $0 < \theta < \pi$, and is given by

$$a_c = \frac{\pi}{m} - \frac{\zeta}{mU^{1/2}} + O\left(\frac{1}{U^{3/2}}\right) \tag{4.45}$$

if $-\pi < \theta < 0$, where $\zeta = \zeta(\theta)$ is a root of the cubic polynomial equation

$$8\sin^2\theta\zeta^3 + 6\sqrt{5}\sin\theta\zeta^2 + 5\sqrt{5}\cos\theta = 0 \tag{4.46}$$

that is real in the interval $-\pi < \theta < 0$. The real roots of (4.46) are shown in figure 4.10, in which the root corresponding to the full-rivulet solution is shown with a solid line while the other real roots, which correspond to higher (unphysical) branches of solutions, are shown with dashed lines. The root ζ of (4.46) that corresponds to the full-rivulet solution may be written as

$$\zeta = \begin{cases} -\dfrac{\sqrt{5}}{4\sin\theta}\left[1 + 2\cosh\left(\dfrac{1}{3}\cosh^{-1}\left[1 + 2\sin(2\theta)\right]\right)\right] & \text{if } -\pi < \theta < -\pi/2, \\ \dfrac{3\sqrt{5}}{4} & \text{if } \theta = -\pi/2, \\ -\dfrac{\sqrt{5}}{4\sin\theta}\left[1 + 2\cos\left(\dfrac{1}{3}\cos^{-1}\left[1 + 2\sin(2\theta)\right]\right)\right] & \text{if } -\pi/2 < \theta < 0, \end{cases} \tag{4.47}$$

which has a corner at $\theta = -\pi/4$. From (4.44) and (4.45) we see that the effect of large but finite rotation speed U is to decrease the critical semi-width a_c from $a_c = \pi/m$ (an $O(1)$ quantity) on the bottom of the cylinder near $\theta = -\pi/2$, while

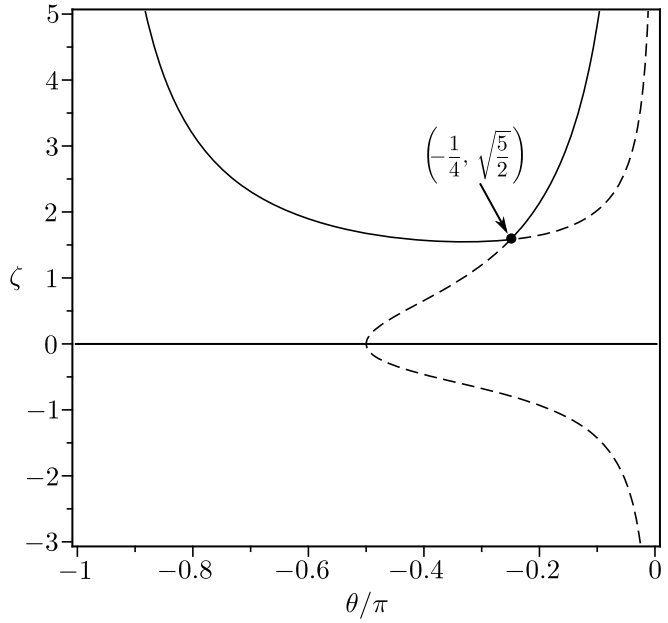

Figure 4.10: Plot of the real roots of the cubic equation (4.46), ζ, as a function of θ/π, with the root that corresponds to the full-rivulet solution shown with a solid line and the other real roots, which correspond to higher (unphysical) branches of solutions, shown with dashed lines.

on the top of the cylinder near $\theta = \pi/2$ a_c is large and of $O(U^{1/2})$. It is also interesting to note that there is no corner at leading order in the solution for a_c when $-\pi < \theta < 0$ given by (4.45); the corner does, however, appear at first order. In the boundary layers near $\theta = 0$ and $|\theta| = \pi$, a_c is given by

$$a_c = \begin{cases} a_1 U^{1/4} - \dfrac{\operatorname{sgn}(\cos\theta) F(a_1|T|^{1/2})}{9U^{1/4}|T|^{3/2}G'(a_1|T|^{1/2})} + O\left(\dfrac{1}{U^{3/4}}\right) & \text{if } \theta \neq 0, \\ \dfrac{2\sqrt{\pi}U^{1/4}}{5^{1/4}} + \dfrac{8\pi^{3/2}\operatorname{sgn}(\cos\theta)}{35(125U)^{1/4}} + O\left(\dfrac{1}{U^{3/4}}\right) & \text{if } \theta = 0 \text{ or } \theta = \pi, \end{cases} \tag{4.48}$$

where $a_1 = a_1(T)$ is the smallest positive root of

$$G\big(a_1|T|^{1/2}\big) = \frac{8\pi|T|}{3\sqrt{5}} \tag{4.49}$$

and T ($\neq 0$) is given by $T = \theta U^{1/2}$ with $a_1 = a_{c0}$ in the boundary layer near $\theta = 0$ and by $T = (\operatorname{sgn}(\theta)\pi - \theta)U^{1/2}$ with $a_1 = a_{c\pi}$ in the boundary layer near $|\theta| = \pi$. A

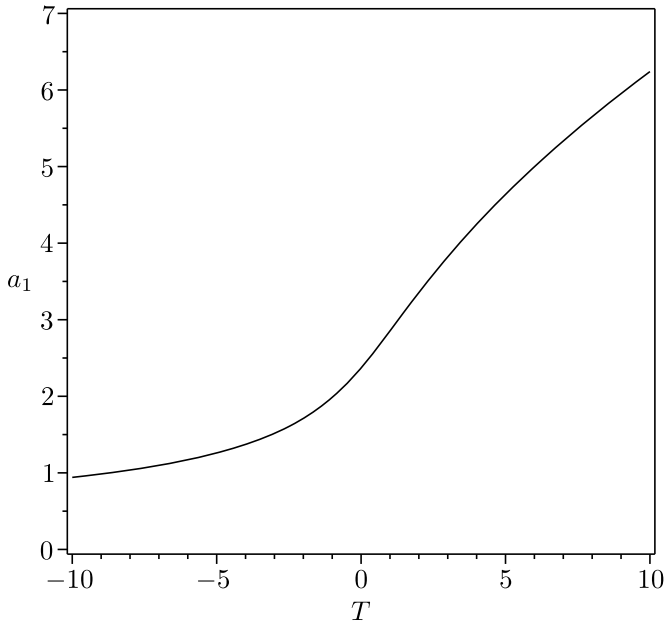

Figure 4.11: Plot of a_1 as a function of T given by the smallest positive root to (4.49).

plot of a_1 as a function of T from (4.49) is shown in figure 4.11. The solution for a_c given by (4.48) shows that at leading order in the limit of large rotation speed the critical semi-width a_c is large and of $O(U^{1/4})$ on the right-hand and left-hand sides of the cylinder near $\theta = 0$ and $\theta = \pi$, respectively. A sketch showing the structure of the solution for a_c in the limit $U \to \infty$ is shown in figure 4.12(a). A composite solution for a_c may be written as

$$a_c = \frac{4\pi U^{1/2}}{3\sqrt{5}}\big(m-(\pi-\theta)^{1/2}-\theta^{1/2}\big)+\frac{1}{m}-\frac{1}{(\pi-\theta)^{1/2}}-\frac{1}{\theta^{1/2}}+(a_{c0}+a_{c\pi})U^{1/4} \quad (4.50)$$

if $0 < \theta < \pi$, and as

$$a_c = \frac{\pi}{m} - \frac{\pi}{|\theta|^{1/2}} - \frac{\pi}{(\pi+\theta)^{1/2}} - \frac{1}{U^{1/2}}\left(\frac{\zeta}{m} - \frac{3\sqrt{5}}{4}\left[\frac{1}{|\theta|^{3/2}} + \frac{1}{(\pi+\theta)^{3/2}} - \frac{8}{27|\theta|^{1/2}} + \frac{8}{27(\pi+\theta)^{1/2}}\right]\right) + (a_{c0}+a_{c\pi})U^{1/4} \quad (4.51)$$

if $-\pi < \theta < 0$. This composite solution for a_c is shown as a dashed line in figure 4.5(a), and shows that the effect of an increasingly large rotation speed is to make

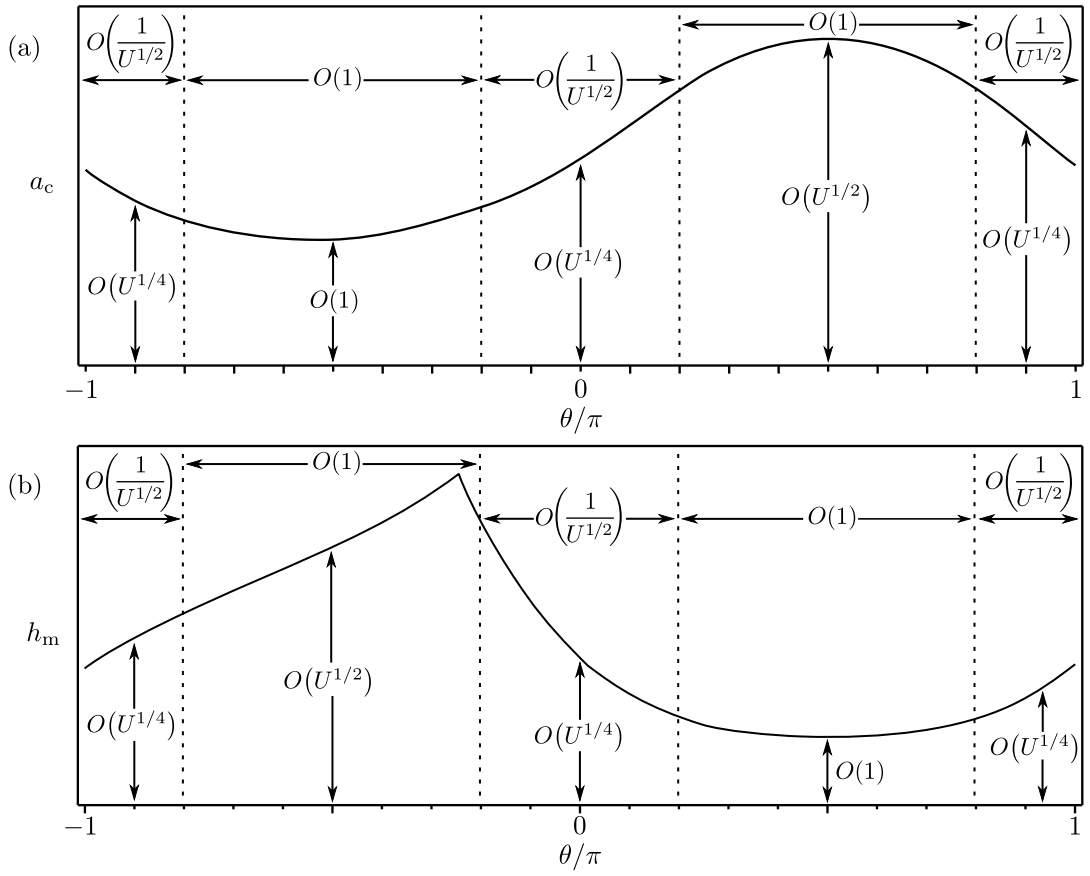

Figure 4.12: Sketch showing the structure of the solution for (a) the critical semi-width a_c, and (b) the critical maximum thickness h_{mc} (which is also typical of h_c), in the limit $U \to \infty$.

the semi-width approach an $O(1)$ value near the bottom of the cylinder and become large and of $O(U^{1/2})$ near the top of the cylinder.

The solution for the critical rivulet profile h_c is given by

$$h_c = \xi(m) + O\left(\frac{1-|y|}{U^{1/2}} \exp\left[\frac{-4\pi m^2(1-|y|)U^{1/2}}{3\sqrt{5}}\right]\right) \tag{4.52}$$

if $0 < \theta < \pi$ where

$$\xi(m) = \frac{1}{m}\left[1 - 2\exp\left(-\frac{4\pi m^2 U^{1/2}}{3\sqrt{5}} - 1\right)\cosh\left(\frac{4\pi m^2 U^{1/2} y}{3\sqrt{5}} + y\right)\right], \tag{4.53}$$

and is given by

$$h_{\rm c} = \frac{1+\cos(\pi y)}{\zeta m} U^{1/2} + \frac{y\sin(\pi y)}{m} + O\left(\frac{1}{U^{1/2}}\right) \tag{4.54}$$

if $-\pi < \theta < 0$ with ζ as in (4.47). From (4.52) and (4.54) we see that at leading order in the limit of large rotation speed, the critical rivulet profile $h_{\rm c}$ at the bottom of the cylinder near $\theta = -\pi/2$ is large and of $O(U^{1/2})$, while at the top of the cylinder near $\theta = \pi/2$ the effect of large but finite rotation speed U is to decrease the critical rivulet profile $h_{\rm c}$ away from its leading order value $h_{\rm c} = 1/m$ (an $O(1)$ quantity) except near $y = \pm 1$ where $h_{\rm c}$ is exponentially small. We note that, unlike in the asymptotic solution for $a_{\rm c}$ when $-\pi < \theta < 0$ given by (4.45), the corner appears at leading order in the solution for $h_{\rm c}$ when $-\pi < \theta < 0$, given by (4.54). In the boundary layers near $\theta = 0$ and $|\theta| = \pi$, $h_{\rm c}$ is given by

$$h_{\rm c} = \eta(T,y) = \begin{cases} \dfrac{\cosh(a_1 T^{1/2}) - \cosh(a_1 T^{1/2} y)}{T^{1/2}\sinh(a_1 T^{1/2})} U^{1/4} + O\left(\dfrac{1}{U^{1/4}}\right) & \text{if } 0 < \theta < \pi, \\ \dfrac{a_1 U^{1/4}}{2}(1-y^2) + O\left(\dfrac{1}{U^{1/4}}\right) & \text{if } \theta = 0 \text{ or } \theta = \pi, \\ \dfrac{\cos(a_1 |T|^{1/2} y) - \cos(a_1 |T|^{1/2})}{|T|^{1/2}\sin(a_1 |T|^{1/2})} U^{1/4} + O\left(\dfrac{1}{U^{1/4}}\right) & \text{if } -\pi < \theta < 0, \end{cases} \tag{4.55}$$

This solution for $h_{\rm c}$ shows that at leading order in the limit of large rotation speed, the critical rivulet profile $h_{\rm c}$ is large and of $O(U^{1/4})$ on the right-hand and left-hand sides of the cylinder near $\theta = 0$ and $\theta = \pi$, respectively. A plot detailing the structure of the solution for $h_{\rm mc}$ (which is also typical of $h_{\rm c}$) in the limit $U \to \infty$ is shown in figure 4.12(b). A composite solution for $h_{\rm c}$ may be written as

$$h_{\rm c} = \xi(m) - \xi(\theta^{1/2}) - \xi([\pi-\theta]^{1/2}) + \eta(\theta U^{1/2}, y) + \eta([\pi-\theta]U^{1/2}, y) \tag{4.56}$$

if $0 < \theta < \pi$, and as

$$\begin{aligned} h_{\rm c} &= U^{1/2}(1+\cos(\pi y))\left(\frac{1}{m\zeta} - \frac{4}{3\sqrt{5}}(|\theta|^{1/2} + (\pi+\theta)^{1/2})\right) \\ &+ y\sin(\pi y)\left(\frac{1}{m} - \frac{1}{|\theta|^{1/2}} - \frac{1}{(\pi+\theta)^{1/2}}\right) + \eta(\theta U^{1/2}, y) + \eta([\pi+\theta]U^{1/2}, y) \end{aligned} \tag{4.57}$$

if $-\pi < \theta < 0$ where ζ, ξ and η are given by (4.47), (4.53) and (4.55), respectively. This composite solution for the critical rivulet profile h_c is shown as a dashed line in figure 4.5(b) and is also shown in figure 4.9(b), which shows a three-dimensional plot of the asymptotic critical rivulet profile h_c given by (4.56) and (4.56) for $U = 10$ which may be compared with the corresponding three-dimensional plot of the numerical solution shown in figure 4.7(e). In particular, these solutions show that effect of an increasingly large rotation speed is to make the critical rivulet thin and wide near the top of the cylinder and thick and narrow near the bottom of the cylinder; this effect can be attributed to the combination of increased load and the effect of gravity on the rivulet.

The slopes on either side of the corner in the solutions for a_c and h_c, $A_c^{\pm}$ and $H_c^{\pm}$, are given by

$$A_c^{\pm} = \frac{\pi}{2^{3/4}} - \frac{2^{3/4}\sqrt{5}}{12U^{1/2}}\left(9 \pm 2\sqrt{6}\right) + \frac{15\pi}{2^{15/4}U} + O\left(\frac{1}{U^{3/2}}\right) \tag{4.58}$$

and

$$H_c^{\pm} = \mp\frac{2^{3/4}(5U)^{1/2}}{30}\big(1 + \cos(\pi y)\big)\left(2\sqrt{6} \pm 3\right) + \frac{y\sin(\pi y)}{2^{3/4}} + O\left(\frac{1}{U^{1/2}}\right). \tag{4.59}$$

These solutions are shown as dashed lines in figure 4.8 and show that the effect of a large but finite rotation speed is to decrease $A_c^{\pm}$ away from its leading order value $A_c^{\pm} = \pi/2^{3/4}$ (specifically $A_c^{\pm} = \pi/2^{3/4} + O(1/U^{1/2})$ as $U \to \infty$), while at leading order in the limit of large rotation speed the slope H_c^- (the slope H_c^+) is large and positive (negative) and of $O(U^{1/2})$. We note that A_c^- and A_c^+ take the same (constant) value at leading order (as we would expect given that at leading order the asymptotic solution for a_c when $-\pi < \theta < 0$, given by (4.45), has no corner in it) while H_c^- and H_c^+ have the same magnitude but opposite sign at leading order.

With the solution for a_c known we find from (4.28) that the critical load M_c is given by

$$M_c = U^{1/2}\left(\frac{8\pi^2}{3\sqrt{5}} + \int_{-\pi}^{0}\frac{2\pi}{m^2\zeta}\,\mathrm{d}\theta\right) + O(1) \simeq 24.25391U^{1/2} + O(1). \tag{4.60}$$

This solution is shown as a dashed line in figure 4.4(c), and shows that at leading order in the limit of large rotation speed the critical load M_c is large and of $O(U^{1/2})$.

4.3 The Non-Critical Solution

In this Section we consider in detail the behaviour of the non-critical full-rivulet solution with both the rotation speed U and load M prescribed such that U and M satisfy $M < M_c$ (sub-critical load) and $U > U_c$ (super-critical rotation speed) so that $Q < Q_c$, i.e. the point (U, M) lies below the curve in figure 4.4(c). Figure 4.13 shows the semi-width a and maximum thickness h_m plotted as functions of θ/π for three different values of the rotation speed U and a range of values of the load M in each case (including the critical load M_c), while figure 4.14 shows the semi-width a and maximum thickness h_m plotted as functions of θ/π for five different values of the load M and a range of values of the rotation speed U in each case (including the critical rotation speed U_c); these figures clearly show the behaviour of the rivulet as one parameter varies while the other remains constant. In particular, figures 4.13 and 4.14 show that both the semi-width a and the maximum thickness h_m are increasing functions of the load M (a property that also holds for the rivulet profile h) and are decreasing functions of the rotation speed U on the right-hand-side of the cylinder near $\theta = 0$ and are increasing functions of the rotation speed U on the left-hand-side near $\theta = \pi$ (and again, these properties also hold for the rivulet profile h). It may also be seen that the semi-width a (maximum thickness h_m) is a decreasing (increasing) function of θ on the left-hand-side of the cylinder near $\theta = \pi$ but is a non-monotonic function of θ elsewhere. Another feature that is seen in figures 4.13 and 4.14 is that varying the load M has a substantial effect on the behaviour of the solution, as would be expected. However, varying the rotation speed U varies the solution only slightly, with the most significant changes occurring for values of U close to the critical (i.e. close to $U = U_c$) and values of θ close to the corner in the critical solution (i.e. close to $\theta = \hat{\theta}_c(U_c)$); this

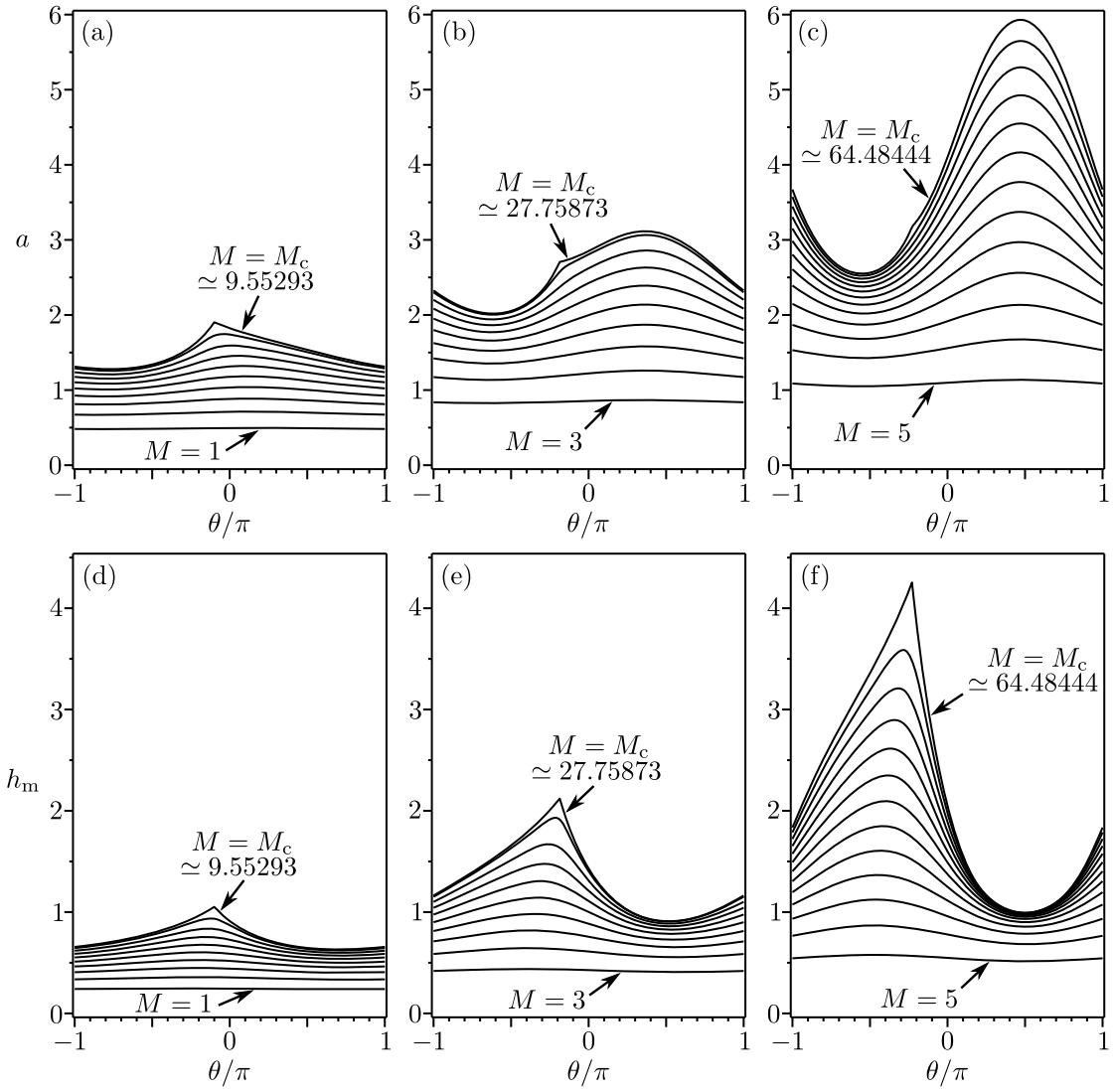

Figure 4.13: (a,b,c) The semi-width a and (d,e,f) the maximum thickness $h_{\rm m}$ plotted as functions of θ/π for (a,d) $M = 1, 2, 3, \ldots, 9$ and $M = M_{\rm c} \simeq 9.55293$ with $U = 1/2$, (b,e) $M = 3, 6, 9, \ldots, 27$ and $M = M_{\rm c} \simeq 27.75873$ with $U = 2$ and (c,f) $M = 5, 10, 15, \ldots, 60$ and $M = M_{\rm c} \simeq 64.48444$ with $U = 8$.

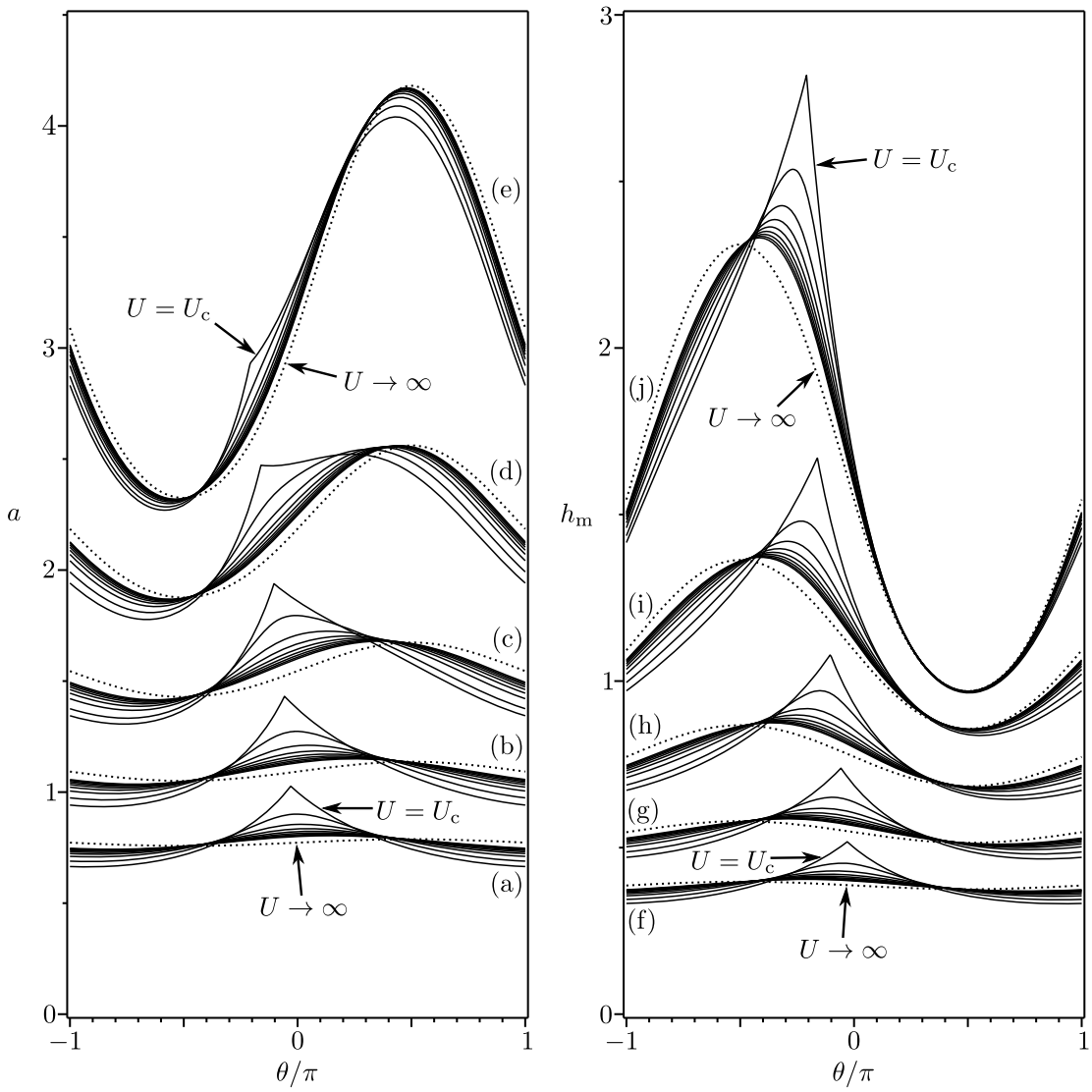

Figure 4.14: (a-e) The semi-width a and (f-j) the maximum thickness $h_{\rm m}$ plotted as functions of θ/π for (a,f) $U = U_{\rm c} \simeq 0.12240$ and $U = 0.15$, 0.2, 0.25, ..., 0.5 with $M = 2.5$, (b,g) $U = U_{\rm c} \simeq 0.24834$ and $U = 0.3$, 0.4, 0.5, ..., 1 with $M = 5$, (c,h) $U = U_{\rm c} \simeq 0.52666$ and $U = 0.6$, 0.8, 1, ..., 2 with $M = 10$, (d,i) $U = U_{\rm c} \simeq 1.24416$ and $U = 1.5$, 2, 2.5, ..., 5 with $M = 20$, and (e,j) $U = U_{\rm c} \simeq 3.51518$ and $U = 4$, 5, 6, ..., 11 with $M = 40$ (solid lines). Also shown for each load is the leading-order asymptotic solutions (4.62), (4.65) and (4.66) in the limit $U \to \infty$ (dotted lines).

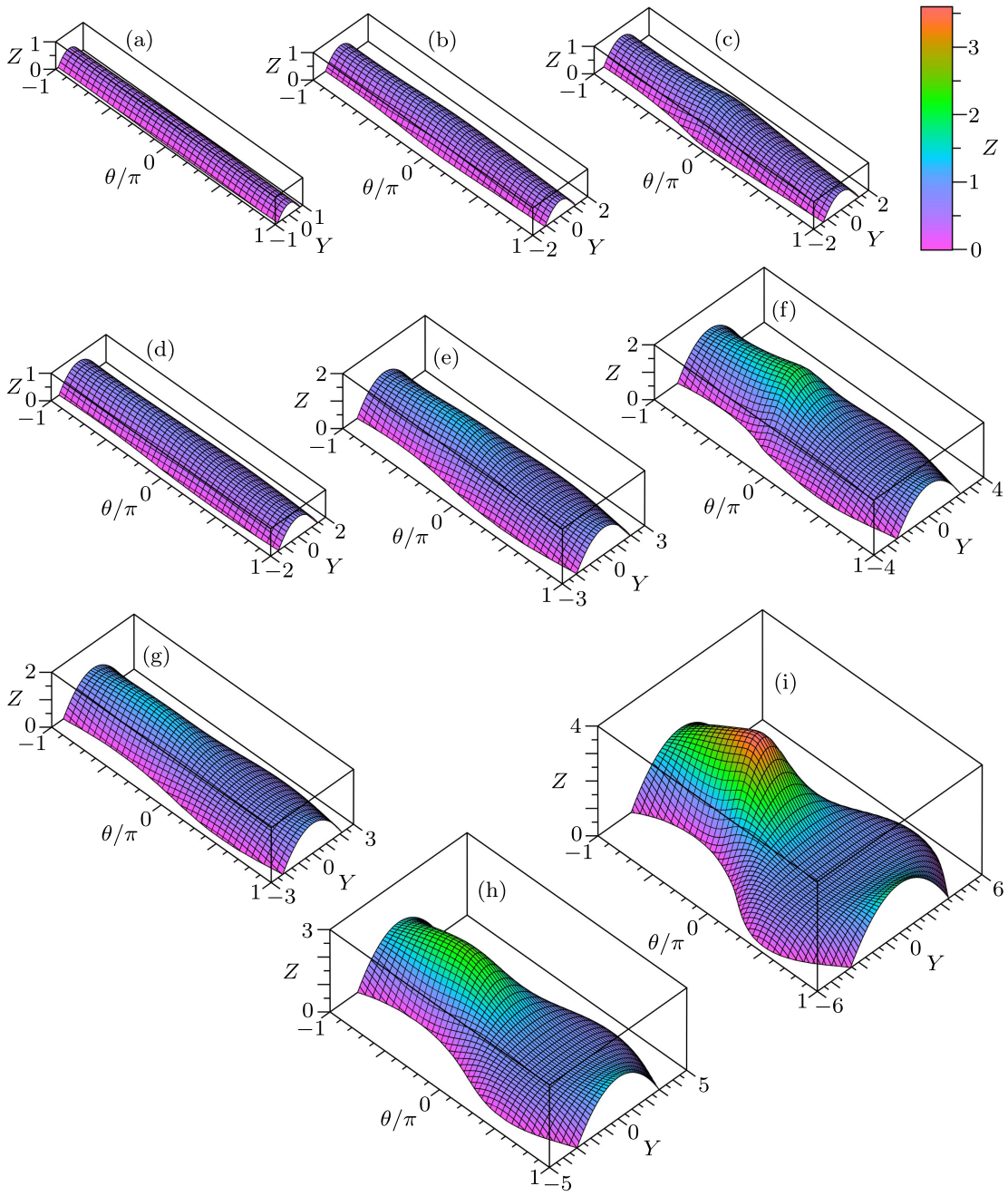

Figure 4.15: Three-dimensional plots of the rivulet profile h as a function of $Y = ay$ and θ/π for (a) $M = 3$, (b) $M = 6$ and (c) $M = 9$ for $U = 1/2$, (d) $M = 9$, (e) $M = 18$ and (f) $M = 27$ for $U = 2$, and (g) $M = 20$, (h) $M = 40$ and (i) $M = 60$ for $U = 8$.

is mainly due to the load being fixed. This result may seem odd because intuitively one might imagine that the increased rotation speed could lead to a uniform rivulet or perhaps critical solution beyond which load shedding occurs, however, both of these would be the result of inertial effects which are outside the regime considered here. Figure 4.15 shows three-dimensional plots of the non-critical rivulet profile h for various values of the rotation speed U and load M, clearly illustrating how the shape of the rivulet changes as U and M vary.

In the following two subsections we analyse the behaviour of the non-critical solution with prescribed rotation speed U or prescribed load M in the asymptotic limits $M \to 0$ and $U \to \infty$, respectively. Note that there is no full-rivulet solution in the limits $M \to \infty$ with prescribed U or $U \to 0$ with prescribed M, since these would exceed the critical (maximum) value M_{c} and the critical (minimum) value U_{c}, respectively.

4.3.1 The limit of large rotation speed $U \to \infty$

In the limit of large rotation speed $U \to \infty$ with the load M prescribed, the flux Q and semi-width a are given from (4.18) and (4.28) by

$$Q = \frac{MU}{2\pi} - \frac{I}{162\pi U} + O\left(\frac{1}{U^3}\right) \tag{4.61}$$

and

$$a = a_0 + \frac{F(ma_0)\cos\theta}{9m^3 U G'(ma_0)} + O\left(\frac{1}{U^2}\right), \tag{4.62}$$

where a_0 is the smallest positive solution of

$$G(ma_0) = \frac{Mm^2}{2\pi} \tag{4.63}$$

when $\theta \neq 0$ and $\theta \neq \pi$, and is $a_0 = \sqrt{3M/\pi}/2$ when $\theta = 0$ or $\theta = \pi$, while $I = I(M)$ is given by

$$I = \int_{-\pi}^{\pi} \frac{\cos^2\theta F(ma_0)F'(ma_0)}{m^6 G'(ma_0)}\,\mathrm{d}\theta \tag{4.64}$$

and is plotted as a function of M in figure 4.16. The leading order solution for a, a_0, is shown as dotted lines in figure 4.14(a) for a range of values of the load M. With the semi-width a given by (4.62) the rivulet profile h is given from (4.10) by $a(1-y^2)/2$ if $\theta = 0$, by

$$h = \frac{\cos(ma_0y) - \cos(ma_0)}{m\sin(ma_0)} - \frac{\cos\theta\big[\cos(ma_0)\cos(ma_0y)+y\sin(ma_0)\sin(ma_0y)-1\big]F(ma_0)}{9Um^3\sin^2(ma_0)G'(ma_0)} + O\left(\frac{1}{U^2}\right) \quad (4.65)$$

if $-\pi < \theta < 0$, and by

$$h = \frac{\cosh(ma_0) - \cosh(ma_0y)}{m\sinh(ma_0)} + \frac{\cos\theta\big[\cosh(ma_0)\cosh(ma_0y) - y\sinh(ma_0)\sinh(ma_0y) -1\big]F(ma_0)}{9Um^3\sinh^2(ma_0)G'(ma_0)} + O\left(\frac{1}{U^2}\right) \quad (4.66)$$

if $0 < \theta < \pi$.

The solution for the flux Q given by (4.61) shows that at leading order in the limit of large rotation speed the flux is large and of $O(U)$. Plots of this solution for Q as a function of U are included as dotted lines in figure 4.17(a) for a range of values of the load M together with the corresponding numerical solutions as solid lines and the critical solution Q_c as a dashed line. In particular, figure 4.17(a) demonstrates the rather surprising conclusion that although (4.61) is strictly valid only in the limit $U \to \infty$, in practice it provides a good approximation to Q for all $U \geq U_c$. This property also holds for the solutions for the semi-width a and rivulet profile h, given by (4.62), (4.65) and (4.66), as may be seen in figure 4.18, which shows three-dimensional plots of the asymptotic rivulet profile h for (a) $U = 1/2$ and $M = 9$, (b) $U = 2$ and $M = 27$, and (c) $U = 8$ and $M = 60$, which may be compared with the corresponding three-dimensional plots of the numerical solution shown in figures 4.15(c), 4.15(f) and 4.15(i), respectively. These solutions show that the effect of large but finite rotation speed is to increase (decrease) both the semi-width a and the rivulet profile h on the right-hand side $|\theta| \leq \pi/2$ (left-hand side $\pi/2 \leq |\theta| \leq \pi$) away from their respective $O(1)$ leading order values.

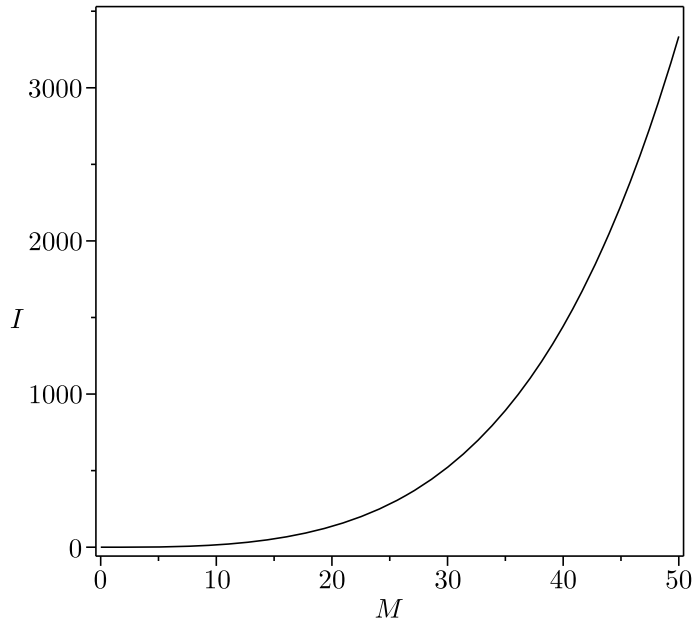

Figure 4.16: Plot of I, given by (4.64), as a function of the load M.

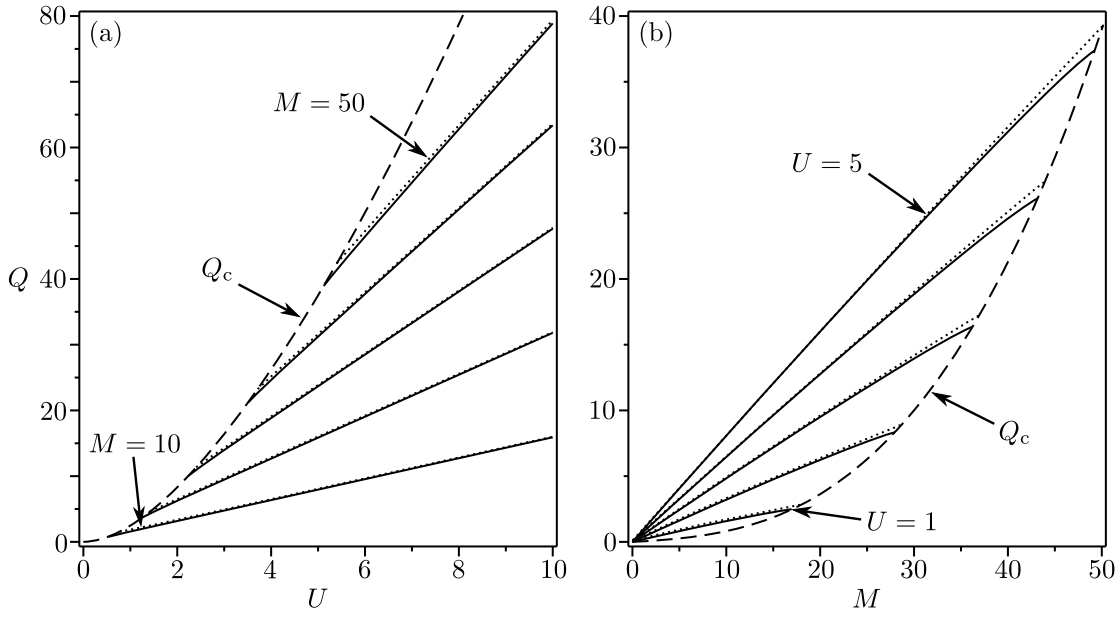

Figure 4.17: The flux Q plotted as a function of (a) U for $M = 10$, 20, 30, 40, 50 (solid lines) with the asymptotic solution (4.61) in the limit $U \to \infty$ (dotted lines) together with the critical flux Q_c (dashed line), and (b) M for $U = 1$, 2, 3, 4, 5 (solid lines) with the asymptotic solution (4.67) in the limit $M \to 0$ (dotted lines) together with the critical flux Q_c (dashed line).

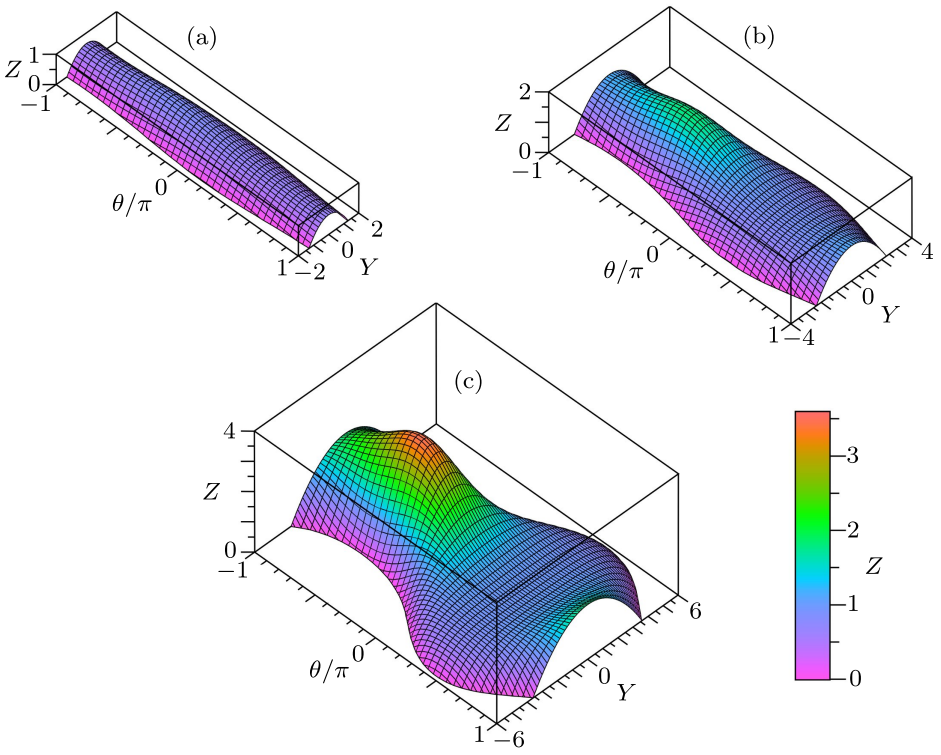

Figure 4.18: Three-dimensional plots of the asymptotic solution in the limit $U \to \infty$ for the rivulet profile h as a function of $Y = ay$ and θ/π for (a) $U = 1/2$ with $M = 9$, (b) $U = 2$ with $M = 27$ and (c) $U = 8$ for $M = 60$. These plots may be compared with figures 4.15(c), 4.15(f) and 4.15(i), respectively.

4.3.2 The limit of small load $M \to 0$

In the limit of small load $M \to 0$ with the rotation speed U prescribed, the flux Q and semi-width a are given from (4.18) and (4.28) by

$$Q = \frac{MU}{2\pi} - \frac{9M^3}{9800\pi^3 U} + O\left(M^5\right) \tag{4.67}$$

and

$$a = \frac{1}{2}\left(\frac{3}{\pi}\right)^{1/2}\left(M^{1/2} + \frac{(7U\sin\theta + 6\cos\theta)}{280\pi U}M^{3/2}\right) + O\left(M^{5/2}\right), \tag{4.68}$$

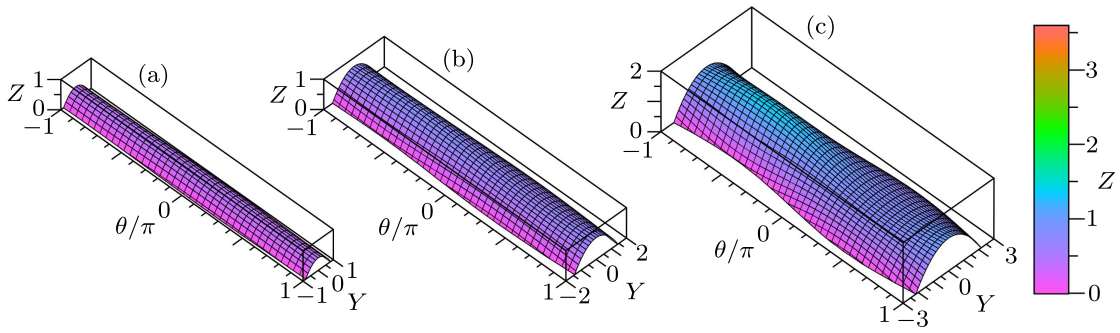

Figure 4.19: Three-dimensional plots of the asymptotic solution in the limit $M \to 0$ for the rivulet profile h as a function of $Y = ay$ and θ/π for (a) $M = 3$ with $U = 1/2$, (b) $M = 8$ with $U = 2$ and (c) $M = 20$ with $U = 8$. These plots may be compared with the corresponding numerical solutions shown in figures 4.15(a), 4.15(d) and 4.15(g), respectively.

and hence, from (4.10), the rivulet profile h is given by

$$h = \frac{1-y^2}{4}\left(\frac{3}{\pi}\right)^{1/2}\left(M^{1/2} + \frac{\left[7(5y^2-3)U\sin\theta + 12\cos\theta\right]}{560\pi U}M^{3/2}\right) + O\left(M^{5/2}\right). \tag{4.69}$$

The solution for the flux Q given by (4.67) shows that at leading order in the limit of small load the flux is small and of $O(M)$ and is the same as the leading order value for Q in the limit of large rotation speed $U \to \infty$ given by (4.61). Plots of Q in (4.67) as a function of M are included as dotted lines in figure 4.17(b) for a range of values of the rotation speed U together with the corresponding numerical solutions as solid lines and the critical solution Q_c as a dashed line. As was the case in the limit $U \to \infty$ discussed previously in subsection 4.3.1, the solution (4.67) a surprisingly good approximation to Q for any $M \leq M_c$, and again this property also holds for the solutions for the semi-width a and rivulet profile h given by (4.68) and (4.69), as may be seen in figure 4.19, which shows three-dimensional plots of the rivulet profile h for (a) $M = 3$ and $U = 1/2$, (b) $M = 8$ and $U = 2$, and (c) $M = 20$ and $U = 8$, which may be compared with the corresponding three-dimensional plots of the numerical solution shown in figures 4.15(a), 4.15(d)

and 4.15(g), respectively. These solutions show that at leading order the effect of a small load is to increase the semi-width a and rivulet profile h, both of which are of $O(M^{1/2})$.

4.4 Backflow

For the two-dimensional full-film flow considered by Moffatt [7], the azimuthal velocity u is always in the same direction as the rotation of the cylinder (i.e. $u \geq 0$ for all $-\pi < \theta \leq \pi$ and $0 \leq z \leq 1$) and so backflow (i.e. $u < 0$ somewhere within the flow) never occurs. In contrast, in this Section we will show that in the present case of three-dimensional rivulet flow backflow is possible, but only within a restricted region of the M–U parameter space, and that when it does occur it is always in a small region on the right-hand side of the cylinder near $\theta = 0$.

From (4.15) we see that the azimuthal velocity may be zero ($u = 0$) only on the three-dimensional surface defined by

$$z = 1 - \left(1 - \frac{2U}{h^2 \cos\theta}\right)^{1/2}, \tag{4.70}$$

in $0 < z \leq 1$. It is immediately apparent that (4.70) may have solutions satisfying $z \geq 0$ only for $-\pi/2 < \theta < \pi/2$ (that is, on the right-hand side of the cylinder), and that the surface (4.70) cannot intersect either the substrate $z = 0$ (by the no-slip condition) or the plane surfaces $\theta = \pm\pi/2$. If it intersects the free surface of the fluid $z = 1$ then it would do so when $h = (2U/\cos\theta)^{1/2}$, which from (4.10) means that it may intersect the free surface only on the curve $y = \pm y_s(\theta)$ defined by

$$y_s = \begin{cases} \dfrac{1}{ma}\cosh^{-1}\left[\cosh(ma) - (2U\tan\theta)^{1/2}\sinh(ma)\right] & \text{if } 0 < \theta < \dfrac{\pi}{2}, \\ \left(1 - \dfrac{2(2U)^{1/2}}{a}\right)^{1/2} & \text{if } \theta = 0, \\ \dfrac{1}{ma}\cos^{-1}\left[\cos(ma) + (-2U\tan\theta)^{1/2}\sin(ma)\right] & \text{if } -\dfrac{\pi}{2} < \theta < 0, \end{cases} \tag{4.71}$$

which provides an explicit expression for the "footprint" of the region of recirculation on the cylinder. From (4.15) it is clear that at any station $\theta =$ constant the azimuthal velocity u on the free surface $z = 1$ has a minimum at $y = 0$ since this is where h takes its maximum value $h = h_{\rm m}$; hence, the endpoints of the region of backflow in the θ direction (where $u = 0$) will lie on $y = 0$. At these endpoints we have $h_{\rm m} = (2U/\cos\theta)^{1/2}$ and the semi-width a is given by

$$a = \begin{cases} \dfrac{2}{m}\tanh^{-1}\left(2U\tan\theta\right)^{1/2} & \text{if } 0 < \theta < \dfrac{\pi}{2}, \\ 2(2U)^{1/2} & \text{if } \theta = 0, \\ \dfrac{2}{m}\tan^{-1}\left(-2U\tan\theta\right)^{1/2} & \text{if } -\dfrac{\pi}{2} < \theta < 0, \end{cases} \tag{4.72}$$

so that the flux equation (4.18) becomes

$$Q = \begin{cases} \dfrac{U}{m^2}G\left(2\tanh^{-1}\left(2U\tan\theta\right)^{1/2}\right) & \\ \qquad -\dfrac{\cos\theta}{9m^4}F\left(2\tanh^{-1}\left(2U\tan\theta\right)^{1/2}\right) & \text{if } 0 < \theta < \dfrac{\pi}{2}, \\ \dfrac{304}{105}U^2 & \text{if } \theta = 0, \\ \dfrac{U}{m^2}G\left(2\tan^{-1}\left(-2U\tan\theta\right)^{1/2}\right) & \\ \qquad -\dfrac{\cos\theta}{9m^4}F\left(2\tan^{-1}\left(-2U\tan\theta\right)^{1/2}\right) & \text{if } -\dfrac{\pi}{2} < \theta < 0, \end{cases} \tag{4.73}$$

which provides an equation determining the values of θ at the endpoints of any region of recirculating flow in terms of the flux Q. The function on the right-hand side of (4.73) is real and positive only for $-\pi/2 < \theta < \theta_{\rm max}$, where $\theta_{\rm max} = \theta_{\rm max}(U) = \cot^{-1}(2U) > 0$; the function decreases with θ from infinity as $\theta \to -\pi/2^+$ to a minimum value $Q_{\rm min}$ at some $\theta = \theta_{\rm min}(U)$ $(-\pi/2 < \theta_{\rm min} < 0)$, and then increases to infinity as $\theta \to \theta_{\rm max}^-$. With U prescribed, it is found that $Q_{\rm min}$ satisfies $0 < Q_{\rm min} \le Q_{\rm c}(U)$ for any U (together with a corresponding minimum load denoted $M_{\rm min}$ satisfying $0 < M_{\rm min} \le M_{\rm c}(U)$), and therefore (4.73) has two solutions $\theta = \theta_1$ and $\theta = \theta_2$ (with $-\pi/2 < \theta_1 < \theta_{\rm min} < \theta_2 < \theta_{\rm max}$) when $Q >$

$Q_{\min}$ (with $Q \leq Q_{\rm c}$), one solution $\theta = \theta_1 = \theta_2 = \theta_{\min}$ when $Q = Q_{\min}$, and no solution when $Q < Q_{\min}$. However, some of these correspond to solutions on higher branches; specifically, it is found that for a full-rivulet solution there may be a region of backflow near the free surface in $\theta_1 \leq \theta \leq \theta_2$ only when $U < 1$ and $Q_{\min} < Q \leq Q_{\rm c}$, and that otherwise the flow is always in the same direction as the rotation of the cylinder. When $Q = Q_{\min}$ the region of recirculating flow collapses to just a single stagnation point on the free surface. Figure 4.20 shows the differences between (a) the critical flux and the minimum flux below which backflow is not possible, $Q_{\rm c} - Q_{\min}$, and (b) the critical load and the minimum load below which backflow is not possible, $M_{\rm c} - M_{\min}$, plotted as functions of U, which, in conjunction with figures 4.4(b) and 4.4(c), shows the regions of Q–U and M–U parameter space in which backflow occurs. In particular, figure 4.20 shows that for a given rotation speed U, backflow occurs only when the load M is very close to the critical load $M_{\rm c}$. With this result in mind we shall further describe backflow only in the critical case.

Figure 4.21(a) shows the endpoints of the region of backflow in the critical case, $\theta_{1\rm c}$ and $\theta_{2\rm c}$, plotted as functions of U together with the position of the corner in the critical solution, $\hat{\theta}_{\rm c}$, and shows that the endpoints always lie on opposite sides of the corner. It may also be shown that in the limit $U \to 0$ the endpoints $\theta_{1\rm c}$ and $\theta_{2\rm c}$ have the same magnitude, with $\theta_{1\rm c} = -\theta_{2\rm c} = -\cos^{-1}(1216/1225) \simeq -0.12129$ ($\simeq -0.03861\pi$), while in the limit $U \to 1^-$ the endpoints take the same value $\theta_{1\rm c} = \theta_{2\rm c} = -\cot^{-1}(2) \simeq -0.46365$ ($\simeq -0.14758\pi$), showing that the region of backflow has zero width.

Figure 4.21(b) shows the footprint of the region of backflow in the Y–θ/π plane (i.e. the curves $y = \pm y_{\rm s}$ given by (4.71)) for a range of values of the rotation speed U in the critical case. Also shown is the maximum width of the region (which always occurs at $\theta = \hat{\theta}_{\rm c}$) given by the curves $Y = \pm\hat{y}_{\rm sc} = \pm\hat{y}_{\rm c}(\theta)$ in which the value of the rotation speed U is determined by the solution of $\theta = \hat{\theta}_{\rm c}(U)$. In particular, figure 4.21(b) shows that in the limit $U \to 0$ the region of backflow

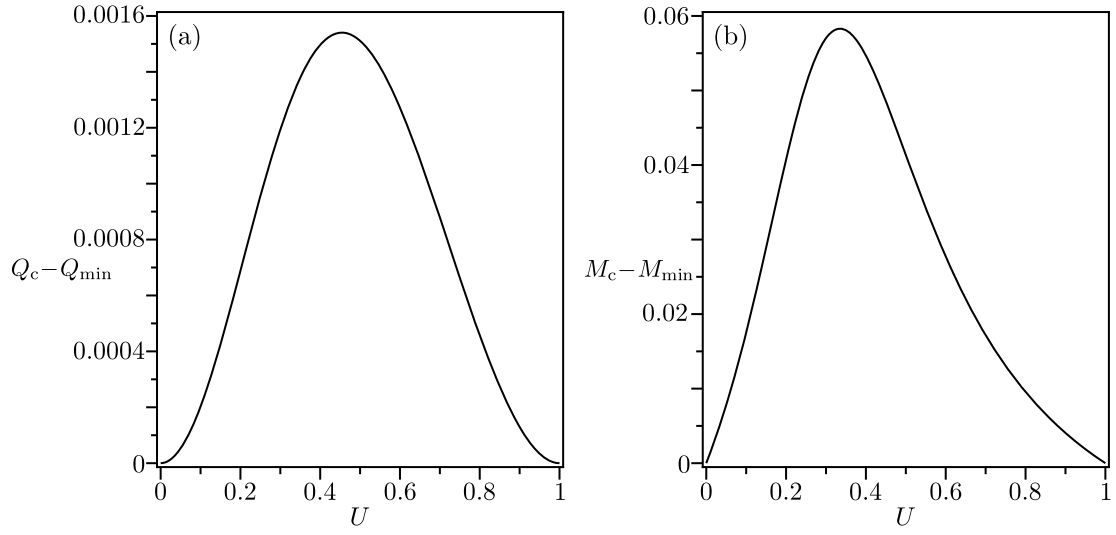

Figure 4.20: (a) The difference between the critical flux and the minimum flux below which backflow is not possible, $Q_c - Q_{min}$, and (b) the difference between the critical load and the minimum load below which backflow is not possible, $M_c - M_{min}$, plotted as functions of U.

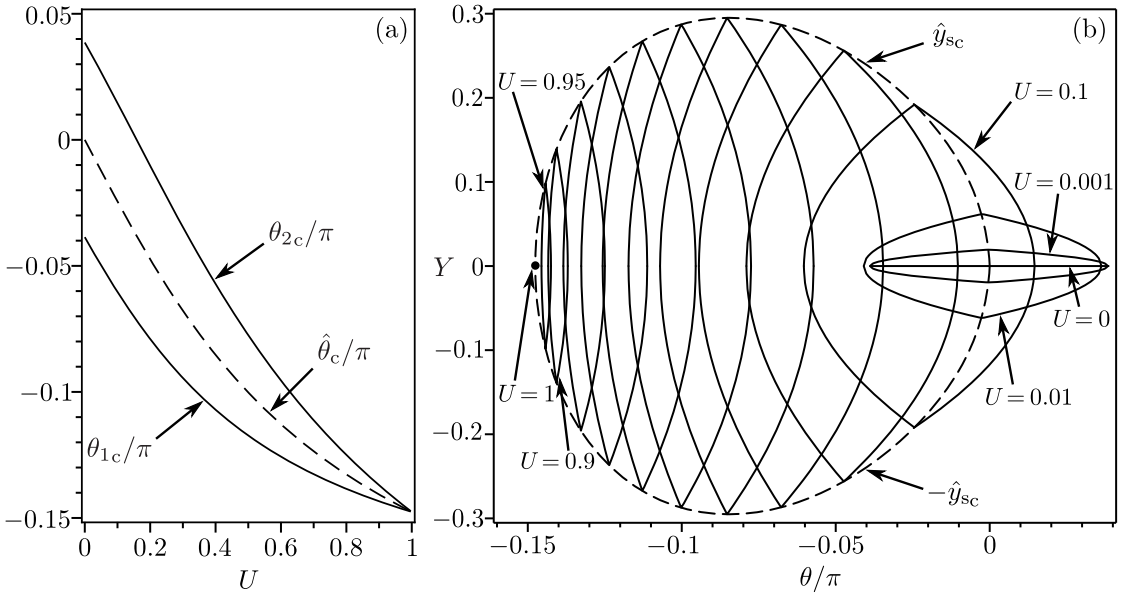

Figure 4.21: (a) The endpoints of the region of backflow, θ_1/π and θ_2/π, plotted as a function of U together with the position of the corner, $\hat{\theta}_c/\pi$. (b) The footprint of the region of backflow Y–θ/π plane (i.e. the curves $y = \pm y_s$ given by (4.71)) in the critical case for $U = 0.1$, 0.2, 0.3, ..., 0.9 and $U = 0$, $U = 0.01$, $U = 0.01$, $U = 0.95$ (solid lines) and $U = 1$ (dot) together with the curve $\hat{y}_{sc}$ as a function of $\hat{\theta}_c/\pi$ which shows the maximum width of the regions.

becomes narrow in the Y direction but tends towards a constant width in the θ direction, eventually becoming a line when $U = 0$ (when, of course, there is no full-rivulet solution), while in the limit $U \to 1^-$ the region of backflow becomes narrow in the Y direction and narrower in the θ direction, eventually becoming a point when $U = 1$ (representing a single stagnation point on the free surface).

4.5 Conclusions

In this Chapter we used the lubrication approximation to obtain a detailed description of the steady flow of a thin, slowly varying, symmetric rivulet of Newtonian fluid on either the outside or the inside of a uniformly rotating horizontal cylinder. We found that, like the two-dimensional full-film flow considered by Moffatt [7], there exists a critical solution corresponding to either a critical load M_c above which no full-rivulet solution exists (if the rotation speed U is prescribed) or a critical rotation speed U_c below which no full-rivulet solution exists (if the load M is prescribed).

In Section 4.2 we showed that the critical solution for the semi-width a is made up of two branches of solutions that meet to form a corner at some point on the bottom-right of the cylinder; this is analogous to the corner found by Moffatt [7] for the two-dimensional problem. However, unlike in Moffatt's problem, in the present problem the position and slopes either side of the corner in the present problem depend on the rotation speed U or the load M. We also showed that the critical flux Q_c, critical semi-width a_c, critical rivulet profile h_c and the critical load M_c are increasing functions of the rotation speed U. In the limit of small rotation speed $U \to 0$ the critical rivulet becomes both narrow and thin, with the critical semi-width a_c and critical rivulet profile h_c both being of $O(U^{1/2})$, leading to small critical load of $O(U)$. In the limit of large rotation speed $U \to \infty$ the critical rivulet becomes narrow and thick at the bottom of the cylinder and wide and thin at the top of the cylinder with the critical semi-width being of $O(1)$ on

the bottom and of $O(U^{1/2})$ on the top of the cylinder and the critical rivulet profile being of $O(U^{1/2})$ on the bottom and $O(1)$ on the top of the cylinder, leading to a large critical load of $O(U^{1/2})$.

In Section 4.3 we considered the case in which both the rotation speed U and load M are prescribed such that non-critical full-rivulet solutions are possible and found that the semi-width a and the rivulet profile h are increasing functions of the load M and are decreasing functions of the rotation speed U, and that varying the load can have a substantial effect on the behaviour of the solution while varying the rotation speed varies the solution only slightly. In particular, we found that at leading order in the limit of large rotation speed $U \to \infty$ both the semi-width a and rivulet profile h are of $O(1)$ while at leading order in the limit of small load $M \to 0$ both the semi-width a and the rivulet profile h are small and of $O(M^{1/2})$.

In Section 4.4 we showed that, for most values of the parameters U and M, the azimuthal velocity is in the same direction as the rotation of the cylinder; however, if $0 < U < 1$ and we are sufficiently close to the critical solution a small region of backflow occurs on the right-hand side of the cylinder.

Chapter 5

Conclusions and Further Work

5.1 Conclusions

In this thesis we obtained a comprehensive description of three problems concerning thin-film flows on horizontal cylinders.

In Chapter 2 we considered steady two-dimensional gravity-driven curtain flow with prescribed volume flux of a Newtonian fluid with temperature-dependent viscosity over a uniformly heated or cooled stationary horizontal cylinder. We showed that, for the exponential viscosity model (2.8), when the thermoviscosity number is positive $V > 0$, the effect of increasing the Biot number B is to decrease the average temperature and the average velocity and to increase the viscosity, film thickness and the load; when $V < 0$ the opposite occurs. Similarly, we showed that the effect of increasing V is always to increase the film thickness and the load. In order to obtain a complete understanding of the influence of varying B and V, we also analysed the behaviour in appropriate asymptotic limits. In the limits $B \to 0^+$ and $B \to \infty$ these solutions revealed that increasing B changes the film thickness everywhere by a constant factor of $\hat{f}^{-1/3}$, where $\hat{f}$ is given by (2.22), which depends only on the specific viscosity model considered. In the limit $V \to -\infty$ the viscosity decreases from $O(1)$ at the cylinder to $O((-V)^{-3}) \ll 1$ at the free surface and the velocity increases from zero at the cylinder to a large value of $O(-V) \gg 1$ at the

free surface, leading to a small film thickness of $O(\log(-V)/(-V)) \ll 1$, while in the limit $V \to \infty$ the viscosity is exponentially large and the velocity is small and uniform of $O(V^{-1/3}) \ll 1$ outside a narrow boundary layer near the cylinder, leading to a large film thickness of $O(V^{1/3}) \gg 1$. The distinguished limit of strong thermoviscosity and weak heat transfer, $|V| \to \infty$ and $B \to 0^+$ with $BV = O(1)$, was also considered.

In Chapter 3 we considered steady two-dimensional coating and rimming flow of a Newtonian fluid with temperature-dependent viscosity on a uniformly heated or cooled rotating horizontal cylinder. We found that, as in the corresponding isothermal problem studied by Moffatt [7], there is a critical solution with a corresponding critical load (which depends, in general, on both the Biot number B and the thermoviscosity number V) above which no full-film solutions exist. The critical film thickness, magnitude of the slope of the corner in the critical film thickness at $\theta = 0$, and the critical load were all found to be increasing (decreasing) functions of B for positive (negative) V, and increasing functions of V. In the limit of $V \to -\infty$ the critical film thickness and the critical load become small like $O(\log(-V)/(-V)) \ll 1$, while in the limit $V \to \infty$ they become large like $O(V^{1/2}) \gg 1$. For a prescribed load M, it was shown that near $\theta = 0$ the film thickness is a decreasing (increasing) function of B for positive (negative) V, and a decreasing function of B, but that near $\theta = \pi$ it behaves in the opposite way. Full-film solutions exist in the limit $B \to \infty$ for $V \geq V_\infty$, but not for $V < V_\infty$, where $V = V_\infty$ satisfies $M = \hat{f}^{-1/2} M_{\mathrm{c}0}$, where $M_{\mathrm{c}0} \simeq 4.44272$ is the critical load in the isothermal problem. In the limit $V \to -\infty$ there is no full-film solution, while in the limit $V \to \infty$ the leading-order film thickness is the constant $h = M/2\pi$. We also showed that for sufficiently small prescribed values of M satisfying $M < 1.50315$ there is a narrow region of the B–V parameter plane in which backflow occurs in a region on the right-hand side of the cylinder. Again, the distinguished limit of strong thermoviscosity and weak heat transfer, $|V| \to \infty$ and $B \to 0^+$ with $BV = O(1)$, was also considered.

In Chapter 4 we considered the steady isothermal flow of a rivulet of Newtonian fluid on either the outside or the inside of a uniformly rotating horizontal cylinder. We found that, like the two-dimensional full-film flow considered by Moffatt [7], there exists a critical solution corresponding to either a fixed rotation speed U and a critical load M_c above which no full-rivulet solution exists or a fixed load M and a critical rotation speed U_c below which no full-rivulet solution exists. It was shown that the critical rivulet profile has a corner at some point on the bottom-right of the cylinder, the position of which depends on the rotation speed or the load; this is analogous to the corner found by Moffatt [7] for the two-dimensional problem. The critical flux, critical semi-width, critical rivulet profile and critical load are all increasing functions of the rotation speed U. In the limit $U \to 0$ the critical rivulet becomes both narrow and thin with width and thickness of $O(U^{1/2})$ and a small critical load of $O(U)$. In the limit $U \to \infty$ the critical rivulet becomes narrow and thick at the bottom of the cylinder and wide and thin at the top of the cylinder with width of $O(1)$ and $O(U^{1/2})$ on the bottom and top of the cylinder, respectively, and a thickness of $O(U^{1/2})$ an $O(1)$ on the bottom and top of the cylinder, respectively, leading to a large critical load of $O(U^{1/2})$. For non-critical solutions we found that the width and thickness are increasing (decreasing) functions of the load M (rotation speed U) and that varying the load can have a substantial effect on the behaviour of the solution while varying the rotation speed varies the solution only slightly. At leading order in the limit $U \to \infty$ the width and thickness are of $O(1)$ while at leading order in the limit of small load $M \to 0$ both width and thickness are small and of $O(M^{1/2})$. We also showed that if $0 < U < 1$ and if we are sufficiently close to the critical solution a small region of backflow (which does not occur in the two-dimensional problem) occurs on the right-hand side of the cylinder.

5.2 Further Work

There are a number of possible interesting extensions to the work described in this thesis that could be considered.

In Chapter 2 we considered thermoviscous curtain flow on a stationary horizontal cylinder and in Chapter 3 we considered thermoviscous coating and rimming flow on a rotating horizontal cylinder. The applications of these problems often involve temperature differences that are important (for example, in heat exchangers or in many coating flows) and so further extensions to these problems would be of much interest. A natural extension to the work of Chapters 2 and 3 would be to consider different viscosity models, as Wilson and Duffy [96] did for the flow of a rivulet down an inclined plane. The inclusion of other thermal effects, such as thermocapillarity, heat transfer to or from the cylinder or evaporation/condensation at the free surface would also be of interest. Some of these of effects have been considered for curtain flow (see Section 1.3.2(a)), though, as far as the author is aware, no work that also includes thermoviscous effects has been performed. In the case of coating and rimming flow very little work (Duffy and Wilson [129] being the only example that the author is aware of) has been done that includes non-isothermal effects (despite their obvious importance to the applications of these flows) and so almost any non-isothermal extension to the work of Chapter 3 would be of interest. Extensions that consider the flow of non-Newtonian fluids would be of interest since in many of the applications the fluids are often non-Newtonian, particularly in the case of coating and rimming flows. Another potentially interesting addition to the work is to include higher order terms in the governing equations, possibly extending to numerical simulations of the full equations as well as the consideration of unsteady solutions; as we saw in Chapter 1, many people have performed these types of extensions, but few include non-isothermal effects (especially for coating and rimming flow) and none include thermoviscous effects. One could also address the important question of if and when these flows are sta-

ble. Carefully controlled laboratory experiments involving non-isothermal effects could also be conducted; this would be very useful for making comparisons with the model and could also help to address the question of stability.

In Chapter 4 we considered the flow of a non-perfectly wetting rivulet on either the outside or the inside of a rotating horizontal cylinder. There are many extensions to this flow that would be of interest. The inclusion of thermoviscous effects (as in Chapters 2 and 3 for two-dimensional flow) would present an interesting problem as would the inclusion of other non-isothermal effects (Holland et al. [94], El-Genk and Saber [92] and Wilson and Duffy [96] all consider non-isothermal effects for rivulet flows down inclined planes). One could also consider the case of a perfectly wetting rivulet or a non-perfectly wetting rivulet with fixed contact lines (but variable contact angle) or a case where both the contact angle and the contact lines vary; for example, Davis [97] considered contact angles that are functions of the contact line speed, for rivulet flow down an incline. The inclusion of higher order terms in the governing equations or unsteady solutions may also lead to interesting results, as would the consideration of surface shear stress effects (Saber and El-Genk [103], Myers et al. [104] and Sullivan et al. [107] all considered the effects of a surface shear stress on the flow of a rivulet down an incline). Studies into the stability of rivulet flows on rotating cylinders would also be useful, as would experimental investigations for the purpose of comparison.

Bibliography

[1] H. E. Huppert, "Flow and instability of a viscous current down a slope," *Nature*, vol. 300, pp. 427–429, 1982.

[2] A. Oron, S. H. Davis, and S. G. Bankoff, "Long-scale evolution of thin liquid films," *Rev. Mod. Phys.*, vol. 69, pp. 931–980, 1997.

[3] P. Colineta, H. Kaya, S. Rossomme, and B. Scheid, "Some advances in lubrication-type theories," *Eur. Phys. J. Special Topics*, vol. 81, pp. 1131–1198, 2007.

[4] R. V. Craster and O. K. Matar, "Dynamics and stability of thin liquid films," *Rev. Mod. Phys.*, vol. 81, pp. 1131–1198, 2009.

[5] W. Nusselt, "Die oberflächenkondensation des wasserdampfes," *Z. Vereines deutscher Ingenieure*, vol. 60, pp. 541–546, 1916.

[6] W. Nusselt, "Die oberflächenkondensation des wasserdampfes," *Z. Vereines deutscher Ingenieure*, vol. 60, pp. 569–575, 1916.

[7] H. K. Moffatt, "Behaviour of a viscous film on the outer surface of a rotating cylinder," *J. Méc.*, vol. 16, pp. 651–673, 1977.

[8] E. M. Sparrow and J. L. Gregg, "Laminar condensation heat transfer on a horizontal cylinder," *J. Heat Transfer*, vol. 80, pp. 291–296, 1959.

[9] A. A. Nicol, Z. L. Aidoun, R. J. Gribben, and G. Wilks, "Heat transfer in the presence of condensate drainage," *Int. J. Multiphase Flow*, vol. 14, pp. 349–359, 1988.

[10] J.-J. Shu and G. Wilks, "Heat transfer in the flow of a cold, two-dimensional draining sheet over a hot, horizontal cylinder," *Eur. J. Mech. B. Fluids*, vol. 28, pp. 185–190, 2009.

[11] I. G. Shekriladze and V. I. Gomelauri, "Theoretical study of laminar film condensation of flowing vapour," *Int. J. Heat Mass Transfer*, vol. 9, pp. 581–591, 1966.

[12] T. Fujii, H. Uehara, and C. Kurata, "Laminar filmwise condensation of flowing vapour on a horizontal cylinder," *Int. J. Heat Mass Transfer*, vol. 15, pp. 235–246, 1972.

[13] J. W. Rose, "Effect of pressure gradient in forced convection film condensation on a horizontal tube," *Int. J. Heat Mass Transfer*, vol. 27, pp. 39–47, 1984.

[14] C.-K. Chen and Y.-T. Lin, "Laminar film condensation from a downward-flowing steam-air mixture onto a horizontal circular tube," *Appl. Math. Modell.*, vol. 33, pp. 1944–1956, 2009.

[15] P. K. Sarma, B. Vijayalakshmi, F. Mayinger, and S. Kakac, "Turbulent film condensation on a horizontal tube with external flow of pure vapors," *Int. J. Heat Mass Transfer*, vol. 41, pp. 537–545, 1998.

[16] S.-A. Yang and Y.-T. Lin, "Turbulent film condensation on a non-isothermal horizontal tube – effect of eddy diffusivity," *Appl. Math. Modell.*, vol. 29, pp. 1149–1163, 2005.

[17] A. T. Conlisk and J. Mao, "Nonisothermal absorption on a horizontal cylindrical tube – 1. the film flow," *Chem. Eng. Sci.*, vol. 51, pp. 1275–1285, 1996.

[18] S.-A. Yang and C.-H. Hsu, "Free- and forced-convection film condensation from a horizontal elliptic tube with a vertical plate and a horizontal tube as special cases," *Int. J. Heat Fluid Flow*, vol. 18, pp. 567–574, 1997.

[19] Y.-T. Lin and S.-A. Yang, "Turbulent film condensation on a horizontal elliptical tube," *Heat Mass Transfer*, vol. 41, pp. 495–50, 2005.

[20] G.-C. Li and S.-A. Yang, "Entropy generation minimization of free convection film condensation on an elliptical cylinder," *Int. J. Therm. Sci.*, vol. 46, pp. 407–412, 2007.

[21] X. Hu and A. M. Jacobi, "The intertube falling film: Part 1 – flow characteristics, mode transitions, and hysteresis," *J. Heat Transfer*, vol. 118, pp. 616–625, 1996.

[22] J. D. Killion and S. Garimella, "Gravity-driven flow of liquid films and droplets in horizontal tube banks," *Int. J. Refrig.*, vol. 26, pp. 516–526, 2003.

[23] J. D. Killion and S. Garimella, "Simulation of pendant droplets and falling films in horizontal tube absorbers," *J. Heat Transfer*, vol. 126, pp. 1003–1013, 2004.

[24] P. Sultana, N. E. Wijeysundera, J. C. Ho, and C. Yap, "Modeling of horizontal tube-bundle absorbers of absorption cooling systems," *Int. J. Refrig*, vol. 30, pp. 709–723, 2007.

[25] B. Ruan, A. M. Jacobi, and L. Li, "Effects of a countercurrent gas flow on falling-film mode transitions between horizontal tubes," *Exp. Therm Fluid Sci.*, vol. 33, pp. 1216–1225, 2009.

[26] G. Ribatskia and A. M. Jacobib, "Falling-film evaporation on horizontal tubes – a critical review," *Int. J. Refrig.*, vol. 28, pp. 635–653, 2005.

[27] W. Li, X.-Y. Wu, Z. Luo, S. c. Yao, and J.-L. Xu, "Heat transfer characteristics of falling film evaporation on horizontal tube arrays," *Int. J. Heat Mass Transfer*, vol. 54, pp. 1986–1993, 2011.

[28] L. Yang and W. Wang, "The heat transfer performance of horizontal tube bundles in large falling film evaporators," *Int. J. Refrig*, vol. 34, pp. 303–316, 2011.

[29] B. Reisfeld and S. G. Bankoff, "Non-isothermal flow of a liquid film on a horizontal cylinder," *J. Fluid Mech.*, vol. 236, pp. 167–196, 1992.

[30] C.-K. Lin, C.-C. Hwang, and T.-C. Ke, "Three-dimensional nonlinear rupture theory of thin liquid films on a cylinder," *J. Colloid Interface Sci.*, vol. 256, pp. 480–482, 2002.

[31] A. A. King, L. J. Cummings, S. Naire, and O. E. Jensen, "Liquid film dynamics in horizontal and tilted tubes: Dry spots and sliding drops," *Phys. Fluids*, vol. 19, no. 042102, 2007.

[32] L. R. Band, D. S. Riley, P. C. Matthews, J. M. Oliver, and S. L. Waters, "Annular thin-film flows driven by azimuthal variations in interfacial tension," *Q. J. Mech. Appl. Math.*, vol. 62, pp. 403–430, 2009.

[33] O. Haimovich and A. Oron, "Nonlinear dynamics of a thin liquid film on an axially oscillating cylindrical surface," *Phys. Fluids*, vol. 22, no. 032101, 2010.

[34] O. Haimovich and A. Oron, "Nonlinear dynamics of a thin nonisothermal liquid film on an axially oscillating cylindrical surface," *Phys. Rev. E*, vol. 84, no. 061605, 2011.

[35] V. V. Pukhnachev, "Motion of a liquid film on the surface of a rotating cylinder in a gravitational field," *J. Appl. Mech. Tech. Phys.*, vol. 18, pp. 344–351, 1977.

[36] R. E. Johnson, "Steady-state coating flows inside a rotating horizontal cylinder," *J. Fluid Mech.*, vol. 190, pp. 321–342, 1988.

[37] E. B. Hansen and M. A. Kelmanson, "Steady, viscous, free-surface flow on a rotating cylinder," *J. Fluid Mech.*, vol. 272, pp. 91–107, 1994.

[38] R. C. Peterson, P. K. Jimack, and M. A. Kelmanson, "On the stability of viscous free-surface flow supported by a rotating cylinder," *Proc. R. Soc. Lond. A*, vol. 457, pp. 1427–1445, 2001.

[39] S. K. Wilson, R. Hunt, and B. R. Duffy, "On the critical solutions in coating and rimming flow on a uniformly rotating horizontal cylinder," *Q. J. Mech. Appl. Math.*, vol. 55, pp. 357–383, 2002.

[40] R. Hunt, "Numerical solution of the free-surface viscous flow on a horizontal rotating elliptical cylinder," *Num. Meth. Part. Diff. Eqns.*, vol. 24, pp. 1094–1114, 2008.

[41] B. R. Duffy and S. K. Wilson, "Thin-film and curtain flows on the outside of a rotating horizontal cylinder," *J. Fluid Mech.*, vol. 394, pp. 29–49, 1999.

[42] M. Tirumkudulu and A. Acrivos, "Coating flows within a rotating horizontal cylinder: Lubrication analysis, numerical computations, and experimental measurements," *Phys. Fluids*, vol. 13, pp. 14–19, 2001.

[43] A. Acrivos and B. Jin, "Rimming flows within a rotating horizontal cylinder: asymptotic analysis of the thin-film lubrication equations and stability of their solutions," *J. Eng. Math.*, vol. 50, pp. 99–120, 2004.

[44] C. H. Tougher, S. K. Wilson, and B. R. Duffy, "On the approach to the critical solution in leading order thin-film coating and rimming flow," *Appl. Math. Lett.*, vol. 22, pp. 882–886, 2009.

[45] E. J. Hinch and M. A. Kelmanson, "On the decay and drift of free-surface perturbations in viscous thin-film flow exterior to a rotating cylinder," *Proc. R. Soc. Lond. A*, vol. 459, pp. 1193–1213, 2003.

[46] E. A. Karabut, "Two regimes of liquid film flow on a rotating cylinder," *J. Appl. Mech. Tech. Phys.*, vol. 48, pp. 55–64, 2007.

[47] M. A. Kelmanson, "On inertial effects in the Moffatt-Pukhnachov coating-flow problem," *J. Fluid Mech.*, vol. 633, pp. 327–353, 2009.

[48] S. D. R. Wilson and J. Williams, "The flow of a liquid film on the inside of a rotating cylinder, and some related problems," *Phys. Fluids*, vol. 9, pp. 2184–2190, 1997.

[49] S. B. G. O'Brien and E. G. Gath, "The location of a shock in rimming flow," *Phys. Fluids*, vol. 10, pp. 1040–1042, 1998.

[50] S. B. G. O'Brien, "A mechanism for linear instability in two-dimensional rimming flow," *Q. Appl. Math.*, vol. 60, pp. 283–299, 2002.

[51] E. S. Benilov, V. N. Lapin, and S. B. G. O'Brien, "On rimming flows with shocks," *J. Eng. Math.*, 2012, to appear.

[52] J. Ashmore, A. E. Hosoi, and H. A. Stone, "The effect of surface tension on rimming flows in a partially filled rotating cylinder," *J. Fluid Mech.*, vol. 479, pp. 65–98, 2003.

[53] E. S. Benilov, M. S. Benilov, and N. Kopteva, "Steady rimming flows with surface tension," *J. Fluid Mech.*, vol. 597, pp. 91–118, 2008.

[54] C. J. Noakes, J. R. King, and D. S. Riley, "The effect of mass transfer on steady two-dimensional rimming flow," *J. Eng. Math.*, vol. 71, pp. 223–236, 2011.

[55] E. S. Benilov, S. B. G. O'Brien, and I. A. Sazonov, "A new type of instability: explosive disturbances in a liquid film inside a rotating horizontal cylinder," *J. Fluid Mech.*, vol. 497, pp. 201–224, 2003.

[56] E. S. Benilov, N. Kopteva, and S. B. G. O'Brien, "Does surface tension stabilize liquid films inside a rotating horizontal cylinder?" *Q. J. Mech. Appl. Math.*, vol. 58, pp. 185–200, 2005.

[57] E. S. Benilov and S. B. G. O'Brien, "Inertial instability of a liquid film inside a rotating horizontal cylinder," *Phys. Fluids*, vol. 17, no. 052106, 2005.

[58] M. Villegas-Díaz, H. Power, and D. S. Riley, "Analytical and numerical studies of the stability of thin-film rimming flow subject to surface shear," *J. Fluid Mech.*, vol. 541, pp. 317–344, 2005.

[59] D. Rajagopalan, R. J. Phillips, R. C. Armstrong, R. A. Brown, and A. Bose, "The influence of viscoelasticity on the existence of steady solutions in two-dimensional rimming flow," *J. Fluid Mech.*, vol. 235, pp. 611–642, 1992.

[60] S. Fomin, T. Hashida, and J. Watterson, "Fundamentals of steady-state non-Newtonian rimming flow," *J. Non-Newtonian Fluid Mech.*, vol. 111, pp. 19–40, 2003.

[61] S. Fomin, K. Kilpatrick, and R. Hubbard, "Rimming flow of a power-law fluid: Qualitative analysis of the mathematical model and analytical solutions," *Appl. Math. Comput.*, vol. 216, pp. 2169–2176, 2010.

[62] P.-J. Chen, Y.-T. Tsai, T.-J. Liu, and P.-Y. Wu, "Low volume fraction rimming flow in a rotating horizontal cylinder," *Phys. Fluids*, vol. 19, no. 128107, 2007.

[63] S. T. Thoroddsen and L. Mahadevan, "Experimental study of coating flows in a partially-filled horizontally rotating cylinder," *Exp. Fluids*, vol. 23, pp. 1–13, 1997.

[64] A. E. Hosoi and L. Mahadevan, "Axial instability of a free-surface front in a partially filled horizontal rotating cylinder," *Phys. Fluids*, vol. 11, pp. 97–106, 1999.

[65] B. Jin and A. Acrivos, "Rimming flows with an axially varying viscosity," *Phys. Fluids*, vol. 16, pp. 633–640, 2004.

[66] P. L. Evans, L. W. Schwartz, and R. V. Roy, "Steady and unsteady solutions for coating flow on a rotating horizontal cylinder: Two-dimensional theoretical and numerical modeling," *Phys. Fluids*, vol. 16, pp. 2742–2756, 2004.

[67] P. L. Evans, L. W. Schwartz, and R. V. Roy, "Three-dimensional solutions for coating flow on a rotating horizontal cylinder: Theory and experiment," *Phys. Fluids*, vol. 17, no. 072102, 2005.

[68] C. J. Noakes, J. R. King, and D. S. Riley, "On three-dimensional stability of a uniform, rigidly rotating film on a rotating cylinder," *Q. J. Mech. Appl. Math.*, vol. 58, pp. 229–256, 2005.

[69] C. J. Noakes, J. R. King, and D. S. Riley, "On the development of rational approximations incorporating inertial effects in coating and rimming flows: a multiple-scales approach," *Q. J. Mech. Appl. Math.*, vol. 59, pp. 163–190, 2006.

[70] K. Pougatch and I. Frigaard, "Thin film flow on the inside surface of a horizontally rotating cylinder: Steady state solutions and their stability," *Phys. Fluids*, vol. 23, no. 022102, 2011.

[71] R. Chicharro, A. Vazquez, and R. Manasseh, "Characterization of patterns in rimming flow," *Exp. Therm. Fluid Sci.*, vol. 35, pp. 1184–1192, 2011.

[72] L. M. Hocking, W. R. Debler, and K. E. Cook, "The growth of leading-edge distortions on a viscous sheet," *Phys. Fluids*, vol. 11, pp. 307–313, 1999.

[73] G. D. Towell and L. B. Rothfeld, "Hydrodynamics of rivulet flow," *AIChE J.*, vol. 12, pp. 972–980, 1966.

[74] R. F. Allen and C. M. Biggin, "Longitudinal flow of a lenticular liquid filament down an inclined plane," *Phys. Fluids*, vol. 17, pp. 287–291, 1974.

[75] M. Bentwich, D. Glasser, J. Kern, and D. Williams, "Analysis of rectilinear rivulet flow," *AIChE J.*, vol. 22, pp. 772–779, 1976.

[76] B. R. Duffy and H. K. Moffatt, "Flow of a viscous trickle on a slowly varying incline," *Chem. Eng. J.*, vol. 60, pp. 141–146, 1995.

[77] B. R. Duffy and S. K. Wilson, "A rivulet of perfectly wetting fluid with temperature-dependent viscosity draining down a uniformly heated or cooled slowly varying substrate," *Phys. Fluids*, vol. 15, pp. 3236–3239, 2003.

[78] S. K. Wilson and B. R. Duffy, "On the gravity-driven draining of a rivulet of viscous fluid down a slowly varying substrate with variation transverse to the direction of flow," *Phys. Fluids*, vol. 10, pp. 13–22, 1998.

[79] C. A. Perazzo and J. Gratton, "Navier–Stokes solutions for parallel flow in rivulets on an inclined plane," *J. Fluid Mech.*, vol. 507, pp. 367–379, 2004.

[80] A. J. Tanasijczuk, C. A. Perazzo, and J. Gratton, "Navier–Stokes solutions for steady parallel-sided pendent rivulets," *Eur. J. Mech. B. Fluids*, vol. 29, pp. 465–471, 2010.

[81] P. A. Kuibin, "An asymptotic description of the rivulet flow along an inclined cylinder," *Russ. J. Eng. Thermophys.*, vol. 6, pp. 33–45, 1996.

[82] S. V. Alekseenko, P. I. Geshev, and P. A. Kuibin, "Free-boundary fluid flow on an inclined cylinder," *Phys. Dokl.*, vol. 42, pp. 269–272, 1997.

[83] S. V. Alekseenko, A. V. Bobylev, and D. M. Markovich, "Rivulet flow on the outer surface of an inclined cylinder," *J. Eng. Thermophys.*, vol. 4, pp. 259–272, 2008.

[84] S. K. Wilson and B. R. Duffy, "A rivulet of perfectly wetting fluid draining steadily down a slowly varying substrate," *IMA J. Appl. Math.*, vol. 70, pp. 293–322, 2005.

[85] P. C. Smith, "A similarity solution for slow viscous flow down an inclined plane," *J. Fluid Mech.*, vol. 58, pp. 275–288, 1973.

[86] B. R. Duffy and H. K. Moffatt, "A similarity solution for viscous source flow on a vertical plane," *Eur. J. Appl. Math.*, vol. 8, pp. 37–47, 1997.

[87] S. K. Wilson, B. R. Duffy, and R. Hunt, "A slender rivulet of a power-law fluid driven by either gravity or a constant shear stress at the free surface," *Q. J. Mech. Appl. Math.*, vol. 55, pp. 385–408, 2002.

[88] J. H. Snoeijer, N. Le Grand-Piteira, L. Limat, H. A. Stone, and J. Eggers, "Cornered drops and rivulets," *Phys. Fluids*, vol. 19, no. 042104, 2007.

[89] Y. M. Yatim, B. R. Duffy, S. K. Wilson, and R. Hunt, "Similarity solutions for unsteady gravity-driven slender rivulets," *Q. J. Mech. Appl. Math.*, vol. 64, pp. 455–480, 2011.

[90] D. Sultanović, B. Bjerke, J. Rekstad, and K. A. Villalonga, "A study of the heat transfer of rivulet flow on inclined plates," *Sol. Energy*, vol. 60, pp. 221–227, 1997.

[91] O. A. Kabov, B. Scheid, I. A. Sharina, and J.-C. Legros, "Heat transfer and rivulet structures formation in a falling thin liquid film locally heated," *Int. J. Therm. Sci.*, vol. 41, pp. 664–672, 2002.

[92] M. S. El-Genk and H. H. Saber, "An investigation of the breakup of an evaporating liquid film, falling down a vertical, uniformly heated wall," *J. Heat Transfer*, vol. 124, pp. 39–50, 2002.

[93] M. S. El-Genk and H. H. Saber, "Minimum thickness of a flowing down liquid film on a vertical surface," *Int. J. Heat Mass Transfer*, vol. 44, pp. 2809–2825, 2001.

[94] D. Holland, B. R. Duffy, and S. K. Wilson, "Thermocapillary effects on a thin viscous rivulet draining steadily down a uniformly heated or cooled slowly varying substrate," *J. Fluid Mech.*, vol. 441, pp. 195–221, 2001.

[95] S. K. Wilson and B. R. Duffy, "On the gravity-driven draining of a rivulet of fluid with temperature-dependent viscosity down a uniformly heated or cooled substrate," *J. Eng. Math.*, vol. 42, pp. 359–372, 2002.

[96] S. K. Wilson and B. R. Duffy, "Strong temperature-dependent-viscosity effects on a rivulet draining down a uniformly heated or cooled slowly varying substrate," *Phys. Fluids*, vol. 15, pp. 827–840, 2003.

[97] S. H. Davis, "Moving contact lines and rivulet instabilities. Part 1. The static rivulet," *J. Fluid Mech.*, vol. 98, pp. 225–242, 1980.

[98] G. W. Young and S. H. Davis, "Rivulet instabilities," *J. Fluid Mech.*, vol. 176, pp. 1–31, 1987.

[99] T. Nakagawa and J. C. Scott, "Stream meanders on a smooth hydrophobic surface," *J. Fluid Mech.*, vol. 149, pp. 89–99, 1984.

[100] T. Nakagawa, "Rivulet meanders on a smooth hydrophobic surface," *Int. J. Multiphase Flow*, vol. 18, pp. 455–463, 1992.

[101] P. Schmuki and M. Laso, "On the stability of rivulet flow," *J. Fluid Mech.*, vol. 215, pp. 125–143, 1990.

[102] R. V. Roy and L. W. Schwartz, "On the stability of liquid ridges," *J. Fluid Mech.*, vol. 391, pp. 293–318, 1999.

[103] H. H. Saber and M. S. El-Genk, "On the breakup of a thin liquid film subject to interfacial shear," *J. Fluid Mech.*, vol. 500, pp. 113–133, 2004.

[104] T. G. Myers, H. X. Liang, and B. Wetton, "The stability and flow of a rivulet driven by interfacial shear and gravity," *Int. J. Non-Linear Mech.*, vol. 39, pp. 1239–1249, 2004.

[105] S. K. Wilson and B. R. Duffy, "Unidirectional flow of a thin rivulet on a vertical substrate subject to a prescribed uniform shear stress at its free surface," *Phys. Fluids*, vol. 17, no. 108105, 2005.

[106] S. K. Wilson, J. M. Sullivan, and B. R. Duffy, "The energetics of the breakup of a sheet and of a rivulet on a vertical substrate in the presence of a uniform surface shear stress," *J. Fluid Mech.*, vol. 674, pp. 281–306, 2011.

[107] J. M. Sullivan, S. K. Wilson, and B. R. Duffy, "A thin rivulet of perfectly wetting fluid subject to a longitudinal surface shear stress," *Q. J. Mech. Appl. Math.*, vol. 61, pp. 25–61, 2008.

[108] N. Le Grand-Piteira, A. Daerr, and L. Limat, "Meandering rivulets on a plane: A simple balance between inertia and capillarity," *Phys. Rev. Lett.*, vol. 96, p. 254503, 2006.

[109] A. Daerr, J. Eggers, L. Limat, and N. Valade, "General mechanism for the meandering instability of rivulets of Newtonian fluids," *Phys. Rev. Lett.*, vol. 106, p. 184501, 2011.

[110] E. S. Benilov, "On the stability of shallow rivulets," *J. Fluid Mech.*, vol. 636, pp. 455–474, 2009.

[111] J. A. Diez, A. G. González, and L. Kondic, "On the breakup of fluid rivulets," *Phys. Fluids*, vol. 21, no. 082105, 2009.

[112] J. A. Diez, A. G. González, and L. Kondic, "Stability of a finite-length rivulet under partial wetting conditions," *J. Phys. Conf. Ser.*, vol. 166, p. 012009, 2009.

[113] B. Reisfeld and S. G. Bankoff, "Nonlinear stability of a heated thin liquid film with variable viscosity," *Phys. Fluids*, vol. 2, pp. 2066–2067, 1990.

[114] R. Selak and G. Lebon, "Bénard-Marangoni thermoconvective instability in [the] presence of a temperature-dependent viscosity," *J. Phys. II France*, vol. 3, pp. 1185–1199, 1993.

[115] N. J. Balmforth and R. V. Craster, "Dynamics of cooling domes of viscoplastic fluid," *J. Fluid Mech.*, vol. 422, pp. 225–248, 2000.

[116] Y. O. Kabova and V. V. Kuznetsov, "Downward flow of a nonisothermal thin liquid film with variable viscosity," *J. Appl. Mech. Tech. Phys.*, vol. 43, pp. 895–901, 2002.

[117] R. Usha, R. Ravindran, and B. Uma, "Dynamics and stability of a thin liquid film on a heated rotating disk film with variable viscosity," *Phys. Fluids*, vol. 17, no. 102103, 2005.

[118] D. Goussis and R. E. Kelly, "Effects of viscosity variation on the stability of film flow down heated or cooled inclined surfaces: Long-wavelength analysis," *Phys. Fluids*, vol. 28, pp. 3207–3214, 1985.

[119] D. A. Goussis and R. E. Kelly, "Effects of viscosity variation on the stability of a liquid film flow down heated or cooled inclined surfaces: Finite wavelength analysis," *Phys. Fluids*, vol. 30, pp. 974–982, 1987.

[120] C.-C. Hwang and C.-I. Weng, "Non-linear stability analysis of film flow down a heated or cooled inclined plane with viscosity variation," *Int. J. Heat Mass Transfer*, vol. 31, pp. 1775–1784, 1988.

[121] M.-C. Wu and C.-C. Hwang, "Nonlinear theory of film rupture with viscosity variation," *Int. Comm. Heat Mass Transfer*, vol. 18, pp. 705–713, 1991.

[122] A. Sansom, J. R. King, and D. S. Riley, "Degenerate-diffusion models for the spreading of thin non-isothermal gravity currents," *J. Eng. Math.*, vol. 48, pp. 43–68, 2004.

[123] D. Bercovici, "A theoretical model of cooling viscous gravity currents with temperature-dependent viscosity," *Geophys. Res. Lett.*, vol. 21, pp. 1177–1180, 1994.

[124] A. A. Osiptsov, "Non-isothermal lava flows over a conical surface," *Fluid Dyn.*, vol. 40, pp. 221–232, 2005.

[125] L. Wu, "Spin coating of thin liquid films on an axisymmetrically heated disk," *Phys. Fluids*, vol. 18, no. 063602, 2006.

[126] G. A. Leslie, S. K. Wilson, and B. R. Duffy, "Non-isothermal flow of a thin film of fluid with temperature-dependent viscosity round a uniformly heated or cooled stationary cylinder," in *proceedings of the 11th UK National Heat Transfer Conference*, 2009.

[127] G. A. Leslie, S. K. Wilson, and B. R. Duffy, "Non-isothermal flow of a thin film of fluid with temperature-dependent viscosity round a uniformly rotating heated or cooled cylinder," in *proceedings of the 12th UK National Heat Transfer Conference*, 2011.

[128] G. A. Leslie, S. K. Wilson, and B. R. Duffy, "Non-isothermal flow of a thin film of fluid with temperature-dependent viscosity on a stationary horizontal cylinder," *Phys. Fluids*, vol. 23, no. 062101, 2011.

[129] B. R. Duffy and S. K. Wilson, "Large-Biot-number non-isothermal flow of a thin film on a stationary or rotating cylinder," *Eur. Phys. J. Special Topics*, vol. 166, pp. 147–150, 2009.

[130] I. S. Gradshteyn and I. M. Ryzhik, *Tables of Integrals, Series and Products*, 2nd ed. Academic Press, 1980, pp. 904–925.